Study of Transport Properties of Strongly Interacting Matter in a Magnetic Field

A thesis submitted for the Degree of

DOCTOR OF PHILOSOPHY (Science)

of

JADAVPUR UNIVERSITY

by

PALLAVI KALIKOTAY

Department of Physics

Jadavpur University

Kolkata - 700032

India

2024

Dedicated to

Baba - Late Bharat Singh Kalikotay

Kanchabhai - Late Sailendra Kalikotay

and

Sanobaba - Late Nependra Kalikotay

Declaration by the Author

This is to certify that this thesis, "***Study of transport properties of strongly interacting matter in a magnetic field***," which is being submitted for the degree of Doctor of Philosophy (Science), contains only my original research and writing, and to the best of my knowledge and belief, neither the thesis nor any portion of it has been approved for the award of any other degree or certificate by the university or other institution of higher learning, with the exception of instances where appropriate credit has been given in the text.

Date: 27/06/2024

Pallavi Kalikotay

Certificate from the Supervisor

This is to certify that the thesis entitled "***Study of Transport Properties of Strongly Interacting Matter in a magnetic field***" submitted by Smt. Pallavi Kalikotay who got her name registered on 11.11.2020 for the award of Ph.D. (Science) degree of Jadavpur University, is absolutely based upon her own work under the supervision of Dr. Sourav Sarkar and that neither this thesis nor any part of it has been submitted for either any degree / diploma or any other academic award anywhere before.

Sourav Sarkar 27/06/2024

Dr. Sourav Sarkar
Scientific Officer (H)
Theoretical Nuclear Physics Division
Variable Energy Cyclotron Centre
1/AF, Bidhannagar
Kolkata-700064

डॉ. सौरव सरकार / Dr. Sourav Sarkar
वैज्ञानिक अधिकारी (एच) / Scientific Officer (H)
भारत सरकार / Government of India
परमाणु ऊर्जा विभाग / Department of Atomic Energy
परिवर्ती ऊर्जा साइक्लोट्रॉन केन्द्र / Variable Energy Cyclotron Centre
1/ए,एफ., बिधान नगर / 1/AF, Bidhan Nagar
कोलकाता / Kolkata-700 064

Acknowledgements

I would like to express my sincere gratitude to my supervisor, Prof. Sourav Sarkar. From the beginning of my PhD tenure he has very helpful, encouraging and kind. His sincerity and dedication to research has always inspired and motivated me. My humble gratitude to our collaborator, Prof. Pradip Roy, for his invaluable insights and encouragement throughout my PhD journey.

My PhD seniors have been instrumental in my PhD journey. Utsab Da, has taught me kinetic theory from scratch. Snigdha Da's computational knowledge and analytical skills have helped me immensely. Nilanjan, my contemporary, in our research group has always been available for help and discussions. Their insightful discussions, constructive feedback, and camaraderie have been invaluable to my research and personal growth. I am deeply thankful for the shared knowledge, teamwork, and the countless moments of inspiration and motivation they provided.

I acknowledge my PhD friends Dipen, Sudipta, Kalyan and Abdul for their valuable academic and non-academic discussions during the early days of my PhD journey.

My deepest gratitude to the Head of the Department, Jadavpur University for all the help he provided with administrative work. Also, I am grateful to the VECC administration for providing me with comfortable accommodation during my PhD work.

I would like to extend my deepest gratitude to my dear friends Subhadip, Madhurima, Sayanti, Ajanta, Divya, Khusboo and Sahin for their unwavering support, which has been instrumental in keeping me grounded and balanced throughout my PhD journey. Their encouragement, understanding, and steadfast companionship have been invaluable, and I am profoundly thankful for their presence in my life. I am thankful to Aritra for giving me invaluable suggestions to improve my thesis.

I thank my parents who have always valued education above anything else. I thank my dearest Fupu, Devika Kalikotay, who made sure that I get the best education. Ama, Maila Kaka, Maili Kaki and Kanchikaki have always been there to cheer me up during difficult times. I am lucky to have Prashant, Nishal and Naivaidya, my brothers who have always believed in me and provided all the love and support. I thank my family members in heaven who worked hard all their life to provide the best for me.

Pallavi Kalikotay
27/06/2024
Pallavi Kalikotay

List of Publications arising from the thesis

Journal

1. **"Viscous coefficients and thermal conductivity of a πKN gas mixture in the medium"**
   Pallavi Kalikotay, Nilanjan Chaudhuri, Snigdha Ghosh, Utsab Gangopadhyaya and Sourav Sarkar.
   Eur. Phys. J. A **56**, no.3, 79 (2020)

2. **"Medium effects on the electrical and Hall conductivities of a hot and magnetized pion gas"**
   Pallavi Kalikotay, Snigdha Ghosh, Nilanjan Chaudhuri, Pradip Roy and Sourav Sarkar.
   Phys. Rev. D **102**, no.7, 076007 (2020)

3. **"Electrical conductivity and shear viscosity of a pion gas in a thermo-magnetic medium"**
   P**allavi Kalikotay**, Snigdha Ghosh, Nilanjan Chaudhuri, Pradip Roy and Sourav Sarkar.
   Eur. Phys. J. A **60**, no.3, 71 (2024)

Conferences

1. **"Medium effects on Relaxation times and Transport coefficients of Pion-Kaon-Nucleon system"**
   Pallavi Kalikotay, Nilanjan Chaudhuri, Snigdha Ghosh, Sourav Sarkar.
   DAE Symp. Nucl. Phys. **63**, 1004 (2018).

2. **Viscous coefficients and thermal conductivity of a πKN gas mixture in the medium**
   at Dynamics of QCD matter — current status
   Pallavi Kalikotay *et al.*
   Int. J. Mod. Phys. E **30**, no. 02, 2130001 (2021)

3. **"Electrical and Hall conductivities of a pion gas in thermal and magnetic medium"**
   Pallavi Kalikotay, Snigdha Ghosh, Nilanjan Chaudhuri, Pradip Roy and Sourav Sarkar.
   DAE Symp. Nucl. Phys. **65**, 589 (2021).

4. **"Shear Viscosity of a pion gas in a thermomagnetic medium"**
   Pallavi Kalikotay, Snigdha Ghosh, Nilanjan Chaudhuri, Pradip Roy and Sourav Sarkar.
   DAE Symp. Nucl. Phys. **66**, 835 (2022).

Pallavi Kalikotay

Contents

List of Figures

Chapter 1

Introduction

Throughout history, humans have been curious about the fundamental building blocks of matter. This relentless quest of mankind has led to the development of high-energy physics, a field of physics dedicated to probing the fundamental building blocks of matter. At the heart of this exploration lie matter particles, which are classified into two categories: leptons and quarks. These particles are fermions and they constitute the basic constituents of all matter. In addition to matter particles, there exists exchange particles which are bosons. These exchange particles mediate the four fundamental forces of nature: gravitational force, electromagnetic force, weak nuclear force, and strong nuclear force. Together, these forces govern the behaviour of matter at both the microscopic (nuclear and subnuclear) and macroscopic (cosmic) scales. The Standard Model provides a comprehensive framework for understanding the interactions between these fundamental particles and forces except the gravitational force. In the Standard model, the strong interaction between the quarks and gluons is described by Quantum Chromodynamics.

1.1 Quantum Chromodynamics

Quantum Chromodynamics (QCD) is a non-abelian gauge field theory based on $SU(3)$ colour symmetry. In QCD, quarks and gluons have colour degrees of freedom. Since gluons are coloured they can self interact unlike the photons in Quantum Electrodynamics (QED). Due to the gluon-gluon self interactions, the QCD coupling which controls the strength of the strong interaction depends on the momentum transfer. When the momentum transfer is small, the coupling constant is large and thus the quarks and gluons are strongly coupled and the quarks are trapped within the hadrons. This is known as colour confinement. As a consequence of colour-confinement, free quarks are not directly observed in nature. However, colour singlet states of quarks and antiquarks known as hadrons are observed in nature. Based on the quark composition hadrons are of two types – mesons and baryons. Mesons are the bound states of a quark and an antiquark pair ($q\bar{q}$) whereas baryons are the bound states of three quarks (qqq) or three antiquarks ($\bar{q}\bar{q}\bar{q}$). When the momentum transfer is large, the QCD coupling is small as a result of which quarks and gluons are weakly coupled. This phenomenon is known as asymptotic freedom. This weakly coupled system of quarks and

gluons occupying a finite volume (∼10 fm/c) at high temperature and/or density is known as Quark Gluon Plasma (QGP). Light quarks being (almost) massless, chiral symmetry or handedness is preserved in this high temperature phase of QCD. At low temperature, the QCD vacuum breaks this symmetry spontaneously leading to the build-up of the chiral condensate which is manifested as the constituent mass of quarks in the hadrons.

In the high energy regime, QCD allows the use of perturbative techniques to estimate various observables. However, perturbative techniques fail at low energy energies due to the fact that the QCD coupling constant becomes large. One of the most successful non-perturbative frameworks is Lattice Quantum Chromodyanmics (LQCD) [14] wherein the field theory of strong interaction is defined in a gauge-invariant way on a discrete space-time domain. However, LQCD at finite baryon density usually suffers from uncontrolled systematic uncertainities in addition to the infamous sign problem [15]. Some of the techniques used to overcome this problem are Taylor expansion around zero chemical potential, analytic continuation from purely imaginary chemical potentials or the complex Langevin approach. On the other hand, effective theories provide an alternative method to study the strongly interacting matter in the low energy non-perturbative region. Effective models are used in situations where there is a natural separation of energy scales. These models are constructed using the basic symmetries of the underlying QCD lagrangian. Some of the well known models like Hadron Resonance Gas (HRG) model [16, 17, 18, 19, 20], Nambu–Jona–Lasinio (NJL) model [21, 22, 23], Polyakov loop extended Quark-Meson (PQM) model [24, 25, 26] have successfully explained the lattice data and also provided insights on the strongly interacting matter at non-zero baryon density.

1.2 Formation of Quark Gluon Plasma

When the density of nuclear matter is increased by compressing it, the distance between the constituents of the nucleons namely the quarks and gluons start to decrease. When the density of the system is greater than a certain critical value of density, the quarks and gluons between different nucleons/hadrons start to overlap and finally move freely in a volume much larger than the hadronic/nucleonic volume. This deconfined phase of matter is QGP. QGP can also be created by heating the nuclear matter above a certain critical temperature wherein the hadronic/nucleonic matter "*melt*" into quarks and gluons. A schematic diagram for the formation of QGP at high temperature and/or density is shown in Fig. 1.1.

As per our current knowledge, there are three scenarios where this deconfined state of matter might exist:

- During the early universe evolution, a few microseconds after the Big Bang, temperature of the universe was around 10^{12}K or 200 MeV which is greater than the critical temperature. Thus, a transient QGP was likely to have been created.

- In the core of the neutron stars where the density is believed to exceed 10^{15} gm/cm^3 (few times of

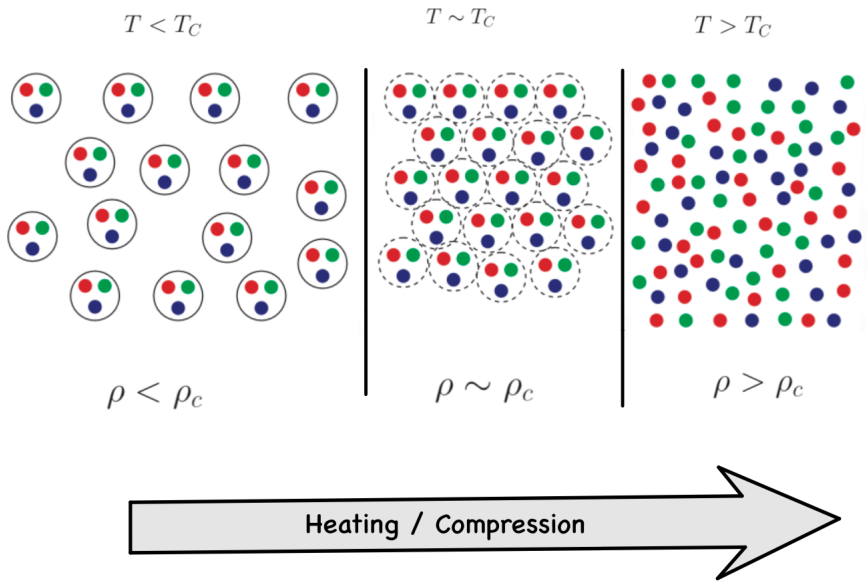

Figure 1.1: Nuclear matter at high temperature and/or density

nuclear density) providing a favourable condition for the formation of QGP.

- In ultra relativistic heavy ion collisions high temperature and/or density is created. This condition is likely to favour the formation of QGP.

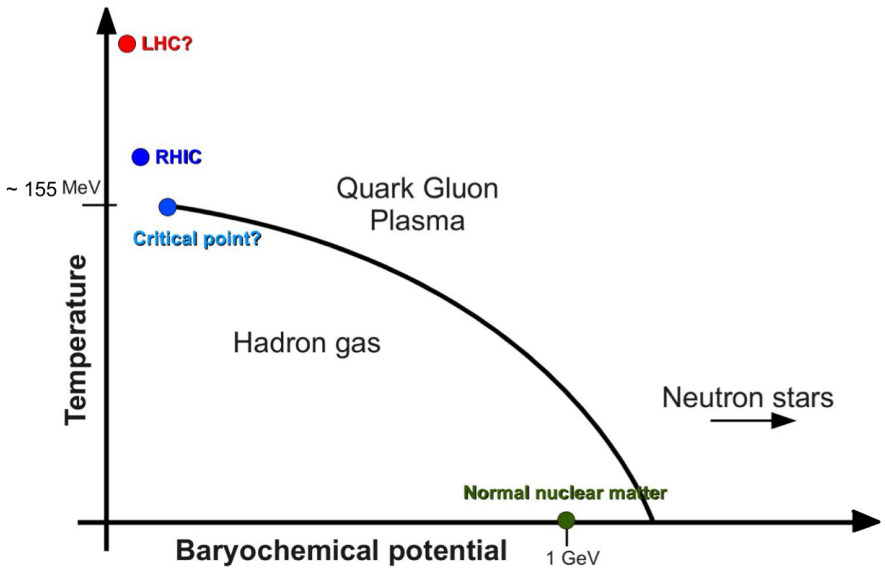

Figure 1.2: QCD Phase diagram in the temperature-baryochemical potential plane.

The above scenarios depict situations when either temperature or baryon density governs the occurence of the phase transition. A graphical representation such as the one shown in Fig. 1.2 is known as the QCD phase diagram. It effectively illustrates the equilibrium phases of QCD matter in the temperature-baryochemical potential plane. Though the exact positions of the phase transitions to deconfined quark

matter are not known, a significant region of the phase space is occupied by hot/dense hadronic matter composed of interacting mesons and baryons at finite temperature and baryon chemical potential.

1.3 Heavy Ion Collisions

The Big Bang occurred a long time ago, and astrophysical objects are far away in space, making the study of QGP through these means quite difficult. Therefore, we focus on studying QGP in the laboratory using relativistic heavy ion collisions.

QGP can be formed at high temperature and/or density. In order to create such an exotic matter in the laboratory, nuclear matter at high temperature and density needs to be produced. This can be achieved in ultra relativistic heavy ion collision experiments. In heavy ion collision (HIC) experiments two highly energetic beams of heavy ions like *Au-Au*, *Pb-Pb* are collided to produce a system of strongly interacting matter at high density and/or temperature. Some of the experimental facilities dedicated to HIC experiments are – Large Hadron Collider (LHC), Relativistic Heavy Ion Colllider (RHIC), Nuclotron-based Ion Collider facility (NICA) and Facility for Antiproton and Ion Research (FAIR). The first evidence of QGP formation in HIC experiment came from the *Au-Au* collisions at RHIC energy of $\sqrt{s_{NN}} = 200$ GeV [27, 28, 29, 30], the same was also confirmed in the *Pb-Pb* collisions at LHC energy of $\sqrt{s_{NN}} = 2.76$ TeV [31, 32, 33, 34].

1.3.1 Stages of Heavy Ion Collisions

The evolution of heavy ion collision starting from the collision of two Lorentz contracted discs to finally the hadrons hitting the detector goes through a pre-equilibrium stage, expansion stage and then finally the freeze-out of the hadrons. A sketch potraying the time evolution of matter created in ultra relativistic heavy ion collision is shown in Fig. 1.3. In the pre-equilibrium stage, the constituents of highly excited fireball collide frequently to reach local thermal equilibrium within a time known as thermalisation time. After the pre-equilibrium stage, the thermalised system consisting of deconfined QGP matter expands in all directions against the surrounding vacuum due to its thermal pressure. As the system expands its temperature decreases thereby decreasing the energy density of the system. When the temperature drops close to crtitical temperature ($T_c \sim 155$ MeV [35]) the system undergoes a phase transition from the QGP phase to the hadronic phase. The system now comprises of hadrons which collide with each other to maintain local equilibrium. The expanding hadronic system further cools and runs out of inelastic collisions. This causes the quark composition of the hadrons to be fixed in the system. This is known as chemical freezeout. The system with fixed hadron abundances undergo elastic collision. Since the system is still expanding and cooling, the mean free path of the elastic collision becomes larger than the range of strong interaction. As elastic collision ceases to occur, local equilibrium cannot be maintained in the system as a result of which hadrons freezeout (kinetic freezeout) and move to the detector.

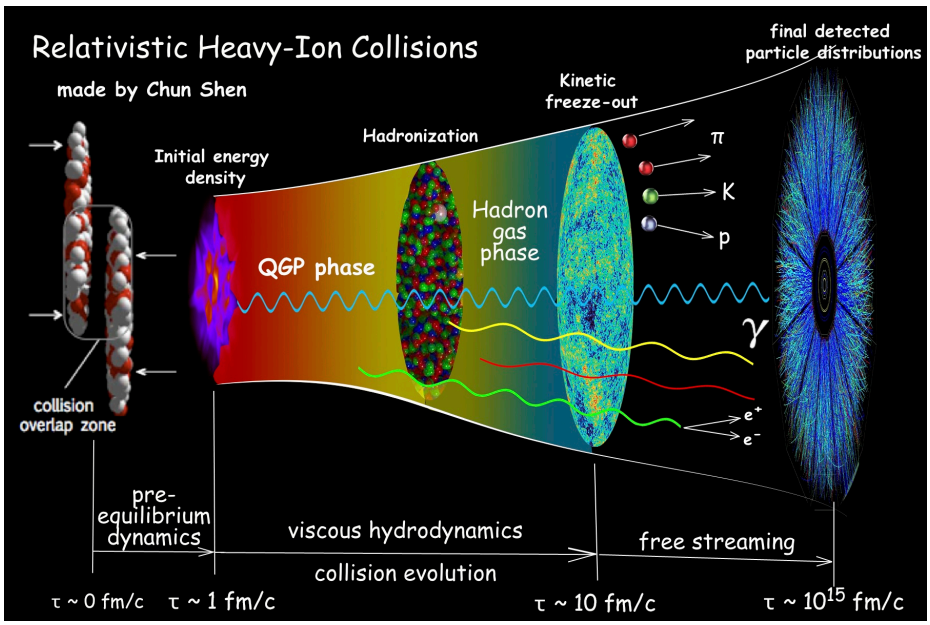

Figure 1.3: Sketch showing time evolution of ultra relativsitic heavy ion collisions. Image source:https://u.osu.edu/vishnu/

1.3.2 Probes of Heavy Ion Collisions

The matter created in a HIC has a very short lifetime and hence cannot be observed directly. Some of the indirect methods to probe the thermodynamic medium produced in heavy ion collisions is through quarkonia dissociation, electromagnetic probes, jet quenching, strangeness enhancement and collective flow. An extensive review on different probes of HIC can be found in Refs. [36, 37, 38, 39]. We will now provide a brief discussion on each of these probes.

- **Quarkonia dissociation:** Bound states of heavy quark and antiquark pair also known as quarkonia are produced in the early stages of heavy ion collisions even before the formation of the QGP. These quarkonia states carry valuable information about their interactions throughout the medium's evolution. Within a deconfined medium, the quark-antiquark ($q\bar{q}$) pairs experience color-screening effects from surrounding quarks and gluons. The screening radius, which decreases as the temperature increases, plays a crucial role in this process. When the screening radius becomes sufficiently smaller than the radius of the quarkonia bound states, these states dissociate. This dissociation leads to a suppression of their yield, a phenomenon that serves as a significant indicator of QGP formation.

- **Electromagnetic Probes:** One of the most important probe in HIC is electromagnetic probes such as photons and dileptons. Photons and dileptons are produced in all stages of nuclear collisions, including the initial hard scattering before the formation of the medium and during hadronic decays. The mean free path of electromagnetic interactions is larger than the size of the deconfined QGP medium. Consequently, these photons and dileptons escape the medium without significant scattering or absorption, retaining the characteristics of their region of origin. When photons and lepton-antilepton pairs or dileptons (like e^+-e^- and μ^+ -μ^-), hit the detector, their spectrum can be analyzed to ex-

tract valuable information about the medium in which they were produced. However, the spectrum of photons and dileptons coming from the hadronic decays must be subtracted to obtain information about the hot deconfined medium under investigation

- **Jet Quenching:** In a p-p collision, the partons produced from hard processes hadronizes into a collimated beam of hadrons produced back-to-back. These stream of particles which are produced back to back are known as jets. However, in heavy ion collisions the initial hard parton-parton collisions travel through the hot and dense QGP medium. This causes the scattered partons to lose their energy because of their interaction with the QGP medium. Having lost their energy, the partons fragment into lesser number of final state hadrons in the jet beam resulting in what is known as jet quenching.

- **Strangeness Enhancement:** An equilibrated QGP with its temperature higher than the mass of the strange quark favors the formation of strange quark and anti-quark pair via $q\bar{q} \rightarrow s\bar{s}$, $gg \rightarrow s\bar{s}$, $g \rightarrow s\bar{s}$, $gs \rightarrow gs$ and $qs \rightarrow qs$ processes, thereby leading to the increased production of final state strange hadrons. Thus, strangeness enhancement in a heavy ion collision compared to nucleon-nucleon collision becomes an essential signature of QGP formation.

- **Collective Flow:** The azimuthal distribution of produced particles is an important observable in HIC [40, 41, 42]. In non-central heavy ion collisions (i.e. collisions with non-zero impact parameter), the participants in the overlapped region of the collision are spatially anisotropic. The initial spatial anisotropy in the overlap zone creates an anisotropic pressure gradient in a plane transverse to the beam pipe which, in turn, causes momentum anisotropy of the produced particles. This observed momentum anisotropy is known as collective flow and it is an essential signature of HIC. It can be best described using hydrodynamic models [43]. This collective flow can be quantified by decomposing the azimuthal dependence of invariant particle spectra in a Fourier series [44]. Each fourier coefficient corresponds to different flow coefficient such as directed flow (v_1), elliptic flow (v_2), triangular flow (v_3) and so on. The directed flow v_1 describes the collective sideward motion of the particles and is believed to have developed in the early stage of the collisions and thus provides information on the equation of state at those early times [45, 46, 47]. The elliptic flow v_2 was proposed as a signature of hydrodynamic behavior of nucelar matter produced in high energy nuclear collisions [41]. It reflects the interactions between the constituents during the early stage of evolution of the produced particles [47] and is therefore sensitive to the equation of state when this system might be in the QGP phase. The triangular flow v_3 corresponds to the the triangular anisotropy of the initial nuclear overlap region and it arises from event- by-event fluctuations in the participant-nucleon collision points [48]. Among these flow coefficients, v_2 has been extensively studied at RHIC [49] and LHC [50] collision energies.

1.4 Theoretical Models to treat Heavy Ion Collisions

The hot and dense matter created in HIC can be treated mathematically through - (i) Covariant transport theory and (ii) Relativistic Hydrodynamics. The transport theory deals with the microscopic description of the system and is used to study the early pre-equilibirum and later hadronic rescattering and freeze-out stage. Some of the transport based models are - A Multi-Phase Transport (AMPT) model [51], Ultra-relativistic Quantum Molecular Dynamics (UrQMD) model [52], Parton-Hadron String Dynamics (PHSD) model [53] and Simulating Many Accelerated Strongly-Interacting Hadrons (SMASH) [54]. The evolution of the system from the early pre-equilibrium phase to the hadronic phase can be studied using hydrodynamics. Hydrodynamics deals with the macroscopic description of the system. The macroscopic quantities are an average of some microscopic quantity (energy, momentum, baryon number etc.), over all the constituent particles.

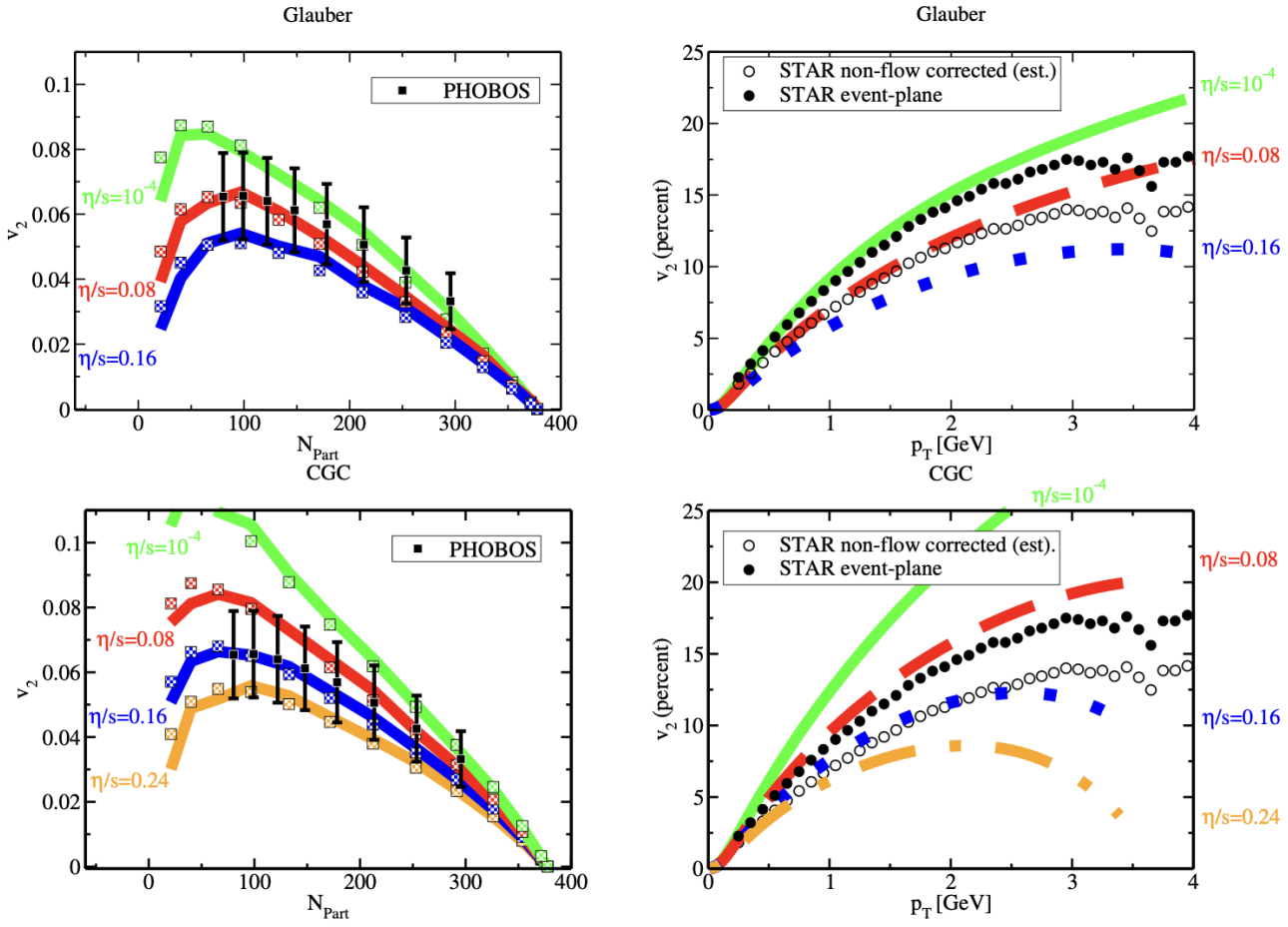

Figure 1.4: Comparison of hydrodynamic models to experimental data on charged hadron integrated (left) and minimum bias (right) elliptic flow by PHOBOS and STAR, respectively. STAR event plane data has been reduced by 20 per cent to estimate the removal of non-flow contributions. [1]

Hydrodynamic simulations of relativistic heavy ion collisions are performed using computational methods. The hydrodynamic equations are solved numerically and matched with the observed momentum distribution of the particles obtained in the experiments. It has been observed that ideal hydrodynamics explains

the experimental data for multiplicity, radial and elliptic flow of low of p_T particles for heavy-ion collisions at RHIC. In ideal hydrodynamics, input parameters like initial energy density, time where the hydrodynamic model is initialized as well as the temperature at which the hydrodynamic evolution is stopped are chosen so as to match with the experimental data obtained for multiplicity and radial flow. The Glauber Model and the Color Glass Condensate (CGC) model are primarily used to describe the initial energy density. In the Glauber model, the energy density profile follows the nucleon distribution, whereas the Color Glass Condensate model uses the gluon number density in binary collisions.

Ideal hydrodynamics does not include any dissipative effects in its formalism. However, due to quantum mechanical uncertainity [55], the system created in a heavy ion collision undergoes irreversible processes as a result of which dissipation is always present in the system. This necessitates the use of relativistic dissipative fluid dynamics in HIC. In Fig. 1.4 we have shown the comparison of hydrodynamic models (CGC and Glauber model) to experimental data on charged hadron integrated (left) and minimum bias (right) elliptic flow by PHOBOS and STAR, respectively [1]. From the figure we can see that ideal hydrodynamics ($\eta/s = 10^{-4}$) overpredicts the data in the high p_T regions, both for STAR and PHOBOS data. From the figure we observe that in hydrodynamic models, elliptic flow v_2 is sensitive to the shear viscosity to entropy density ratio (η/s) of the medium and this fact has been used to extract the η/s of the hot and dense medium from the elliptic flow data [56, 57, 58]. Thus, studying transport properties like viscosity helps us in refining hydrodynamic models, thereby improving our understanding of the evolution of the fireball created in these collisions. In this thesis, we have estimated the values of η/s in both thermal and thermo-magnetic medium.

1.5 Magnetic Field in Heavy Ion Collisions

Apart from high temperature and/or density, in non-central HICs, at RHIC and LHC, strong magnetic fields of the order of $\sim 10^{18}$ Gauss [59, 60] or larger may be generated due to the collision geometry. Fig. 1.5 shows the schematic representation of non-central HICs. At relativistic energies the Lorentz contracted thin discs which travel towards each other in the oppositie direction along the beam pipe (z direction) collide with each other. In HIC the participants carry charges and charges in motion produce electric currents which thereby produces magnetic field. In Ref. [61] it is shown that two ions of radius R with electric charge Ze and colliding impact parameter b, the produced magnetic field, in the centre of mass frame according to the Biot Savart's law, has a magnitude of

$$B \sim \gamma Ze\frac{b}{R^3} \tag{1.1}$$

The magnetic field points in a direction perpendicular to the reaction plane ($x-z$ plane). At RHIC, for Au+Au collisions at $\sqrt{s_{NN}} = 200$ GeV, Lorentz factor $\gamma = 100$ ($\gamma = \sqrt{s_{NN}}$), $z = 79$, $b \sim R_A \sim 7$ fm, the estimated value of magnetic field using Eq. (1.1) is $eB \approx m_\pi^2 \sim 10^{18}$ Gauss. A similar calculation performed

at LHC energies estimates magnetic field to be $eB \approx 10m_\pi^2$.

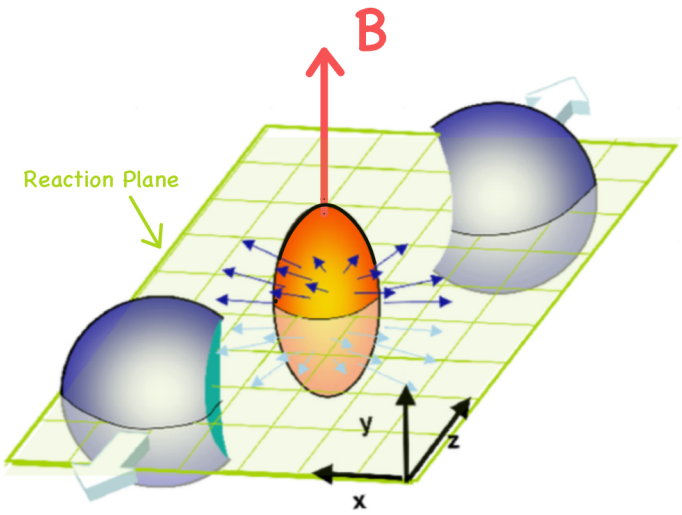

Figure 1.5: The schematic representation of non-central heavy ion collision. The magnetic field is generated in the collision region along the y-axis perpendicular to the reaction plane. This figure has been modified from [2]

The fields produced in HICs are comparable to the QCD scale i.e. $eB \approx m_\pi^2 \approx \Lambda_{QCD}^2$ and hence it can cause noticeable influence on the behaviour of strongly interacting matter. This has motivated a large number of investigations on the properties of hot and dense QCD matter in the presence of background magnetic field in recent times involving several novel and interesting phenomena, such as, Chiral Magnetic Effect (CME) [59, 62, 63, 64], Magnetic Catalysis (MC) [65, 66, 67, 68, 69] and Inverse Magnetic Catalysis (IMC) [70, 71] of dynamical chiral symmetry breaking which may cause significant change in the nature of electro-weak [72, 73, 74, 75], chiral and superconducting phase transitions [76, 77, 78, 79], electromagnetically induced superconductivity and superfluidity [80, 81] and many more. Though, the magnetic field is very transient (few fm/c), the finite electrical conductivity of the medium sustains the magnetic field for a longer time [82, 83, 84, 85]. This magnetic field affects the evolution of the strongly interacting matter which has a noticeable effect on its dynamics and is reflected in the observables like charged hadron spectra and flow harmonics. Thus, a deeper understanding of the various aspects of strongly interacting matter in the presence of magnetic field is important to achieve the consistent dynamical modelling of the matter created in HICs.

Besides heavy ion collisions, such magnetic fields of the order of $\sim 10^{15}$ Gauss can also be realized on the surface of certain compact stars called *magnetars*, while in the interior it is estimated to reach magnitudes of the order of $\sim 10^{18}$ Gauss [86, 87]. Cosmological model calculations, in fact, predict that during electroweak phase transition in the early universe extremely strong magnetic field as high as $\sim 10^{23}$ Gauss might have been produced [88, 89].

The dynamical evolution of such a relativistic matter in the presence of background magnetic field is studied using magnetohydrodynamics (MHD). Transport coefficients are essential for describing the time

evolution of strongly interacting matter and they are the key dynamical inputs to MHD. The transport coefficients are the measure of dissipative processes occurring in the strongly interacting matter. The dissipative processes are brought in by the collisions among the constituents. Thus, the scattering cross-section is an important dynamical input to the transport coefficients. In HICs, the hadronic phase attains a temperature in the range 100 MeV $\lesssim T \lesssim$ 150 MeV. Hence, it becomes important to consider the thermal effects in the presence of background magnetic field in the cross section calculations to provide a more realistic picture of HICs. Thus, in Chapters 5 and 6 we have considered the background magnetic field and thermal medium to calculate the transport coefficients in which thermo-magnetic effects are incorporated in the scattering cross-section. Substantial amount of works which involve the estimation of transport coefficients of quark gluon plasma (QGP) and hadrons in a background magnetic field are available in the literature where these quantities have been evaluated using either a constant cross-section or the relaxation time has been taken as a parameter to evaluate the necessary transport coefficients. Incorporation of the effect of magnetic field along with thermal effects on the relaxation time is the novelty of this thesis.

1.6 Scope and Organization of the thesis

The hot and dense nuclear matter produced in heavy-ion collisions may be near local thermodynamic equilibrium, exhibiting specific thermodynamic and transport properties. If the interaction between quarks and gluons is sufficiently strong to maintain local thermodynamic equilibrium in the subsequent phases, these phases will also exhibit distinct transport properties. Experimentally one can only measure the energy and momentum of the particles that hit the detector after kinetic freeze-out. Therefore, to study the transport in QGP, it is necessary to investigate and model the properties of all stages in heavy-ion collisions. This includes the initial state of two Lorentz-contracted heavy ion nuclei, the formation and thermalization of the QGP, its evolution, the phase transition to the hadronic phase, and the evolution of the hadronic phase. To accurately study the transport properties of the QGP, the transport properties of the latter phase of HIC which is the hadronic phase must also be examined to validate findings through experiments. In this thesis, we have focussed on the transport properties of the hadronic state.

In this thesis, the transport coefficients have been evaluated in the kinetic theory approach in the ambit of relaxation time approximation. The relativistic Boltzmann transport equation in the presence of electromagnetic field is given by [90]

$$p^\mu \partial_\mu f + qF^{\mu\nu} p_\nu \frac{\partial f}{\partial p^\mu} = C[f] \tag{1.2}$$

where, $f(x,p)$ is the single particle distribution function, q is the electric charge of the particle and $g^{\mu\nu} = \text{diag}(1,-1,-1,-1)$ is the metric tensor and the field information is contained in the field strength tensor $F^{\mu\nu}$. The collision integral $C[f]$ appearing on the right-hand side of the above equation carries information of all the microscopic interactions occuring in the system. These microscopic interactions are responsible

for removing the dissipation and bringing the system into equilibrium. In order to evaluate the transport coefficients one has to solve the relativistic Boltzmann transport equation. The in-medium effects on the transport coefficients is studied by solving the collsion integral using the relaxation time approximation. In this approximation only one of the incoming particle's distribution function in a binary interaction is taken to be slightly away from equilibrium whereby we consider $C[f] = -\frac{\delta f}{\tau}$, in which δf is the deviation function and τ is the relaxation time. The deviation function, δf which encapsulates the dissipative processes can be written in terms of the thermodynamic forces. Making use of conservation equation and Gibb's Duhem relation, the left-hand side of Eq.(1.2) can be written in terms of the thermodynamic forces. The irreversible flows such as heat flow, energy momentum flow and charge flow can be expressed in terms of thermodynamic forces and the corresponding transport coefficients and simultaneously these flows can also be written in terms of the deviation function, thus connecting the macroscopic gradients with the microscopic theory. Comparing the two sides of the Boltzmann transport equation one can obtain the expression of the transport coefficients. It is to be noted here that in the presence of magnetic field these coefficients become anisotropic leading to three components of electrical conductivity, five components of shear viscosity, two components of bulk viscosity and three components of thermal conductivity unlike the non-magnetic field case where each of these coefficients have only single isotropic component.

The dynamical input to these coefficients i.e. the relaxation time is evaluated using real time formalism of thermal field theory. In the low temperature regime ($\sim$100-150 MeV) the perturbative QCD breaks down due to larger values of the coupling constant. One then resorts to effective theories constructed using the basic symmetries of the underlying QCD Lagrangian. Using the effective interaction Lagrangian, the matrix elements for the scattering process mediated via various resonance channels are evaluated. The vacuum propagators corresponding to the intermediate resonances appearing in the s-channel diagrams, are replaced with effective ones obtained from a Dyson-Schwinger sum containing one-loop self-energy diagrams in vacuum. This introduces an imaginary part in the matrix elements rendering a Breit-Wigner like structure to the cross- section. The scattering cross-section is normalized to the experimental data fixing a few unknown model parameters in the process. The corresponding in-medium cross-section is then obtained by evaluating the self-energy diagrams in the medium.

In Chapter 2 we have discussed the basics of kinetic theory which will be used to derive the transport coefficients in the later chapters.

Chapter 3 deals with the expressions of shear viscosity, bulk viscosity and thermal conductivity for a multi-component system using relaxation time approximation. We have in brief discussed the real time formalism of finite temperature field theory and have also given a general picture of thermal propagators for different fields. The formalism stated in this chapter is discussed by presenting the results of shear viscosity of a pion gas in a thermal medium.

In Chapter 4 we have studied the relaxation times, thermal conductivity, bulk viscosity and shear viscosity of a hot and dense gas consisting of pions, kaons and nucelons (πKN system). The thermal medium dependent cross-sections for $\pi\pi$, πK and πN scatterings is obtained using the complete propagators for the

exchanged ρ, σ, K^* and Δ resonances. We have obtained appreciable change in the temperature dependence of these transport coefficients upon use of in-medium cross-section.

In Chapter 5 magnetic field has been switched on and its effect on the electrical and hall conductivity of a system of pion gas been studied. Here we have explored the magnetic field influence only through cyclotron frequency and the scattering cross-section is evaluated only in a thermal medium. We have studied the variation of electrical and hall conductivities with the temperature for different values of the magnetic field. It has been observed that electrical conductivity and Hall conductivity are very sensitive to the magnetic field strength and the use of in-medium cross sections.

Chapter 6 concerns the study of effects of thermo-magnetic medium on two important transport coefficients - electrical conductivity and shear viscosity of a pion gas. The magnetic field influences the electrical conductivity and shear viscosity through cyclotron frequency as well as the magnetic field dependent relaxation time. Upon the introduction of magnetic field, the self-energies of $\rho^{\pm}$ and ρ^0 becomes unequal unlike the pure thermal medium case.

Finally, in Chapter 7 we present a summary and some outlook for future work.

Chapter 2

Kinetic Theory

The QGP fluid or a hot hadron gas can be considered as a macroscopic system which is characterised by the thermodynamic state variables like number density, temperature, pressure, energy density etc. The dynamics of the evolution of such a fluid can be obtained using the thermodynamic state variables. This is achieved by solving the Boltzmann transport equation, the solution of which is given by the one-particle distribution function. The one particle distribution function $f(x,p)$ gives the statistical description of the gases in kinetic theory. This distribution function gives the average number of particles with a certain momentum at each space-time point. To find its explicit form one derives kinetic equation or the transport equation which gives the rate of change of distribution function in time and space due to particle interactions. Before deriving the transport equation we will describe some of the macroscopic quantities in terms of the one-particle distribution function.

2.1 Macroscopic Quantities

On the macroscopic level the state of a many-particle system is described by the particle density, energy density and hydrodynamic velocity. In non-uniform system these quantities become function of space and time. We will now discuss each of these quantities.

2.1.1 Particle four-flow

To describe a non-uniform system one introduces a local density $n(\vec{x},t)$. The quantity $n(\vec{x},t)\Delta^3x$ gives the average number of particles in the spatial volume element Δ^3x at point $\vec{x}$ and at time t. The particle flow is denoted by $j(\vec{x},t)$. Thus the particle four flow $N^\mu(x)$ is given by-

$$N^\mu(x) = (n(\vec{x},t), \vec{j}(\vec{x},t)) \tag{2.1}$$

Let us consider a distribution function $f(x,p)$, then $f(x,p)\Delta^3x\Delta^3p$ gives the average number of particles present in the volume element Δ^3x at point x with momentum in the range $(p, p+\Delta p)$ at time t. It is to be noted here that though the volume element Δ^3x is very small from a macroscopic point of view but the

number of particles contained in it is quite large. In terms of the distribution function, the temporal and spatial components of particle four flow is given as-

$$n(\vec{x},t) = \int d^3p\ f(x,p) \tag{2.2}$$

$$\vec{j}(\vec{x},t) = \int \frac{d^3p}{p^0}\ \vec{p}f(x,p) \tag{2.3}$$

where $\vec{u} = \frac{\vec{p}}{p^0}$. Thus,

$$N^\mu(x) = \int \frac{d^3p}{p^0} p^\mu f(x,p) \tag{2.4}$$

2.1.2 Energy-Momentum tensor

Let us now consider the energy density. The energy per particle is p^0, hence the average can be written as,

$$T^{00}(x) = \int d^3p\ p^0 f(x,p) \tag{2.5}$$

the quantity T^{00} is the macroscopic energy density. The energy flow T^{0i} is given by,

$$T^{0i}(x) = \int d^3p\ p^0 u^i f(x,p). \tag{2.6}$$

The momentum density is given by,

$$T^{i0}(x) = \int d^3p\ p^i f(x,p). \tag{2.7}$$

Similarly, the momentum flow (or the pressure tensor) which is the flow of the i^{th} component of the momentum in the j^{th} direction is given by,

$$T^{ij}(x) = \int d^3p\ p^i u^j f(x,p). \tag{2.8}$$

Combining the above equations, the energy momentum tensor can be written as,

$$T^{\mu\nu}(x) = \int \frac{d^3p}{p^0} p^\mu p^\nu f(x,p). \tag{2.9}$$

Hence, in relativistic kinetic theory, the energy-momentum tensor is defined as the second moment of the distribution function, and is thus a symmetric quantity.

2.1.3 Entropy four flow

The H-function as introduced by Boltzmann, implies that the local entropy density for a system outside equilibrium may be defined as,

$$S^0(x) = -k_{_B} \int d^3p f(x,p) \left[\log h^3 f(x,p) - 1\right] \tag{2.10}$$

where $k_{_B}$ is the Boltzmann constant. The entropy flow, corresponding to the entropy density has the form-

$$\vec{S} = -k_{_B} \int d^3p \vec{u} f(x,p) \left[\log h^3 f(x,p) - 1\right]. \tag{2.11}$$

The above two equations may be combined to get the entropy four flow

$$S^\mu(x) = -k_{_B} \int \frac{d^3p}{p^0} p^\mu f(x,p) \left[\log h^3 f(x,p) - 1\right] \tag{2.12}$$

2.1.4 Hydrodynamic four velocity

An important quantity in the description of a continuous media is the hydrodynamic four-velocity $U^\mu(x)$, which is a vector field. Hydrodynamic four velocity is a time like vector with length equal to unity in each space time point $U^\mu(x)U_\mu(x) = 1$. On differentiation of $U^\mu(x)U_\mu(x) = 1$ we get

$$U^\mu(x)\partial_\nu U_\mu(x) = 0. \tag{2.13}$$

We now define a projector, $\Delta^{\mu\nu}(x)$ with the help of hydrodynamic velocity,

$$\Delta^{\mu\nu}(x) = g^{\mu\nu} - U^\mu U^\nu \tag{2.14}$$

$g^{\mu\nu} = (1, -1, -1, -1)$ is a metric tensor. If $\Delta^{\mu\nu}(x)$ is contracted with an arbitrary four vector, it acts as a projector since it annihilates the part of the four vector which is parallel to U^μ,

$$\Delta^{\mu\nu}(x)U_\nu(x) = 0. \tag{2.15}$$

Some properties of the projector $\Delta^{\mu\nu}(x)$ are as follows -

$$\Delta^{\mu\nu} = \Delta^{\nu\mu} \tag{2.16}$$

$$\Delta^{\mu\nu}\Delta_{\nu\sigma} = \Delta^\mu_\sigma \tag{2.17}$$

$$\Delta^\mu_\mu = 3. \tag{2.18}$$

In the local rest frame $U^\mu_{LR} = (1, 0, 0, 0)$. The two mainly used definitions of hydrodynamic velocity in the literature are the Eckart's definition of hydrodynamic velocity and the Landau and Lifshitz's definition of

hydrodynamic velocity.

Eckart relates the hydrodynamic velocity directly to the particle four flow N^μ by relation $U^\mu = \frac{N^\mu}{\sqrt{N^\nu N_\nu}}$. Using this definition of U^μ we get $\Delta^{\mu\nu} N_\nu = 0$, which thus implies that in the local rest frame the spatial components of the particle four flow N^μ vanishes $N^i_{LR} = 0$. The hydrodynamic velocity as defined by Eckart is the mean particle velocity.

Landau and Lifshitz's definition of hydrodynamic velocity $U^\mu = \frac{T^{\mu\nu} U_\nu}{\sqrt{U_\rho T^{\rho\sigma} T_{\sigma\tau} U^\tau}}$ is related to the flow of energy. Using this definition of U^μ we find $\Delta^{\mu\nu} T_{\nu\sigma} U^\sigma = 0$, which shows that in the local rest frame associated with the Landau and Lifshitz's velocity the momentum density and the energy flow vanish $T^{i0}_{LR} = T^{0i}_{LR} = 0$.

2.1.5 Thermodynamic quantities

With the help of hydrodynamic four velocity $U^\mu(x)$ one may define the relevant macroscopic quantities, namely the particle density, the energy density, the heat flow, the pressure tensor and the entropy density, in a covariant manner.

The scalar quantity particle density is defined as

$$n = N^\mu U_\mu \tag{2.19}$$

where N^μ is the particle four-flow. In the local rest frame $n = N^0_{LR}$, which implies that n is the density of the particles with respect to this frame.

The scalar energy density is defined as

$$en = U_\mu T^{\mu\nu} U_\nu \tag{2.20}$$

where e is the energy per particle. In the local rest frame $en = T_{LR}$, implies that en is the energy density of the particles with respect to this frame.

The heat flow is defined as the difference of the energy flow and the flow of enthalpy h carried by the particles

$$I^\mu_q = \left(U_\nu T^{\nu\mu} - hN^\sigma\right) \Delta^\mu_\sigma. \tag{2.21}$$

The enthalpy or heat function per particle is $h = e + pn^{-1}$, where p is the local hydrostatic pressure. In the local rest frame the heat flow has spatial components only i.e. $I^0_{qLR} = 0$ and $I^i_{qLR} = T^{0i}_{LR} - hN^i_{LR}$.

The pressure tensor is defined as

$$P^{\mu\nu} = \Delta^\mu_\sigma T^{\sigma\tau} \Delta^\nu_\tau. \tag{2.22}$$

The pressure tensor contains a reversible part and an irreversible part according to the splitting

$$P^{\mu\nu} = -p\Delta^{\mu\nu} + \Pi^{\mu\nu} \tag{2.23}$$

where $\Pi^{\mu\nu}$ is the viscous pressure tensor.

The scalar entropy density is defined as

$$sn = S^{\mu}U_{\mu} \tag{2.24}$$

where S^{μ} is the entropy four-flow and s is the entropy per particle. In the local rest frame $sn = S^{0}_{LR}$, which implies that sn is the local entropy density in the local rest frame.

2.2 Relativistic Boltzmann Transport Equation

The distribution function which is used to define the macroscopic quantities satisfies an integro-differential equation widely known as Boltzmann transport equation(BTE). This equation is used to study the statistical behaviour of a system consisting of a large number of particles. It deals with the study of microscopic description of the gas given by one particle distribution function. It gives the rate of change of distribution function in space and time brought in by the collisions or interaction among the particles. The distribution function is the solution of the BTE and it can be used to obtain the macroscopic quantities governing the fluid behaviour. In order to derive the relativistic BTE following assumptions are considered-

1. Only binary collisions among the constituents are taken, implying that the fluid under consideration is dilute.

2. We take into account the hypothesis of molecular chaos. As a consequence, particle correlation before each individual collision is neglected. The number of binary collisions is proportional to the product of the distribution function of the colliding particles.

3. The distribution function varies slowly in space and time. The time variation of the distribution function is only allowed over time scales larger than the collision time and the spatial variation over distances larger than the mean free path of the collision.

2.2.1 BTE for systems without collision

In the particle four flow, $N^{\mu}(x) = \int \frac{d^3p}{p^0} p^{\mu} f(x,p)$ we introduce a scalar quantity $\Delta N(x)$, which is given by

$$\Delta N(x) = \int_{\Delta^3\sigma} d^3\sigma_{\mu} N^{\mu}(x) \tag{2.25}$$

where $d^3\sigma_\mu = (dxdydz, dtdydz, dtdxdz, dtdxdy)$ is a hyper surface. Using $N^\mu(x)$ in Eq. (2.25) we get,

$$\Delta N(x) = \int_{\Delta^3\sigma} \int d^3\sigma_\mu \frac{d^3p}{p^0} p^\mu f(x,p). \tag{2.26}$$

In the lorentz frame, $d^3\sigma_\mu$ is a purely time like quantity i.e. $d^3\sigma_\mu = \left(d^3x, 0, 0, 0\right)$. Thus we get,

$$\Delta N(x) = \int_{\Delta^3 x} \int d^3x d^3p f(x,p) \tag{2.27}$$

$\Delta N(x)$ is the number of particles present in the element $\Delta^3(x)$. It can also be considered as the number of world lines crossing the segment $\Delta^3\sigma$ with momenta in the range $\Delta^3 p$ around p and is given as-

$$\int_{\Delta^3\sigma'} \int_{\Delta^3 p} d^3\sigma_\mu \frac{d^3p}{p^0} p^\mu f(x,p) - \int_{\Delta^3\sigma} \int_{\Delta^3 p} d^3\sigma_\mu \frac{d^3p}{p^0} p^\mu f(x,p) = 0. \tag{2.28}$$

Let us consider a closed region enclosed by the surface elements $\Delta^3\sigma$, $\Delta^3\sigma'$ and the surface of the tube formed by the world lines considered. For a system without collision no world lines crosses the tube like surface. Thus, the net flow through the surface $\Delta^3\sigma$ of the Minkowski-space element $\Delta^4 x$ vanishes. Hence,

$$\int_{\Delta^3\sigma} \int_{\Delta^3 p} d^3\sigma_\mu \frac{d^3p}{p^0} p^\mu f(x,p) = 0. \tag{2.29}$$

Using Gauss' theorem we obtain

$$\int_{\Delta^4 x} \int_{\Delta^3 p} d^4x \frac{d^3p}{p^0} p^\mu \partial_\mu f(x,p) = 0. \tag{2.30}$$

Since the intervals $\Delta^4 x$ and $\Delta^3 p$ are arbitrary, it follows that

$$p^\mu \partial_\mu f(x,p) = 0. \tag{2.31}$$

This is the relativistic transport equation for the case without collisions which can also be written as,

$$\left(\partial_t + \vec{u} \cdot \vec{\nabla}\right) f(x,p) = 0 \tag{2.32}$$

where $\vec{u} = \frac{\vec{p}}{p^0}$.

2.2.2 BTE for systems with collisions

In order to obtain the full transport equation collisions among the constituents should be taken into account. Due to the collision, the momenta of the particle changes, as a result of which the number of particles crossing the segment $\Delta^3\sigma$ and $\Delta^3\sigma'$ will be different unlike the case without collisions. The amount by which the

number of particles in the ranges Δ^4x and Δ^3p changes is given by

$$\Delta^4 x \frac{\Delta^3 p}{p^0} C(x,p) \tag{2.33}$$

where $C(x,p)$ is an invariant function which is to be determined. To determine the form of $C(x,p)$, let us consider a collision between two particles with initial four momentum p^μ and k^μ which after collision attains the four momentum p'^μ and k'^μ. The average number of such collision in a Minkowski-space element Δ^4x around x, i.e. in a time interval Δt around t and a volume element Δ^3x around x, is proportional to:

1. The average number of particles per unit volume with three momentum in the range $(\vec{p}, \vec{p}+\Delta\vec{p})$ i.e. $\Delta^3 p\ f(x,p)$.

2. The average number of particles per unit volume with three momentum in the range $\left(\vec{k}, \vec{k}+\Delta\vec{k}\right)$ i.e. $\Delta^3 k\ f\left(x,k\right)$.

3. The intervals Δ^3p' and Δ^3k' and Δ^4x.

The proportionality term is given by $\frac{W(p,k|p',k')}{p^0k^0p'k'}$. The quanity $W\left(p,k \mid p',k'\right)$ is called the transition rate. The average number of particles in the range Δ^4x with momentum in the range Δ^3p which are lost through collisions is given by-

$$\frac{1}{2}\Delta^4x\Delta^3p \int \frac{d^3k}{k^0}\frac{d^3p'}{p'^0}\frac{d^3k'}{k'^0} f(x,p) f\left(x,k\right) W\left(p,k \mid p',k'\right). \tag{2.34}$$

A factor of $\frac{1}{2}$ is added because of the fact that a final state with momenta (p',k') can not be distinguished from (k',p'). Similarly, the gain in average number of particles in the range Δ^4x with momenta in the range Δ^3p through collisions is-

$$\frac{1}{2}\Delta^4x\Delta^3p \int \frac{d^3k}{k^0}\frac{d^3p'}{p'^0}\frac{d^3k'}{k'^0} f\left(x,p'\right) f\left(x,k'\right) W\left(p',k' \mid p,k\right). \tag{2.35}$$

Thus, the net change in the number of particles in range Δ^4x and Δ^3p is given by

$$\frac{1}{2}\Delta^4x\Delta^3p \int \frac{d^3k}{k^0}\frac{d^3p'}{p'^0}\frac{d^3k'}{k'^0} \left[f\left(x,p'\right) f\left(x,k'\right) W\left(p',k' \mid p,k\right) - f(x,p) f\left(x,k\right) W\left(p,k \mid p',k'\right)\right]. \tag{2.36}$$

Comparing Eqs. (2.33) and (2.36) and using the principle of detailed balancing $W\left(p',k' \mid p,k\right) = W\left(p,k \mid p',k'\right)$ we obtain

$$C(x,p) = \frac{1}{2}\int \frac{d^3k}{k^0}\frac{d^3p'}{p'^0}\frac{d^3k'}{k'^0} \left[f\left(x,p'\right) f\left(x,k'\right) - f(x,p) f\left(x,k\right)\right]\ W\left(p,k \mid p',k'\right). \tag{2.37}$$

Since we are taking collisions into account, Eq. (2.30) can be written for the case with collisions as

$$\int_{\Delta^4 x}\int_{\Delta^3 p} d^4x \frac{d^3p}{p^0} p^\mu \partial_\mu f(x,p) = \Delta^4 x \frac{\Delta^3 p}{p^0} C(x,p). \tag{2.38}$$

Since the intervals $\Delta^4 x$ and $\Delta^3 p$ are arbitrary we obtain,

$$p^\mu \partial_\mu f(x,p) = C(x,p) \tag{2.39}$$

or using the expression for $C(x,p)$ we can write the above expression as follows

$$p^\mu \partial_\mu f(x,p) = \frac{1}{2}\int \frac{d^3k}{k^0}\frac{d^3p'}{p'^0}\frac{d^3k'}{k'^0}\left[f\left(x,p'\right) f\left(x,k'\right) - f(x,p) f\left(x,k\right)\right]\; W\left(p,k \mid p',k'\right) \tag{2.40}$$

which is the required single particle relativistic transport equation when collisions are taken into consideration.

For a multicomponent system, each component $k = 1,2,3,...N$ is described by separate distribution function $f_k(x,p)$. We now aim to write the relativisitic Boltzmann transport equation for a multiparticle system. A binary collision of the form $p_k + p_l \longrightarrow p'_k + p'_l$ will satifsy the following transport equation-

$$p_k^\mu \partial_\mu f_k(x,p) \;=\; \sum_{l=1}^{N} \frac{g_l}{1+\delta_{kl}}\; C_{kl}[f_k] \tag{2.41}$$

where g_l is the degeneracy of the l^{th} particle. The collision term on the right hand side is given as-

$$C_{kl}[f_k] \;=\; \int \frac{d^3p_l}{(2\pi)^3 p_l^0}\frac{d^3p'_k}{(2\pi)^3 p'^0_k}\frac{d^3p'_l}{(2\pi)^3 p'^0_l}\left[f_k(x,p'_k) f_l(x,p'_l) \;-\; f_k(x,p_k) f_l(x,p_l)\right] W\left(p_k,p_l \mid p'_k,p'_l\right). \tag{2.42}$$

for collisions considering Maxwell-Boltzmann statistics and for collisions involving Fermi-Dirac and Bose-Einstein statistics C_{kl} is given as

$$\begin{aligned} C_{kl}[f_k] \;=\; \int \frac{d^3p_l}{(2\pi)^3 p_l^0}\frac{d^3p'_k}{(2\pi)^3 p'^0_k}\frac{d^3p'_l}{(2\pi)^3 p'^0_l}\; & \left[f_k(x,p'_k) f_l(x,p'_l)\{1 \pm f_k(x,p_k)\}\{1 \pm f_l(x,p_l)\}\right. \\ & \left. - f_k(x,p_k) f_l(x,p_l)\{1 \pm f_k(x,p'_k)\}\{1 \pm f_l(x,p'_l)\}\right] W\left(p_k,p_l \mid p'_k,p'_l\right). \end{aligned} \tag{2.43}$$

where the $\pm$ sign in the above equation denotes Bose enhancement and Pauli blocking.

2.2.3 BTE in presence of background magnetic field

The BTE in presence of external force field is valid if the deviations caused by this external force in the particle trajectories during the collision is small. First, we shall derive the transport equation subject to external force field for the collisionless case. In presence of external force field $F^\mu(x,p)$ the particle momenta p^μ will be modified to $p^\mu + F^\mu \Delta\tau$ while travelling from the surface element $\Delta^3\sigma$ to $\Delta^3\sigma'$ in the proper time

interval $\Delta\tau$. Thus, Eq. (2.28) will be modified to

$$\int_{\Delta^3\sigma'}\int_{\Delta^3 p} d^3\sigma_\mu \frac{d^3p}{p^0} p^\mu f(x,p+F\Delta\tau) - \int_{\Delta^3\sigma}\int_{\Delta^3 p} d^3\sigma_\mu \frac{d^3p}{p^0} p^\mu f(x,p) = 0. \tag{2.44}$$

The four volume $\Delta^4 x$ enclosed by the surface element $\Delta^3\sigma$, $\Delta^3\sigma'$ and the surface of the tube formed by these surface elements is given by -

$$\Delta^4 x = \Delta\tau \frac{p^\mu}{m} \int_{\Delta^3\sigma} d^3\sigma_\mu \tag{2.45}$$

Making use of Taylor series expansion of $f(x,p+F\Delta\tau)$, Eq. (2.45), and Gauss's theorem Eq. (2.44) we obtain-

$$\int_{\Delta^4 x}\int_{\Delta^3 p} d^4x \frac{d^3p}{p^0}\left[p^\mu\partial_\mu + mF^\mu(x,p)\frac{\partial}{\partial p^\mu}\right] f(x,p) = 0. \tag{2.46}$$

Since the intervals $\Delta^4 x$ and $\Delta^3 p$ are arbitrary we obtain

$$p^\mu\partial_\mu f(x,p) + mF^\mu(x,p)\frac{\partial}{\partial p^\mu} f(x,p) = 0. \tag{2.47}$$

For the BTE in presence of external force field with collisions we have

$$p^\mu\partial_\mu f(x,p) + mF^\mu(x,p)\frac{\partial}{\partial p^\mu} f(x,p) = C(x,p) \tag{2.48}$$

with collision term as given in Eqs. (2.42) and (2.43).

In the derivation of transport equation in presence of external field we have assumed that the external force is mechanical and hence it does not change the rest mass of the particle i.e. we have

$$p^\mu F_\mu(x,p) = 0. \tag{2.49}$$

Also, we consider that upto first order in $\Delta\tau$, the momentum range is invariant as a result of which force $F^\mu(x,p)$ satisfies

$$\frac{\partial F^\mu(x,p)}{\partial p^\mu} = 0 \tag{2.50}$$

Eqs. (2.49) and (2.50) are satisfied by the Lorentz force

$$F^\mu(x,p) = \frac{q}{m} p_\nu F^{\mu\nu}(x) \tag{2.51}$$

where q is the charge of the positive particle and $F^{\mu\nu}$ is the antisymmetric electromagnetic tensor. The components $F^{0i} = E^i$ and $F^{ij} = B^k$ $(i,j,k = x,y,z:$ cyclic) where $\vec{E}$ and $\vec{B}$ are respectively the electric

and magnetic field vectors. Using Eq. (2.51) in Eq. (2.48) we obtain

$$p^{\mu}\partial_{\mu}f(x,p) + q\ p_{\nu}F^{\mu\nu}(x)\frac{\partial}{\partial p^{\mu}}f(x,p) = C(x,p) \tag{2.52}$$

2.3 Conservation laws

The macroscopic quantities that describe a relativistic system outside equilibrium obey equations which follow from the conservation laws of particle number and energy-momentum. In the framework of a kinetic theory the conservation laws can be derived from the corresponding laws valid at the microscopic level. It can be proved that the production of entropy is always greater than or equal to zero. In kinetic theory this is known as the H-theorem, originally due to Boltzmann. Equilibrium is then defined as the state in which there is no entropy production.

2.3.1 Conservation Equations

Let us consider a dilute mixture of N-components interacting via elastic and inelastic collisions. The total number of particles are assumed to be conserved during the collision. The distribution function of each component given by $f_k(x,p_k)$ $(k = 1,2,...N)$ satisfies the following set of BTE -

$$p_k^{\mu}\partial_{\mu}f_k\left(x,p_k\right) = \sum_{l=1}^{N} C_{kl}\left(x,p_k\right) \tag{2.53}$$

where the collsion term for the reaction of type k and l species colliding and forming i and j species, $k + l \longrightarrow i + j$ is given as

$$C_{kl} = \frac{1}{2}\sum_{i,j=1}^{N}\int \frac{d^3p_l}{p_l^0}\frac{d^3p_i}{p_i^0}\frac{d^3p_j}{p_j^0}\left(f_i f_j W_{ij|kl} - f_k f_l W_{kl|ij}\right) \tag{2.54}$$

As a consequence of the microscopic conservation laws obeyed by various reactions, the collision term in Eq. (2.54) possess the following property-

$$\sum_{k,l=1}^{N}\int \frac{d^3p_k}{p_k^0}\ \psi_k\left(x,p_k\right)C_{kl}\left(x,p_k\right) = 0 \tag{2.55}$$

where,

$$\psi_k\left(x,p_k\right) = a_k(x) + b_{\mu}(x)p_k^{\mu}. \tag{2.56}$$

The space-time dependent function $a_k(x)$ and $b_{\mu}(x)$ satisfies

$$a_k(x) + a_l(x) = a_i(x) + a_j(x). \tag{2.57}$$

In order to prove Eq. (2.55), we substitute Eqs. (2.56) and (2.57) on the L.H.S. of Eq. (2.55)

$$\frac{1}{2}\sum_{i,j,k,l}\int \frac{d^3p_i}{p_i^0}\frac{d^3p_l}{p_l^0}\frac{d^3p_i}{p_i^0}\frac{d^3p_j}{p_j^0}\psi_k\left(f_if_jW_{ij|kl}-f_kf_lW_{kl|ij}\right) \tag{2.58}$$

Now interchanging the variables, $i \longleftrightarrow k$ and $j \longleftrightarrow l$ we obtain

$$\frac{1}{2}\sum_{i,j,k,l}\int \frac{d^3p_i}{p_i^0}\frac{d^3p_l}{p_l^0}\frac{d^3p_i}{p_i^0}\frac{d^3p_j}{p_j^0}\left[\psi_k-\psi_i\right]f_if_jW_{ij|kl} \tag{2.59}$$

Similarly on interchanging the variables, $i \longleftrightarrow j$ and $k \longleftrightarrow l$ we obtain

$$\frac{1}{2}\sum_{i,j,k,l}\int \frac{d^3p_i}{p_i^0}\frac{d^3p_l}{p_l^0}\frac{d^3p_i}{p_i^0}\frac{d^3p_j}{p_j^0}\left[\psi_l-\psi_j\right]f_if_jW_{ij|kl}. \tag{2.60}$$

On adding Eqs. (2.59) and (2.60) we obtain

$$\frac{1}{4}\sum_{i,j,k,l}\int \frac{d^3p_i}{p_i^0}\frac{d^3p_l}{p_l^0}\frac{d^3p_i}{p_i^0}\frac{d^3p_j}{p_j^0}\left[\psi_k+\psi_l-\psi_i-\psi_j\right]f_if_jW_{ij|kl}. \tag{2.61}$$

Using Eq. (2.56) and the conservation of energy and momentum ($p_k^\mu + p_l^\mu = p_i^\mu + p_j^\mu$) in the above equation we get

$$\psi_k+\psi_l-\psi_i-\psi_j=0. \tag{2.62}$$

Substituting Eq. (2.62) in Eq. (2.61) we obtain,

$$\sum_{k,l=1}^{N}\int \frac{d^3p_k}{p_k^0}\psi_k\left(x,p_k\right)C_{kl}\left(x,p_k\right)=0 \tag{2.63}$$

2.3.2 Conservation of particle number

Substituting $b^\mu(x)=0$ and $a_k(x)=a(x)$

$$\sum_{k,l=1}^{N}\int \frac{d^3p_k}{p_k^0}a(x)C_{kl}\left(x,p_k\right)=0 \tag{2.64}$$

Since $a(x)$ is arbitrary, above equation can be written as,

$$\sum_{k,l=1}^{N}\int \frac{d^3p_k}{p_k^0}C_{kl}\left(x,p_k\right)=0. \tag{2.65}$$

Making use of Eq. (2.53) in the above equation we get

$$\sum_{k=1}^{N}\int \frac{d^3p_k}{p_k^0}\,p_k^\mu\,\partial_\mu f_k\left(x,p_k\right)=0. \tag{2.66}$$

Thus we have,

$$\partial_\mu \sum_{k=1}^{N} \int \frac{d^3p_k}{p_k^0} p_k^\mu f_k\left(x, p_k\right) = 0. \tag{2.67}$$

Making use of particle four flow for each component we get

$$\partial_\mu \sum_{k=1}^{N} N_k^\mu = \partial_\mu N^\mu = 0. \tag{2.68}$$

Eq. (2.68) represents the particle number conservation in the system. Apart from the particle number, the system may possess some other conserved intrinsic quantum numbers like lepton number or baryon number. The form for such a conservation law is given as

$$q_k + q_l = q_i + q_j. \tag{2.69}$$

Substituting $a_k(x) = q_k a(x)$ and $b^\mu(x) = 0$ in Eq. (2.56)and then making use of Eq. (2.53)we get

$$\partial_\mu \sum_{k=1}^{N} \left[q_k \int \frac{d^3p_k}{p_k^0} p_k^\mu f_k\left(x, p_k\right) \right] = 0. \tag{2.70}$$

Again, making use of particle four flow we get

$$\partial_\mu \sum_{k}^{N} q_k N_k^\mu = \partial_\mu J^\mu = 0 \tag{2.71}$$

where the current $J^\mu = \sum_k^N q_k N_k^\mu$. This shows that any conserved quantum number implies the existence of a conserved macroscopic current.

2.3.3 Conservation of Energy and Momentum

Substituting $a_k(x) = 0$ in Eq. (2.56) we get

$$\sum_{k,l=1}^{N} \int \frac{d^3p}{p_k^0} p_k^\mu C_{kl}\left(x, p_k\right) = 0 \tag{2.72}$$

Using Eq. (2.53) in the above equation we get

$$\partial_\mu \sum_{k=1}^{N} \int \frac{d^3p_k}{p_k^0} p_k^\mu p_k^\nu f_k\left(x, p_k\right) = 0 \tag{2.73}$$

Applying Eq. (2.9) in the above equation we get

$$\partial_\mu \sum_{k=1}^{N} T_k^{\mu\nu} = \partial_\mu T^{\mu\nu} = 0. \tag{2.74}$$

Eq. (2.74) expresses the conservation of energy for $\mu = 0$ and for $\mu = 1, 2, 3$ it expresses the conservation of momentum.

2.4 Equations of motion of fluids and H-theorem

The equation of motion of fluids can be derived from the conservation of particle number and conservation of energy and momentum. These equations give the rate of change of particle densities, hydrodynamic four velocity and the energy density.

2.4.1 Time derivative and gradient

The time-space derivative ∂^μ is decomposed into time derivative and space derivative in the rest frame using the hydrodynamic velocity. The four derivative is hence given as -

$$\begin{aligned} \partial^\mu &= U^\mu U^\nu \partial_\nu + \left(g^{\mu\nu} - U^\mu U^\nu\right) \partial_\nu \\ &= U^\mu D + \nabla^\mu \end{aligned} \tag{2.75}$$

where

$$D = U^\nu \partial_\nu, \qquad \nabla^\mu = \Delta^{\mu\nu} \partial_\nu \tag{2.76}$$

In addition to the convective time derivative D, let us introduce the concept of substantial time derivative $\mathscr{D}$ as

$$\mathscr{D} = nD + N^\mu \Delta_\mu. \tag{2.77}$$

In Eckart's frame $N^\mu \nabla_\mu = 0$, thus in this frame Eq. (2.77) reduces to

$$\mathscr{D} = nD \tag{2.78}$$

while in Landau's frame $I_q^\mu = -h\Delta^{\mu\nu} N_\nu$, as a consequence of which in this frame Eq. (2.77) reduces to

$$\mathscr{D} = nD - h^{-1} I_q^\nu \partial_\nu \tag{2.79}$$

2.4.2 Equations of Continuity

The particle four flow N^μ can be decomposed into a component parallel to and perpendicular to the hydrodynamic velocity. Thus

$$N^\mu = U^\mu U^\nu N_\nu + \left(g^{\mu\nu} - U^\mu U^\nu\right) N_\nu = nU^\mu + V^\mu \tag{2.80}$$

where

$$V^\mu = \Delta^{\mu\nu} N_\nu. \tag{2.81}$$

Using Eq. (2.80) in the particle number conservation equation $\partial_\mu N^\mu = 0$ we get

$$U_\mu U^\alpha \partial_\alpha (nU\mu) + U_\mu U^\alpha \partial_\alpha V^\mu + \Delta_{\mu\alpha}\partial^\alpha (nU^\mu) + \nabla_\mu V^\mu = 0. \tag{2.82}$$

Substituting $U_\mu V^\mu = 0, U^\mu \Delta\mu\alpha = 0$ and $U_\mu \partial_\alpha U^\mu = 0$ in the above equation we obtain

$$Dn = -n\nabla_\mu U^\mu - \nabla_\mu V^\mu + V_\mu DU^\mu \tag{2.83}$$

This is the required equation of continuity.

2.4.3 Equation of Motion

Equation of motion can be derived from the conservation of energy momentum tensor. Since it should only involve the space part of the energy momentum tensor we contract $\partial_\mu T^{\mu\nu} = 0$ with the projector operator. We thus get

$$\Delta^\mu_\nu \partial_\sigma T^{\nu\sigma} = 0 \tag{2.84}$$

The heat flow I^μ_q is given by

$$I^\mu_q = U_\nu T^{\nu\sigma}\Delta^\mu_\sigma - hV^\mu \tag{2.85}$$

$$U_\nu T^{\nu\sigma}\Delta^\mu_\sigma = I^\mu_q + hV^\mu = W^\mu \tag{2.86}$$

where the quantity W^μ introduced above is orthogonal to U_μ. The energy momentum tensor in terms of W^μ can be written as

$$T^{\mu\nu} = enU^\mu U^\nu - p\Delta^{\mu\nu} + W^\mu U^\nu + W^\nu U^\mu + \Pi^{\mu\nu}. \tag{2.87}$$

Using Eq. (2.87) and equations $U_\sigma \Pi^{\mu\sigma} = 0, U_\nu \partial_\sigma U^\nu = 0$, $W^\mu U_\mu = 0$ and $h = e + pn^{-1}$ in Eq. (2.84) we obtain

$$hnDU^\mu = \nabla^\mu p - \Delta^\mu_\nu \nabla_\sigma \Pi^{\nu\sigma} + \Pi^{\mu\nu} DU_\nu - \Delta^\mu_\nu DW^\nu - W^\mu \nabla_\nu U^\nu - W^\nu \nabla_\nu U^\mu \tag{2.88}$$

This is the required equation of motion.

If the quantities $\Pi^{\mu\nu}$ and W^{μ} are ignored, the equation of motion reduces to the zeroth order form

$$DU^{\mu} = \frac{1}{nh}\nabla^{\mu}p. \tag{2.89}$$

valid for perfect fluids.

In Eckart's frame, $V^{\mu} = 0$, and hence $W^{\mu} = I_q^{\mu}$. So using these in Eq. (2.88) we get

$$hnDU^{\mu} = \nabla^{\mu}p - \Delta^{\mu}_{\nu}\nabla_{\sigma}\Pi^{\nu\sigma} + \frac{1}{nh}\Pi^{\mu\nu}\nabla_{\nu}p - \left[\Delta^{\mu}_{\nu}DI_q^{\nu} + T_q^{\mu}\nabla_{\nu}U^{\nu} + T_q^{\nu}\nabla_{\nu}U^{\mu}\right] \tag{2.90}$$

However, in Landau's frame, $W^{\mu} = U^{\nu}T_{\nu\sigma}\Delta^{\mu\sigma} = 0$. So using $W^{\mu} = 0$ in Eq. (2.88), equation of motion in Landau's frame is given by

$$hnDU^{\mu} = \nabla^{\mu}p - \Delta^{\mu}_{\nu}\nabla_{\sigma}\Pi^{\nu\sigma} + \Pi^{\mu\nu}DU_{\nu}. \tag{2.91}$$

Again, if the quantities $\Pi^{\mu\nu}$ and W^{μ} are ignored in Eqs. (2.90) and (2.91), the equation of motion reduces to the zeroth order form as obtained in Eq. (2.89).

2.4.4 Equation of energy

Equation of energy can be derived from the conservation of energy momentum tensor. Since the equation of energy should only involve the time part of the energy momentum tensor we contract $\partial_{\nu}T^{\mu\nu} = 0$ with the hydrodynamic velocity U_{μ}

$$U_{\mu}\partial_{\nu}T^{\mu\nu} = 0. \tag{2.92}$$

Using Eq. (2.87) and equations $W^{\mu}U_{\mu} = 0,\ \Pi^{\mu\nu}U_{\nu} = 0, D = U^{\mu}\partial_{\mu},\ \nabla^{\mu} = \Delta^{\mu\nu}\partial_{\nu}$ in the above equation we get

$$D(en) = -nh\nabla_{\mu}U^{\mu} + \Pi^{\mu\nu}\nabla_{\nu}U_{\mu} - \nabla_{\mu}W^{\mu} + 2W^{\mu}DU_{\mu} \tag{2.93}$$

Using the equation of continuity given in Eq. (2.83) in the above equation we obtain

$$nDe = -p\nabla_{\mu}U^{\mu} + \Pi^{\mu\nu}\nabla_{\nu}U_{\mu} - \nabla_{\mu}W^{\mu} + e\nabla_{\mu}V^{\mu} + (2W^{\mu} - eV^{\mu})\,DU_{\mu}. \tag{2.94}$$

This equation gives the rate of change of energy per particle.

If we omit the quantities $\Pi^{\mu\nu}$ and W^{μ} we get

$$nDe = -p\partial_{\mu}U^{\mu} \tag{2.95}$$

which is the relativistic Euler or zeroth order equation of energy valid for perfect fluids.

If we choose the Eckart's frame then, $V^\mu = 0$, hence $W^\mu = I_q^\mu$. Equation of energy in Eckart's frame can thus be written as

$$nDe = -p\nabla_\mu U^\mu + \Pi^{\mu\nu}\nabla_\nu U_\mu - \nabla_\mu I_q^\mu + 2I_q^\mu DU_\mu. \tag{2.96}$$

In landau's frame $W^\mu = 0$, hence $I_q^\mu = -hV^\mu$, thus the equation of energy can be written as

$$nDe = -p\nabla_\mu U^\mu + \Pi^{\mu\nu}\nabla_\nu U_\mu - e\nabla_\mu \left(h^{-1} I_q^\mu\right) + eh^{-1} I_q^\mu DU_\mu. \tag{2.97}$$

2.4.5 First law of thermodynamics

The first law of thermodynamics is an energy law which relates the change of energy to the work term and a heat term. Thus, the first law of thermodynamics is the equation which relates the quantity $De + pDn^{-1}$ to the other relevant local quantities. We already have an expression for De from Eq. (2.94) and the quantity nDn^{-1} can be calculated from equation of continuity i.e. Eq. (2.83). Thus, nDn^{-1} is obtained to be

$$nDn^{-1} = -\frac{1}{n}\left[-n\nabla_\mu U^\mu - \nabla_\mu V^\mu + V_\mu DU^\mu\right] \tag{2.98}$$

Thus using Eqs. (2.94) and (2.98) we obtain

$$n\left(De + pdn^{-1}\right) = \Pi^{\mu\nu}\nabla_\nu U_\mu - \nabla_\mu I_q^\mu - v^\mu \nabla_\mu h + \left(2I_q^\mu + hV^\mu\right) DU_\mu. \tag{2.99}$$

which is the relativistic first law of thermodynamics. In the absence of transport quantities Eq. (2.99) reduces to

$$De + pDn^{-1} = 0 \tag{2.100}$$

which has the usual appearance of the first law of thermodynamics for systems which are adiabaticaly insulated from their surroundings. In Eckart's frame, $V^\mu = 0$, $W^\mu = I_q^\mu$ hence the first law of thermodynamics reduces to

$$n\left(De + pDn^{-1}\right) = \Pi^{\mu\nu}\nabla_\nu U_\mu - \nabla_\mu I_q^\mu + 2I_q^\mu DU_\mu. \tag{2.101}$$

In Landau's frame, $W^\mu = 0$, $V^\mu = -h^{-1} I_q^\mu$, thus the first law of thermodynamics in this frame reduces to

$$n\left(De + pDn^{-1}\right) = \Pi^{\mu\nu}\nabla_\nu U_\mu - \nabla_\mu I_q^\mu + h^{-1} I_q^\mu \nabla_\mu h + I_q^\mu DU_\mu. \tag{2.102}$$

Substituting Eqs. (2.77) and (2.89) in Eq. (2.99) we obtain

$$\mathscr{D}e + p\mathscr{D}n^{-1} = \Pi^{\mu\mu}\nabla_\nu U_\mu - \nabla_\mu I_q^\mu + 2(nh)^{-1} I_q^\mu \nabla_\mu p. \tag{2.103}$$

The term $\mathscr{D}e$ is the change of energy, $p\mathscr{D}n^{-1}$ is the work done due to local pressure, $\Pi^{\mu\nu}\nabla_\nu U_\mu$ is the work done due to viscous pressure, $-\nabla_\mu I_q^\mu$ is the heat term with divergence of heat flow and the term $2(nh)^{-1}I_q^\mu\nabla_\mu p$ is the purely relativistic term involving the pressure gradient.

2.4.6 H-theorem

The local entropy production is given by-

$$\sigma_s(x) = \partial_\mu S^\mu(x). \tag{2.104}$$

Substituting Eq. (2.12) in the above equation we obtain

$$\sigma_s = -k_B \int \frac{d^3p}{p^0}\left[\log h^3 f(x,p)\right] p^\mu \partial_\mu f(x,p) \tag{2.105}$$

For the reactive mixture we have

$$\sigma_s = -k_B \sum_{k=1}^{N} \int \frac{d^3p_k}{p^0}\left[\log h^3 f_k(x,p)\right] p_k^\mu \partial_\mu f_k(x,p). \tag{2.106}$$

Using Eq. (2.53) in the above equation we obtain

$$\sigma_s = -k_B \sum_{k,l} \int \frac{d^3p_k}{p^0}\left[\log\mathrm{h}^3\, f_k(x,p)\right] C_{kl} \tag{2.107}$$

$$= -k_B \mathcal{F}\left[\log\mathrm{h}^3\, f_k\right]. \tag{2.108}$$

Using the form for $\mathcal{F}$ from Eq. (2.61) in the above equation we obtain

$$\sigma_s = -\frac{1}{4}\sum_{ijkl}\int \frac{d^3p_i}{p_i^0}\frac{d^3p_j}{p_j^0}\frac{d^3p_k}{p_k^0}\frac{d^3p_l}{p_l^0}\left[\log\frac{f_k f_l}{f_i f_j}\right] f_i f_j W_{ij|kl}. \tag{2.109}$$

We now assume that the transition rate satisfies

$$\sum_{ij}\int \frac{d^3p_i}{p_i^0}\frac{d^3p_j}{p_j^0} W_{kl|ij} = \sum_{ij}\int \frac{d^3p_i}{p_i^0}\frac{d^3p_j}{p_j^0} W_{ij|kl} \tag{2.110}$$

Multiplying both sides by $\frac{f_k f_l}{p_k^0 p_l^0}$ and integrating over p_k and p_l we obtain

$$\sum_{ijkl}\int \frac{d^3p_i}{p_i^0}\frac{d^3p_j}{p_j^0}\frac{d^3p_k}{p_k^0}\frac{d^3p_l}{p_l^0}\left[f_k f_l W_{ij|kl} - f_k f_l W_{kl|ij}\right] = 0. \tag{2.111}$$

Interchanging $k \longleftrightarrow l$ and $i \longleftrightarrow j$ we get

$$\sum_{ijkl}\int \frac{d^3p_i}{p_i^0}\frac{d^3p_j}{p_j^0}\frac{d^3p_k}{p_k^0}\frac{d^3p_l}{p_l^0}\left[f_k f_l - f_i f_j\right] W_{ij|kl} = 0 \tag{2.112}$$

As the left hand side of the above equation equates to zero we can add it to Eq. (2.109). We thus obtain

$$\sigma_s = -\frac{1}{4}\sum_{ijkl}\int \frac{d^3p_i}{p_i^0}\frac{d^3p_j}{p_j^0}\frac{d^3p_k}{p_k^0}\frac{d^3p_l}{p_l^0}\left[\frac{f_kf_l}{f_if_j} - \log\frac{f_kf_l}{f_if_j} - 1\right] f_if_jW_{ij|kl}. \tag{2.113}$$

Let $\frac{f_kf_l}{f_if_j} = x$, we know that $x - \log x - 1 > 0$ for $x > 0$ and $x - \log x - 1 = 0$ for $x = 1$, hence

$$\sigma_s \geq 0. \tag{2.114}$$

This is the H theorem which states that the entropy production can never be negative.

2.5 First Chapman-Enskog Approximation

Experimental observation shows that many-particle systems usually approaches equilibrium in two different stages. First, the system reaches a state of equilibrium which means that its state may be specified in terms of the local density, local hydrodynamic velocity and local temperature. During the second stage the spatial non-uniformities slowly disappear and the system relaxes to complete equilibrium.

2.5.1 Chapman-Enskog Method

The Chapman-Enskog approximation aims at obtaining a solution of the transport equation valid in the last hydrodynamic stage. In this method we assume that in the hydrodynamic regime the distribution function can be expressed as a function of the hydrodynamic variables and their gradients. As in the non-relativistic theory the main interest of the Chapman-Enskog method lies in the first approximation. It yields the second law of thermodynamics outside equilibrium and explicit expressions for the transport co-efficient in terms of the particle interaction. We know that the transport equation is given by

$$p^\mu U_\mu Df = -p^\mu \nabla_\mu f + C[f,f] \tag{2.115}$$

where $C[f,f]$ is given by equation

$$C[f,f] = \frac{1}{2}\int \frac{d^3p_1}{p_1^0}\frac{d^3p_1'}{p_1^{0'}}\frac{d^3p'}{p'^0}\left(f'f_1' - ff_1\right)W\left(p'p_1' \mid pp_1\right) \tag{2.116}$$

On dividing Eq. (2.115) by mcf, both the terms on the right hand side of the equation acquires inverse length dimension. The length associated with the first term is the characteristic for the spatial non-uniformities in the system, while the second length associated with the collision term characterizes the mean free path. In the hydrodynamic regime the latter length is much smaller than the former and one may try to find a solution of the transport equation with the ratio of these lengths as an expansion parameter. This is the chapman-Enskog procedure.

Let us intoduce a parameter ϵ in the transport equation

$$p^\mu U_\mu Df = -\epsilon p^\mu \nabla_\mu f + C[f,f]. \tag{2.117}$$

The parameter ϵ measures the relative strength of the gradient and is called the non-uniformity parameter. To find the solution of Eq. (2.117) we adopt the expansions

$$f = f^{(0)} + \epsilon f^{(1)} + \epsilon^2 f^{(2)} + \ldots \tag{2.118}$$

$$Df = \epsilon (Df)^{(1)} + \epsilon^2 (Df)^{(2)} + \ldots \tag{2.119}$$

Substituing Eqs. (2.118) and (2.119) in Eq. (2.117) we get

$$p^\mu U_\mu \left[\epsilon (Df)^{(1)} + \epsilon^2 (Df)^{(2)} + \ldots\right] = -\epsilon p^\mu \nabla_\mu \left[f^{(0)} + \epsilon f^{(1)} + \epsilon^2 f^{(2)} + \ldots\right] + C[f,f]. \tag{2.120}$$

On equating the coefficients of equal powers in ϵ in the above equation, we obtain

$$C\left[f^{(0)}, f^{(0)}\right] = 0 \tag{2.121}$$

$$p^\mu U_\mu (Df)^{(1)} = -p^\mu \nabla_\mu f^{(0)} + C\left[f^{(0)}, f^{(1)}\right] + C\left[f^{(1)}, f^{(0)}\right]. \tag{2.122}$$

Thus, in general we can write

$$p^\mu U_\mu (Df)^{(r)} = -p^\mu \nabla_\mu f^{(r-1)} + \sum_{s=0}^{r} C\left[f^{(s)}, f^{(r-s)}\right] \quad r \geq 1 \tag{2.123}$$

where $f^{(0)}$ is the equilibrium distribution function and is given by

$$f^{(0)}(x,p) = \frac{1}{2\pi\hbar^3} \exp\left(\frac{\mu - p^\mu U_\mu}{k_B T}\right). \tag{2.124}$$

Let us now introduce a linearized collision operator $\mathcal{L}[\phi]$ which is given as

$$\mathcal{L}[\phi] = \frac{1}{2}\int \frac{d^3p_1}{p_1^0}\frac{d^3p'}{p'^0}\frac{d^3p_1'}{p_1'^0} f_1^{(0)} \left(\phi + \phi_1 - \phi' - \phi_1'\right) W\left(p', p_1' \mid p, p_1\right). \tag{2.125}$$

Using Eq. (2.125) we obtain

$$C\left[f^{(0)}, f^{(r)}\right] + C\left[f^{(r)}, f^{(0)}\right] = -f^{(0)} \mathcal{L}\left[\phi^{(r)}\right] \tag{2.126}$$

Making use of the above equation in Eq. (2.123) the Chapman-Enskog hierarchy becomes

$$p^\mu U_\mu (Df)^{(r)} + p^\mu \nabla_\mu f^{(r-1)} - \sum_{s=1}^{r-1} C\left[f^{(s)}, f^{(r-s)}\right] = -f^{(0)} \mathcal{L}\left[\phi^{(r)}\right] \tag{2.127}$$

We now make an assumption that

$$n = \int \frac{d^3p}{p^0} p^\mu U_\mu f = \int \frac{d^3p}{p^0} p^\mu U_\mu f(0) \tag{2.128}$$

$$ne = \int \frac{d^3p}{p^0} (p^\mu U_\mu)^2 f = \int \frac{d^3p}{p^0} (p^\mu U_\mu)^2 f^{(0)} \tag{2.129}$$

i.e. we have assumed particle density and energy density to be determined by local distribution function alone. Similarly, we make an assumption for the hydrodynmaic velocity.

In Eckart's frame

$$\Delta^{\mu\nu} N_\nu = \int \frac{d^3p}{p^0} \Delta^{\mu\nu} p_\nu f^{(0)} \tag{2.130}$$

and in Landau's frame

$$\Delta^{\mu\nu} T_{\nu\sigma} U^\sigma = \int \frac{d^3p}{p^0} \Delta^{\mu\nu} p_\nu p_\sigma U^\sigma f^{(0)} = 0. \tag{2.131}$$

Eqs. (2.128), (2.129), (2.130) and (2.131) are satisfied if we impose on the functions $f^{(r)}$ for all values of $r > 0$ the following conditions

$$\int \frac{d^3p}{p^0} p^\mu U_\mu f(r) = 0 \tag{2.132}$$

$$\int \frac{d^3p}{p^0} (p^\mu U_\mu)^2 f^{(r)} = 0 \tag{2.133}$$

$$\int \frac{d^3p}{p^0} \Delta^{\mu\nu} p_\nu f^{(r)} = 0 \tag{2.134}$$

$$\int \frac{d^3p}{p^0} \Delta^{\mu\nu} p_\nu p_\sigma U^\sigma f^{(r)} = 0 \tag{2.135}$$

2.5.2 Solubility Conditions

We will now try to find the explicit expression for $(Df)^{(r)}$. Integrating Eq. (2.117) over $\frac{d^3p}{p^0}$ and using the condition $\int \frac{d^3p}{p^0} C[f,f] = 0$ we get

$$\int \frac{d^3p}{p^0} p^\mu U_\mu Df = -\epsilon \int \frac{d^3p}{p^0} p^\mu \nabla_\mu f. \tag{2.136}$$

Using the expansions of f and Df from Eqs. (2.118) and (2.119) in Eq. (2.136) we get

$$\int \frac{d^3p}{p^0} p^\mu U_\mu (Df)^{(r)} = -\int \frac{d^3p}{p^0} p^\mu \nabla_\mu f^{(r-1)}. \tag{2.137}$$

On multiplying Eq. (2.117) with p^ν and integrating over $\frac{d^3p}{p^0}$ we obtain

$$\int \frac{d^3p}{p^0} p^\mu p^\nu U_\nu Df = -\epsilon \int \frac{d^3p}{p^0} p^\mu p^\nu \nabla_\nu f. \tag{2.138}$$

Using the expansions of f and Df from Eqs. (2.118) and (2.119) in Eq. (2.138) we get

$$\int \frac{d^3p}{p^0} p^\mu p^\nu U_\nu (Df)^{(r)} = -\int \frac{d^3p}{p^0} p^\mu p^\nu \nabla_\nu f^{(r-1)}. \tag{2.139}$$

The integral Eq. (2.123) are solvable only if equations Eqs. (2.137) and (2.139) are satisfied. Eqs. (2.137) and (2.139) are called the solubility conditions. The solubility conditions can be satisfied by assuming that the time and space dependence of the distribution function is given solely by its dependence upon the independent variables $n(x), T(x), U^\mu(x)$ and their gradients, so that

$$\begin{aligned}(Df)^{(r)} = \sum_{s=1}^{r} \left[\frac{\partial f^{(r-s)}}{\partial n} (Dn)^{(s)} \frac{\partial f^{(r-s)}}{\partial T} (DT)^{(s)} + \frac{\partial f^{(r-s)}}{\partial U^\mu} (DU^\mu)^{(s)} \right] \\ + \sum_{s=2}^{r} \left[\frac{\partial f^{(r-s)}}{\partial (\nabla^\mu n)} (D\nabla^\mu n)^{(s)} + \ldots + \ldots \right] + \ldots\end{aligned} \tag{2.140}$$

Substituting Eq. (2.140) on the left handside of solubility condition Eq. (2.137)

$$\begin{aligned}\int \frac{d^3p}{p^0} p^\mu U_\mu (Df)^{(r)} = \int \frac{d^3p}{p^0} p^\mu U_\mu \sum_{s=1}^{r} \left[\frac{\partial f^{(r-s)}}{\partial n} (Dn)^{(s)} \frac{\partial f^{(r-s)}}{\partial T} (DT)^{(s)} + \frac{\partial f^{(r-s)}}{\partial U^\mu} (DU^\mu)^{(s)} \right] \\ + \int \frac{d^3p}{p^0} p^\mu U_\mu \sum_{s=2}^{r} \left[\frac{\partial f^{(r-s)}}{\partial (\nabla^\mu n)} (D\nabla^\mu n)^{(s)} + \ldots + \ldots \right] + \ldots\end{aligned} \tag{2.141}$$

We will now calculate each term in the above equation. Considering the first term on R.H.S of Eq. (2.141) we get

$$\sum_{s=1}^{r} \int \frac{d^3p}{p^0} p^\mu U_\mu \frac{\partial f^{(r-s)}}{\partial n} (Dn)^{(s)} = \sum_{s=1}^{r} (Dn)^{(s)} \frac{\partial}{\partial n} \int \frac{d^3p}{p^0} p^\mu U_\mu f^{(r-s)} \tag{2.142}$$

We know from Eq. (2.132), the quantity $s \neq r$ does not contribute in the above expression, thus for $s = r$ we have

$$\sum_{s=1}^{r} \int \frac{d^3p}{p^0} p^\mu U_\mu \frac{\partial f^{(r-s)}}{\partial n} (Dn)^{(s)} = \sum_{s=1}^{r} (Dn)^{(s)} \frac{\partial}{\partial n} \int \frac{d^3p}{p^0} p^\mu U_\mu f^{(0)} = (Dn)^{(r)} \tag{2.143}$$

Considering the second term on R.H.S of Eq. (2.141) we get

$$\sum_{s=1}^{r} \int \frac{d^3p}{p^0} p^\mu U_\mu \frac{\partial f^{(r-s)}}{\partial T} (DT)^{(s)} = \sum_{s=1}^{r} (DT)^{(s)} \frac{\partial}{\partial T} \int \frac{d^3p}{p^0} p^\mu U_\mu f^{(r-s)}. \tag{2.144}$$

From Eq. (2.133) we know that the quantity $s \neq r$ does not contribute in the above expression, hence we have for $s = r$

$$\sum_{s=1}^{r} \int \frac{d^3p}{p^0} p^\mu U_\mu \frac{\partial f^{(r-s)}}{\partial T} (DT)^{(s)} = \sum_{s=1}^{r} (DT)^{(s)} \frac{\partial}{\partial T} \int \frac{d^3p}{p^0} p^\mu U_\mu f^{(0)} = (DT)^{(r)} \frac{\partial n}{\partial T} \tag{2.145}$$

Since particle density n is independent of temperature T we have from the above equation

$$\sum_{s=1}^{r} \int \frac{d^3p}{p^0} p^\mu U_\mu \frac{\partial f^{(r-s)}}{\partial T} (DT)^{(s)} = 0 \tag{2.146}$$

Considering the third term on R.H.S of Eq. (2.141)

$$\begin{aligned}
\sum_{s=1}^{r} \int \frac{d^3p}{p^0} p^\mu U_\mu \frac{\partial f^{(r-s)}}{\partial U^\mu} (DU^\mu)^{(s)} &= \sum_{s=1}^{r} (DU^\mu)^{(s)} \frac{\partial}{\partial U^\mu} \int \frac{d^3p}{p^0} p^\mu U_\mu f^{(r-s)} + \sum_{s=1}^{r} (DU^\mu)^{(s)} \int \frac{d^3p}{p^0} p^\mu f^{(r-s)} \\
&= (DU^\mu)^{(r)} \frac{\partial n}{\partial U^\mu} + \sum_{s=1}^{r} N_\mu^{(r-s)} (DU^\mu)^{(s)} \\
&= \sum_{s=1}^{r} N_\mu^{(r-s)} (DU^\mu)^{(s)} .
\end{aligned} \tag{2.147}$$

Similarly other terms on R.H.S of Eq. (2.141) can be calculated to be zero identically. Thus substituting Eqs. (2.143), (2.146) and (2.147) in Eq. (2.140) we get

$$\int \frac{d^3p}{p^0} p^\mu U_\mu (Df)^{(r)} = (Dn)^{(r)} - \sum_{s=1}^{r} N_\mu^{(r-s)} (DU^\mu)^{(s)} \tag{2.148}$$

Using Eq. (2.148), equations $U^\mu (DU_\mu)^{(s)} = 0$ and $N_\mu^0 (DU^\mu)^{(r)} = nU_\mu^0 (DU^\mu)^{(r)} = 0$ in Eq. (2.137) we obtain

$$(Dn)^{(r)} - \sum_{s=1}^{r-1} N_\mu^{(r-s)} (DU^\mu)^{(s)} = - \int \frac{d^3p}{p^0} p_\mu \nabla^\mu f^{(r-1)} \tag{2.149}$$

$$(Dn)^{(r)} = \sum_{s=1}^{r-1} N_\mu^{r-s} (DU^\mu)^{(s)} - \nabla^\mu N_\mu^{(r-1)}. \tag{2.150}$$

Eq. (2.150) for $r = 1$ can be written as

$$(Dn)^{(1)} = -\nabla^\mu U^\mu \tag{2.151}$$

where we have made use of $N_\mu^0 = nU_\mu$. Similarly from Eq. (2.136) we get

$$Dn = N^\mu DU_\mu - \epsilon \nabla^\mu N_\mu \tag{2.152}$$

2.5.3 First Chapman-Enskog Approximation

The first Chapman-Enskog approximation is determined by Eq. (2.136) for $r = 1$. Thus, we have

$$p^\mu U_\mu (Df)^{(1)} + p^\mu \nabla_\mu f^{(0)} = -f^{(0)} \mathcal{L} \left[\phi^{(1)} \right]. \tag{2.153}$$

We know $Df^{(1)}$ is given by

$$(Df)^{(1)} = \frac{\partial f^{(0)}}{\partial n}(Dn)^{(1)} + \frac{\partial f^{(0)}}{\partial T}(DT)^{(1)} + \frac{\partial f^{(0)}}{\partial U^{\mu}}(DU^{\mu})^{(1)} \tag{2.154}$$

where $f^{(0)}$ is given by Eq. (2.124). Substituting for $(Df)^{(1)}$ from Eq. (2.154) in Eq. (2.153) we get

$$p^{\mu}U_{\mu}\left(\frac{\partial f^{(0)}}{\partial n}(Dn)^{(1)} + \frac{\partial f^{(0)}}{\partial T}(DT)^{(1)} + \frac{\partial f^{(0)}}{\partial U^{\mu}}(DU^{\mu})^{(1)}\right) p^{\mu}\nabla_{\mu}f^{(0)} = -f^{(0)}\mathcal{L}\left[\phi^{(1)}\right]. \tag{2.155}$$

On calculating each term in the above equation we obtain

$$\frac{\partial f^{(0)}}{\partial n} = \frac{1}{k_{B}T}f^{(0)}\frac{\partial \mu}{\partial n} \tag{2.156}$$

$$\frac{\partial f^{(0)}}{\partial U^{\nu}} = -\frac{p^{\nu}}{k_{B}T}f^{(0)} \tag{2.157}$$

$$\frac{\partial f^{(0)}}{\partial T} = \frac{1}{k_{B}}\left[\frac{\partial}{\partial T}\left(\frac{\mu}{T}\right) + \frac{p^{\nu}U_{\nu}}{T^{2}}\right]. \tag{2.158}$$

$$\nabla_{\mu}f^{(0)} = \frac{1}{k_{B}}f^{(0)}\left[\nabla_{\mu}\left(\frac{\mu}{T}\right) - \frac{p^{\nu}}{T}\nabla_{\mu}U_{\nu} + \frac{p^{\nu}U_{\nu}}{T^{2}}\nabla_{\mu}T\right]. \tag{2.159}$$

Using Eqs. (2.156), (2.157), (2.158) and (2.159) in Eq. (2.155) we get

$$p^{\mu}U_{\mu}\left[\frac{\partial \mu}{\partial n}(Dn)^{(1)} + \left[T^{2}\frac{\partial}{\partial T}\left(\frac{\mu}{T}\right) + p^{\nu}U_{\nu}\right]\frac{(DT)^{(1)}}{T} - p^{\nu}\left(DU_{\nu}\right)^{(1)}\right] + p^{\mu}T\nabla_{\mu}\left(\frac{\mu}{T}\right)$$
$$-p^{\mu}p^{\nu}\nabla_{\mu}U_{\nu} + \frac{p^{\mu}p^{\nu}U_{\nu}}{T}\nabla_{\mu}T = -k_{B}T\mathcal{L}\left[\phi^{(1)}\right]. \tag{2.160}$$

For $r = 1$, Eq. (2.139) becomes

$$\int \frac{d^{3}p}{p^{0}}p^{\mu}p^{\nu}U_{\nu}(Df)^{(1)} = -\int \frac{d^{3}p}{p^{0}}p^{\mu}p^{\nu}\nabla_{\nu}f^{(0)}. \tag{2.161}$$

Using Eq. (2.154) and $\int \frac{d^{3}p}{p(0)}p^{\mu}P^{\nu}f^{(0)} = enU^{\mu}U^{\nu} - p\Delta^{\mu\nu}$ in the above equation we get

$$U^{\mu}\left[e(Dn)^{(1)} + n\frac{\partial e}{\partial T}(DT)^{(1)}\right] + nh\left(DU^{\mu}\right)^{(1)} = -nhU^{\mu}\nabla_{\nu}U^{\nu} + \nabla^{\mu}p. \tag{2.162}$$

Contracting Eq. (2.162) with $\Delta_{\mu\nu}$ we get

$$(DU^{\mu})^{(1)} = \frac{1}{nh}\nabla^{\mu}p \tag{2.163}$$

which is the lowest order approximation to the equation of motion.

Again, contracting Eq. (2.162) with U^{μ} and using Eq. (2.151), $h = e + pn^{-1}$ and $c_{v} = \frac{\partial e}{\partial T}$ we obtain

$$c_{v}(DT)^{(1)} = -k_{B}T\nabla_{\mu}U^{\mu} \tag{2.164}$$

which is the lowest order approximation to the equation of energy. Using Eqs. (2.151), (2.163) and (2.164) in Eq. (2.160) we get

$$p^\mu U_\mu p^\nu \left(\frac{\nabla_\nu T}{T} - \frac{\nabla_\nu p}{nh}\right) + p^\nu T \nabla_\nu \frac{\mu}{T} - p^\mu p^\nu \left(\nabla_\mu U_\nu - \frac{1}{3}\Delta_{\mu\nu}\nabla_\sigma U^\sigma\right) + Q\nabla^\mu U_\mu = -k_{_B} T \mathcal{L}[\phi^{(1)}] \tag{2.165}$$

where

$$Q = -\frac{1}{3}\Delta^{\mu\nu} p_\mu p_\nu + (1-\gamma)\left(p^\mu U_\mu\right)^2 + \left[T^2(1-\gamma)\frac{\partial}{\partial T}\left(\frac{\mu}{T}\right) - n\frac{\partial \mu}{\partial n}\right] p^\mu U_\mu. \tag{2.166}$$

Using $\gamma = \frac{k_B}{c_v} + 1$, $\frac{\partial \mu}{\partial n} = \frac{k_B T}{n}$ and $\frac{\partial}{\partial T}\left(\frac{\mu}{T}\right) = -\frac{e}{T^2}$ in Eq. (2.166) we get

$$Q = \left(\frac{4}{3} - \gamma\right)\left(p^\mu U_\mu\right)^2 + \left[(\gamma-1)h - \gamma k_{_B} T\right] p^\mu U_\mu - \frac{1}{3}m^2. \tag{2.167}$$

The first order perturbation function $\phi^{(1)}$ is uniquely determined by the Eq. (2.165) and the conditions of fit Eqs. (2.132)-(2.135)

$$\int \frac{d^3p}{p^0} p^\mu U_\mu f(0)\phi^{(1)} = 0 \tag{2.168}$$

$$\int \frac{d^3p}{p^0}\left(p^\mu U_\mu\right)^2 f^{(0)}\phi^{(1)} = 0 \tag{2.169}$$

and

$$\int \frac{d^3p}{p^0}\Delta^{\mu\nu} p_\nu f^{(0)}\phi^{(1)} = 0 \tag{2.170}$$

$$\int \frac{d^3p}{p^0}\Delta^{\mu\nu} p_\nu p_\sigma U^\sigma f^{(0)}\phi^{(1)} = 0. \tag{2.171}$$

2.5.4 Second law of thermodynamics

The second law of thermodynamics expresses the fact that the entropy production is zero for a reversible process, and positive for an irreversible transformation of the system. Within the framework of kinetic theory this statement is called the H-theorem. In a wider sense it may mean either the Gibbs relation or the entropy balance law. Sometimes it comprises both of them. We shall consider the later point of view.

2.5.5 Gibbs relation

Gibbs relation relates the entropy change to the changes of the other thermodynamic variables which determines the state of the system. In the Chapman-Enskog hierarchy the conditions of fit are such that the macroscopic variables are always determined by the distribution function alone. In particular, we have for an N-component mixture-

$$n_k = n_k^{(0)} \qquad k = 1, 2, \ldots, \quad Ne = e^{(0)} \tag{2.172}$$

If reactive collisions are allowed,

$$n_a = \sum_k q_{ak} n_k^{(a)} \quad a = 1, 2, \ldots, N' \tag{2.173}$$

where q_{ak} are the conserved quantum numbers associated with the system. The entropy four flow for a mixture is given by equation

$$S^\mu = -k_{_B} \sum_{k=1}^{N} \int \frac{d^3 p_k}{p_k^0} p_k^\mu f_k \left[\log(2\pi\hbar)^3 f_k - 1\right]. \tag{2.174}$$

Let us consider the distribution function slightly deviated from equilibrium position

$$f_k(x, p_k) = f_k^{(0)}(x, p_k)\left[1 + \phi_k(x, p_k)\right]. \tag{2.175}$$

Substituting Eq. (2.175) in Eq. (2.174) and ignoring all the higher powers of the perturbation function ϕ_k we get

$$S^\mu = \frac{1}{T}\left[T^{\mu\nu} U_\nu - \sum_k \mu_k N_k^\mu\right] + k_{_B} N^{(0)\mu}. \tag{2.176}$$

Contracting Eq. (2.176)with U^μ we obtain

$$Ts = e + pn^{-1} - \sum_k x_k \mu_k \tag{2.177}$$

where we have made use of $U_\mu S^\mu = sn$ and $x_k = \frac{n_k}{n}$. Thus, contraction with U^μ yields for the entropy density the same expression as in equilibrium.

The corresponding expression for a reactive mixture is

$$Ts = e + pn^{-1} - \sum_{a=1}^{N'} x_a \mu_a. \tag{2.178}$$

Taking the derivative of above equation we get

$$T\partial_\nu s + s\partial_\nu T = \partial_\nu e + p\partial_\nu n^{-1} + n^{-1}\partial_\nu p - \sum_a \mu_a \partial_\nu x_a - \sum_a x_a \partial_\nu \mu_a. \tag{2.179}$$

Let us consider T and μ to be independent variables. We know

$$p = nk_{_B} T. \tag{2.180}$$

Differentiating the above equation we get

$$\partial_\nu p = k_{_B} T \sum_{ak} \frac{\partial n_k^{(0)}}{\partial \mu_a} \partial_\nu \mu_a + k_{_B} \sum_k n_k^{(0)} + k_{_B} T \sum k \frac{\partial n_k^{(0)}}{\partial T} \partial_\nu T. \tag{2.181}$$

The quantity $n_k^{(0)}$ in terms of the Bessel's function is given by

$$n_k^{(0)} = \frac{4\pi m_k^2 k_{_B} T}{(2\pi\hbar^3)} K_2 \left(\frac{m_k}{k_{_B} T} \right) \exp \left(\frac{\mu_k}{k_{_B} T} \right). \tag{2.182}$$

Differentiating Eq. (2.182) with temperature T we get

$$\frac{\partial n_k^{(0)}}{\partial T} = \frac{n_k^{(0)}}{k_{_B} T^2} \left(e_k^{(0)} - \mu_k \right) \tag{2.183}$$

where we have made use of $\frac{\partial}{\partial z} \left[K_n(z) \right] = -\frac{1}{2} \left[K_{n-1}(z) + K_{n+1} \right]$ and $K_{n+1}(z) = 2n \frac{K_n}{z} + K_{n-1}$. Differentiating Eq. (2.182) with chemical potential μ_a we get

$$\frac{\partial n_k^{(0)}}{\partial \mu_a} = q_{ak} \frac{n_k^{(0)}}{k_{_B} T}. \tag{2.184}$$

Using Eqs. (2.183) and (2.184) in Eq. (2.181) we get

$$n^{-1} \partial_\nu p - \sum_a x_a \partial_\nu \mu_a = s \partial_n u T \tag{2.185}$$

which is the relativistic version of Gibbs-Duhem relation. Using Eq. (2.185) in Eq. (2.179) we obtain

$$T \partial_\nu s = \partial_\nu e + p \partial_\nu n^{-1} - \sum_a \mu_a \partial_\nu x_a \tag{2.186}$$

which is the required Gibbs relation which proves to be valid in the linear theory and, hence, in the first order chapman-Enskog approximation. This relation is not valid beyond first approximation as we have ignored the higher order terms while obtaining Eq. (2.176).

2.5.6 Irreversible flows

In the linear theory, the thermodynamic variables are independent of the perturbation functions. The perturbation functions manifest themselves primarily in the expression for the flows. Let us first consider the diffusion flow

$$I_k^\mu = N_k^\mu - x_k N^\mu. \tag{2.187}$$

If reactive processes are taking place in the system then

$$I_a^\mu = \sum_k q_{ak} \left(N_k^\mu - x_k N^\mu \right). \tag{2.188}$$

In zeroth order the particle flow is given by-

$$N_k^{(0)\mu} = \int \frac{d^3 p_k}{p_k^0} p_k^\mu f_k^{(0)} = n_k^{(0)} U^\mu. \tag{2.189}$$

Using Eq. (2.189) in Eq. (2.188) we obtain

$$I_a^{(0)\mu} = 0. \tag{2.190}$$

Thus, in terms of the perturbation function the diffusion flow is given as

$$I_a^\mu = \sum_k \left(q_{ak} - x_a \right) \int \frac{d^3 p_k}{p_k^0} p_k^\mu f_k^{(0)} \phi_k \tag{2.191}$$

The heat flow is given by

$$I_q^\mu = \left(U_\nu T^{\nu\sigma} - h N^\sigma \right) \Delta_\sigma^\mu. \tag{2.192}$$

The zeroth order approximation to the heat flow vanishes

$$I_q^{(0)\mu} = 0. \tag{2.193}$$

In terms of the perturbation function the heat flow is given by

$$I_q^\mu = \sum_k \int \frac{d^3 p_k}{p_k^0} p_k^\mu \left(p_k^\nu U_\nu - h \right) f_k^{(0)} \phi_k \tag{2.194}$$

The viscous pressure tensor is defined as

$$\Pi^{\mu\nu} = \Delta_\sigma^\mu T^{\sigma\tau} \Delta_\tau^\nu + p \Delta^{\mu\nu} \tag{2.195}$$

The zeroth order approximation vanishes i.e.

$$\overset{o}{\Pi}{}^{\mu\nu} = 0 \tag{2.196}$$

and the viscous pressure tensor in terms of the perturbation function is given by,

$$\Pi^{\mu\nu} = \sum_k \int \frac{d^3 p_k}{p_k^0} \Delta_\sigma^\mu \Delta_\tau^\nu p_k^\sigma p_k^\tau f_k^{(0)} \phi_k. \tag{2.197}$$

The viscous pressure tensor can be split into a traceless part $\overset{o}{\Pi}{}^{\mu\nu}$ and the remainder:

$$\Pi^{\mu\nu} = \overset{o}{\Pi}{}^{\mu\nu} - \Pi\Delta^{\mu\nu}. \tag{2.198}$$

The viscous pressure Π is defined as negative one third of the trace of the viscous pressure tensor and in terms of the perturabation function it is given as

$$\Pi = -\frac{1}{3}\Pi^{\mu}_{\mu} = -\frac{1}{3}\sum_k \frac{d^3p_k}{p^0_k}\Delta_{\mu\nu}p^{\mu}_k p^{\nu}_k f^{(0)}_k \phi_k. \tag{2.199}$$

Thus, the traceless part in terms of the perturbation function is given by

$$\overset{o}{\Pi}{}^{\mu\nu} = \sum_k \int \frac{d^3p_k}{p^0_k}\left(\Delta^{\mu}_{\sigma}\Delta^{\nu}_{\tau} - \frac{1}{3}\Delta_{\sigma\tau}\Delta^{\mu\nu}\right) p^{\sigma}_k p^{\tau}_k f^{(0)}_k \phi_k. \tag{2.200}$$

The entropy four flow is given by

$$I^{\mu}_s = S^{\mu} - sN^{\mu}. \tag{2.201}$$

The zeroth order approxiamtion to the entropy flow S^{μ} is

$$S^{(0)\mu} = snU^{\mu}. \tag{2.202}$$

Using Eq. (2.176) and $\mu_k = \sum_{a=1}^{N'} q_{ak}\mu_a$ in Eq. (2.201) we get

$$I^{\mu}_s = \frac{1}{T}\left(\Delta^{\mu\nu}T_{\nu\sigma}U^{\sigma} - \sum_a \mu_a \sum_k q_{ak}N^{\mu}_k + nhU^{\mu}\right) - sN^{\mu}. \tag{2.203}$$

Using Eqs. (2.178),(2.188) and (2.192) in the above equation.we get

$$I^{\mu}_s = \frac{1}{T}\left(I^{\mu}_q - \sum_a \mu_a I^{\mu}_a\right). \tag{2.204}$$

Thus, in the linear approximation, the entropy flow is not an independent quantity, but a particular linear combination of the heat flow and the diffusion flows.

2.6 Transport coefficients

The irreversible phenomenon taking place in non-equilibrium systems is dominated by thermodynamic forces and flows. The flows tend to smooth out or remove the non-uniformities caused by the forces. The proportionality constants are known as the transport coefficients. The transport coefficients are dependant on the kind of system and on the local thermodynamic variables, but independent of the local variations of these quantities. We will try to find the transport coefficients in terms of the interactions between the

constituent particles using Chapman-Enskog approximation.

2.6.1 First order distribution function

In the Chapman-Enskog approximation the one-particle distribution function $f(x,p)$, describing the state of a simple system, is written as

$$f(x,p) = f^{(0)}(x,p)[1+\phi(x,p)] \tag{2.205}$$

where $f^{(0)}$ is the local equilibrium distribution function

$$f^{(0)}(x,p) = \frac{1}{(2\pi\hbar)^3}\exp\left(\frac{\mu(x)-p^\mu U_\mu(x)}{k_{_B}T}\right). \tag{2.206}$$

The first order perturbation function $\phi(x,p)$ is determined from the integral Eq. (2.165). Using Gibbs-Duhem relation in the integral equation we obtain

$$\left[\left(\frac{4}{3}-\gamma\right)(p^\mu U_\mu)^2 + ((\gamma-1)h-\gamma k_{_B}T)\,p^\mu U_\mu - \frac{1}{3}m^2\right]X - (p^\mu U_\mu - h)\,p_\nu X_q^\nu + p^\mu p^\nu \overset{o}{X}_{\mu\nu} = k_{_B}T\mathcal{L}[\phi] \tag{2.207}$$

where X, X_q^μ and $\overset{0}{X}_{\mu\nu}$ indicate the thermodynamic forces and is given by

$$X = -\nabla^\mu U_\mu \tag{2.208}$$

$$X_q^\mu = \nabla^\mu \log T - \frac{k_{_B}T}{h}\nabla^\mu \log p \tag{2.209}$$

$$\overset{0}{X}^{\mu\nu} = \left(\Delta^\mu_\sigma\Delta^\nu_\tau - \frac{1}{3}\Delta^{\mu\nu}\Delta_{\sigma\tau}\right)\nabla^\sigma U^\tau \tag{2.210}$$

and $\mathcal{L}$ is the linearized collision operator given by equation

$$\mathcal{L}[\phi] = \frac{1}{2}\int \frac{d^3p_1}{p_1^0}\frac{d^3p'}{p'^0}\frac{d^3p_1'}{p_1'^0} f_1^{(0)}\left(\phi+\phi_1-\phi'-\phi_1'\right)W\left(p',p_1' \mid p,p_1\right). \tag{2.211}$$

Let us consider ϕ to be

$$\phi = \frac{1}{n\sigma}\left(AX - B_\mu X_q^\mu + C^{\mu\nu}\overset{o}{X}_{\mu\nu}\right) \tag{2.212}$$

where σ is the scattering cross-section and the factors at the right-hand side is chosen in such a way that the coefiicients A, B^μ and $C^{\mu\nu}$ becomes dimensionless.

The coefficient A, being dimensionless, can only be a function of a scalar and dimensionless combinations that can be constructed from the momentum vector p^μ, the metric tensor $g^{\mu\nu}$ and the thermodynamic

variables n, T and U^μ. These are

$$\tau = \frac{p^\mu U_\mu}{k_B T}, \quad z = \frac{m}{k_B T} \tag{2.213}$$

and the dimensionless quantity containing the density. It will be shown that the coefficient A is independent of the density, so that we have

$$A = A(\tau, z). \tag{2.214}$$

The vector term B^μ constructed from the same variables is given as

$$B^\mu = \frac{1}{k_B T} B(\tau, z) \Delta^{\mu\nu} p_\nu \tag{2.215}$$

where the scalar function B turns out to be dimensionless and also independent of density. It contains contribution from U^μ which however can be omitted since upon contraction with the thermodynamic force X_q^μ in Eq. (2.212) it vanishes. Finally, we take

$$C^{\mu\nu} = \left(\frac{1}{k_B T}\right)^2 C(\tau, z) \left(\Delta^\mu_\sigma \Delta^\nu_\rho - \frac{1}{3}\Delta^{\mu\nu}\Delta_{\rho\sigma}\right) p^\rho p^\sigma \tag{2.216}$$

where C is dimensionless and independent of the density. The tensor $C^{\mu\nu}$ must have the particular form Eq. (2.216) since contributions proportional to $\Delta^{\mu\nu}$ as well as to U^μ vanish upon contraction with the thermodynamic force $\overset{o}{X}{}^{\mu\nu}$.

The thermodynamic forces appearing in the integral Eq. (2.207) as well as in trial solution (2.212) are independent quantities. We now substitute Eq. (2.212) into Eq. (2.207) and equate the coefficients of each of the thermodynamic forces separately. In terms of a dimensionless linearized collision operator defined as

$$L[\phi] = \frac{1}{n k_B T \sigma(T)} \mathcal{L}[\phi] \tag{2.217}$$

we obtain the following set of integral equations for the functions (2.214), (2.215) and (2.216)

$$\left(\frac{4}{3} - \gamma\right)\tau^2 + [(\gamma - 1)\hat{h} - \gamma]\tau - \frac{1}{3}z^2 = L[A(\tau, z)] \tag{2.218}$$

$$(\tau - \hat{h})\Delta^{\mu\nu} p_\nu = L\left[B(\tau, z)\Delta^{\mu\nu} p_\nu\right] \tag{2.219}$$

$$\left(\Delta^\mu_\sigma \Delta^\nu_\rho - \frac{1}{3}\Delta^{\mu\nu}\Delta_{\rho\sigma}\right) p^\sigma p^\rho = L\left[C(\tau, z)\left(\Delta^\mu_\sigma \Delta^\nu_\rho - \frac{1}{3}\Delta^{\mu\nu}\Delta_{\sigma\rho} p^\sigma p^\rho\right)\right] \tag{2.220}$$

where $\hat{h} = \frac{h}{k_B T}$.

2.6.2 Heat conduction and viscous flow

We will now determine the relationship between gradients in the system and the irreversible flows. In order to write the irreversible flows in concise form, we introduce few notations to indicate the symmetrized space-like part of a vector a^μ, a tensor $b^{\mu\nu}$

$$a^{\bar{\mu}} = \Delta^\mu_\nu a^\nu \tag{2.221}$$

$$b^{\overline{\mu\nu}} = \frac{1}{2}\left(\Delta^\mu_\sigma\Delta^\nu_\tau + \Delta^\nu_\sigma\Delta^\mu_\tau\right) b^{\sigma\tau} \tag{2.222}$$

and a traceless part of the tensor as

$$b^{\overset{o}{\mu\nu}} = b^{\overline{\mu\nu}} - \frac{1}{3}\Delta^{\mu\nu}\Delta_{\sigma\tau}b^{\sigma\tau}. \tag{2.223}$$

We also introduce a dimensionless inner product of two functions $F(p)$ and $G(p)$ as the momentum integral

$$(F,G) = \frac{k_B T}{n}\int \frac{d^3p}{p^0}F(p)G(p). \tag{2.224}$$

Let us introduce a dimensionless momentum vector $\pi^\mu = \frac{p^\mu}{k_B T}$. With the help of these notation we can write equations for (2.191),(2.194) and (2.200) in the following manner: the viscous pressure as

$$\Pi = -\frac{1}{3}nk_B T\left(\overline{\pi^\mu\pi_\mu}, \phi\right) \tag{2.225}$$

the heat flow as

$$I^\mu_q = nk_B T\left(\pi^{\bar{\mu}}(\tau - \hat{h}), \phi\right) \tag{2.226}$$

and the traceless viscous pressure tensor as

$$\overset{o}{\mu\nu}^{\mu\nu} = nk_B T\left(\frac{o}{\pi^\mu\pi^\nu}, \phi\right). \tag{2.227}$$

We now consider the viscous pressure as given in Eq. (2.225) and substitute the expression for ϕ in the equation to get

$$\Pi = -\frac{1}{3}\frac{1}{nk_B\sigma T}\int \frac{d^3p}{p^0}\Delta^{\mu\nu}p_\mu p_\nu f^{(0)}\left(AX - B_\alpha X^\alpha_q + C^{\alpha\beta}\overset{o}{X}_{\alpha\beta}\right). \tag{2.228}$$

Let us consider the first term as Π_1. Calculating the first term in Eq. (2.228) we obtain

$$\Pi_1 = -\frac{1}{3}\frac{1}{nk_B\sigma T}\int \frac{d^3p}{p^0}\Delta^{\mu\nu}p_\mu p_\nu f^{(0)}AX. \tag{2.229}$$

Substituing the expression for A from Eq. (2.214) and X from Eq. (2.208) in the above equation we get

$$\Pi_1 = -\frac{1}{3}\frac{1}{nk_{_B}\sigma T}\int \frac{d^3p}{p^0}\Delta^{\mu\nu}p_\mu p_\nu f^{(0)}A(\tau,z)\left(-\nabla^\alpha U_\alpha\right). \tag{2.230}$$

This equation can be written as

$$\Pi_1 = -\zeta\ \nabla^\alpha U_\alpha \tag{2.231}$$

where ζ is the bulk viscosity coefficient and is given as

$$\zeta = -\frac{1}{3}\frac{k_{_B}T}{\sigma}\left(\overline{\pi^\mu\pi_\mu}, A\right). \tag{2.232}$$

Now considering the second term say Π_2 in Eq. (2.228)

$$\Pi_2 = \frac{1}{3}\frac{1}{nk_{_B}\sigma T}\int \frac{d^3p}{p^0}\Delta^{\mu\nu}p_\mu p_\nu f^{(0)}B_\alpha X_q^\alpha. \tag{2.233}$$

Substituing the expression for B_α from Eq. (2.215) and the expression for X_q^α from Eq. (2.209) we get

$$\begin{aligned}
\Pi_2 &= \frac{1}{3}\frac{1}{nk_{_B}\sigma T}\int \frac{d^3p}{p^0}\Delta^{\mu\nu}p_\mu p_\nu B(\tau,z)\Delta_{\alpha\beta}p^\beta\left[\frac{\nabla^\alpha T}{T} - \frac{k_{_B}T}{h}\frac{\nabla^\alpha p}{p}\right]f^{(0)} &(2.234)\\
&= \frac{1}{3}\frac{1}{nk_{_B}\sigma T}\left[\frac{\nabla^\alpha T}{T} - \frac{k_{_B}T}{h}\frac{\nabla^\alpha p}{p}\right]\Delta_{\alpha\beta}\int \frac{d^3p}{p^0}\Delta^{\mu\nu}p_\mu p_\nu B(\tau,z)p^\beta f^{(0)} &(2.235)\\
&= \frac{1}{3}\frac{1}{nk_{_B}\sigma T}\left[\frac{\nabla^\alpha T}{T} - \frac{k_{_B}T}{h}\frac{\nabla^\alpha p}{p}\right]\Delta_{\alpha\beta}\left[\text{ constant }\times U^\beta\right] &(2.236)
\end{aligned}$$

where the last equation is obtained using equation

$$\int \frac{d^3p}{p^0}F\left(p_\sigma U^\sigma\right)p_\mu = \text{ constant }\times U_\mu. \tag{2.237}$$

Thus, we get

$$\Pi_2 = 0 \tag{2.238}$$

since $\Delta_{\alpha\beta}U^\beta = 0$. Considering the third term say Π_3

$$\Pi_3 = -\frac{1}{3}\frac{1}{nk_{_B}\sigma T}\int \frac{d^3p}{p^0}\Delta^{\mu\nu}p_\mu p_\nu f^{(0)}C^{\alpha\beta}\ \overset{o}{X}_{\alpha\beta}. \tag{2.239}$$

Substituing the expression for $C^{\alpha\beta}$ from Eq. (2.216) and the expression for $\overset{o}{X}_{\alpha\beta}$ from Eq. (2.210) we get

$$\begin{aligned}\Pi_3 &= -\frac{1}{3}\frac{1}{k_{_B}Tn\sigma(T)}\int\frac{d^3p}{p^0}\Delta^{\mu\nu}p_\mu p_\nu f^{(0)}C(\tau,z)\left(\Delta^\alpha_\sigma\Delta^\beta_\rho-\frac{1}{3}\Delta^{\alpha\beta}\Delta_{\sigma\rho}\right)p^\sigma p^\rho\left(\Delta^\gamma_\alpha\Delta^\delta_\beta-\frac{1}{3}\Delta_{\alpha\beta}\Delta^{\gamma\delta}\right)\nabla_\gamma U_\delta\\ &= -\frac{1}{3}\frac{1}{k_{_B}Tn\sigma(T)}\left(\Delta^\alpha_\sigma\Delta^\beta_\rho-\frac{1}{3}\Delta^{\alpha\beta}\Delta_{\sigma\rho}\right)\left(\Delta^\gamma_\alpha\Delta^\delta_\beta-\frac{1}{3}\Delta_{\alpha\beta}\Delta^{\gamma\delta}\right)\nabla_\gamma U_\delta\int\frac{d^3p}{p^0}\Delta^{\mu\nu}p_\mu p_\nu C(\tau,z)p^\sigma p^\rho f^{(0)}\\ &= -\frac{1}{3}\frac{1}{k_{_B}\,\mathrm{T}n\,\sigma(T)}\left(\Delta^\alpha_\sigma\Delta^\beta_\rho-\frac{1}{3}\Delta^{\alpha\beta}\Delta_{\sigma\rho}\right)\left(\Delta^\gamma_\alpha\Delta^\delta_\beta-\frac{1}{3}\Delta_{\alpha\beta}\Delta^{\gamma\delta}\right)\nabla_\gamma\\ &\qquad\times U_\delta[\text{constant}_1\times U^\sigma U^\rho+\text{constant}_2\times\Delta^{\sigma\rho}]\end{aligned}\tag{2.240}$$

where the last equation has been derived using equation

$$\int\frac{d^3p}{p^0}F\left(p_\sigma U^\sigma\right)p_\mu p_\nu=\left[\text{constant}_1\times U_\mu U_\nu+\text{constant}_2\times\Delta_{\mu\nu}\right].\tag{2.241}$$

Thus, we get

$$\Pi_3=0\tag{2.242}$$

since $\Delta_{\alpha\beta}U^\beta=0$. Combining Eqs. (2.231), (2.238) and (2.242) we get

$$\Pi=-\zeta\nabla^\mu U_\mu.\tag{2.243}$$

Considering the heat flow as given in Eq. (2.226) and substituting the expression for ϕ in the equation we get

$$I^\mu_q=\frac{k_{_B}T}{n\sigma(T)}\int\frac{d^3p}{p^0}\Delta^\mu_\nu p^\nu(\tau-\hat{h})f^{(0)}\left(AX-B_\alpha X^\alpha_q+C^{\alpha\beta}\overset{o}{X}_{\alpha\beta}\right).\tag{2.244}$$

A similar treatment to the heat flow as done in the calculation of viscous pressure yields

$$I^\mu_q=\lambda^{\mu\nu}\left(\nabla_\nu T-\frac{T}{nh}\nabla_\nu p\right)\tag{2.245}$$

where

$$\lambda^{\mu\nu}=-\frac{k_{_B}}{\sigma(T)}\left(\pi^{\bar{\mu}}(\tau-\hat{h}),B\pi^{\bar{\nu}}\right).\tag{2.246}$$

The quantity $\lambda^{\mu\nu}=c\lambda^{\mu\nu}$ since $\lambda^{\mu\nu}$ contains only the space part. Hence, we can write

$$\Delta_{\mu\nu}\lambda^{\mu\nu}=\lambda\lambda^{\mu\nu}\lambda_{\mu\nu}\tag{2.247}$$

$$\lambda=\frac{1}{3}\Delta_{\mu\nu}\lambda^{\mu\nu}\tag{2.248}$$

where λ is the scalar heat conductivity coefficient.

With the same arguments as followed above we get for the traceless pressure tensor

$$\overset{o}{\Pi}{}^{\mu\nu} = 2\eta\overset{o}{\overline{\nabla^\mu U^\nu}} \tag{2.249}$$

where the shear viscosity is found as

$$\eta = \frac{1}{10}\frac{k_B T}{\sigma(T)}\left(\overset{o}{\overline{\pi^\mu\pi^\nu}}, C\overset{o}{\overline{\pi_\mu\pi_\nu}}\right). \tag{2.250}$$

In deriving the above equation we have made use of

$$\Delta^\mu_\sigma\Delta^\nu_\tau\overset{o}{\overline{\Delta^\sigma_\mu\Delta^\tau_\nu}} = 5 \tag{2.251}$$

Thus, we have derived all the three kinetic coefficients.

We now introduce the collision bracket notation

$$[F, G] = (L[F], G). \tag{2.252}$$

In terms of the collision bracket the three kinetic coefficients are given as

$$\zeta = \frac{k_B T}{\sigma(T)}[A, A] \tag{2.253}$$

$$\lambda = -\frac{1}{3}\frac{k_B}{\sigma(T)}[B\overline{\pi^\mu}, B\overline{\pi_\mu}] \tag{2.254}$$

$$\eta = \frac{1}{10}\frac{k_B T}{\sigma(T)}\left[C\overset{o}{\overline{\pi^\mu\pi^\nu}}, C\overset{o}{\overline{\pi_\mu\pi_\nu}}\right] \tag{2.255}$$

2.7 Calculating the transport coefficients using relaxation time approximation

We will now calculate kinetic equations using the relaxation time approximation on the right hand side of the transport equation. Using the relaxation time approximation we will calculate the quantities A, B^ν and $C^{\mu\nu}$ snd substitute them in the equation for kinetic coefficients obtained using Chapman-Enskog approximation in Eqs. (2.232), (2.248) and (2.250) .

Let us consider a binary collision of form $p+k \longrightarrow p'+k'$. In this collision, if only particles with incoming momentum $\vec{p}$ is out of equilibrium and the remaining particles are in equilibrium then the transport equation takes the following form,

$$\frac{p^\mu\partial_\mu f}{p^0} \simeq -\frac{\delta f}{\tau}. \tag{2.256}$$

This approximation is called the Relaxation time approximation.

Eq. (2.256) can be solved using Chapman-Enskog approximation in the left hand side of the equation

and taking $\delta f = f^{(0)}\phi$. To solve Eq. (2.256) we use similar treatment as was used to obtain Eq. (2.165), we thus get for Eq. (2.256)

$$QX - (p^\mu U_\mu - h)\, p_\nu X_q^\nu + p^\mu p^\nu \overset{o}{X}_{\mu\nu} = \frac{k_B T p^0 \phi}{\tau} \tag{2.257}$$

where Q, X, X_q^ν and $\overset{o}{X}\ \mu\nu$ are given by Eqs. (2.167), (2.208), (2.209) and (2.210). Substituting for ϕ from Eq. (2.212)in the above equation we obtain

$$QX - (p^\mu U_\mu - h)\, p_\nu X_q^\nu + p^\mu p^\nu \overset{o}{X}_{\mu\nu} = \frac{k_B T p^0}{n\sigma(T)\tau}\left[AX - B_\mu X_q^\mu + C^{\mu\nu}{}_{X}^{X_{\mu\nu}}\right]. \tag{2.258}$$

Now comparing the coefficients we obatin

$$A = \frac{n\sigma\tau}{k_B T p^0} Q \tag{2.259}$$

$$B^\nu = \frac{n\sigma\tau}{k_B T p^0}\,(p^\mu p_\mu - h)\, p^\nu \tag{2.260}$$

$$C^{\mu\nu} = \frac{n\sigma\tau}{k_B T p^0} p^\mu p^\nu. \tag{2.261}$$

Using Eq. (2.259) and $d^3p = 4\pi|\vec{p}|^2 d|p|$ in Eq. (2.232) we obtain

$$\zeta = -\frac{4\pi}{3k_B T}\int \frac{\vec{p}^2}{p^{0^2}} \Delta^{\mu\nu} p_\mu p_\nu Q\tau f^{(0)} dp \tag{2.262}$$

which is the required coefficient of Bulk viscosity.

Again using Eq. (2.260) and $d^3p = 4\pi|\vec{p}|^2 d|p|$ in Eq. (2.248) we get

$$\lambda = -\frac{4\pi}{3k_B T^2}\int \frac{p^2}{p^0}\tau\,(p^\mu U_\mu - h)^2\, f^{(0)} dp \tag{2.263}$$

where λ is the coefficient of scalar thermal conductivity. Similarly, using Eq. (2.261) and $d^3p = 4\pi|\vec{p}|^2 d|p|$ in Eq. (2.250) we get

$$\eta = \frac{4\pi n}{10}(k_B T)^2 \left[\Delta_\lambda^\sigma - \frac{1}{3}\Delta_{\lambda\theta}\Delta^{\sigma\tau}\right] \int \frac{\vec{p}^2}{p^{0^2}} \tau p_\sigma p_\tau p^\lambda p^\theta f^{(0)} dp \tag{2.264}$$

where η is the coefficient of shear viscosity.

Chapter 3

Formalism for evaluation of transport coefficients in thermal medium

In this chapter we will evaluate the expressions of shear viscosity, bulk viscosity and thermal conductivity in the ambit of relaxation time approximation. First, we will derive the expressions of the transport coefficients and then discuss the recipe for evaluating the in-medium cross-section which is an important dynamical input to these coefficients. The in-medium cross-sections are obtained in the following manner. In the matrix elements for $2 \to 2$ scattering processes, evaluated from well-known effective interaction Lagrangians, the vacuum propagators corresponding to the intermediate resonances appearing in the s-channel diagrams, are replaced with effective ones obtained from a Dyson-Schwinger sum containing one-loop self-energy diagrams in *vacuum*. This introduces an imaginary part in the matrix elements rendering a Breit-Wigner like structure to the cross-section. The scattering cross-section thus obtained is normalized to experimental data fixing a few unknown model parameters in the process. The corresponding in-medium cross-sections are then obtained by evaluating the self-energy diagrams in the medium using standard techniques of finite temperature field theory. We will in brief discuss the real time formalism of finite temperature field theory and give a general picture of thermal propagators for different fields. To illustrate this methodology a system of pion gas is considered and the formalism stated in this chapter is discussed by presenting the results of shear viscosity of a pion gas in a thermal medium.

In Sec. 3.1 we have discussed the formalism of obtaining the transport coefficients using the Boltzmann transport equation. In Sec. 3.2 the invariant amplitudes for scattering cross-section of a pion gas has been discussed. A brief discussion on the techniques of thermal field theory and therefore the thermal propagators is discussed in Sec. 3.3 and in Sec. 3.4 we have evaluated the one-loop self-energies of the ρ and σ resonances. This is then followed by numerical results of the in-medium cross-section, average relaxation time and shear viscosity of a pion gas in Sec. 3.5

3.1 Viscosities and thermal conductivity from the transport equation

The relationship between thermodynamic forces and the corresponding fluxes for a dissipative system is given by [91, 92]

$$T^{\mu\nu} = en\ u^\mu u^\nu\ -\ P\Delta^{\mu\nu}\ +\ \Pi^{\mu\nu}\ +\ [(I_q^\mu + h\Delta^{\mu\sigma}N_\sigma)u^\nu\ +\ (I_q^\nu + h\Delta^{\nu\sigma}N_\sigma)u^\mu]\ , \tag{3.1}$$

$$\Pi^{\mu\nu} = 2\eta\ \langle\partial^\mu u^\nu\rangle\ +\ \zeta\ (\partial\cdot u)\ \Delta^{\mu\nu} \tag{3.2}$$

where the heat flow I_q^μ and the viscous part $\Pi^{\mu\nu}$ arises due to dissipation in the system and is quantified by shear viscosity η and bulk visocosity ζ. In the above equation P is the pressure, e is the energy per particle, n is the particle density and u^ν is the particle four flow.

In terms of h_k, enthalpy per particle of type k and heat flow I_q^μ we can define a quantity known as reduced heat flow $\bar{I}_q^\mu$ [93]

$$\bar{I}_q^\mu\ =\ I_q^\mu - \sum_k h_k I_k^\mu\ ,\quad I_k^\mu = N_k^\mu - x_k N^\mu\ , \tag{3.3}$$

$$\bar{I}_q^\mu\ =\ L_{qq}\left(\frac{\nabla^\mu T}{T} - \frac{\nabla^\mu P}{nh}\right) + \sum_{j=1}^{N-1} L_{qj}\left((\nabla^\mu\mu_j)_{P,T} - (\nabla^\mu\mu_N)_{P,T} - \frac{h_j - h_N}{nh}\nabla^\mu P\right). \tag{3.4}$$

where k and j denotes the particle type and x_k denotes the particle fraction of type k. Considering mechanical equilibrium i.e. the state with vanishing pressure gradients $\nabla^\mu P = 0$ and also considering vanishing gradients of particle fraction i.e. $\nabla^\mu x = 0$ we have $(\nabla^\mu\mu_j)_{P,T} = 0$, thus Eq. (3.4) can be written as

$$\bar{I}_q^\mu\ =\ L_{qq}\frac{\nabla^\mu T}{T} \tag{3.5}$$

where $L_{qq} = \lambda T$, λ being the thermal conductivity.

The flow and collisions of the constituent particles causes transfer of energy and momentum in the system. For the systems which are out of equilibrium dissipative processes work to bring the system to equilibrium and hence the correlation between transport theory and viscous hydrodynamics is established by considering the distribution function f_k for the $k-$th species to be slightly away from the equilibrium distribution function $f_k^{(0)}$. The measure of the deviation which quantifies the dissipative processes is given by the quantity δf_k. Thus we have,

$$f_k(x,p) = f_k^{(0)}(x,p) + \delta f_k(x,p) \tag{3.6}$$

where,

$$\delta f_k(x,p) = f_k^{(0)}(x,p)\left[1 \pm f_k^{(0)}(x,p)\right]\phi_k(x,p). \tag{3.7}$$

The $\pm$ sign in the above expression denotes the Bose enhancement and Pauli blocking. The equilibrium

distribution function $f_k^{(0)}$ is given by

$$f_k^{(0)} = \left[\exp\left\{\frac{p\cdot u(x) - \mu_k(x)}{T(x)}\right\} \pm 1\right]^{-1} \tag{3.8}$$

where p is the four momentum of the particle, $u_\mu(x)$, $\mu_k(x)$ and $T(x)$ are the local flow velocity, chemical potential and temperature respectively. The $\pm$ sign in the distribution function denotes fermions $(+)$ and bosons $(-)$. We will now express the dissipative terms like viscous part of energy momentum tensor $\Pi^{\mu\nu}$ and reduced heat flow $\bar{I}_q^\mu$ in terms of the distribution function. Thus, in terms of the distribution function $\Pi^{\mu\nu}$ is given as

$$\Pi^{\mu\nu} = \sum_{k=1}^{N}\int \frac{d^3p_k}{(2\pi)^3 E_{p_k}} \Delta_\sigma^\mu \Delta_\tau^\nu p_k^\sigma p_k^\tau \delta f_k \tag{3.9}$$

where N is the number of different species of particles present in the system and $E_{p_k} = \sqrt{\vec{p}_k^2 + m_k^2}$ is the energy corresponding to particle of k. The reduced heat flow in terms of the distribution function is given by

$$\bar{I}_q^\mu = \sum_{k=1}^{N} \Delta_\sigma^\mu \; g_k \int \frac{d^3p_k}{(2\pi)^3 E_{p_k}} [(p_k^\nu u_\nu) - h_k] \; p_k^\sigma \; \delta f_k. \tag{3.10}$$

In order to realize the form of $\Pi^{\mu\nu}$ as expressed in Eq. (3.2) and $\bar{I}_q^\mu$ as expressed in Eq. (3.4), the expression for ϕ_k which is related to δf_k by Eq. (3.7) is written as a linear combination of thermodynamic forces of different tensorial ranks multiplied by suitable coefficients [92]. Thermal conductivity, shear viscosity and bulk viscosity correspond to temperature gradients and velocity gradients and thus ϕ_k can be written as

$$\phi_k = A_k(\partial\cdot u) - B_{kq}^\nu \Delta_{\mu\nu}\left(\frac{\nabla^\mu T}{T}\right) - C_k^{\mu\nu}\;\langle\partial_\mu u_\nu\rangle \tag{3.11}$$

where A_k, B_{kq}^ν and $C_k^{\mu\nu}$ are the unknown coefficients to be determined. The viscous part of the energy momentum tensor can be separated into a traceless part and the remainder as

$$\Pi^{\mu\nu} = \overset{o}{\Pi}{}^{\mu\nu} + \Pi\Delta^{\mu\nu} \tag{3.12}$$

where Π is the viscous pressure

$$\Pi = \sum_{k=1}^{N}\frac{1}{3}\int \frac{d^3p_k}{(2\pi)^3 E_{p_k}} \Delta_{\sigma\tau} p_k^\sigma p_k^\tau \delta f_k \;, \tag{3.13}$$

so that

$$\overset{o}{\Pi}{}^{\mu\nu} = \Pi^{\mu\nu} - \Pi\Delta^{\mu\nu} = \sum_{k=1}^{N}\int \frac{d^3p_k}{(2\pi)^3 E_{p_k}} \left\{\Delta_\sigma^\mu\Delta_\tau^\nu - \frac{1}{3}\Delta_{\sigma\tau}\Delta^{\mu\nu}\right\} p_k^\sigma p_k^\tau \delta f_k. \tag{3.14}$$

Substituting Eqs. (3.7) and (3.11) in Eqs. (3.4), (3.13) and (3.14) and hence making the comparison of

the coefficients with Eq. (3.2) the expressions for thermal condcutivity λ, shear viscosity η and bulk viscosity ζ is obtained as:

$$\lambda = -\sum_{k=1}^{N} \frac{1}{3T} g_k \int \frac{d^3p_k}{(2\pi)^3 E_k} \; (p_k^\nu u_\nu - h_k) \; f_k^{(0)}(1 \pm f_k^{(0)}) \; \Delta_\sigma^\alpha \; p_k^\sigma \; B_\alpha^{kq}, \tag{3.15}$$

$$\eta = -\sum_{k=1}^{N} \frac{1}{10} \int \frac{d^3p_k}{(2\pi)^3 E_{p_k}} \langle p_{k\mu} p_{k\nu} \rangle f_k^{(0)}(1 \pm f_k^{(0)}) C_k^{\mu\nu}, \tag{3.16}$$

$$\zeta = \sum_{k=1}^{N} \frac{1}{3} \int \frac{d^3p_k}{(2\pi)^3 E_{p_k}} \Delta_{\mu\nu} p_k^\mu p_k^\nu f_k^{(0)}(1 \pm f_k^{(0)}) A_k. \tag{3.17}$$

To obtain the explicit form of thermal conductivity, shear and bulk viscosity we need to find the unknown coefficients A_k, B_α^{kq} and $C_k^{\mu\nu}$ and for that we will make use of the Boltzmann transport equation

$$p_k^\mu \partial_\mu f_k(x,p) = \sum_{l=1}^{N} \left(\frac{g_l}{1+\delta_{kl}} \right) C_{kl}[f_k] \tag{3.18}$$

where we have considered the binary collision $p_k + p_l \to p_k' + p_l'$ and g_l is the degeneracy of the l^{th} particle. The collision term on the right hand side is

$$C_{kl}[f_k] = \int\int\int \frac{d^3p_l}{(2\pi)^3 E_{p_l}} \frac{d^3p_k'}{(2\pi)^3 E_{p_k'}} \frac{d^3p_l'}{(2\pi)^3 E_{p_l'}} \Big[f_k(x,p_k') f_l(x,p_l') \left\{ 1 \pm f_k(x,p_k) \right\} \left\{ 1 \pm f_l(x,p_l) \right\}$$
$$- f_k(x,p_k) f_l(x,p_l) \left\{ 1 \pm f_k(x,p_k') \right\} \left\{ 1 \pm f_l(x,p_l') \right\} \Big] W_{kl} \tag{3.19}$$

where W_{kl} is the interaction rate. The derivative ∂_μ can be separated in terms of a temporal and a spatial part in the local rest frame by writing $\partial_\mu = u_\mu D + \nabla_\mu$ where $D = u_\mu \partial^\mu$ and $\nabla_\mu = \Delta_{\mu\nu}\partial^\nu$. Then Eq. (3.18) can be written as

$$p^\mu u_\mu D f_k + p^\mu \nabla_\mu f_k = \sum_{l=1}^{N} \left(\frac{g_l}{1+\delta_{kl}} \right) C_{kl}[f_k]. \tag{3.20}$$

In the Chapman-Enskog approach, the distribution function and its derivative is expanded in terms of ϵ which is called the non-uniformity parameter or Knudsen number as

$$f = f^{(0)} + \epsilon f^{(1)} + \epsilon^2 f^{(2)} + \dots ,$$
$$Df = \epsilon D f^{(1)} + \epsilon^2 D f^{(2)} + \dots . \tag{3.21}$$

Considering only the first order in the above expansion and substituting in Eq. (3.18), the transport equation reduces to

$$p^\mu u_\mu D f_k^{(0)} + p^\mu \nabla_\mu f_k^{(0)} = \sum_{l=1}^{N} \frac{g_l}{1+\delta_{kl}} C_{kl}[f_k^{(1)}]. \tag{3.22}$$

Using conservation equations, the left hand side of the above equation can be simplified to obtain (see

Appendices A and B).

$$\frac{1}{T}f_k^{(0)}(1\pm f_k^{(0)})\left[Q_k\partial\cdot u-\langle p_k^\mu\, p_k^\nu\rangle\langle\partial_\mu u_\nu\rangle\ +\ (p_k^\sigma u_\sigma-h_k)\ p_k^\mu\ \left(\frac{\nabla_\mu T}{T}\right)\right]\ =\ \sum_{l=1}^{N}\ \frac{g_l}{1+\delta_{kl}}\ C_{kl}[f_k^{(1)}]. \quad (3.23)$$

where

$$Q_k=T^2\left[-\frac{1}{3}z_k^2+\tau_k^2\left(\frac{4}{3}-\gamma'\right)+\tau_k\{(\gamma_k''-1)\hat{h}_k-\gamma_k'''\}\right] \quad (3.24)$$

with $z_k=m_k/T$, $\tau_k=(p_k\cdot u)/T$ and $\hat{h}_k=h_k/T$. Here h_k is the enthalpy per particle of type k. The steps connecting Eq. (3.22) to Eq. (3.23) and the expressions for γ's are provided in Appendix B.

In order to proceed further and solve Eq. (3.22) we assume that in the interaction $p_k+p_l\to p_k'+p_l'$, only particles with momentum p_k are out of equilibrium and the remaining ones i.e. particles with momentum p_l, p_k' and p_l' are in equilibrium. This assumption is the well known Relaxation Time Approximation (RTA). Thus substituting $f_k^{(1)}$, $f_l^{(1)}$, $f_k^{(1')}$ and $f_l^{(1')}$ in Eq. (3.19) with $f_k^{(0)}+\delta f_k$, $f_l^{(0)}$, $f_k^{(0')}$ and $f_l^{(0')}$ respectively, the rhs of Eq. (3.22) reduces to

$$\sum_{l=1}^{N}\left(\frac{g_l}{1+\delta_{kl}}\right)C_{kl}[f_k]=-\frac{\delta f_k}{\tau_k}E_k \quad (3.25)$$

where,

$$\tau_k=\sum_{l=1}^{N}\left(\frac{1}{\tau_{kl}^{-1}}\right) \quad (3.26)$$

with

$$\begin{aligned}[\tau_{kl}]^{-1}\ &=\ \left(\frac{g_l}{1+\delta_{kl}}\right)\frac{1}{2E_{p_k}}\int\int\int\frac{d^3p_l}{(2\pi)^3 2E_{p_l}}\frac{d^3p_{k'}}{(2\pi)^3 2E_{p_{k'}}}\frac{d^3p_{l'}}{(2\pi)^3 2E_{p_{l'}}}(2\pi)^4\delta^4\left(p_k+p_l-p_{k'}-p_{l'}\right)|\mathscr{M}_{kl}|^2\\ &\qquad\times\left[\,f_l^{(0)}(1\pm f_{k'}^{(0)})(1\pm f_{l'}^{(0)})\mp(1\pm f_l^{(0)})f_{k'}^{(0)}\,f_{l'}^{(0)}\right]\\ &=\ \left(\frac{g_l}{1+\delta_{kl}}\right)\frac{\mathrm{csh}(\epsilon_k/2)}{E_k}\int\int\int d\Gamma_{p_l}d\Gamma_{p_{k'}}d\Gamma_{p_{l'}}(2\pi)^4\delta^4\left(p_k+p_l-p_{k'}-p_{l'}\right)|\mathscr{M}_{kl}|^2\end{aligned} \quad (3.27)$$

in which, for four-momenta q, $d\Gamma_q=\dfrac{1}{2\mathrm{csh}(\epsilon_k/2)}\dfrac{d^3q}{(2\pi)^2 2E_q}$, $\epsilon_q=\dfrac{E_q-\mu_q}{T}$ and $\mathrm{csh}(\epsilon_q)=\cosh(\epsilon_q)\left(\ \sinh(\epsilon_q)\right)$ if q represents a Fermion(Boson). In the above equations, $\mathscr{M}_{kl}$ is the invariant amplitude for elastic $kl\to kl$ scattering. Following Ref. [3], we will assume $f_{p'}^{(0)}\sim f_p^{(0)}$ and $f_{k'}^{(0)}\sim f_k^{(0)}$ so that we can analytically integrate over the momenta of final particles k' and p' respectively. This results in the expression for the relaxation time as

$$[\tau_k]^{-1}=\sum_{l=1}^{N}\left(\frac{g_l}{1+\delta_{kl}}\right)\int\frac{d^3p_k}{(2\pi)^3}\left(\sigma^{kl}v_{\mathrm{rel}}^{kl}\right)f_l\left(1\pm f_l\right). \quad (3.28)$$

Thus, using the RTA and Eq. (3.7), the transport equation can be reduced to

$$\frac{1}{TE_k}\left[Q_k\ \partial\cdot u\ -\ \langle p_k^\mu\, p_k^\nu\rangle\langle\partial_\mu\ u_\nu\rangle\ +\ (p_k^\sigma u_\sigma-h_k)\ p_k^\mu\ \left(\frac{\nabla_\mu T}{T}\right)\right]=\ -\frac{\phi_k}{\tau_k}. \quad (3.29)$$

Substituting the expression for ϕ_k from Eq. (3.11) in Eq. (3.29) and comparing the coefficients of $(\partial\cdot u)$,

$\langle \partial_\mu u_\nu \rangle$ and $\frac{\nabla_\mu T}{T}$ on both sides the unknown quantities A_k, B^ν_{kq} and $C^{\mu\nu}_k$ is found to be:

$$A_k = -\frac{\tau_k}{TE_k} Q_k \ , \tag{3.30}$$

$$B^{kq}_\nu \ \Delta^{\mu\nu} = \frac{\tau_k}{E_k T} \ (p^\sigma_k u_\sigma - h_k) \ \Delta^{\mu\nu} \ p_{k\nu} \ , \tag{3.31}$$

$$C^{\mu\nu}_k = -\frac{\tau_k}{TE_k} \langle p^\mu_k p^\nu_k \rangle. \tag{3.32}$$

Finally, substituting the values of A_k, B^ν_{kq} and $C^{\mu\nu}_k$ in Eq. (3.17), (3.15) and (3.16) respectively we obtain the final expressions for thermal conductivity, shear and bulk viscosities as

$$\lambda = \frac{1}{3T^2} \sum_{k=1}^{N} \int \frac{d^3p_k}{(2\pi)^3} \ \frac{g_k \tau_k}{E^2_{p_k}} \ p^2_k \ (p^\nu_k u_\nu - h_k)^2 \ f^{(0)}_k (1 \pm f^{(0)}_k), \tag{3.33}$$

$$\eta = \frac{1}{15T} \sum_{k=1}^{N} \int \frac{d^3p_k}{(2\pi)^3} \frac{g_k \tau_k}{E^2_{p_k}} |\vec{p}_k|^4 f^{(0)}_k (1 \pm f^{(0)}_k), \tag{3.34}$$

$$\zeta = \frac{1}{T} \sum_{k=1}^{N} \int \frac{d^3p_k}{(2\pi)^3} \frac{g_k \tau_k}{E^2_{p_k}} Q^2_k f^{(0)}_k (1 \pm f^{(0)}_k). \tag{3.35}$$

It is clear from the above expressions that the relaxation times are the essential dynamical components responsible for dissipative processes occurring in the system evolving towards equilibrium. It is to be noted here that the simplistic approach of treating the collision integral is limited by the fact that it is not possible to have control over the degree of accuracy of the method and neither can one go to higher orders to increase the accuracy as is possible in the Chapman-Enskog (CE) approach. In addition, the latter method involves the transport cross-section with an angular weight of $(1 - \cos^2\theta)$ in first-order calculations which accounts for the momentum transfer in collisions desirable for the evaluation of viscosities which is lacking in the RTA featuring the total cross-section. These aspects have been discussed in [94] and [95] along with a comparison of the two methods for various cases. The study by Wiranata et al [94] reveal that the extent of agreement between the CE and the RTA approaches depend sensitively on the energy dependence of the differential cross sections employed. It was shown that for an interacting pion gas where the cross-section involves the ρ resonance, the ratio of shear viscosities calculated in the CE and RTA methods varies between 1.18 at a temperature of 100 MeV to about 1.1 at 160 MeV.

Since the cross-sections used here have a similar nature as far as the energy dependence is concerned, this not so large disagreement could justify use of the simplistic approach of RTA keeping in mind that the present study is basically aimed at bringing out the relative effect brought about by the in-medium cross-sections on the temperature dependence of the transport coefficients compared to the vacuum ones.

In the next section we consider a system of pion gas and will evaluate the scattering cross-section, σ for a system of pion gas in a thermal medium as σ carries information about all the microscopic dynamics of the system as evident from Eqs. (3.27) and (3.28).

3.2 Scattering cross-section of a pion gas

In order to calculate the scattering cross-section for a system of pion gas we evaluate the matrix elements of $\pi(k)\pi(p) \to \pi(k')\pi(p')$. The $\pi(k)\pi(p) \to \pi(k')\pi(p')$ is considered to be mediated via the ρ and σ resonances. This is done by taking an effective Lagrangian for $\rho\pi\pi$ and $\sigma\pi\pi$ interactions [96]

$$\mathscr{L}_{\rm int} = g_{\rho\pi\pi}\vec{\rho}_\mu \cdot \vec{\pi} \times \partial^\mu \vec{\pi} + \frac{1}{2} g_{\sigma\pi\pi} m_\sigma \vec{\pi} \cdot \vec{\pi}\sigma \ . \tag{3.36}$$

The values of the coupling constants in Eq. (3.36) follow from the experimental decay widths of ρ and σ mesons and we get $g_{\rho\pi\pi} = 6.05$ and $g_{\sigma\pi\pi} = 2.5$. We have made use of isospin basis for expressing the invariant amplitudes in different isospin channels. Denoting the invariant amplitude in a channel with total isospin I by $\mathscr{M}_I^{\pi\pi}$, we get [97]

$$\mathscr{M}_2^{\pi\pi} = g_{\rho\pi\pi}^2 \left[-\left(\frac{s-u}{t-m_\rho^2}\right) - \left(\frac{s-t}{u-m_\rho^2}\right)\right] + 4g_{\sigma\pi\pi}^2 \left[\frac{1}{t-m_\sigma^2} + \frac{1}{u-m_\sigma^2}\right] \tag{3.37}$$

$$\mathscr{M}_1^{\pi\pi} = g_{\rho\pi\pi}^2 \left[2\left(\frac{t-u}{s-m_\rho^2-\Pi_\rho}\right) + \left(\frac{s-u}{t-m_\rho^2}\right) - \left(\frac{s-t}{u-m_\rho^2}\right)\right] + 4g_{\sigma\pi\pi}^2 \left[\frac{1}{t-m_\sigma^2} - \frac{1}{u-m_\sigma^2}\right] \tag{3.38}$$

$$\mathscr{M}_0^{\pi\pi} = g_{\rho\pi\pi}^2 \left[2\left(\frac{s-u}{t-m_\rho^2}\right) + 2\left(\frac{s-t}{u-m_\rho^2}\right)\right] + 4g_{\sigma\pi\pi}^2 \left[\frac{3}{s-m_\sigma^2-\Pi_\sigma} + \frac{1}{t-m_\sigma^2} + \frac{1}{u-m_\sigma^2}\right] \tag{3.39}$$

where $s = (k+p)^2$, $t = (k-k')^2$ and $u = (k-p')^2$ are the Mandelstam variables. The vacuum ρ and σ propagator in the s-channel diagrams is replaced by the complete ones obtained from a Dyson-Schwinger sum involving the one-loop self energies of ρ and σ mesons denoted by Π_ρ and Π_σ respectively. Since we will be calculating isospin averaged cross sections, we define the corresponding isospin averaged invariant amplitude by

$$\overline{|\mathscr{M}|^2} = \sum_I (2I+1)\,|\mathscr{M}_I|^2 \Big/ \sum_I (2I+1) \ , \tag{3.40}$$

which is used to obtain the cross-section from

$$\sigma(s) = \frac{1}{64\pi^2 s}\int d\Omega \overline{|\mathscr{M}|^2} \ . \tag{3.41}$$

In order to evaluate the in-medium scattering cross-section we need to calculate the one-loop self-energies of different hadrons at finite temperature and/or density. In this chapter, we will show the calculation of the one-loop self energy of ρ and σ resonance Π_ρ and Π_σ appearing respectively in Eqs.(3.38) and (3.39). This can be achieved by using quantum field theory in a thermal medium i.e. the thermal field theory. There are two methods available in the literature which is used for studying thermal field theory (TFT)- (i) Imaginary time formalism (ITF) and (ii) Real time formalism (RTF). The difference between the two formalisms involves in the form of the propagators. In the ITF, the propagators are written as a sum over frequencies known as Matsubara frequency, a consequence of the finite interval of imaginary time resulting

in the discrete Matsubara frequencies. However, in the RTF the propagator is a 2×2 matrix owing to the two infinite intervals of time. In this thesis, RTF of TFT has been used to evaluate the one-loop self energies of the hadrons. In the next section we briefly describe the thermal propagators for different fields.

3.3 Thermal Propagators

For a general field $\phi_l(x)$, the free thermal propagator is defined as

$$D_{ll'}(x, x') = i\left\langle \mathcal{T}_C\left\{\phi_l(x)\,\phi_{l'}^{\dagger}(x')\right\}\right\rangle \tag{3.42}$$

where $\langle\rangle$ denotes ensemble average. The temporal component τ and τ' respectively take complex values on the contour C in complex time plane. The ensemble average of products of various fields converges in the domain $-\beta \leq \mathrm{Im}(\tau - \tau') \leq 0$ where β is the inverse temperature. This condition defines the region of analyticity and puts restriction on the time contour C. The contour chosen is shown in Fig. 3.1. This

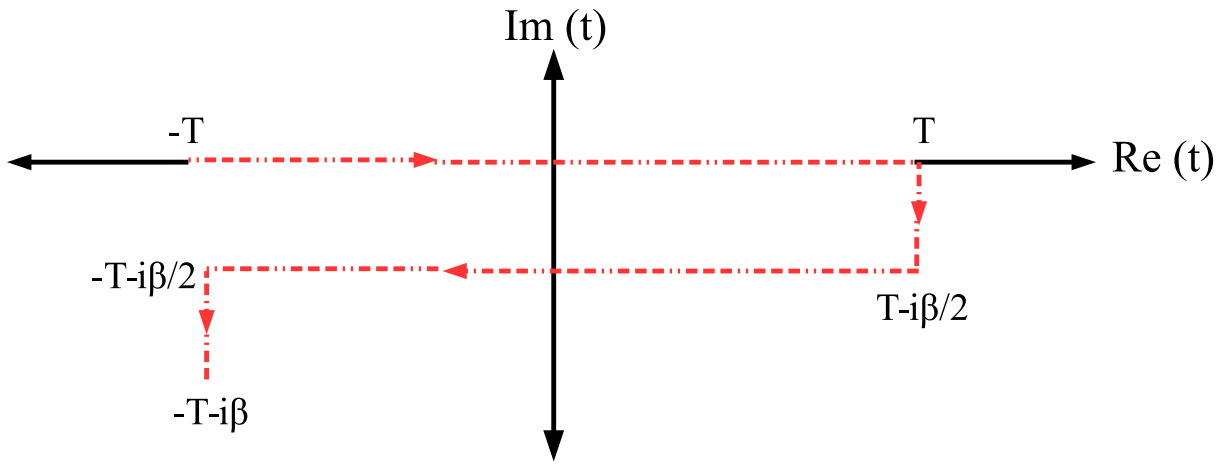

Figure 3.1: The contour C in the complex time plane for RTF with $T \to \infty$

particular choice of the time contour breaks up the propagator into pieces with points on different segment of the contour. If τ_h and τ_v are points respectively on the horizontal and vertical segments, the pieces, $D_{ll'}\left(\vec{x}, \vec{x'}; \tau_h, \tau_v\right) \to 0$ by Riemann-Lebesgue lemma. The contour essentially reduces to two parallel lines, one being the real axis and the other shifted from it by $-i\beta/2$. The points on this two lines are denoted by subscripts 1 and 2 respectively so that $\tau_1 = t$ and $\tau_2 = t - i\beta/2$. The propagator then consists of four pieces and may be put into the form of 2×2. The Fourier transform of each component can be written as

$$\begin{aligned}\begin{bmatrix} D_{ll'}\left(\vec{x}, \vec{x'}; t, t'\right) & D_{ll'}\left(\vec{x}, \vec{x'}; t, t' - i\beta/2\right) \\ D_{ll'}\left(\vec{x}, \vec{x'}; t - i\beta/2, t'\right) & D_{ll'}\left(\vec{x}, \vec{x'}; t', t\right) \end{bmatrix} \\ = \int \frac{d^3q}{(2\pi)^3} e^{-iq.(t-t')} e^{i\vec{q}.\left(\vec{x}-\vec{x'}\right)} \boldsymbol{D}_{ll'}(q)\end{aligned} \tag{3.43}$$

where $\boldsymbol{D}_{ll'}(q)$ is the momentum space thermal propagator matrix. We will briefly dicuss the forms of

momentum space thermal propagator matrices for different spin fields.

For a real scalar field, the momentum space thermal propagator matrix is given by $\boldsymbol{D}(k)$ is given by

$$\boldsymbol{D}(k) = \begin{bmatrix} \left(1+n^k\right)\Delta_F - n^k\Delta_F^* & \sqrt{n^k\left(1+n^k\right)}\left(\Delta_F - \Delta_F^*\right) \\ \sqrt{n^k\left(1+n^k\right)}\left(\Delta_F - \Delta_F^*\right) & n^k\Delta_F - \left(1+n^k\right)\Delta_F^* \end{bmatrix} \tag{3.44}$$

where, $\Delta_F = \frac{-1}{k^2-m^2+i\epsilon}$ and n_k is the single particle Bose-Einstein thermal distribution function

$$n^k(\omega, T) = \left[e^{\beta\omega} - 1\right]^{-1} \tag{3.45}$$

with $\omega = \sqrt{\vec{k}^2 + m^2}$. Eq. (3.44) can be diagonalized as follows

$$\boldsymbol{D}(k) = \boldsymbol{U}_0 \begin{bmatrix} \Delta_F & 0 \\ 0 & -\Delta_F^* \end{bmatrix} \boldsymbol{U}_0 \tag{3.46}$$

where,

$$\boldsymbol{U}_0(\omega, T) = \begin{bmatrix} \sqrt{1+n^k} & \sqrt{n^k} \\ \sqrt{n^k} & \sqrt{1+n^k} \end{bmatrix}. \tag{3.47}$$

Although the free thermal propagators are 2×2 matrices, only the 11-component will be needed for our calculations. The 11-component of the thermal propagator matrix for a scalar field $D_{11}(k)$

$$\left.\begin{aligned} D_{11}(k) &= \Delta_F(k,m) + 2\pi i N_1^2(k,m)\,\delta\left(k^2 - m^2\right) \\ &= \Delta_F(k,m) + 2iN_1^2(k,m)\,\mathrm{Im}\;\Delta_F(k,m) \end{aligned}\right\} \tag{3.48}$$

The momentum space propagator matrix for a complex field is

$$\boldsymbol{D}(k) = \boldsymbol{U} \begin{bmatrix} \Delta_F & 0 \\ 0 & -\Delta_F^* \end{bmatrix} \boldsymbol{U}\ , \tag{3.49}$$

where the diagonalizing matrix $\boldsymbol{U}$ containing chemical potential to account for conserved charges is given by

$$\boldsymbol{U}(\omega, T, \mu) = \begin{bmatrix} N_2 & N_1 e^{\beta\mu/2} \\ N_1 e^{-\beta\mu/2} & N_2 \end{bmatrix}. \tag{3.50}$$

where,

$$\left.\begin{aligned} N_1(k,m) &= \Theta(k_0)\sqrt{n_+^k} + \Theta(-k_0)\sqrt{n_-^k} \\ N_2(k,m) &= \Theta(k_0)\sqrt{1+n_+^k} + \Theta(-k_0)\sqrt{1+n_-^k} \end{aligned}\right\} \tag{3.51}$$

with $n_\pm^k$ being the Bose-Einstein distribution functions for particles and antiparticles,

$$n_\pm^k(\omega, T, \mu) = \left[e^{\beta(\omega\mp\mu)} - 1\right]^{-1}\ . \tag{3.52}$$

The 11-component of the thermal propagator matrix for a complex scalar field $\tilde{D}_{11}(p)$ is

$$\left.\begin{aligned}\tilde{D}_{11}(p) &= \Delta_F(p,m) - 2\pi i \tilde{N}_1^2(p,m)\,\delta\left(p^2-m^2\right) \\ &= \Delta_F(p,m) - 2i\tilde{N}_1^2(p,m)\,\mathrm{Im}\;\Delta_F(p,m)\end{aligned}\right\}. \tag{3.53}$$

Similarly, the Dirac thermal propagator matrix can be written as,

$$\boldsymbol{S}(p) = (\not{p}+m)\,\boldsymbol{V}\begin{bmatrix}\Delta_F & 0\\ 0 & -\Delta_F^*\end{bmatrix}\boldsymbol{V} \tag{3.54}$$

where,

$$\boldsymbol{V}(\omega,T,\mu) = \begin{bmatrix}\tilde{N}_2 & \tilde{N}_1 e^{\beta\mu/2}\\ \tilde{N}_1 e^{-\beta\mu/2} & \tilde{N}_2\end{bmatrix} \tag{3.55}$$

with,

$$\left.\begin{aligned}\tilde{N}_1(p,m) &= \Theta(p_0)\sqrt{\tilde{n}_+^p} + \Theta(-p_0)\sqrt{\tilde{n}_-^p} \\ \tilde{N}_2(p,m) &= \Theta(p_0)\sqrt{1+\tilde{n}_+^p} + \Theta(-p_0)\sqrt{1+\tilde{n}_-^p}\;.\end{aligned}\right\} \tag{3.56}$$

$\tilde{n}_\pm^p$ are the Fermi-Dirac distribution functions for particles and antiparticles

$$\tilde{n}_\pm^p(\omega,T,\mu) = \left[e^{\beta(\omega\mp\mu)}+1\right]^{-1}\;. \tag{3.57}$$

Thus, the 11-component of the thermal propagator matrix for a Dirac field $S_{11}(p)$ is

$$S_{11}(p) = (\not{p}+m)\tilde{D}_{11}(p) \tag{3.58}$$

For a real vector field the thermal propagator matrix is

$$\boldsymbol{D}^{\alpha\beta}(k) = V^{\alpha\beta}\boldsymbol{U}_0\begin{bmatrix}\Delta_F & 0\\ 0 & -\Delta_F^*\end{bmatrix}\boldsymbol{U}_0 \tag{3.59}$$

whereas for a complex vector field it is

$$\boldsymbol{D}^{\alpha\beta}(k) = V^{\alpha\beta}\boldsymbol{U}\begin{bmatrix}\Delta_F & 0\\ 0 & -\Delta_F^*\end{bmatrix}\boldsymbol{U} \tag{3.60}$$

with $V^{\alpha\beta}(k) = \left(-g^{\alpha\beta}+\frac{k^\alpha k^\beta}{m^2}\right)$. The 11-component of the thermal propagator matrix for a vector field $D_{11}^{\alpha\beta}(k)$ is

$$D_{11}^{\alpha\beta}(k) = V^{\alpha\beta}(k)D_{11}(k)\,. \tag{3.61}$$

For the spin-$\frac{3}{2}$ particle which is described by the Rarita-Schwinger field, the thermal propagator matrix is given by

$$\boldsymbol{S}^{\alpha\beta}(p) = R^{\alpha\beta}\boldsymbol{V}\begin{bmatrix}\Delta_F & 0\\ 0 & -\Delta_F^*\end{bmatrix}\boldsymbol{V} \tag{3.62}$$

where,

$$R^{\alpha\beta}(p) = (\not{p}+m)\left\{-g^{\alpha\beta}+\frac{2}{3m^2}p^\alpha p^\beta+\frac{1}{3}\gamma^\alpha\gamma^\beta+\frac{1}{3m}\left(\gamma^\alpha p^\beta-\gamma^\beta p^\alpha\right)\right\}. \tag{3.63}$$

The 11-component of the thermal propagator matrix for a vector field $S_{11}^{\alpha\beta}(p)$ is

$$S_{11}^{\alpha\beta}(p) = R^{\alpha\beta}(p)\,\tilde{D}_{11}(p) \tag{3.64}$$

Let us consider the two-point correlation functions of general currents $J_l(x)$ and $J_{l'}^\dagger(x')$ defined through

$$G_{ll'}(x,x') = i\left\langle \mathcal{T}_C\left\{J_l(x)\,J_{l'}^\dagger(x')\right\}\right\rangle . \tag{3.65}$$

The currents may be composed of free fields or interacting ones and also may be Bosonic or Fermionic (the time-ordering is taken accordingly). Due to the choice of the time contour C as of Fig. 3.1, the correlation function becomes a 2×2 matrix and can be Fourier transformed as,

$$\begin{bmatrix} G_{ll'}\left(\vec{x},\vec{x'};t,t'\right) & G_{ll'}\left(\vec{x},\vec{x'};t,t'-i\beta/2\right)\\ G_{ll'}\left(\vec{x},\vec{x'};t-i\beta/2,t'\right) & G_{ll'}\left(\vec{x},\vec{x'};t',t\right)\end{bmatrix} = \int\frac{d^4q}{(2\pi)^4}e^{-iq.(t-t')}e^{i\vec{q}.\left(\vec{x}-\vec{x'}\right)}\boldsymbol{G}_{ll'}(q) \tag{3.66}$$

where, $\boldsymbol{G}_{ll'}(q)$ is the momentum space correlator matrix. We now introduce the spectral functions $\Gamma_{ll'}^{\mp}(q)$ (- for Bosonic, + for Fermionic) as the Fourier transform of the commutator/anti-commutator as

$$\Gamma_{ll'}^{\mp}(q) = \int_{-\infty}^{+\infty}\frac{dt}{2\pi}\int\frac{d^3x}{(2\pi)^3}e^{iq^0\cdot(t-t')}e^{-i\vec{q}\cdot\left(\vec{x}-\vec{x'}\right)}\left\langle\left[J_l(t,\vec{x}),J_{l'}^\dagger\left(t',\vec{x'}\right)\right]_{\mp}\right\rangle . \tag{3.67}$$

The momentum space correlator matrix $\boldsymbol{G}_{ll'}(q)$ can be written in a diagonal form in terms of the spectral function as

$$\begin{aligned}\boldsymbol{G}_{ll'}(q) &= \int_{-\infty}^{+\infty}\frac{dq_0'}{2\pi}\Gamma_{ll'}^{\mp}\left(q_0',\vec{q}\right)\times\\ &\quad \boldsymbol{W}(|q_0|)\begin{bmatrix}\frac{1}{q_0'-q_0-i\epsilon\ \mathrm{sign}(q_0)} & 0\\ 0 & \frac{-1}{q_0'-q_0+i\epsilon\ \mathrm{sign}(q_0)}\end{bmatrix}\boldsymbol{W}(|q_0|)\\ &= \boldsymbol{W}(|q_0|)\begin{bmatrix}\overline{G}_{ll'}(q) & 0\\ 0 & -\overline{G}_{ll'}^*(q)\end{bmatrix}\boldsymbol{W}(|q_0|) \qquad (3.68)\\ &= \boldsymbol{W}(|q_0|)\,\overline{\boldsymbol{G}}_{ll'}\boldsymbol{W}(|q_0|) \qquad (3.69)\end{aligned}$$

where, the diagonalizing matrix $\boldsymbol{W} = \boldsymbol{U}$ for Bosonic currents and $\boldsymbol{W} = \boldsymbol{V}$ for Fermionic currents respectively and the diagonal matrix correlator is given by

$$\overline{\boldsymbol{G}}_{ll'} = \begin{bmatrix} \overline{G}_{ll'}(q) & 0 \\ 0 & -\overline{G}^{*}_{ll'}(q) \end{bmatrix} \tag{3.70}$$

with the diagonal element

$$\overline{G}_{ll'}\left(q^0, \vec{q}\right) = \int_{-\infty}^{+\infty} \frac{dq'_0}{2\pi} \frac{\Gamma^{\mp}_{ll'}\left(q'_0, \vec{q}\right)}{q'_0 - q_0 - i\epsilon \ \mathrm{sign}\left(q_0\right)} \ . \tag{3.71}$$

It is to be noted that, the general (interacting) two-point matrix correlator is diagonalized by the same matrix $\boldsymbol{U}$ or $\boldsymbol{V}$ which diagonalize the free thermal propagator. To obtain the diagonal element it is sufficient to know any one, say the 11-component of the matrix $\boldsymbol{G}_{ll'}$ since they are related by

$$\mathrm{Re}\ \overline{G}_{ll'}(q) = \mathrm{Re}\ G^{11}_{ll'} \tag{3.72}$$

$$\mathrm{Im}\ \overline{G}_{ll'}(q) = \begin{cases} \mathrm{sign}\left(q_0\right) \tanh\left\{\frac{\beta}{2}\left(q_0 - \mu\right)\right\} \mathrm{Im}\ G^{11}_{ll'} & \text{(Bosonic)} \\ \mathrm{sign}\left(q_0\right) \coth\left\{\frac{\beta}{2}\left(q_0 - \mu\right)\right\} \mathrm{Im}\ G^{11}_{ll'} & \text{(Fermionic)} \ . \end{cases} \tag{3.73}$$

Let us first consider the complete (interacting) scalar matrix propagator. It can be generalized for higher spins also. The complete propagator $\boldsymbol{D'}(k)$ is obtained by summing up loop diagrams perturbatively leading to the Dyson-Schwinger equation

$$\boldsymbol{D'}(k) = \boldsymbol{D}(k) - \boldsymbol{D}(k)\,\boldsymbol{\Pi}(k)\,\boldsymbol{D'}(k) \tag{3.74}$$

where, $\boldsymbol{D}(k)$ is the free scalar matrix propagator and $\boldsymbol{\Pi}(k)$ is the 1-loop thermal self energy matrix. As discussed in the previous section, being a two-point correlator matrix, $\boldsymbol{D'}(k)$ and $\boldsymbol{D}(k)$ are diagonalized by the same matrix $\boldsymbol{U}\left(\left|k^0\right|\right)$ i.e.

$$\boldsymbol{D'}(k) = \boldsymbol{U}\left(\left|k^0\right|\right) \overline{\boldsymbol{D'}}(k)\, \boldsymbol{U}\left(\left|k^0\right|\right) \tag{3.75}$$

$$\boldsymbol{D}(k) = \boldsymbol{U}\left(\left|k^0\right|\right) \overline{\boldsymbol{D}}(k)\, \boldsymbol{U}\left(\left|k^0\right|\right) \tag{3.76}$$

where

$$\overline{\boldsymbol{D}}(k) = \begin{bmatrix} \Delta_F(k) & 0 \\ 0 & -\Delta^{*}_F(k) \end{bmatrix}. \tag{3.77}$$

Using the above equations, we get

$$\overline{\boldsymbol{D'}}(k) = \overline{\boldsymbol{D}}(k) - \overline{\boldsymbol{D}}(k)\,\overline{\boldsymbol{\Pi}}(k)\,\overline{\boldsymbol{D'}}(k) \tag{3.78}$$

where we have used

$$\boldsymbol{\Pi}(k) = \boldsymbol{U}^{-1}\left(\left|k^0\right|\right) \overline{\boldsymbol{\Pi}}(k)\, \boldsymbol{U}^{-1}\left(\left|k^0\right|\right) \ . \tag{3.79}$$

Hence the diagonal element of the complete propagator satisfies

$$\overline{D'}\left(k\right)=\overline{D}\left(k\right)-\overline{D}\left(k\right)\overline{\Pi}\left(k\right)\overline{D'}\left(k\right) \tag{3.80}$$

which is an ordinary algebraic equation and has the solution

$$\overline{D'}\left(k\right)=\left(\frac{-1}{k^2-m^2-\overline{\Pi}\left(k\right)}\right). \tag{3.81}$$

The diagonalized Dyson-Schwinger equation for field containing spin/polaization/Lorentz indices becomes

$$\overline{G'}_{ll'}\left(k\right)=\overline{G}_{ll'}\left(k\right)-\overline{G}_{lj}\left(k\right)\overline{\Pi}^{jj'}\left(k\right)\overline{G'}_{j'l'}\left(k\right)\ . \tag{3.82}$$

The above equation is quite non-trivial to solve for fields which contain arbitrary number of indices in the set l. However, we can take spin/polarization averages to obtain the scalar form of the self energy and propagators and hence use Eq. (3.81) to calculate the complete propagator.

3.4 One-loop self energy of ρ and σ

In this section we will evaluate the one-loop self energy of ρ and σ resonances, Π_ρ and Π_σ appearing respectively in Eqs.(3.38) and (3.39). Contributions to Π_h ($h\in\{\rho,\sigma\}$) come from different loop graphs containing other hadrons (i,j). In a most general notation, the real part of the self energy reads

$$\begin{aligned}\text{Re }\Pi_h(q) \;=\; & \sum_{\{i,j\}\in\{\text{loops}\}}\int\frac{d^3k_i}{(2\pi)^3}\frac{1}{2\omega_{k_i}\omega_{p_j}}\mathcal{P}\left[\left(\frac{n_+^{k_i}\omega_{p_j}\mathcal{N}_{ij}^h(k_i^0=\omega_{k_i})}{(q_0-\omega_{k_i})^2-\omega_{p_j}^2}\right)+\left(\frac{n_-^{k_i}\omega_{p_j}\mathcal{N}_{ij}^h(k_i^0=-\omega_{k_i})}{(q_0+\omega_{k_i})^2-\omega_{p_j}^2}\right)\right.\\ & \left.-\left(\frac{a_j n_+^{p_j}\omega_{k_i}\mathcal{N}_{ij}^h(k_i^0=q_0-\omega_{p_j})}{(q_0-\omega_{p_j})^2-\omega_{k_i}^2}\right)-\left(\frac{a_j n_-^{p_j}\omega_{k_i}\mathcal{N}_{ij}^h(k_i^0=q_0+\omega_{p_j})}{(q_0+\omega_{p_j})^2-\omega_{k_i}^2}\right)\right]\end{aligned} \tag{3.83}$$

whereas the imaginary part is

$$\begin{aligned}\text{Im }\Pi_h(q) \;=\; & -\pi\epsilon(q_0)\sum_{\{i,j\}\in\{\text{loops}\}}\int\frac{d^3k_i}{(2\pi)^3}\frac{1}{4\omega_{k_i}\omega_{p_j}}\\ & \times\left[\mathcal{N}_{ij}^h(k_i^0=\omega_{k_i})\left\{(1+n_+^{k_i}-a_jn_+^{p_j})\delta(q_0-\omega_{k_i}-\omega_{p_j})+(-n_+^{k_i}-a_jn_-^{p_j})\delta(q_0-\omega_{k_i}+\omega_{p_j})\right\}\right.\\ & \left.+\mathcal{N}_{ij}^h(k_i^0=-\omega_{k_i})\left\{(-1-n_-^{k_i}+a_jn_-^{p_j})\delta(q_0+\omega_{k_i}+\omega_{p_j})+(n_-^{k_i}+a_jn_+^{p_j})\delta(q_0+\omega_{k_i}-\omega_{p_j})\right\}\right]\end{aligned} \tag{3.84}$$

where, the distribution functions for loop particles are given by $n_\pm^{k_i}=\left[e^{\beta\left(\omega_{k_i}\mp\mu_i\right)}\mp1\right]^{-1}$ (according to boson/fermion) with $\omega_{k_i}=\sqrt{\vec{k}_i^2+m_i^2}$. In the above equations, i-type particles are always bosons and $a_j=\mp1$ depending upon whether the j-type particle is a boson/fermion. The self energy may contain additional Lorentz/Dirac indices, however in this work we have used the spin/polarization averaged self energies for the calculation of the S-matrix elements. The ρ self energy consists of $\{i,j\}=\{\pi,\pi\}$, $\{\pi,\omega\}$, $\{\pi,h_1\}$ and $\{\pi,a_1\}$ loops whereas the σ self energy has contribution from only $\{i,j\}=\{\pi,\pi\}$ loop. The

detailed expressions of $\mathcal{N}_{ij}^{\rho}$ and $\mathcal{N}_{ij}^{\sigma}$ can be read from Ref. [97]. The four different terms containing the Dirac delta functions in imaginary part of the self energy correspond to different physical processes like decay and scattering owing to the annihilation of hadron h in the thermal medium.

3.5 Numerical Results

In this section we have discussed the numerical results for shear viscosity of a pion gas in a thermal medium evaluated using the formalism discussed so far.

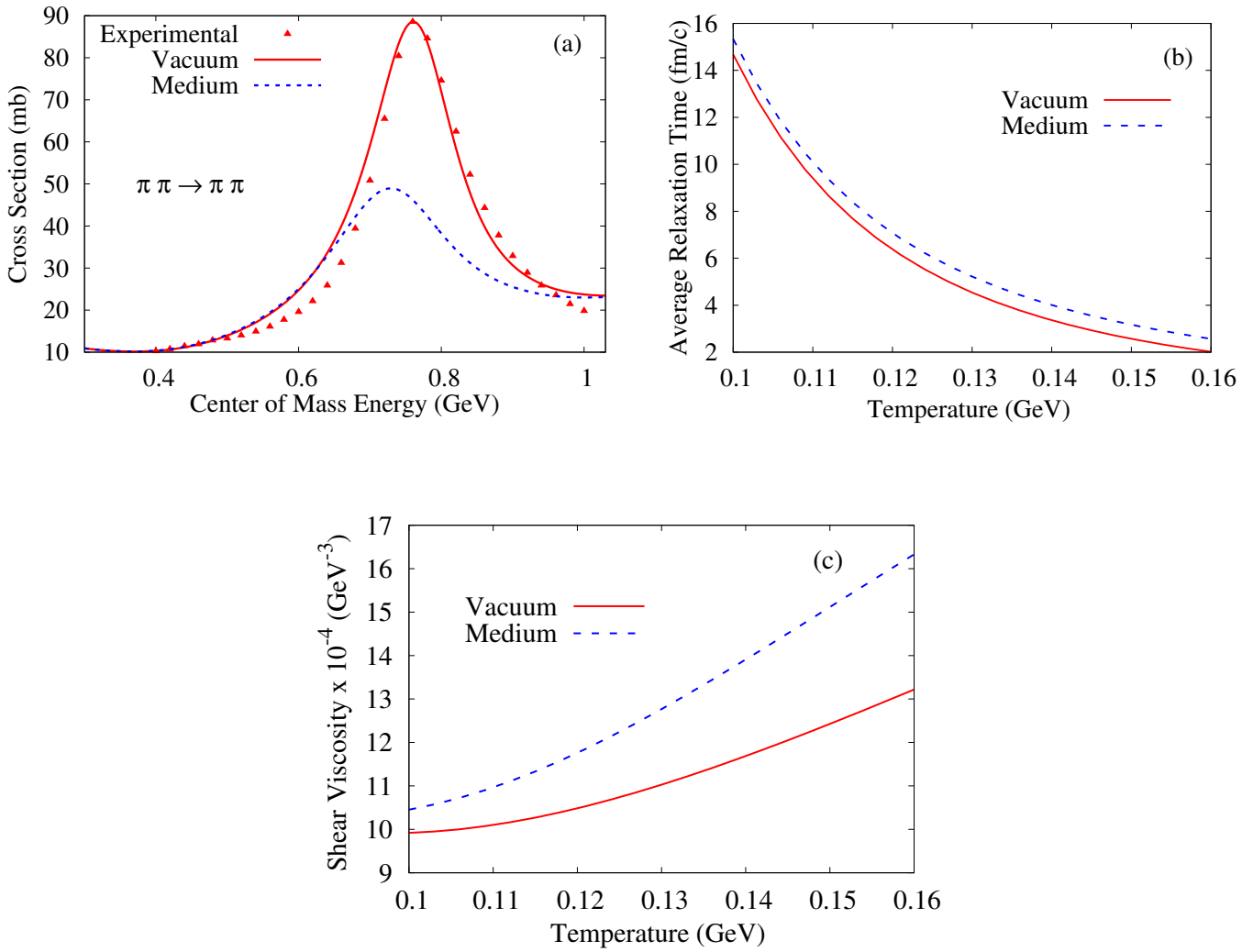

Figure 3.2: (a) The $\pi\pi \to \pi\pi$ elastic scattering cross section as a function of centre of mass energy compared among experiment, vacuum and medium corresponding to $T = 160$ MeV. Experimental data have been taken from Ref. [3] (b) The average relaxation time of $\pi\pi \to \pi\pi$ compared among vacuum and medium. (c) Shear viscosity of a pion system compared among vacuum and medium.

In Fig.3.2(a) we observe that the in-medium elastic cross-section of the pion system is less compared to its vacuum counterpart. This is due to the spectral broadening of the ρ and σ resonances in the thermal medium which is reflected in the suppression of the in-medium cross-section. From Fig.3.2(b) it can be seen that the in-medium relaxation times are significantly larger compared to the vacuum values. This is due to the additional decay and scattering experienced by the ρ and σ in the thermal medium. As seen in

Eq.(3.34), shear viscosity is directly proportional to the relaxation time. Hence, it is natural that the use of in-medium relaxation time will show an increase in its magnitude as observed in Fig.3.2(c).

This difference in magnitude of the quantities evaluated in vacuum and thermal-medium has provided motivation to make a detailed study of the transport coefficients in a medium using the medium dependent cross-section. In the next chapter we will make a detail study of thermal conductivity, shear viscosity and bulk viscosity of a pion-nucleon-kaon (πKN) mixture.

Chapter 4

Viscous coefficients and thermal conductivity of a πKN gas mixture in the medium

The STAR data on elliptic flow of charged hadrons in Au+Au collisions at $\sqrt{s} = 200$ GeV per nucleon pair could be described (see e.g. [1]) using very small but finite values of shear viscosity over entropy density ratio η/s in viscous hydrodynamic simulations, thus clearly indicating that the matter produced in relativistic heavy ion collision behaves more like a strongly interacting liquid than a weakly interacting gas. The viscous coefficients namely shear viscosity and bulk viscosity are useful signatures of phase transition or cross-over between quark and hadronic matter. The kinematic viscosity (η/s) shows a minimum near QGP to hadronic phase transition temperature T_c [98, 99, 100, 101], close to the lower bound [102], whereas ζ/s shows large or diverging [103, 104, 105, 99] values around T_c. Thus the effects of dissipative processes have a significant influence on the hydrodynamical evolution of the matter produced in relativistic heavy ion collisions [106]. The hadrons which are produced during the later stages of the heavy ion collisions will be at a high temperature and presumably also at finite baryon density (CBM experiment at FAIR), thus making it important to consider medium effects in the scattering cross-section which is responsible for the dissipative phenomena.

In this chapter, we have considered a gas mixture consisting of the pions, kaons and nucleons. For this three component mixture we have considered the effect of the thermal medium on the relaxation times and consequently the thermal conductivity and viscous coefficients of the pion system, pion-kaon system and the pion-kaon-nucleon system in the ambit of kinetic theory approach. The expressions for these coefficients have been taken from chapter 3. We have estimated the in-medium scattering cross-sections for $\pi\pi$, πK and πN scattering. The $\pi\pi$, πK and πN interactions are dominated by the ρ, K^* and Δ resonances respectively. The propagation of these resonances gets modified in the thermal medium. The effective propagator in thermal medium is evaluated using the techniques discussed in chapter 3. The effective propagator is then used in the matrix elements to obtain the in-medium cross-sections of scattering which turn out to be significantly

different compared to their vacuum versions usually used in the literature. The in-medium cross-section is then used to obtain the transport coefficients.

Viscous coefficients have been studied both for quark and hadronic matter [107, 3, 108, 109, 110, 111, 112, 103, 113, 98, 104, 114, 4, 101, 115, 105, 116, 99, 117, 118, 119, 120, 121, 122, 123, 124, 125, 126, 127, 128]. In general, there are two different formalisms for evaluating the transport coefficients of a medium-one is the kinetic theory approach [129, 130, 90] where one solves the Boltzmann transport equation, the other being the Kubo formalism [131, 132] where one calculates the in-medium spectral functions in the long wavelength limit. In Kubo formalism a resummation of all the complicated higher-loop diagrams needs to be performed as a naive skeleton expansion in terms of thermal width may have convergence issues as was demonstrated in Refs. [133, 134]. However, the kinetic theory approach is computationally more efficient in evaluating T_c.

In one of the earlier works [107] the viscosities and thermal conductivities of both deconfined as well as hadronic matter have been estimated using relaxation time approximation (RTA) in which a variational approach is used to determine the relaxation times. Transport coefficients of a single component bosonic system were calculated in [108] employing Chapman-Enskog method to first order where the Bose-Einstein distribution function was used instead of the classical one. Pions being the most abundant species of the hadron gas produced in heavy ion collisions at RHIC and LHC [38], a large number of works can be found in the literature considering a system of only pions in the study of transport coefficients [105, 135, 136, 137]. Multicomponent hadronic systems, have been reported in Refs. [3, 110, 112, 138]. In one of the earlier works Ref. [109], Uehling-Uhlenbeck equation is solved to obtain the shear viscosity of a pion gas and the $\pi\pi$ scattering cross section has obtained from chiral perturbation theory. Similar calculations for a multicomponent hadronic mixture (composed of π, K and η mesons) were performed in Ref. [110]. The occurence of minima of η/s evaluated using linear sigma model has been reported in Ref. [112] and Refs. [104, 116] has shown the occurence of maxima of the bulk viscosity to entropy density ratio (ζ/s) near the phase transition.

Such behaviour of both shear and bulk viscosities near the phase transition is also reported in Ref. [99] using parton-hadron-string dynamics (PHSD) off-shell transport approach. In Ref. [114] viscosities of a Hadron resonance gas (HRG) has been evaluated and an upper bound of the η/s near the transition temperature has been obtained. Transport coefficients of hot quark matter and their behaviour near the chiral phase transition has been evaluated using the Nambu Jona-Lasinio (NJL) model in Ref [101]. In Refs. [105, 139], Kubo formalism has been used to study the viscosity of a pion gas and that of a QCD matter in Ref. [103]. In [126, 127, 128] this formalism has been used to estimate the shear viscous coefficient in a hadronic gas mixture of pions and nucleons. The thermal widths used in these calculations arise from the Landau damping of the hadrons in the thermal medium resulting from $2 \to 1$ scattering. Wiranata et al [140] have evaluated η/s in a hadronic resonance gas with resonances up to a mass 2 GeV formed by interactions among the components of a $\pi KN\eta$ mixture and have also shown that the inclusion of more resonances in a multicomponent mixture decreases the value of shear viscosity along with an increase in entropy density which combinedly decreases η/s with an increasing temperature.

In Sec.4.1 the invariant amplitudes for scattering cross-section has been discussed which is followed the discussion on numerical results of the transport coefficients in Sec.4.2

4.1 Invariant Amplitudes

The calculation of the invariant amplitudes for $\pi(k)N(p) \to \pi(k')N(p')$, $\pi(k)K(p) \to \pi(k')K(p')$ and $K(k)K(p) \to K(k')K(p')$ is done by taking an effective Lagrangian like in the case of pions in Sec. 3.2. In this case the interaction Lagrangians read [141, 142]

$$\mathscr{L}_{\pi N\Delta} = \frac{f_{\pi N\Delta}}{m_\pi}\bar{\Delta}_\alpha \mathcal{O}^{\alpha\mu}\vec{\boldsymbol{T}}^\dagger \cdot \partial_\mu \vec{\pi}\Psi + \text{Hermitian Conjugate} \tag{4.1}$$

$$\mathscr{L}_{\pi KK^*} = ig_{\pi KK^*}\overline{K}^*_\mu \vec{\boldsymbol{\tau}} \cdot \left[K\left(\partial^\mu \vec{\pi}\right) - \left(\partial^\mu K\right)\vec{\pi}\right] + \text{Hermitian Conjugate} \tag{4.2}$$

$$\mathscr{L}_{KK\phi} = ig_{KK\phi}\left[\overline{K}(\partial_\mu K) - (\partial_\mu \overline{K})K\right]\phi^\mu \ . \tag{4.3}$$

where, $\Delta^\mu = \begin{bmatrix} \Delta^{++} \\ \Delta^{+} \\ \Delta^{0} \\ \Delta^{-} \end{bmatrix}^\mu$ is the Δ isospin quadruplet, $\Psi = \begin{bmatrix} p \\ n \end{bmatrix}$, $K = \begin{bmatrix} K^+ \\ K^0 \end{bmatrix}$ and $K^*_\mu = \begin{bmatrix} K^{*+} \\ K^{*0} \end{bmatrix}_\mu$ are respectively the isospin doublets for the nucleon, Kaon and K^*. The coupling constants are analogously fixed from the experimental decay widths of Δ and K^* and we get $f_{\pi N\Delta} = 2.8$, $g_{\pi KK^*} = 10.80$. The invariant amplitudes in different isospin channels are given by

$$\left|\mathscr{M}^{\pi N}_{3/2}\right|^2 = \frac{1}{2}\left(\frac{f_{\pi N\Delta}}{m_\pi}\right)^4 \left[\frac{T_s}{\left|s - m^2_\Delta - \Pi_\Delta\right|^2} + \frac{T_u}{\left(u - m^2_\Delta\right)^2} + \frac{2T_m(s - m^2_\Delta - \mathrm{Re}\Pi_\Delta)}{3(u - m^2_\Delta)\left|s - m^2_\Delta - \Pi_\Delta\right|^2}\right], \tag{4.4}$$

$$\left|\mathscr{M}^{\pi N}_{1/2}\right|^2 = \frac{1}{2}\left(\frac{f_{\pi N\Delta}}{m_\pi}\right)^4 \left(\frac{16}{9}\right)\left[\frac{T_u}{\left(u - m^2_\Delta\right)^2}\right], \tag{4.5}$$

$$\mathscr{M}^{\pi K}_{3/2} = 2g^2_{\pi KK^*}\left[\frac{(t-s) + (m^2_k - m^2_\pi)/m^2_{K^*}}{u - m^2_{K^*}}\right], \tag{4.6}$$

$$\mathscr{M}^{\pi K}_{1/2} = g^2_{\pi KK^*}\left[3\frac{(t-u) + (m^2_k - m^2_\pi)/m^2_{K^*}}{s - m^2_{K^*} - \Pi_{K^*}} - \frac{(t-s) + (m^2_k - m^2_\pi)/m^2_{K^*}}{u - m^2_{K^*}}\right], \tag{4.7}$$

$$\mathscr{M}^{KK}_1 = g^2_{KK\phi}\left[\frac{u-s}{t - m^2_\phi} + \frac{t-s}{u - m^2_\phi}\right], \tag{4.8}$$

$$\mathscr{M}^{KK}_0 = g^2_{KK\phi}\left[\frac{u-s}{t - m^2_\phi} - \frac{t-s}{u - m^2_\phi}\right] \tag{4.9}$$

where, T_s, T_u and T_m contain traces over Dirac matrices and details can be found in Ref. [143]. In the above equations, Π_Δ and Π_{K^*} are the one-loop self energies of Δ and K^* which will be obtained in the next section. It is worth mentioning that, to take into account the finite size effect of the hadrons we have considered hadronic form factors $F(p,k) = \Lambda^2\left[\Lambda^2 + \frac{(p\cdot k)^2}{m^2_p} - k^2\right]^{-1}$ in each of the $\pi N\Delta$ and πKK^* vertices where p is the momentum of nucleon/kaon and k is the momentum of pion. In this work we have taken $\Lambda_{\pi N} = 600$ MeV and $\Lambda_{\pi K} = 350$ MeV. In Eqs. (4.4) and (4.5), we have made an average over initial spin states and

a sum over final spin states of the nucleon. The invariant amplitude of $\pi(k)\pi(p) \to \pi(k')\pi(p')$ has been discussed in chapter 3. Using the isospin averaged invariant amplitude $\overline{|\mathscr{M}|^2}$ the scattering cross-section for each of the processes is evaluated.

The real and imaginary part of one-loop self energies Π_Δ and Π_{K^*} appearing in Eqs. (4.4) and (4.7) can be read off from Eqs. (3.83) and (3.84) in Sec. 3.4. For Δ self energy, we consider loop graphs containing $\{i,j\} = \{\pi, N\}$, $\{\rho, N\}$, $\{\pi, \Delta\}$ and $\{\rho, \Delta\}$ and detailed expressions of $\mathcal{N}_{ij}^{\Delta}$ may be found in Ref. [143]. For the K^*, the contribution to the self energy comes from $\{i,j\} = \{\pi, K\}$ and $\mathcal{N}_{\pi K}^{K^*}$ is given by

$$\mathcal{N}_{\pi K}^{K^*} = g_{\pi K K^*}^2 \left[-(q-2k)^2 + \frac{1}{m_{K^*}^2}(q^2 - 2q\cdot k)^2 \right]. \tag{4.10}$$

4.2 Numerical Results

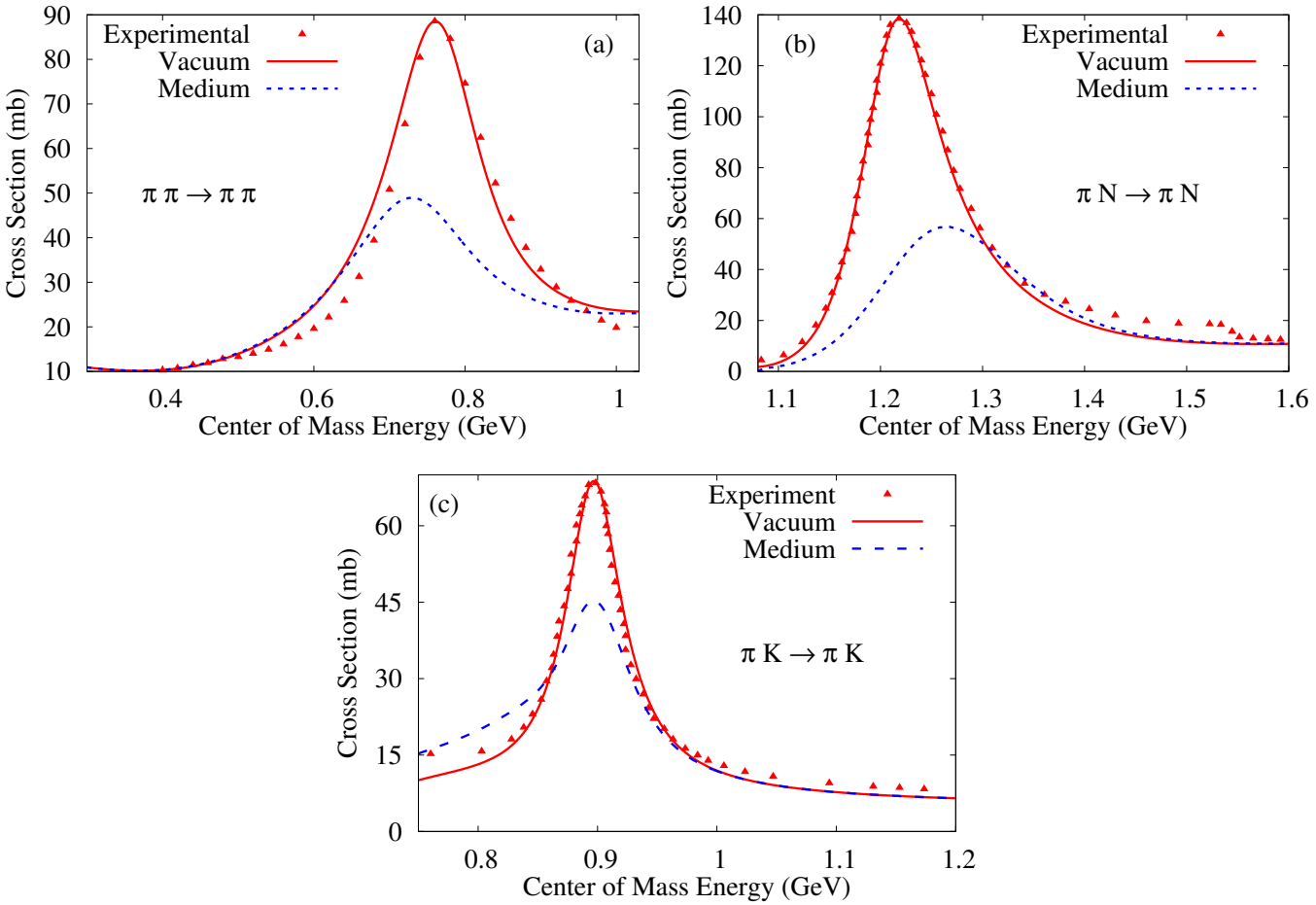

Figure 4.1: The (a)$\pi\pi \to \pi\pi$, (b)$\pi N \to \pi N$ and (c) $\pi K \to \pi K$ elastic scattering cross section as a function of centre of mass energy compared among experiment, vacuum and medium corresponds to $T = 160$ MeV, $\mu_\pi = \mu_K = 0$ and $\mu_N = 200$ MeV. Experimental data have been taken from Ref. [3]

We begin this section by discussing the elastic scattering cross sections for $\pi\pi \to \pi\pi$, $\pi N \to \pi N$ and $\pi K \to \pi K$. In Fig. 4.1 both vacuum and in-medium cross-sections are plotted along with the experimental data [3]. Since the matrix elements obtained in Sec. 4.1 contain the one-loop in-medium self energies of ρ, σ, Δ and K^*, the scattering cross sections also depend on the temperature and density of the thermal medium.

Using the approach described above we have been able to obtain a very good fit of the vacuum cross-section with the experimental data for the given set of model parameters for the tree types of scattering mentioned above. Having thus fixed our model in vacuum we replace the propagators with their thermal versions as described above to obtain the in-medium cross-section. The broadening of the widths of the resonances in the medium are reflected in the suppression of the cross section at the resonance energy and this is seen to be about $50 - 70\%$ at $T = 160$ MeV. The small shift lateral of the peak of the cross section is due to the small contribution from the real part of the thermal self energy function.

Chemical potential	μ_π	μ_K	μ_N
Set-1	0	0	0
Set-2	0	0	200
Set-3	50	100	200

Table 4.1: Different set of values of π, K and N chemical potentials used in this work.

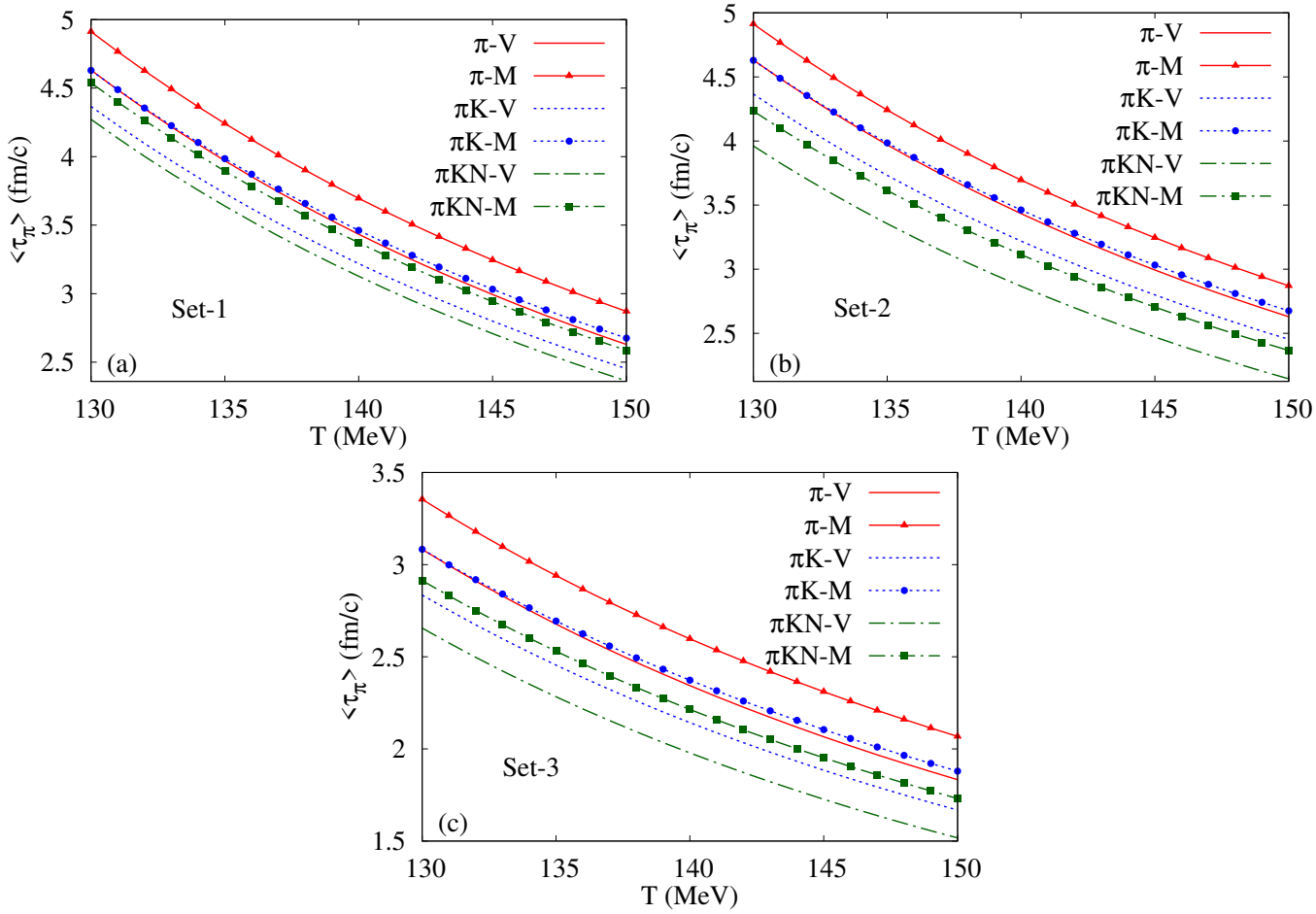

Figure 4.2: Mean relaxation time of pions for three different systems under consideration where V and M indicate the use of vacuum and in-medium cross-sections for (a) Set-1, (b) Set-2 and (c) Set-3.

Here in the upcoming part of this section, we have calculated all the results for three different set of values of pion, nucleon and kaon chemical potential, the choice of these sets have been tabulated in Table 4.1. In our system the only baryon present is the nucleon and hence baryonic chemical potential is essentially

nucleon chemical potential. It is to be noted that non-zero values of μ_π and μ_K are a consequence of pion and kaon number conservation after chemical freezeout [144] and the values taken here are demonstrative (see e.g. [110]).

Now we turn our attention to the numerical results for the temperature dependence of the momentum averaged relaxation time or collision time of π, K and N. The momentum averaged relaxation time is given by the expression,

$$\langle \tau_l \rangle = \int d^3p \tau_l f_l \Big/ \int d^3p f_l \tag{4.11}$$

where $l \in \{\pi, K, N\}$ and f_l is the equilibrium thermal distribution function of the l^{th} species. In all the figures of this chapter, V and M respectively indicates the use of vacuum and in-medium cross-sections in the calculation of relaxation times.

In Fig. 4.2, we have shown the average relaxation time of pions as a function of temperature in pion, pion-kaon and pion-kaon-nucleon system with and without medium effects taken into consideration. Essentially there are three noticeable features in the figure. First the decreasing trend of the relaxation time with increasing temperature which can be understood in the following manner. The relaxation time goes like $\sim 1/n\sigma$ where n is the number density and σ is the cross section. With the increase in temperature, n increases resulting in a reduction of the relaxation time. Secondly, for a given temperature the system relaxes faster when the number of components rises, as the addition of species increases the net density of particles effectively reducing the mean free path. And since the mean free path is directly proportional to the relaxation time, the relaxation time goes down. Finally, we note that the in-medium relaxation times are considerably larger ($\sim 10 - 15\%$) compared to their vacuum counterparts. This is due to the decrease in cross-section because of the additional scattering and decay processes at finite temperature. The vacuum results are in good agreement with Ref. [3]. From the different sets we see that with the increase in chemical potential the magnitude of average relaxation time of pions have decreased.

In Figs. 4.3(a)-(c) we have presented the dependence of mean relaxation time of individual species of the hadron gas mixture, i.e. pion, kaons and nucleons, on temperature with and without medium effects. It is noted that the mean relaxation time of kaon remains larger compared to the other constituents of the system in all cases over the temperature range considered because of their smaller cross-section. From Eq. (3.26), it is evident that mean relaxation time of the components are interdependent. With increasing baryonic density, the relaxation mechanism in the system gets enhanced as the number of particles with which collision is possible increases, and hence a relative decrease in the relaxation time as seen in Figs. 4.3(a)-(c). The in-medium behaviour of the relaxation time can also be explained along similar lines as done before.

Having studied the behaviour of the relaxation times of different species, we now turn our attention to the transport coefficients. The temperature dependence of scaled thermal conductivity λ/T^2 for different sets of chemical potential of the constituents is shown in Figs. 4.4(a)-(c). The quantity λ/T^2 decreases with increase in temperature and also decreases with the increase in chemical potential of the constituents. The fall of

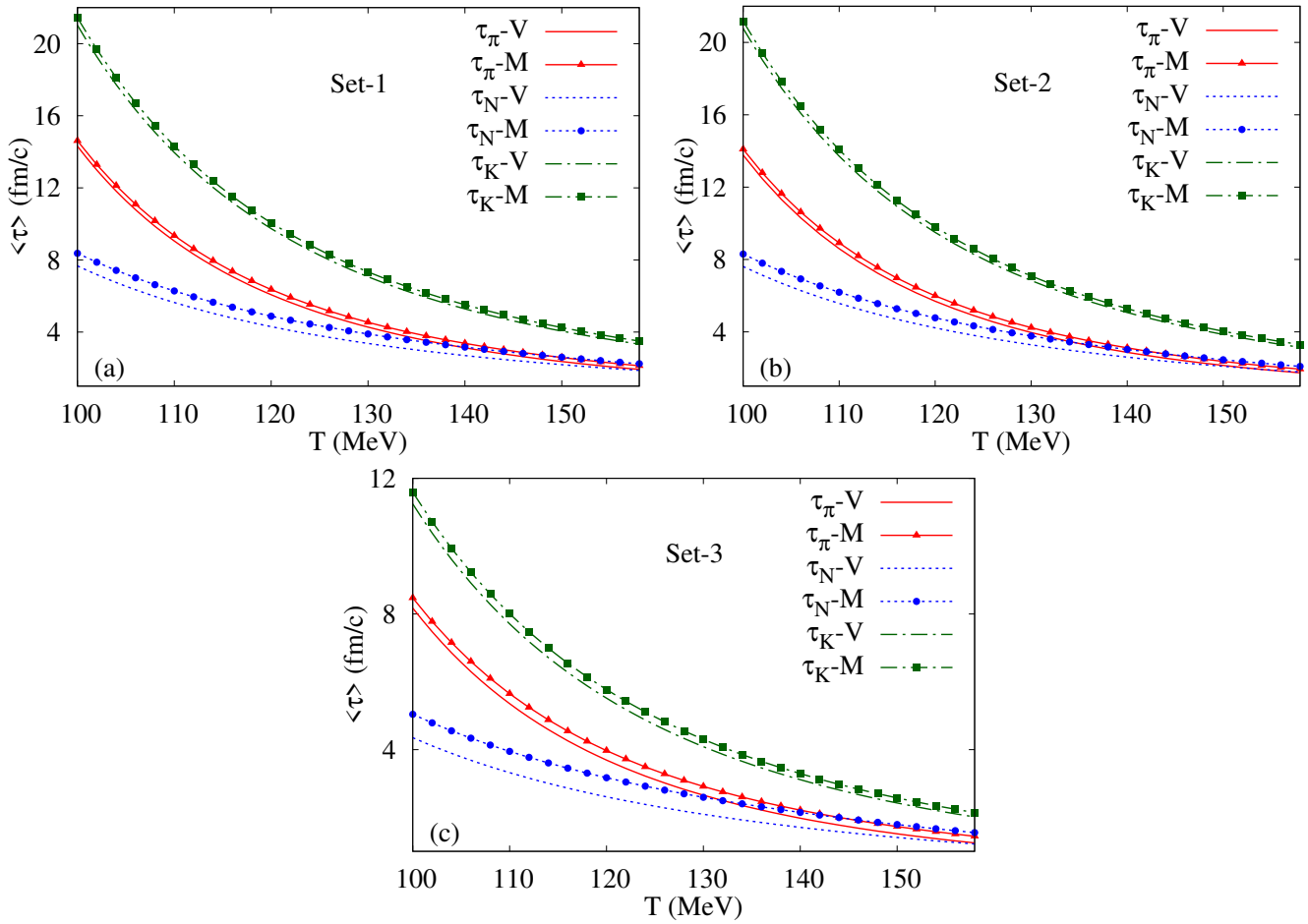

Figure 4.3: Momentum averaged relaxation time of pions, nucleons and kaons in a pion-nucleon-kaon hadronic gas as function of temperature for (a) Set-1, (b) Set-2 and (c) Set-3 of chemical potentials of individual components.

λ/T^2 is similar to that of relaxation time, steeper at lower temperature and gradual as temperature increases. Medium effects are reflected by the increase in magnitude of λ/T^2. With the increase in chemical potential the density of the heavier particles like nucleons and kaons increases which brings down the relaxation time, thus reducing the thermal conductivity.

We now proceed to present the numerical evaluation of shear and bulk viscosity using Eqs. (3.34) and (3.35). The results are shown for the temperature range starting from 100 to 160 MeV which is typical of a hadron gas produced in the later stages of heavy ion collisions. In Figs. 4.5(a)-(c) and Figs. 4.5(d)-(f), the vacuum and in-medium evolution of shear viscosity (η) and bulk viscosity (ζ) as a function of temperature are shown. Classically, for a single component gas, one can write $\eta \propto \bar{p}/\sigma$, where $\bar{p}$ and σ are the average momentum and binary cross section respectively. Fig. 4.1 shows that the cross-section reduces with increasing temperature (T) and since $\bar{p}$ goes as $\sqrt{T}$, the rise in magnitude of η due to inclusion of medium effects is understandable from the expression of η. The medium effects are reflected in the increase in magnitude of ζ as compared to that of ζ calculated using vacuum cross-sections.

Let us now proceed to study the behaviour of the ratios of viscosities to the entropy density η/s and ζ/s which are also termed as the specific shear and bulk viscosity. For this, we need the expression of the

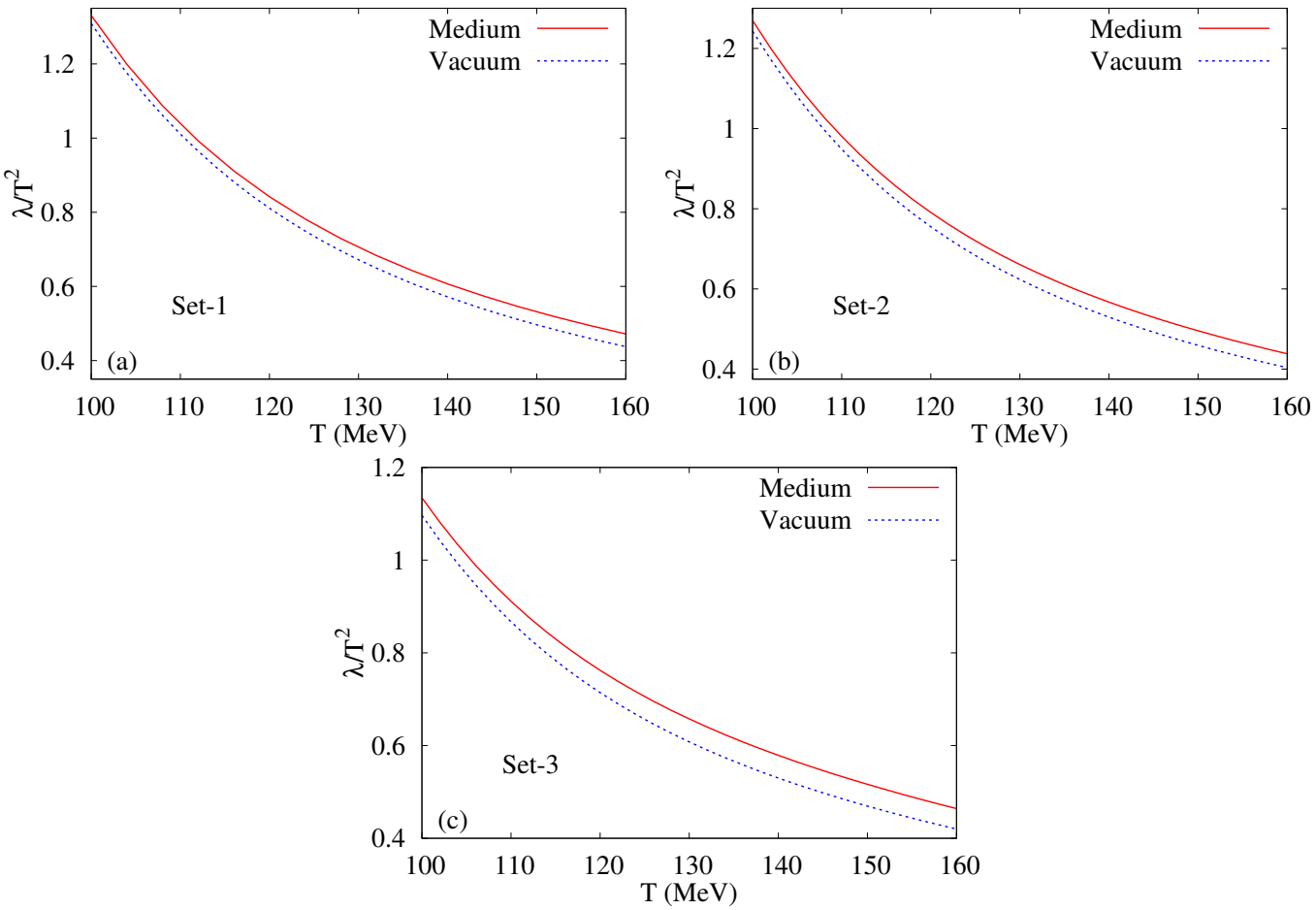

Figure 4.4: λ/T^2 as a function of temperature for (a) Set-1, (b) Set-2 and (c) Set-3 of chemical potentials of individual components.

entropy density. First we note that, the entropy density of a non-interacting hadronic gas mixture is given by [17]

$$s_{\text{free}} = T^3 \sum_{h\in\{\text{hadrons}\}} \frac{g_h}{2\pi^2}\left(\frac{m_h}{T}\right)^2 \left[\left(\frac{m_h}{T}\right)\mathcal{S}^1_{h3}\left(\frac{m_h}{T},\frac{\mu_h}{T}\right) - \left(\frac{\mu_h}{T}\right)\mathcal{S}^1_{h2}\left(\frac{m_h}{T},\frac{\mu_h}{T}\right)\right] \tag{4.12}$$

where, the sum runs over all the hadronic species taken into consideration, m_h is the mass, g_h is the spin-isospin degeneracy, μ_h is the chemical potential of the hadron h and

$$\mathcal{S}^{\alpha}_{hn}(x,y) = \sum_{j=1}^{\infty}(a_h)^{j+1}e^{jy}j^{-\alpha}K_n(jx) \tag{4.13}$$

in which $a_h = 1$ if h is a Boson and $a_h = -1$ if h is a Fermion.

In order to take into account the effect of interactions among the different hadrons, we use the relativistic virial expansion as discussed in Refs. [17, 140]. The total entropy then comes out to be the sum of the free and interacting parts $s = s_{\text{free}} + s_{\text{int}}$. The leading contribution to s_{int} comes from the second virial coefficient

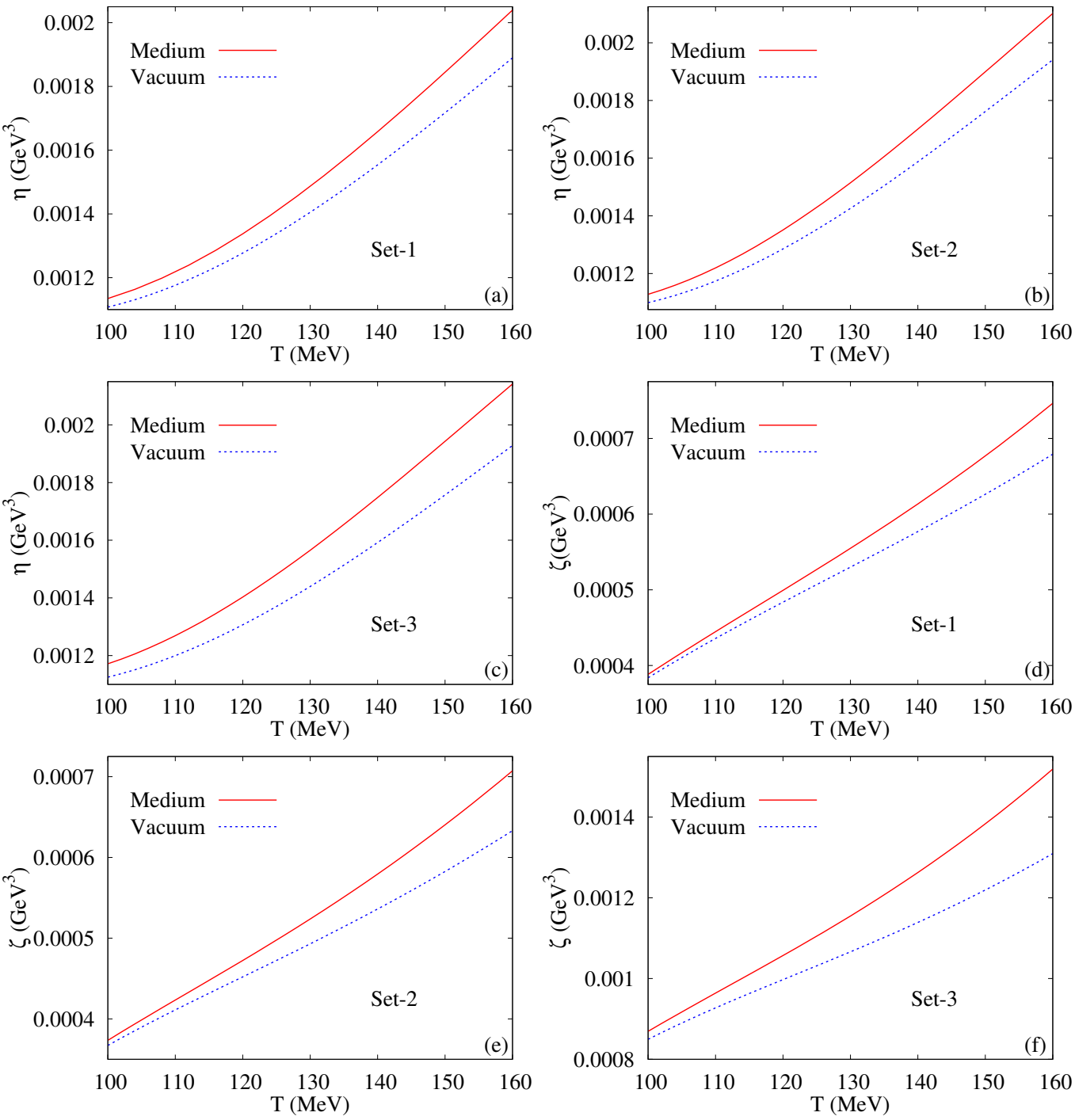

Figure 4.5: Shear viscosity(η) and bulk viscosity (ζ) as a function of temperature (T) for a pion-kaon-nucleon hadronic gas mixture for (a) Set-1, (b) Set-2 and (c) Set-3 of chemical potentials of individual components with and without including medium effects.

which can be calculated from two body phase shifts as

$$s_{\rm int} = \sum_{i,j\geq i} e^{\mu_i/T} e^{\mu_j/T} \frac{1}{2\pi^3} \int_{m_i+m_j}^{\infty} d(\sqrt{s}) s \left[\frac{\sqrt{s}}{T} K_2\left(\frac{\sqrt{s}}{T}\right) - \left(\frac{\mu_i}{T} + \frac{\mu_j}{T}\right) K_2\left(\frac{\sqrt{s}}{T}\right) \right] \sum_{c\in \text{channels}} g_c \delta_c^{ij} \quad (4.14)$$

where the indices i, j run over all the hadronic species taken into consideration, $\sqrt{s}$ is the center of mass energy for the hadronic pair $\{i, j\}$, g_c is the spin-isospin degeneracy of the resonance being exchanged in the channel c and δ_c^{ij} is the corresponding phase shift. The dominant contribution to $s_{\rm int}$ come from those

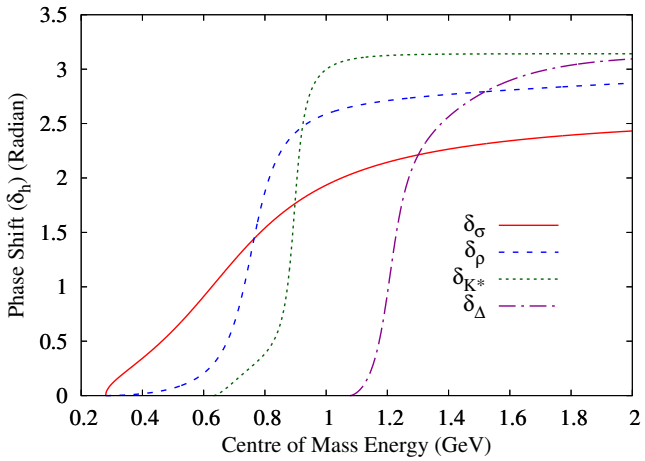

Figure 4.6: Phase shifts in different resonance channels as a function of center of mass energy.

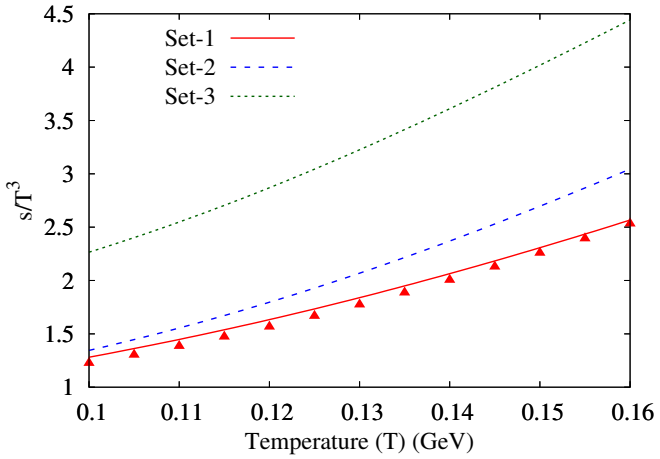

Figure 4.7: Entropy density scaled by the cube of temperature (s/T^3) as a function of temperature for different sets of chemical potentials. The triangles correspond to the result for a free gas mixture of $\pi, K, N, \sigma, \rho, K^*$ and Δ.

channels where explicit resonance exchanges occur [17]. For consistency with the calculations of in-medium cross-sections here we only take into account ρ, σ, Δ and K^* resonances which appear in the s-channel scattering matrix elements. The phase shift (δ_R) for the resonance (R) exchange can be obtained from

$$\delta_R(s) = \frac{\pi}{2} + \tan^{-1}\left(\frac{\sqrt{s} - m_R}{\Gamma_R(s)/2}\right) \tag{4.15}$$

where, $\Gamma_R(s)$ is the decay width of the resonance R with four-momentum $(\sqrt{s}, \vec{0})$.

For $\pi\pi$, we consider the σ and ρ exchange, whereas for πK and πN we consider K^* and Δ exchange. The decay width of σ and ρ are taken from Refs. [140] and they are given by

$$\Gamma_\sigma(s) = 2.06q\ , \tag{4.16}$$

$$\Gamma_\rho(s) = 0.095q\left(\frac{q/m_\pi}{1 + q^2/m_\rho^2}\right)^2 \tag{4.17}$$

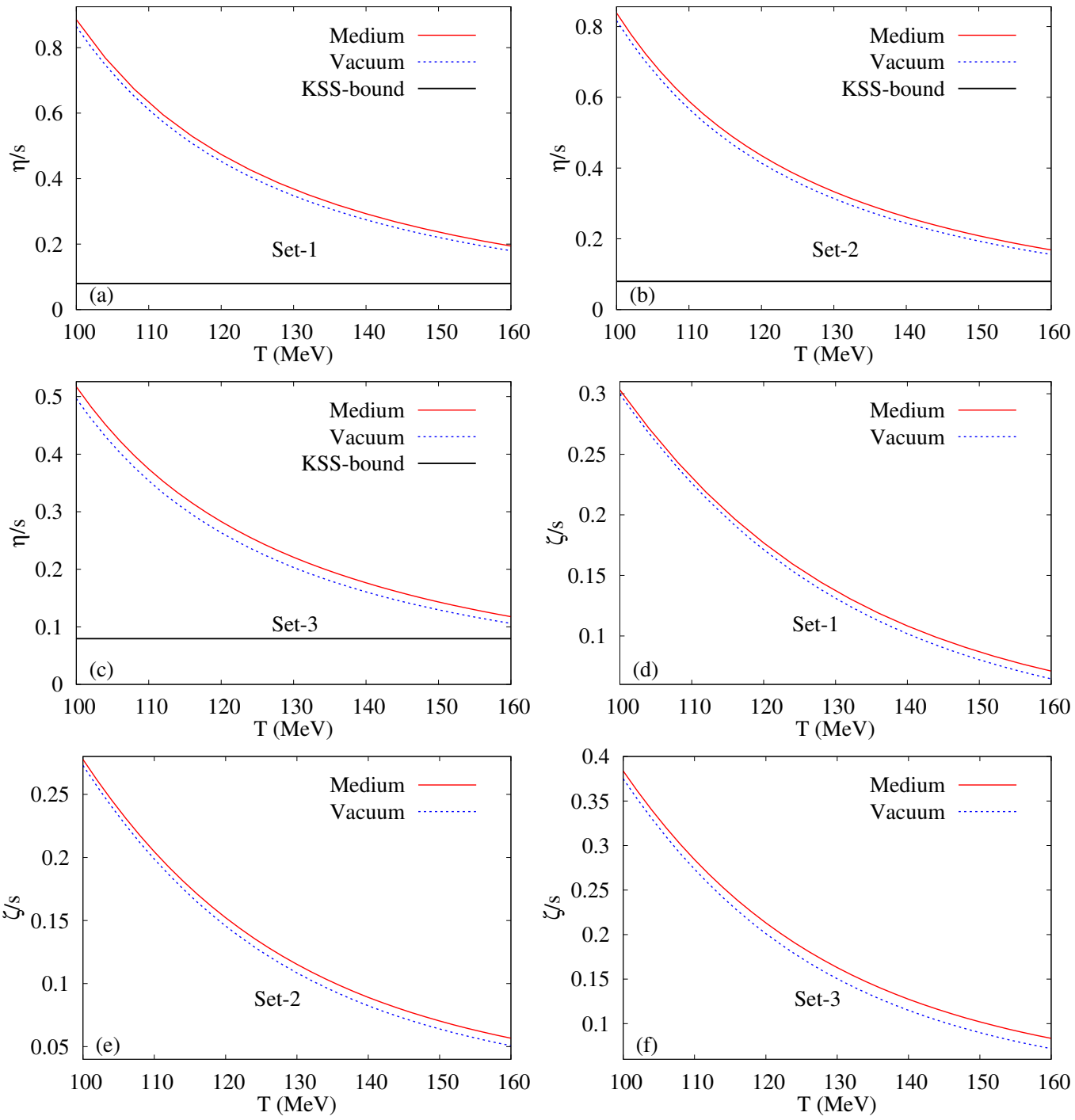

Figure 4.8: Specific shear viscosity (η/s) and specific bulk viscosity (ζ/s) as a function of temperature (T) for a pion-kaon-nucleon hadronic gas mixture for (a) Set-1, (b) Set-2 and (c) Set-3 of chemical potentials of individual components with and without including medium effects.

where, $q = \frac{1}{2}\sqrt{s-4m_\pi^2}$. The decay widths of K^* and Δ are calculated from the effective Lagrangians of Eqs. (4.2) and (4.1) and are given by

$$\Gamma_{K^*}(s) = \frac{g^2_{\pi KK^*}}{16\pi}F^2(s)\frac{1}{s^{3/2}}\lambda^{1/2}(s,m_\pi^2,m_K^2)\left[s-2m_K^2-2m_\pi^2+\frac{1}{s}(m_K^2-m_\pi^2)^2\right], \tag{4.18}$$

$$\Gamma_{\Delta}(s) = \frac{f^2_{\pi N\Delta}}{192\pi m_\pi^2}F^2(s)\frac{1}{s^{5/2}}\lambda^{3/2}(s,m_\pi^2,m_N^2)\left[(\sqrt{s}-m_N)^2-m_\pi^2\right] \tag{4.19}$$

where, the form factor $F(s) = \Lambda^2_{K,N}\left[\Lambda^2_{K,N} + \frac{1}{4m^2_{K,N}}\lambda(s, m^2_\pi, m^2_{K,N})\right]^{-1}$ with $\lambda(x, y, z) = x^2 + y^2 + z^2 - 2xy - 2yz - 2zx$ being the Källén function.

In Fig. 4.6, the phase shifts in the different resonance channels (σ, ρ, K^* and Δ) are shown as a function of the center of mass energy. The slope of δ_σ is least among the other three due to the largest decay width of σ. All the δ_ρ, δ_{K^*} and δ_Δ show rapid changes around the respective pole mass values (m_ρ, m_{K^*} and m_Δ) of the center of mass energies. The δ_{K^*} is the steepest among all due to the smallest vacuum decay width of K^* which is ~ 50 MeV.

Next in Figs. 4.7, the entropy density with interactions scaled by the cube of inverse temperature (s/T^3) has been depicted as a function of temperature for the three sets of chemical potentials. Shown with triangles is the result for a free gas of $\pi, K, N, \sigma, \rho, K^*$ and Δ for Set-1. They appear to be in good agreement [140, 17].

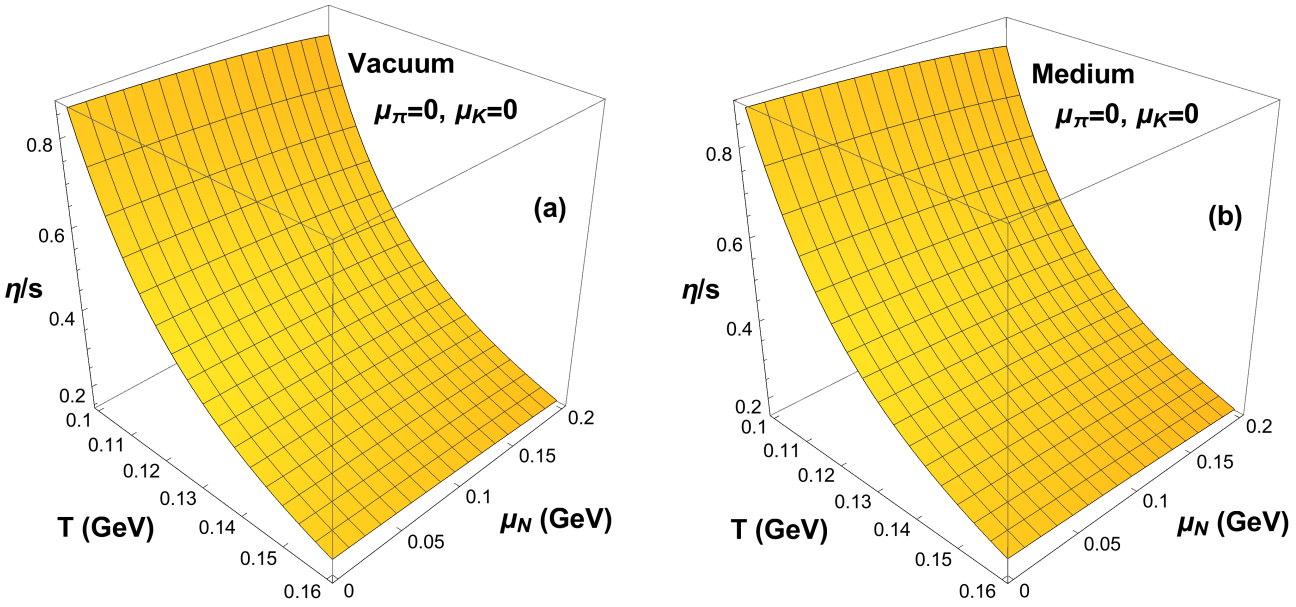

Figure 4.9: Shear viscosity to entropy density ratio (η/s) as a function of temperature and nucleon chemical potential at $\mu_\pi = \mu_K = 0$ with (a) vacuum and (b) in-medium cross sections.

We are now in a position to plot the specific viscosities. In Figs. 4.8(d)-(f) η/s is plotted with temperature for three sets of chemical potentials. We see a monotonic decrease of the specific shear viscosity with increase of temperature. This is because of the fact that the entropy density rises with increase of temperature with a rate faster than η. The increase in magnitude of η for different sets of increasing chemical potential, even though there is a decrease in relaxation time with the increase in chemical potential, is mainly due to the increase in density which turns out to be the governing factor here. η/s on the other hand decreases with the increase in chemical potential because with the increase in chemical potential the entropy increases faster due to the rapid increase in the degrees of freedom, and the value of η/s is within the KSS-bound. Here, we note that with the inclusion of more resonances the shear viscosity decreases as one approaches temperatures close to the critical temperature. Owing to the corresponding increase in the entropy density there is a further decrease in the value of η/s [140].

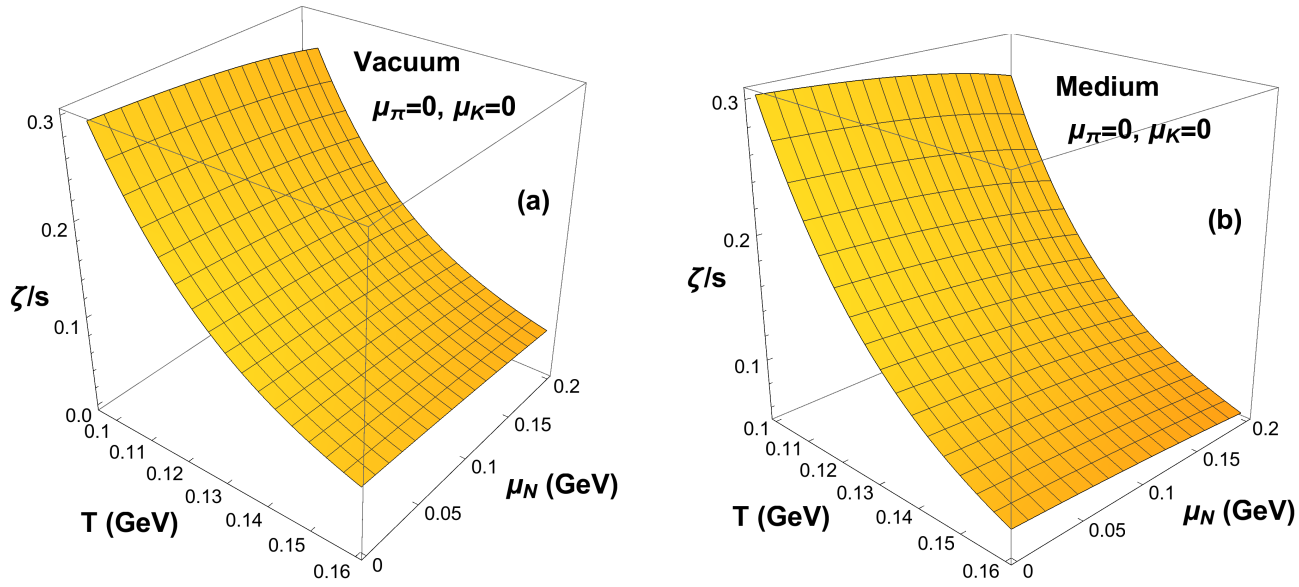

Figure 4.10: Bulk viscosity to entropy density ratio (ζ/s) as a function of temperature and nucleon chemical potential at $\mu_\pi = \mu_K = 0$ with (a) vacuum and (b) in-medium cross sections.

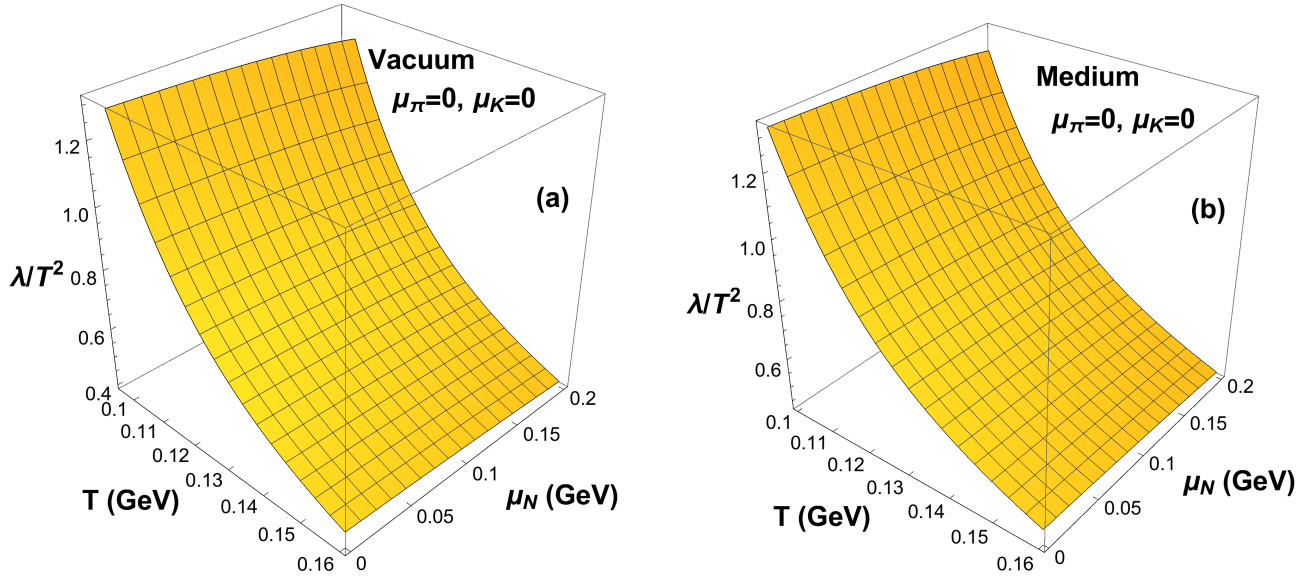

Figure 4.11: Thermal conductivity scaled with inverse of temperature squared (λ/T^2) as a function of temperature and nucleon chemical potential at $\mu_\pi = \mu_K = 0$ with (a) vacuum and (b) in-medium cross sections.

We now show the results of specific bulk viscosity. In Figs. 4.8(d)-(f) one can also observe the sizeable difference in magnitude of ζ/s calculated for vacuum and medium. The figures show increase in magnitude of ζ for increasing value of chemical potential just like in the case for η, which is again attributed to the dominance of increase in density over the decrease in magnitude of relaxation time. And like η/s we find that ζ/s increases with increase in chemical potential.

In Figs. 4.9 and 4.10, we have studied the effect of temperature and baryonic chemical potential on η/s and ζ/s with and without medium effects taken into consideration, for $\mu_\pi = \mu_K = 0$. We find that on introducing the medium effects, there is an increase in the magnitude but very little change in its behaviour.

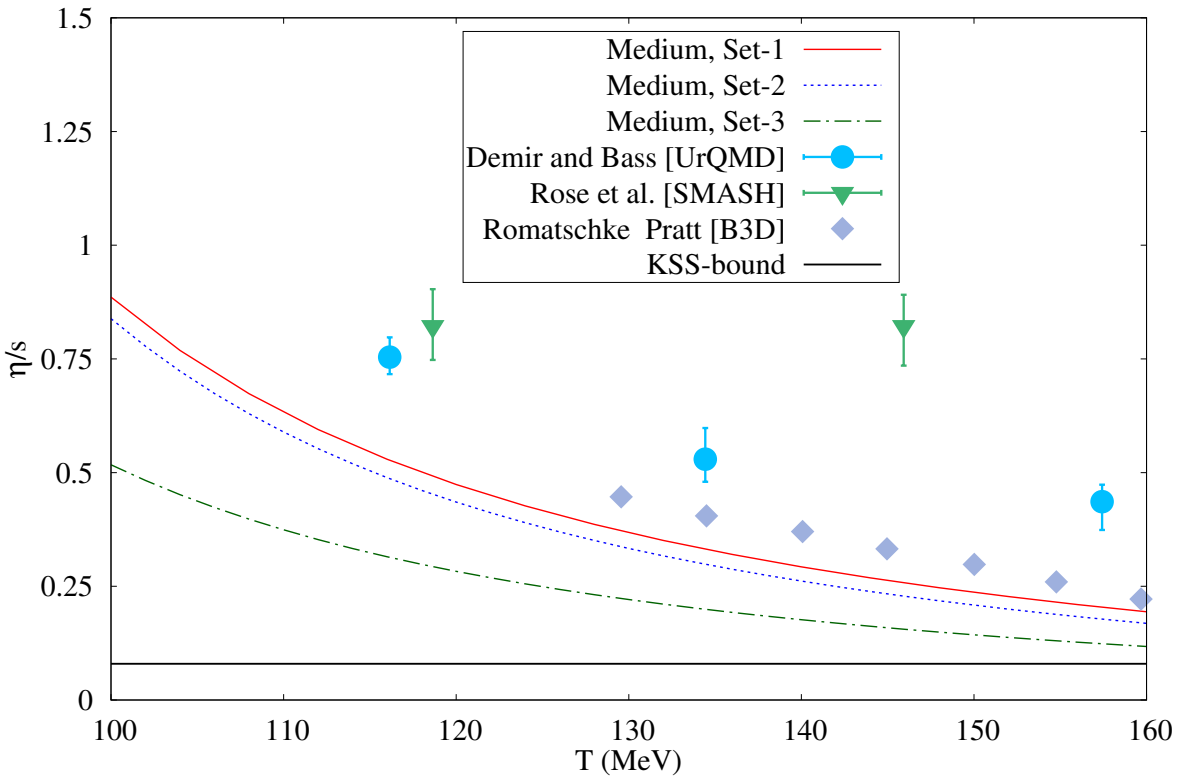

Figure 4.12: The result obtained in this work compared to various data of the specific shear viscosity η/s as a function of temperature available in the literature [4, 5, 6]. A line of KSS bound has been drawn as a reference.

Also, with increase in baryonic chemical potential the value of η/s decreases while the value increases for ζ/s. The drop in the value of η/s with increase in temperature is found to be sharper at lower baryonic chemical potential while we observe the opposite trend in the case of ζ/s where the drop is sharper at higher chemical potential. At lower temperature the effect of the baryonic chemical potential on ζ/s is found to be more pronounced than at higher temperature, this pattern is also ovserved in the case of η/s. The analogous plots for the variation of λ/T^2 as a function of T and μ_N shown in Fig. 4.11(a) and (b) show features similar to that of η/s.

Finally, to check consistency we have plotted in Fig. 4.12, η/s calculated using different techniques such as hadronic cascades URQMD [4], B3D [5] and SMASH [6] along with our result using medium dependent cross-sections for the three sets of chemical potentials. In particular, the in-medium η/s calculated with Set-1 i.e. for $\mu_\pi = 0$, $\mu_K = 0$ and $\mu_N = 0$ are in reasonable agreement with that of [5].

In the next two chapters we will switch on the magnetic field and study the effect of the thermal medium in the presence of background magnetic field on the transport coefficients.

Chapter 5

Electrical and Hall Conductivity of a hot pion gas in a magnetic medium

The estimation of transport coefficients of relativistic systems in the presence of a magnetic field is important in the context of magnetized neutron stars, cosmology and relativistic HICs. In case of HICs, transport coefficients such as the shear and the bulk viscosities and the diffusion coefficients are essential to describe the hydrodynamical evolution of the matter transiently produced in such collisions. In the presence of a magnetic field this evolution is described by magnetohydrodynamics (MHD) which takes into account the coupling of the magnetic field to the relativistically evolving fluid in a self-consistent way.

From a phenomenological point of view, electrical conductivity is important in the sense that if it is large, the created magnetic field in non-central HICs persists for a longer time [83]. However, as of now it is a general belief that the value of the magnetic field is quite small in the hadronic matter (HM) due to the smaller value of the conductivity. As a result, relevant physical quantities calculated in HM will have minor modifications as compared to that in quark matter. In order to substantiate this conjecture, it is necessary to calculate the magnetic field dependent electrical conductivity of HM as accurately as possible taking into account finite temperature and/or density and magnetic field effects.

In this chapter, we have evaluated the electrical as well as Hall conductivites of a relativistic pion gas using kinetic theory approach within the RTA by incorporating the finite temperature effects in the cross-section vis a vis the relaxation time. We have chosen to calculate the electrical conductivity of pions as they are the most abundant species among the other hadrons produced in the HICs at RHIC and LHC [38]. This type of study is also important as the magnetic field produced in heavy ion collisions is of hadronic scale and hence the evaluation of transport coefficients of the QGP and the hadronic medium will provide a better insight into the time evolution of strongly interacting matter in the presence of a background magnetic field.

A good deal of progress has been made in recent times in the evaluation of magnetic field dependent transport coefficients such as electrical conductivity [145, 146, 147, 148, 149, 150, 151, 152], shear viscosity [151, 153, 61, 154] heavy quark diffusion constant [154, 155], and the jet quenching parameter [156]. One of the most important transport coefficients required in the formulation of MHD is the electrical conduc-

tivity. Electrical conductivity of a QGP in strong magnetic field has been evaluated in Ref. [157] where it was shown that it diverges in the massless limit and is very sensitive to the value of the current quark mass. In Ref. [10], the electrical as well as the Hall conductivities of the QGP have been estimated in a strong magnetic field using a kinetic theory approach as well as the Kubo formalism. It is found that, the electrical conductivity decreases in the presence of a magnetic field, specially at low temperature. Also in Ref. [158], the electrical conductivity of a hot and dense quark matter has been computed in the presence of a magnetic field using kinetic theory beyond the lowest Landau level (LLL) approximation. It is observed that the transverse electrical conductivity is dominated by the Hall conductivity and the parallel conductivity has a nominal dependence on both T and μ.

An attempt has been made in Refs. [13, 11] to calculate the electrical conductivity of Hadron Resonance Gas (HRG) which has been studied using the Relaxation Time Approximation (RTA) with a constant cross section whereas in Ref. [159], electrical conductivity along with other transport coefficients of HRG have been computed treating the relaxation time as a free parameter. However, the hadronic phase in HICs attains sufficiently high temperature (100 MeV $\leq T \leq$ 155 MeV) and/or high (baryon) density (note that the QGP–hadron phase transition occurs nearly at temperature $T_c \simeq 155$ MeV, which is the (pseudo) critical temperature for the chiral phase transition as obtained in the Lattice QCD calculations [35]). Hence in order to obtain a more realistic picture, one should incorporate the thermal effects in the cross-sections required to evaluate the transport coefficients which have been ignored in Ref. [11].

The chapter is organized in the following manner. In the Sec. 5.1 we have evaluated the conductivity tensor using the dissipative term obtained from the BTE in the presence of external magnetic field employing RTA and in Sec. 5.2, numerical results are shown.

5.1 Electrical and Hall conductivities from kinetic theory

The BTE in presence of external electromagnetic field [90] which is satisfied by the on-shell single particle phase space distribution function $f_\pm = f_\pm(t, \vec{r}, \vec{p})$ of the charged pions ($\pi^\pm$) is given by -

$$\frac{\partial f_\pm}{\partial t} + \vec{v} \cdot \frac{\partial f_\pm}{\partial \vec{r}} \pm q \left[\vec{E} + (\vec{v} \times \vec{H})\right] \cdot \frac{\partial f_\pm}{\partial \vec{p}} = C[f_\pm] \tag{5.1}$$

where, q is the charge of a proton, $\vec{v} = \vec{p}/\omega_p$ is the velocity, $\omega_p = \sqrt{\vec{p}^2 + m^2}$ is the energy, $\vec{E}$ is the electric field, $\vec{H}$ is the magnetic field and $C[f_\pm]$ denotes the collision kernel. We note that, the equilibrium Bose-Einstein distribution function $f_0 = f_0(\omega_p)$ for which $C[f_0] = 0$ is given by

$$f_0(\omega_p) = \frac{1}{e^{\omega_p/T} - 1} \tag{5.2}$$

where T is temperature.

Few comments on the use of the classical dispersion relation $\omega_p = \sqrt{\vec{p}^2 + m^2}$ for the pions are in order here. It is well known that in the presence of an external magnetic field the momentum states of the charged

pions will be Landau quantized and their classical dispersion relation $\omega_p = \sqrt{\vec{p}^2 + m^2}$ with continuous transverse momentum modifies to

$$\omega_{pl} = \sqrt{p_z^2 + (2l+1)qH + m^2} \tag{5.3}$$

where l is the Landau level. However, in this work we have ignored the Landau quantization (LQ) in the calculation of conductivity assuming the magnetic field to be weak. For low values of the external magnetic field, the Landau levels become closely spaced such that the continuum approximation of the transverse momentum of pions hold good. Moreover, we have used the RTA, where the pion distribution function is assumed to be slightly away from equilibrium which allows linearization of the BTE. The use of RTA implies that the external magnetic field cannot be too high. Finally, the magnitude of external magnetic field in hadronic phase of HIC is usually small which in turn justifies the use of weak field approximation in our calculation. A more quantitative analysis on the validity of the continuum approximation will be performed later in Sec. 5.2.

When the system is out of equilibrium, the dissipative processes within the system try to bring it back to equilibrium. Let us consider the system to be slightly away from equilibrium which is characterized by the non-equilibrium distribution function $f_\pm = f_0 + \delta f_\pm$ with $\delta f_\pm = -\phi_\pm \dfrac{\partial f_0}{\partial \omega_p} \ll f_0$. As $\delta f_\pm$ is small, the BTE can be linearized.

In order to solve Eq. (5.1) we treat the right hand side of Eq. (5.1) using the RTA and consider only the $2 \to 2$ scattering process $k + p \to k' + p'$. In the RTA the collision integral in Eq. (5.1) reduces

$$C[f_\pm] = \frac{\delta f_\pm}{\tau} = -\frac{\phi_\pm}{\tau}\frac{\partial f_0}{\partial \omega_p} \tag{5.4}$$

where τ is the relaxation time. Substituting Eq. (5.4) into Eq. (5.1) yields

$$\frac{\partial f_\pm}{\partial t} + \vec{v}\cdot\frac{\partial f_\pm}{\partial \vec{r}} \pm q\left[\vec{E} + (\vec{v}\times\vec{H})\right]\cdot\frac{\partial f_\pm}{\partial \vec{p}} = -\frac{\phi_\pm}{\tau}\frac{\partial f_0}{\partial \omega_p} \tag{5.5}$$

Since we are dealing with a uniform and static medium, both $f_\pm$ and f_0 are independent of time and space. Also the electric field under consideration is very small. Thus Eq. (5.5) reduces to

$$\pm q\vec{E}\cdot\vec{v}\frac{\partial f_0}{\partial \omega_p} \pm q(\vec{v}\times\vec{H})\cdot\frac{\partial \phi_\pm}{\partial \vec{p}}\left(\frac{\partial f_0}{\partial \omega_p}\right) = -\frac{\phi_\pm}{\tau}\frac{\partial f_0}{\partial \omega_p} \tag{5.6}$$

In order to solve for the electrical and Hall conductivities, we take the following ansatz for the functional form of $\phi_\pm$ [149] as

$$\phi_\pm = \vec{p}\cdot\vec{\Xi}_\pm(\omega_p) \tag{5.7}$$

where the vector $\vec{\Xi}_\pm$ contains information of the dissipation produced due to electric and magnetic fields

and can be expressed most generally as

$$\vec{\Xi}_{\pm} = \alpha_{\pm}\hat{e} + \beta_{\pm}\hat{h} + \gamma_{\pm}\left(\hat{e}\times\hat{h}\right) \tag{5.8}$$

where, $\hat{e} = \vec{E}/|\vec{E}|$ and $\hat{h} = \vec{H}/|\vec{H}|$ are the unit vectors along the directions of electric and magnetic fields respectively. Substituting Eq. (5.7) and Eq. (5.8) into Eq. (5.6), we get after some simplification

$$\begin{aligned}\pm\frac{q|\vec{E}|}{\omega_p}(\hat{e}\cdot\vec{p}) \pm \alpha_{\pm}\frac{q|\vec{H}|}{\omega_p}(\hat{e}\times\hat{h})\cdot\vec{p} \pm \gamma_{\pm}\frac{q|\vec{H}|}{\omega_p}(\hat{e}\cdot\vec{p}) \pm \gamma_{\pm}\frac{q|\vec{H}|}{\omega_p}(\hat{h}\cdot\vec{p})(\hat{h}\cdot\hat{e}) \\ = -\alpha_{\pm}(\hat{e}\cdot\vec{p})\tau^{-1} - \beta_{\pm}(\hat{h}\cdot\vec{p})\tau^{-1} - \gamma_{\pm}(\hat{e}\times\hat{h})\cdot\vec{p}\tau^{-1}.\end{aligned} \tag{5.9}$$

Comparing the coefficients of $\hat{e}\cdot\vec{p}$, $\hat{e}\times\hat{h}$ and $\hat{h}\cdot\vec{p}$ on both sides of Eq. (5.9), we obtain

$$\alpha_{\pm} = \pm\frac{q|\vec{E}|}{\omega_p}\frac{\tau}{1+\omega_c^2\tau^2}, \tag{5.10}$$

$$\frac{\beta_{\pm}}{\alpha_{\pm}} = -(\omega_c\tau)^2(\hat{h}\cdot\hat{e}), \tag{5.11}$$

$$\frac{\gamma_{\pm}}{\alpha_{\pm}} = -\omega_c\tau \tag{5.12}$$

where $\omega_c = |q\vec{H}|/\omega_p$ is the cyclotron frequency. Using Eqs. (5.10)-(5.12) in Eq. (5.8), we can now obtain the vector $\vec{\Xi}_{\pm}$ which in turn is used to get $\phi_{\pm}$ from Eq. (5.7) as

$$\phi_{\pm} = \alpha_{\pm}\omega_p\vec{v}\cdot\left[1+(\omega_c\tau)^2(\hat{e}\cdot\hat{h})\hat{h} - (\omega_c\tau)(\hat{e}\times\hat{h})\right] = \pm\frac{q\tau}{1+(\omega_c\tau)^2}v^i\left[\delta^{ij} - \omega_c\tau\epsilon^{ijk}h^k + (\omega_c\tau)^2h^ih^j\right]E^j \tag{5.13}$$

where the Einstein summation convention has been used.

In order to extract the electrical and Hall conductivities from $\phi_{\pm}$, we first note that the macroscopic electrical current density j^i is given by

$$j^i = \sigma^{ij}E^j = \int\frac{d^3p}{(2\pi)^3}v^iq(\phi_+ - \phi_-)\left(\frac{\partial f_0}{\partial\omega_p}\right). \tag{5.14}$$

In Eq. (5.14), σ^{ij} is the conductivity tensor. Now substitution of Eq. (5.13) into Eq. (5.14) yields

$$\sigma^{ij} = \delta^{ij}\sigma_0 - \epsilon^{ijk}h^k\sigma_1 + h^ih^j\sigma_2 \tag{5.15}$$

where

$$\sigma_0 = \frac{gq^2}{3T}\int\frac{d^3p}{(2\pi)^3}\frac{\vec{p}^2}{\omega_p^2}\frac{\tau}{1+(\omega_c\tau)^2}f_0(\omega_p)\left\{1+f_0(\omega_p)\right\}, \tag{5.16}$$

$$\sigma_1 = \frac{gq^2}{3T}\int\frac{d^3p}{(2\pi)^3}\frac{\vec{p}^2}{\omega_p^2}\frac{\tau(\omega_c\tau)}{1+(\omega_c\tau)^2}f_0(\omega_p)\left\{1+f_0(\omega_p)\right\}, \tag{5.17}$$

$$\sigma_2 = \frac{gq^2}{3T}\int\frac{d^3p}{(2\pi)^3}\frac{\vec{p}^2}{\omega_p^2}\frac{\tau(\omega_c\tau)^2}{1+(\omega_c\tau)^2}f_0(\omega_p)\left\{1+f_0(\omega_p)\right\} \tag{5.18}$$

in which $g = 2$ is the degeneracy of charged pions in the gas since only the charged pions π^+ and π^- participate in the charge conduction. σ_0 is the electrical conductivity in presence of the magnetic field, σ_1 is the Hall conductivity and $\sigma_0 + \sigma_2$ is the electrical conductivity in absence of external magnetic field. In compact notation, Eqs. (5.16)-(5.18) can be written as

$$\sigma_n = \frac{gq^2}{3T}\int \frac{d^3p}{(2\pi)^3}\frac{\vec{p}^2}{\omega_p^2}\frac{\tau(\omega_c\tau)^n}{1+(\omega_c\tau)^2} f_0(\omega_p)\left\{1+f_0(\omega_p)\right\} \quad ; \quad n = 0, 1, 2. \tag{5.19}$$

The steps involving the calculation of relaxation time of pions τ appearing in Eq. (5.19) has been discussed in detail in chapter 3.

5.2 Results and Discussions

We begin this section by showing the in-medium $\pi\pi \to \pi\pi$ total cross section as a function of center of mass energy in Fig. 5.1(a) for different temperatures. At $T = 0$, the cross section obtained using the vacuum self energies of ρ and σ mesons is seen to agree with the experimental data [3] shown with red triangles. With the increase in temperature, the imaginary part of the self energy increases owing to the in-medium broadening of the resonance spectral functions. Physically, it corresponds to the increase in annihilation probabilities (due to decay and scattering) of ρ and σ in the thermal bath. This in-medium spectral-broadening of ρ and σ in turn makes substantial suppression in the cross section at high temperature as can be noticed from the figure.

Next, in Fig. 5.1(b) we have shown the variation of the average relaxation time $\langle\tau\rangle$ of pions with temperature evaluated using vacuum and in-medium cross sections. Note that, the momentum averaged relaxation time $\langle\tau\rangle$ is obtained from the relation

$$\langle\tau\rangle = \int d^3p\tau(p)f(\omega_p) \Big/ \int d^3p f(\omega_p). \tag{5.20}$$

It is seen that the relaxation time obtained using the in-medium cross section is always greater than the same calculated using the vacuum cross section which is also obvious from Eq. (6.27). Since, the in-medium cross section is suppressed with respect to the vacuum cross section, $\langle\tau\rangle_{\text{Vacuum}}$ comes out to be less than $\langle\tau\rangle_{\text{Medium}}$. In order to extract the leading behaviour of $\langle\tau\rangle$ as a function of temperature, we fit the in-medium relaxation time $\langle\tau\rangle_{\text{Medium}}$ with a polynomial function of the form $\sum_{i=0}^{3} a_i \left(\frac{m}{T}\right)^i \frac{1}{T^3}$. This is shown in Fig. 5.1(c) where we have plotted the fitted function along with $\left(\frac{a_0}{T^3}\right)$ and $\sum_{i=1}^{3} a_i \left(\frac{m}{T}\right)^i \frac{1}{T^3}$ separately to understand the leading behaviour. It is easy to check from Eqs. (6.27) and (5.20) that a_i's are dimensionfull quantities and have the dimensions of the inverse of the cross section, $[\sigma^{-1}]$. It is clearly seen that the leading behaviour is well represented by the first term in the fitting function. This can be explained by considering $\langle\tau\rangle \sim 1/(n\sigma)$ where n is the pion density which goes as $n \sim T^3$ in the massless limit and σ is the (T-independent) cross section. The observed deviation from the $1/T^3$ behaviour of $\langle\tau\rangle$ at lower and higher temperatures is quite

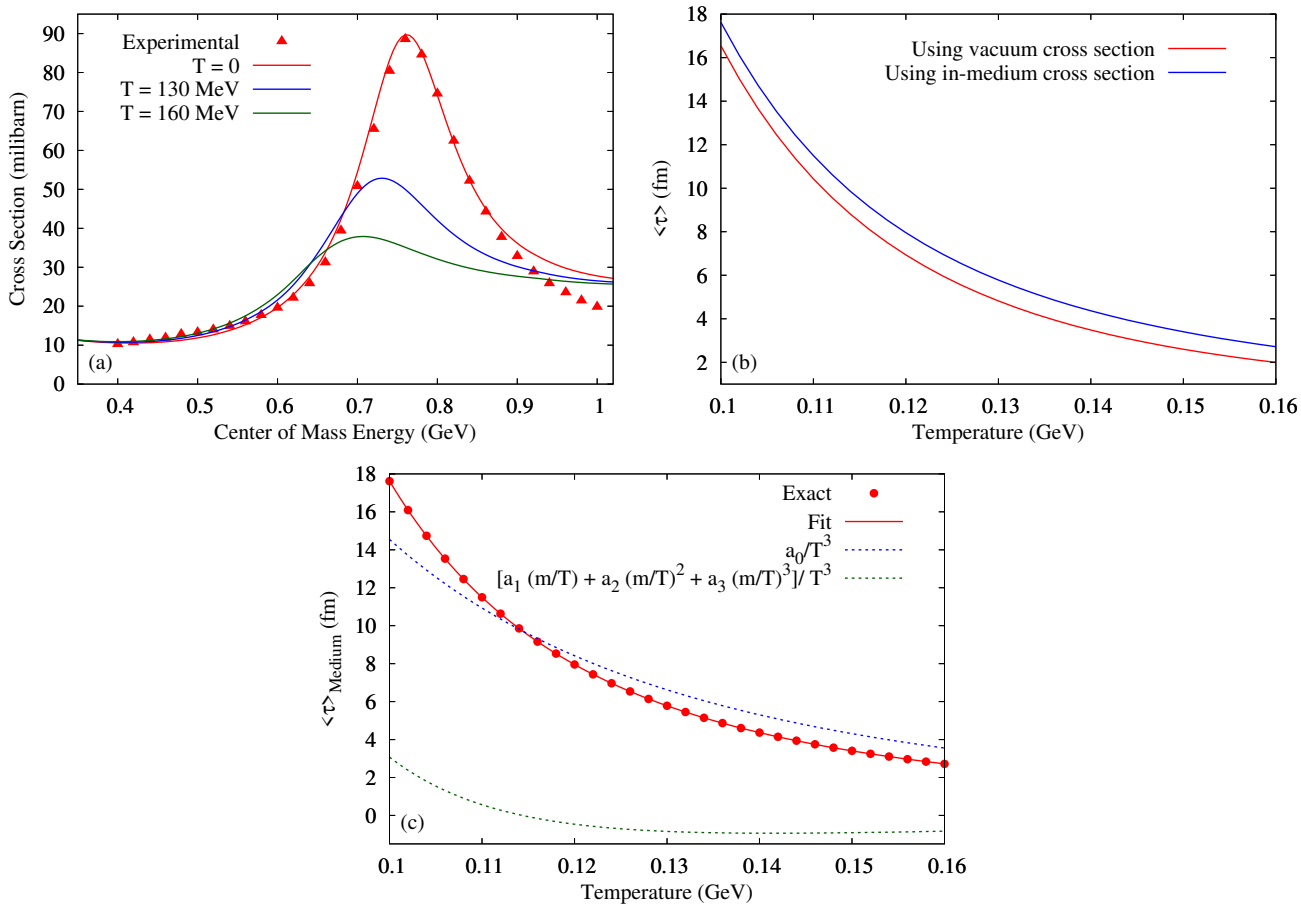

Figure 5.1: (a) The variation of isospin averaged total $\pi\pi \to \pi\pi$ cross section as a function of centre of mass energy for different temperatures. The experimental data is taken from Ref. [3]. (b) The variation of average relaxation time $\langle\tau\rangle$ of pions as a function of temperature calculated using the vacuum and in-medium cross sections. (c) The in-medium $\langle\tau\rangle$ as a function of T fitted with a polynomial funtion of the form $\sum_{i=0}^{3} a_i \left(\frac{m}{T}\right)^i \frac{1}{T^3}$ with $a_0 = 0.0145$ fm-GeV^3, $a_1 = -0.0109$ fm-GeV^3, $a_2 = 0.0058$ fm-GeV^3 and $a_3 = 0.0026$ fm-GeV^3.

understandable and may be attributed to several factors. Most important among these is the contribution coming from the phase space integrals due to the non-zero pion mass which contain higher inverse powers of T. The T-dependence of the cross-section can also make a contribution. However, for purposes of discussion $\langle\tau\rangle$ may well be taken to go as $1/T^3$ in the relevant temperature range and the deviations therefrom will not affect the conclusions significantly.

The variation of σ_0/T as a function of temperature is shown in Figs. 5.2(a) and 5.2(b) for different values of magnetic field using both the vacuum and in-medium cross sections. To understand the behaviour of σ_0/T with temperature, we first note, from Eq. (5.16), that the temperature dependence of σ_0/T roughly comes from $\sigma_0/T \sim \frac{\tau T}{1+(\omega_c\tau)^2}$. At lower values of the magnetic field, $\omega_c\tau \ll 1$ so that the temperature dependence of τT would dictate the temperature dependence of σ_0/T. We have discussed the T-dependence of the average relaxation time earlier by fitting a simple function and argued that $\langle\tau\rangle \propto 1/T^3$ is a good approximation in the relevant temperature range. Thus, at lower values of magnetic field, we expect $\sigma_0/T \sim 1/T^2$ which is quite compatible with Fig. 5.2(a). The situation is reversed at higher values of the external magnetic field for which $\omega_c\tau \gg 1$ and consequently the temperature dependence of σ_0/T approximately comes from

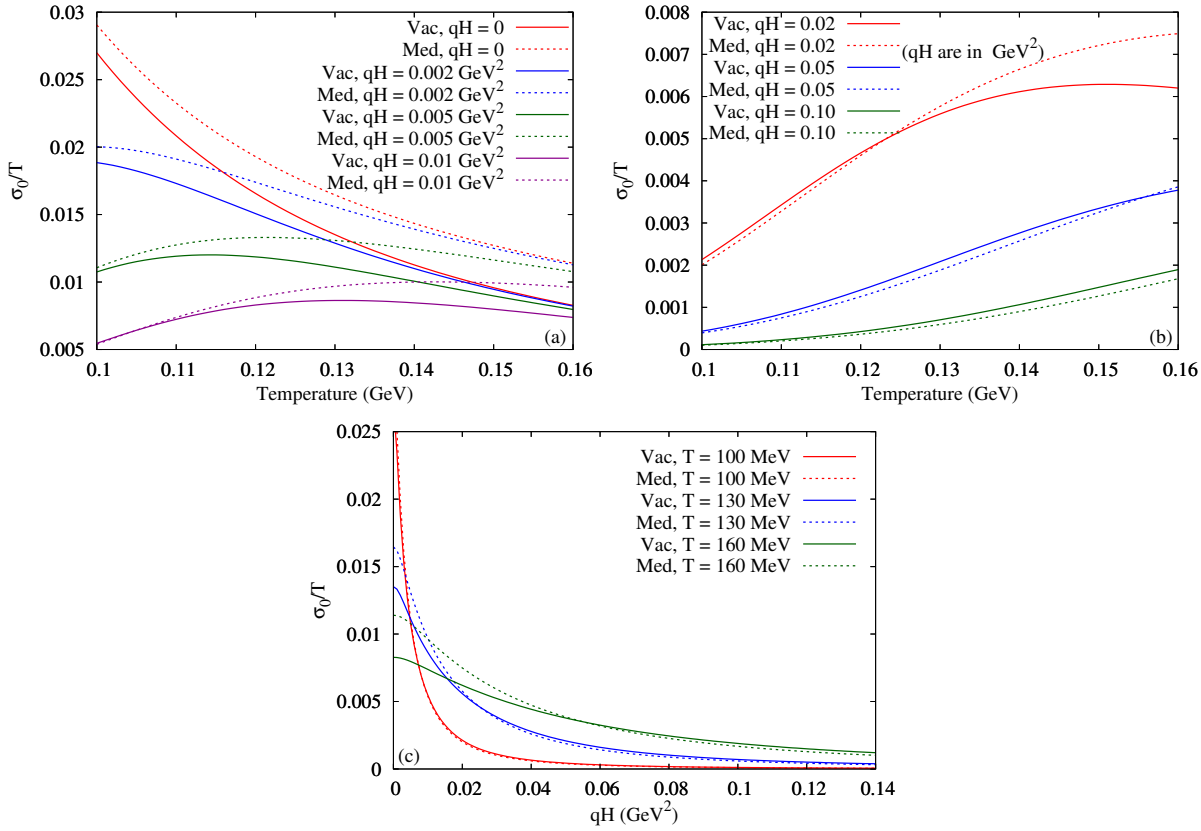

Figure 5.2: The variation of σ_0/T (a)-(b) as a function of temperature for different values of magnetic field strength and (c) as a function of magnetic field for different values of temperature. The solid and dashed curves correspond to the estimations of σ_0/T using vacuum and in-medium cross sections respectively.

$\sigma_0/T \sim \frac{T}{\tau} \sim T^4$. We thus expect a monotonically increasing trend of σ_0/T with temperature at higher values of magnetic field as can be noticed in Fig. 5.2(b). At intermediate values of the magnetic field we observe a non-monotonic behaviour of σ_0/T with temperature. In Fig. 5.2(c), σ_0/T has been plotted as a function of external magnetic field for different temperatures. Unlike the temperature dependence, σ_0/T has a trivial magnetic field dependence as $\sigma_0/T \sim \frac{1}{1+(\omega_c\tau)^2}$. With the increase in magnetic field values, the cyclotron frequency ω_c increases linearly so that a monotonically decreasing trend of σ_0/T with external magnetic field is visible in Fig. 5.2(c). The effect of in-medium cross section on σ_0/T can be understood similarly from the τ dependence of σ_0/T. As already argued, at a given temperature, for lower values of magnetic field, $\sigma_0/T \sim \tau$ whereas for higher values of magnetic field $\sigma_0/T \sim 1/\tau$. Since, the relaxation time is larger for the in-medium cross section, it is obvious that the use of in-medium cross section instead of the vacuum cross section will increase (decrease) σ_0/T for lower (higher) values of the external magnetic field. This is clearly observed in Figs. 5.2(a) and 5.2(b). This argument also explains the crossing of the dashed curves with the respective solid curves in Fig. 5.2(c).

Next in Figs. 5.3(a) and 5.3(b), the Hall conductivity scaled with inverse temperature (σ_1/T) has been depicted as a function of temperature for different values of the external magnetic field using both the vacuum and in-medium cross sections. The behaviour of σ_1/T with temperature can be understood by a similar analysis as done in the last paragraph. We notice from Eq. (5.17), the temperature dependence of

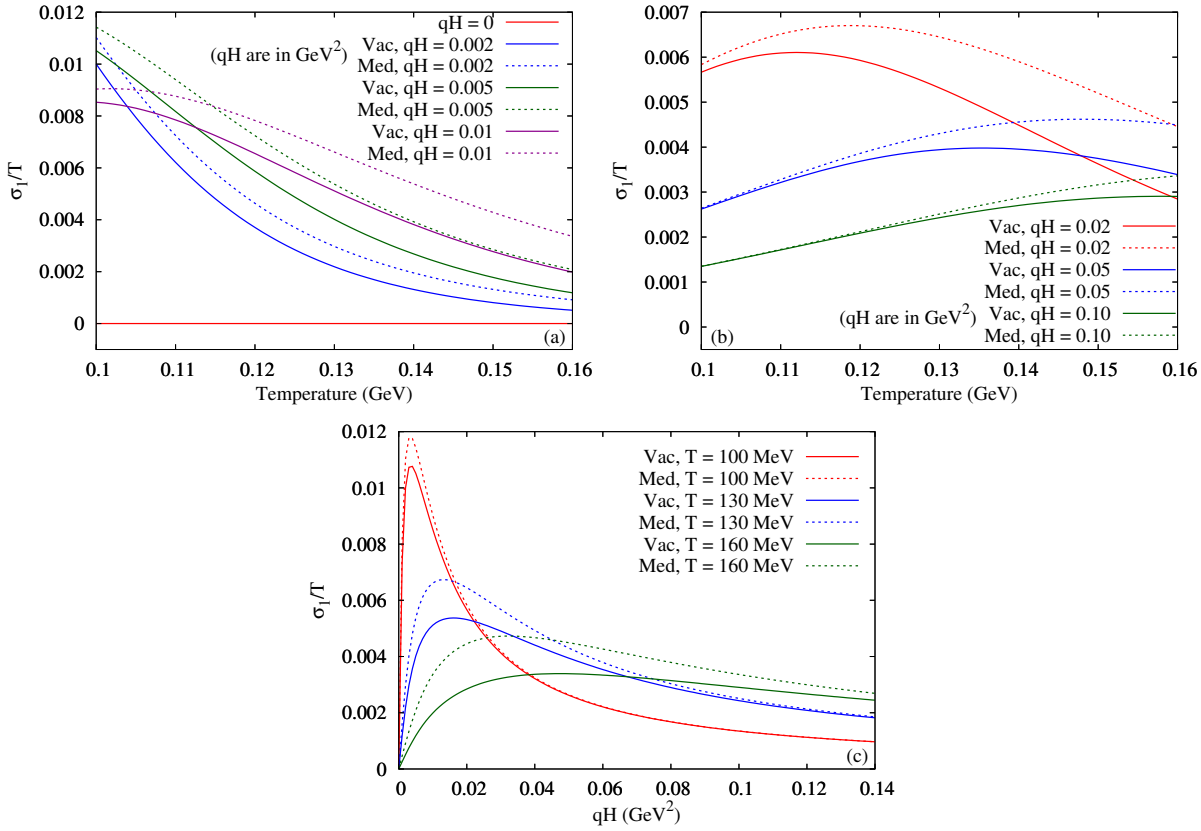

Figure 5.3: The variation of σ_1/T (a)-(b) as a function of temperature for different values of magnetic field strength and (c) as a function of magnetic field for different values of temperature. The solid and dashed curves correspond to the estimations of σ_1/T using vacuum and in-medium cross sections respectively.

σ_1/T approximately comes from $\sigma_1/T \sim \frac{\tau^2 T}{1+(\omega_c\tau)^2}$. Therefore, at lower values of the magnetic field, $\omega_c\tau \ll 1$ so that $\sigma_1/T \sim \tau^2 T \sim 1/T^5$. On the other hand, at higher values of the external magnetic field ($\omega_c\tau \gg 1$), the leading temperature dependence of σ_1/T goes as $\sigma_1/T \sim T$. Thus, at lower values of magnetic field, σ_1/T decreases with temperature more rapidly than σ_0/T whereas at higher values of magnetic field, we notice a linear increase of σ_1/T with temperature. This also makes σ_1/T to vary non-monotonically at intermediate values of the external magnetic field as can be noticed in Figs. 5.3(a) and 5.3(b). In Fig. 5.3(c), we have shown σ_1/T as a function of external magnetic field for different temperatures. The dependence of σ_1/T on the magnetic field goes as $\sigma_1/T \sim \frac{\omega_c}{1+(\omega_c\tau)^2}$ which is basically a Breit-Wigner function of the magnetic field with peak position $\sim 1/\tau \sim T^3$ and width $\sim \tau \sim 1/T^3$. The Breit-Wigner like behaviour of σ_1/T can be observed in Figs. 5.3(c) in which the peak position of σ_1/T moves towards higher magnetic field values and the width increases with temperature. As before, the effect of in-medium cross section on σ_1/T can be understood from the τ dependence of σ_1/T, i.e. from $\sigma_1/T \sim \frac{\tau^2\omega_c}{1+(\omega_c\tau)^2}$ which is a monotonically increasing and saturating function of τ. The saturation occurs in the low temperature (where τ is large) and low magnetic field region in which the overall τ dependence of σ_1/T becomes weaker. Since the in-medium cross section yields a larger relaxation time, the use of in-medium cross section over the vacuum cross section always increases σ_1/T for any value of the external magnetic field as can be noticed in Figs. 5.3(a)-5.3(c). However, in the high magnetic field and low temperature region, due to the weakening of the τ dependence in

σ_1/T, the medium effect in cross section becomes negligible as one can notice by comparing the separations between the dashed and solid curves of Fig. 5.3(b) (low temperature region) and Fig. 5.3(c) (high magnetic field region).

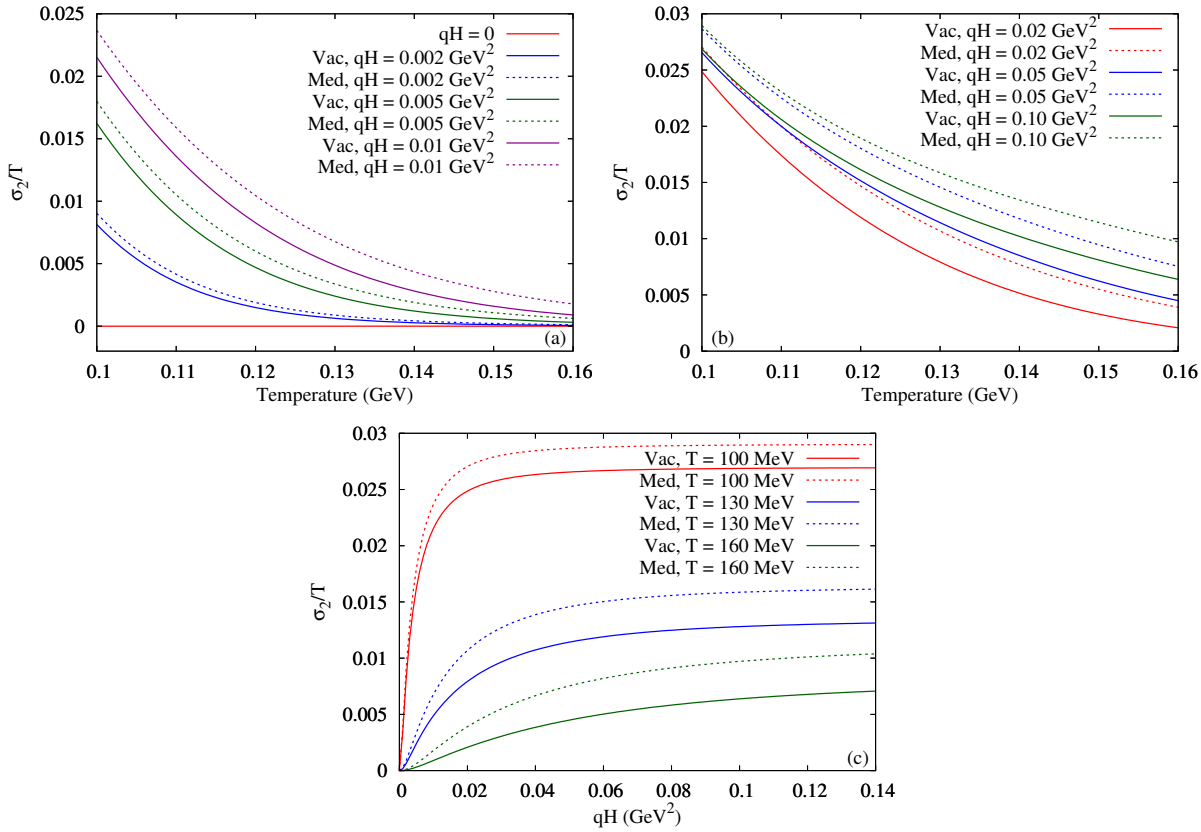

Figure 5.4: The variation of σ_2/T (a)-(b) as a function of temperature for different values of magnetic field strength and (c) as a function of magnetic field for different values of temperature. The solid and dashed curves correspond to the estimations of σ_2/T using vacuum and in-medium cross sections respectively.

We now proceed to show the behaviour of the quantity σ_2/T as a function of temperature for different values of external magnetic field with both the vacuum and in-medium cross sections in Figs. 5.4(a) and 5.4(b). The behaviour of σ_2/T with temperature can be analogously understood from Eq. (5.18) in which the temperature dependence of σ_2/T approximately goes as $\sigma_2/T \sim \frac{\tau^3 T}{1+(\omega_c\tau)^2}$. Therefore, at lower values of the magnetic field ($\omega_c\tau \ll 1$), $\sigma_2/T \sim \tau^3 T \sim 1/T^8$. On the other hand, at higher values of the external magnetic field ($\omega_c\tau \gg 1$), the leading temperature dependence of σ_2/T is approximately given by $\sigma_2/T \sim \tau \sim 1/T^3$. Thus, σ_2/T always decreases monotonically with the increase in temperature even more rapidly than σ_1/T in all the values of the magnetic field considered here (see Figs. 5.4(a) and 5.4(b)). Next, in Fig. 5.4(c), the magnetic field dependence of σ_2/T has been depicted for different temperatures. σ_2/T depends on the magnetic field as $\sigma_2/T \sim \frac{(\omega_c\tau)^2}{1+(\omega_c\tau)^2}$ which is a monotonically increasing and saturating function of magnetic field thus explaining the analogous behaviour of the curves in the figure. To understand the effect of in-medium cross section on σ_2/T, we first note that the τ dependence of σ_2/T is given by $\sigma_2/T \sim \frac{\tau^3\omega_c^2}{1+(\omega_c\tau)^2}$ which is a monotonically increasing function of τ for a particular value of magnetic field. The rate of increase is more for higher magnetic field values. Thus, we notice, from Figs. 5.4(a)-5.4(c), that the use of

in-medium cross section over the vacuum cross section always increases σ_2/T for the values of the magnetic field considered here. Moreover, at higher values of the external magnetic field, due to the increase of τ dependence in σ_2/T, the medium effects become more significant as can be observed by comparing the separations between the dashed and solid curves of Fig. 5.4(a)-5.4(c).

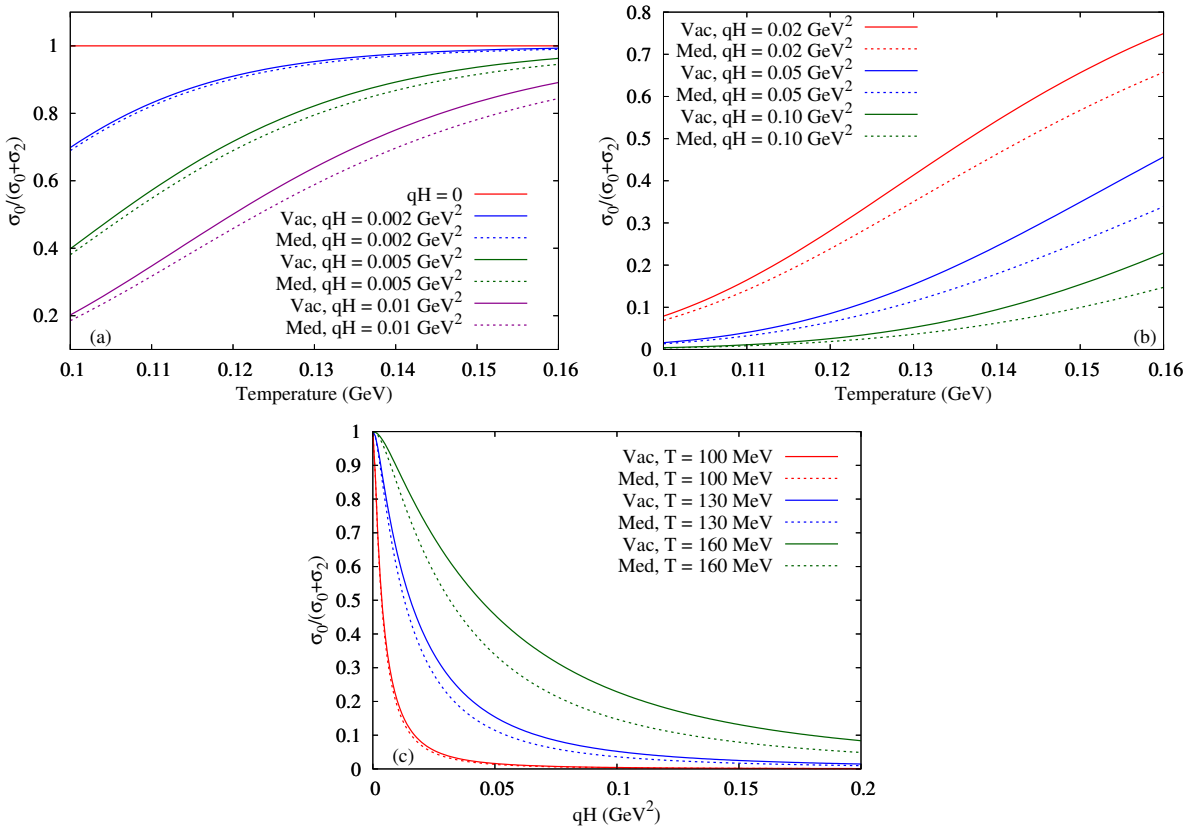

Figure 5.5: The variation of the anisotropy measure $\frac{\sigma_0}{\sigma_0+\sigma_2}$ (a)-(b) as a function of temperature for different values of magnetic field strength and (c) as a function of magnetic field for different values of temperature. The solid and dashed curves correspond to the estimations of $\frac{\sigma_0}{\sigma_0+\sigma_2}$ using vacuum and in-medium cross sections respectively.

Finally, we note that, the normalized ratio $\frac{\sigma_0}{\sigma_0+\sigma_2}$ could be a measure of anisotropy brought in by the external magnetic field since the quantity $\sigma_0+\sigma_2$ is the electrical conductivity in absence of magnetic field. We therefore plot $\frac{\sigma_0}{\sigma_0+\sigma_2}$ as a function of temperature and magnetic field in Figs. 5.5(a)-5.5(c). With the increase in temperature, the ratio increases towards its asymptotic value 1 whereas with the increase in magnetic field, the ratio rapidly decreases from 1. Physically it corresponds to the fact that, the magnetic field tries to bring anisotropy in the medium whereas the thermal fluctuation tries to diminish it. Moreover, comparing the solid and dashed curves in Figs. 5.5(a)-5.5(c), we find that the use of medium effects in the cross section makes the system more anisotropic in presence of external magnetic field.

We have already mentioned in Sec. 5.1 that we are neglecting the LQ of the charged pion dispersion relation (see Eq. (5.3)) while calculating the conductivities. However, to check the validity of this continuum approximation, let us now calculate the conductivities incorporating the LQ of pion transverse momentum. To a first approximation, the LQ can be incorporated in the final expression of the conductivities in Eq. (5.19)

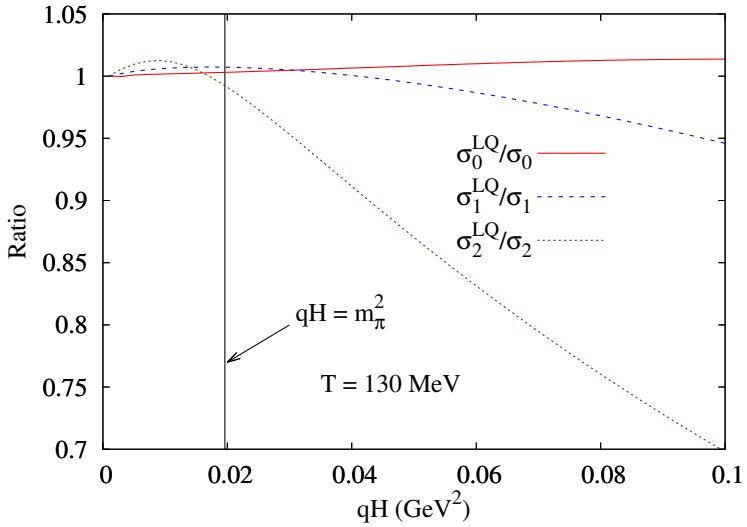

Figure 5.6: The ratio $\sigma_n^{\rm LQ}/\sigma_n$ as a function of external magnetic field at $T = 130$ MeV. The solid-black vertical line corresponds to $qH = m^2$. Upto 300 Landau levels are taken into consideration.

by the following replacements:

$$\omega_p \rightarrow \omega_{pl} = \sqrt{p_z^2 + (2l+1)qH + m^2}, \tag{5.21}$$

$$|\vec{p}| \rightarrow \sqrt{p_z^2 + (2l+1)qH}, \tag{5.22}$$

$$\int \frac{d^3p}{(2\pi)^3} \rightarrow \frac{qH}{2\pi} \sum_{l=0}^{\infty} \int_{-\infty}^{\infty} \frac{dp_z}{2\pi}, \tag{5.23}$$

so that the conductivities with LQ becomes

$$\sigma_n^{\rm LQ} = \frac{gq^2}{3T} \frac{qH}{2\pi} \sum_{l=0}^{\infty} \int_{-\infty}^{\infty} \frac{dp_z}{2\pi} \frac{p_z^2 + (2l+1)qH}{\omega_{pl}^2} \frac{\tau(\omega_{c,l}\tau)^n}{1+(\omega_{c,l}\tau)^2} f_0(\omega_{pl}) \{1 + f_0(\omega_{pl})\} \quad ; \quad n = 0, 1, 2, \tag{5.24}$$

where $\omega_{c,l} = qH/\omega_{pl}$. In Fig. 5.6, we have shown the ratio $\sigma_n^{\rm LQ}/\sigma_n$ as a function of external magnetic field at $T = 130$ MeV. From the figure, we can see that in the low magnetic field region ($qH \precsim m^2$), the ratios are almost unity which imply that the use of continuum approximation is well justified in the weak field region. However, for higher magnetic field values, the continuum approximation breaks down and the LQ becomes important. For example, at $qH = 0.10$ GeV^2, LQ modifies the values of σ_0 and σ_1 by less than 5% whereas the change in σ_2 is about 30%. Therefore, even if we have shown numerical results for a wider range of magnetic field values ($0 \leq qH \leq 0.1$ GeV^2) neglecting the LQ, our results are strictly valid for the weak magnetic field ($0 \leq qH < m^2$) likely to be realised in the hadronic phase of HIC.

In Fig. 5.7(a), we have made a comparison of the electrical conductivity obtained in this work with the other available estimations in the literature. We see that, our estimation of electrical conductivity at zero-magnetic field agrees well with the earlier estimations by Grief et al [7] and Fraile et al [8] whereas it does not agree well with the Lattice QCD estimation [9]. Also, our result at $qH = 0.02$ GeV^2 is lower than the values obtained by Feng. [10] for a system of relativistic quark-gluon gas. This is expected as the

conductivity of QGP is much larger than of hadron gas. Finally, our result at $qH = 0.05$ GeV^2 is in good qualitative and quantitative agreement with the result of Das et al [11] calculated for hadron resonance gas.

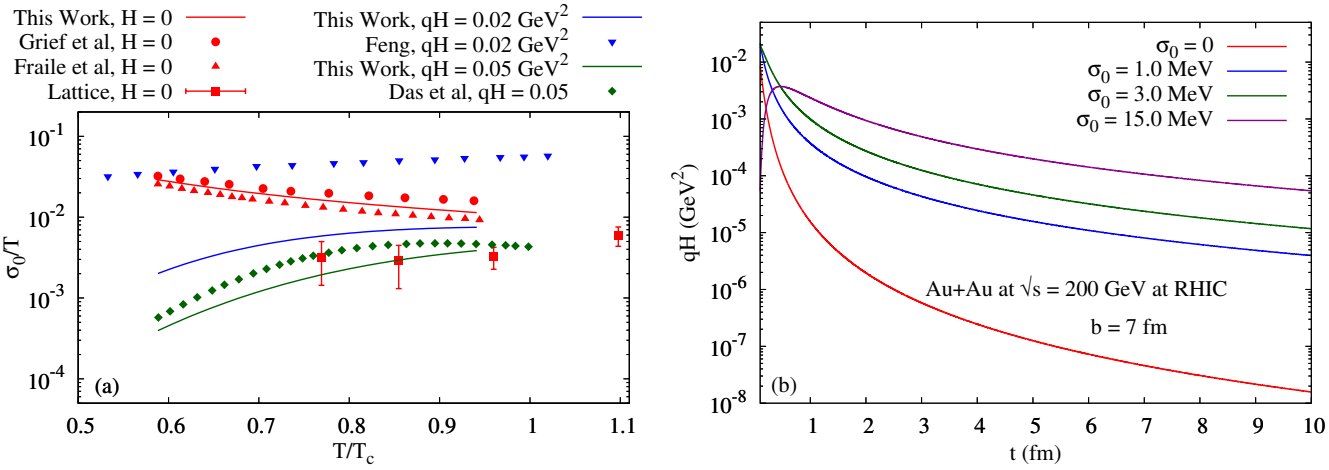

Figure 5.7: (a) The comparison of σ_0/T at zero magnetic field with Grief et al [7], Fraile et al [8] and Lattice QCD calculation [9] and at non-zero magnetic field with Feng [10] and Das et al [11]. (b) The decay of maximum magnetic field value in peripheral Au+Au collision at RHIC for different values of electrical conductivities.

As mentioned earlier, a sufficiently high value of electrical conductivity of the medium can sustain the rapidly decaying magnetic field in a HIC [83, 60, 160, 61]. To see how our estimated electrical conductivity (for a system of pion gas) modifies the decay of the magnetic field in HIC, we have calculated the time (t) dependence of the maximum value of magnetic field for peripheral Au+Au collision at RHIC energy ($\sqrt{s}$=200 GeV) using the simplified expression used by Tuchin [61] for a static medium. In Fig. 5.7(b), we have plotted the decay of the maximum magnetic field value in peripheral Au+Au collision at RHIC for different values of electrical conductivities. In our calculation, we have obtained maximum value of σ_0 as 3 MeV whereas in a QGP medium it has typical value of $\simeq$ 15 MeV [161, 162, 83, 160]. From the figure, it can be noticed that, for a constant $\sigma_0 = 15$ MeV throughout the evolution, a magnetic field value of the order of 10^{-4} GeV^2 is sustained even at $t = 10$ fm. But if we consider constant $\sigma_0 = 1 - 3$ MeV (as obtained in the current work for a pion gas) throughout the evolution, the sustained value of magnetic field at $t = 10$ fm is of the order of 10^{-5} GeV^2. In reality, electrical conductivity is not expected to be constant throughout the evolution. In the early stage (QGP phase), σ_0 will be large ($\sim$ 15 MeV) and in the later stages (hadronic phase) σ_0 will be small ($\sim$ 5 MeV). Therefore the time evolution of the actual magnetic field value is expected to lie in between the violet and green curves in the figure. Moreover, in Fig. 5.7(b), we have considered a medium with no hydrodynamic expansion for the estimation of the decay of magnetic field. For an expanding medium (which is the more realistic scenario for HIC), the magnetic field will sustain for a longer period as shown in Ref. [61]. Thus, we can conclude that a weak magnetic field can be present in the later stages of HIC and could be phenomenologically relevant.

Chapter 6

Electrical conductivity and shear viscosity of a pion gas in a thermo-magnetic medium

In this chapter, we have evaluated the electrical conductivity and shear viscosity of a hot and magnetized pion gas. In the previous chapter we have studied the magnetic field influence on the transport coefficient using only cyclotron frequency. However, it must be noted that the magnetic field also influences the collisions occuring in the system. This has motivated us to calculate the magnetic field dependent cross-section and relaxation time. Incorporation of the effect of magnetic field along with thermal effects on the relaxation time is the novelty of this chapter.

This chapter is organized as follows. Sec. 6.1 deals with the evaluation of shear viscosity using the BTE in the presence of background magnetic field RTA framework. In Sec. 6.2, we discuss the evaluation of the relaxation time of pions in a thermo-magnetic medium which is followed with a discussion on numerical results in Sec. 6.3.

6.1 Shear Viscosity in magnetic field

In order to derive the expression for shear viscosity in a magnetized medium, we start with the standard expression of relativistic BTE in background electromagnetic field (characterized by the field strength tensor $F^{\mu\nu}$), which is given by

$$p^{\mu}\partial_{\mu}f + qF^{\mu\nu}p_{\nu}\frac{\partial f}{\partial p^{\mu}} = C[f] \tag{6.1}$$

where, f is the single particle phase space distribution function, q is the electric charge of the particle and the metric tensor with signature $g^{\mu\nu} = \mathrm{diag}(1, -1, -1, -1)$ has been used throughout the work. The collision term on the right hand side of Eq. (6.1) will be solved using the relaxation time approximation whereby

we consider $C[f] = -\frac{\delta f}{\tau}$, in which δf is the deviation function and τ is the relaxation time. The deviation function δf encapsulates the dissipative processes occurring in the system brought in by the collisions among the constituents.

The velocity gradients in the strongly interacting matter give rise to the shear viscosity in the medium. In order to extract the shear viscosity coefficients in presence of external magnetic field, Eq. (6.1) can be reduced to (taking $\boldsymbol{E} = \boldsymbol{0}$)

$$-\frac{1}{T}p_i p_j V_{ij} f_0(1+f_0) + q(\boldsymbol{v}\times\boldsymbol{B})\cdot\frac{\partial(\delta f)}{\partial \boldsymbol{p}} = -\frac{\delta f}{\tau} \tag{6.2}$$

where $\boldsymbol{v} = \boldsymbol{p}/\omega_{\boldsymbol{p}}$, and the tensor $V_{ij} = \frac{1}{2}\left(\partial_i v_j + \partial_j v_i\right)$ contains the velocity gradients. Eq. (6.2) can be further reduced to

$$-\frac{1}{T}p_i p_j V_{ij} f_0(1+f_0) + \frac{q|\boldsymbol{B}|}{\omega_{\boldsymbol{p}}}\epsilon_{ijk} v_j b_k \frac{\partial(\delta f)}{\partial v_i} = -\frac{\delta f}{\tau}. \tag{6.3}$$

In order to solve Eq. (6.3) for shear viscosities, the deviation function δf containing the velocity gradients is taken to be of the form

$$\delta f = \sum_{n=0}^{n=4} g_n V_{ij}^n v_i v_j \tag{6.4}$$

where g_n's are the coefficients to be determined, and the velocity gradients V_{ij}^n's in presence of magnetic field are constructed using the available vector b_i, the unit tensor δ_{ij} and the Levi-Civita symbol ϵ_{ijk} as follows [129]

$$V_{ij}^0 = (3b_ib_j - \delta_{ij})\left(b_k b_l V_{kl} - \frac{1}{3}\boldsymbol{\nabla}\cdot\boldsymbol{V}\right), \tag{6.5}$$

$$V_{ij}^1 = 2V_{ij} + \delta_{ij}V_{kl}b_k b_l - 2V_{ik}b_k b_j - 2V_{jk}b_k b_i + (b_{ij} - \delta_{ij})\boldsymbol{\nabla}\cdot\boldsymbol{V} + b_i b_j V_{kl} b_k b_l, \tag{6.6}$$

$$V_{ij}^2 = 2\left(V_{ik}b_j b_k + V_{jk}b_i b_k - 2b_i b_j V_{kl} b_k b_l\right), \tag{6.7}$$

$$V_{ij}^3 = V_{ik}b_{jk} + V_{jk}b_{ik} - V_{kl}b_{ik}b_j b_l - V_{kl}b_{jk}b_i b_l, \tag{6.8}$$

$$V_{ij}^4 = 2\left(V_{kl}b_{ik}b_j b_l + V_{kl}b_{jk}b_i b_l\right), \tag{6.9}$$

in which $b_{ij} = \epsilon_{ijk}b_k$. In order to calculate the transverse shear viscosity, we use $\boldsymbol{\nabla}\cdot\boldsymbol{V} = 0$ and $V_{kl}b_k b_l = 0$, as a result of which $V_{ij}^0 = 0$. We now proceed to solve Eq. (6.3) for the deviation function δf for which we substitute Eq. (6.4) into Eq. (6.3) and make use of Eqs. (6.5)-(6.9), to obtain (after some algebra):

$$\begin{aligned}
\frac{\omega_{\boldsymbol{p}}}{T}v_i v_j V_{ij} f_0(1+f_0) &= 2\omega_c g_1\left[2V_{ik}b_{ij}v_j v_k - 2V_{ik}b_{ij}b_k v_j(\boldsymbol{b}\cdot\boldsymbol{v})\right] + 2\omega_c g_2\left[2V_{ik}b_{ij}b_k v_j(\boldsymbol{b}\cdot\boldsymbol{v})\right] \\
&+ 2\omega_c g_3\left[2V_{ij}v_i v_j - 4V_{ij}b_j v_i(\boldsymbol{b}\cdot\boldsymbol{v})\right] + 2\omega_c g_4\left[2V_{ij}b_j v_i(\boldsymbol{b}\cdot\boldsymbol{v})\right] \\
&+ \frac{g_1}{\tau}\left[2V_{ij}v_i v_j - 4V_{ij}b_j v_i(\boldsymbol{b}\cdot\boldsymbol{v})\right] + \frac{g_2}{\tau}\left[4V_{ij}b_j v_i(\boldsymbol{b}\cdot\boldsymbol{v})\right] \\
&+ \frac{g_3}{\tau}\left[2V_{ik}b_{jk}v_i v_j - 2V_{kj}b_{ik}b_j v_i(\boldsymbol{b}\cdot\boldsymbol{v})\right] + \frac{g_4}{\tau}\left[4V_{kj}b_{ik}b_j v_i(\boldsymbol{b}\cdot\boldsymbol{v})\right].
\end{aligned} \tag{6.10}$$

Comparing the coefficients of tensor structures in Eq. (6.10) on both sides, we arrive at the following set of linear equations in g's

$$2\omega_c g_3 + \frac{g_1}{\tau} = \frac{\omega_{\boldsymbol{p}}}{2T} f_0(1+f_0), \tag{6.11}$$

$$g_3 - 2\omega_c \tau g_1 = 0, \tag{6.12}$$

$$2\omega_c g_1 - 2\omega_c g_2 - \frac{g_3}{\tau} + \frac{2g_4}{\tau} = 0, \tag{6.13}$$

$$2\omega_c g_3 - \omega_c g_4 + \frac{g_1}{\tau} - \frac{g_2}{\tau} = 0. \tag{6.14}$$

By solving Eqs. (6.11)-(6.14), the unknown quantities g_n with $n = 1, 2, 3, 4$ is obtained as

$$g_1 = \frac{\omega_{\boldsymbol{p}}}{2T} \frac{\tau}{[1+4(\omega_c\tau)^2]} f_0(1+f_0), \tag{6.15}$$

$$g_2 = \frac{\omega_{\boldsymbol{p}}}{2T} \frac{\tau}{[1+(\omega_c\tau)^2]} f_0(1+f_0), \tag{6.16}$$

$$g_3 = \frac{\omega_{\boldsymbol{p}}}{2T} \frac{2\omega_c\tau^2}{[1+4(\omega_c\tau)^2]} f_0(1+f_0), \tag{6.17}$$

$$g_4 = \frac{\omega_{\boldsymbol{p}}}{2T} \frac{\omega_c\tau^2}{[1+(\omega_c\tau)^2]} f_0(1+f_0). \tag{6.18}$$

Viscosity is characterized by the non-uniformity in the fluid flow and this information is carried by the deviation function. Therefore, having calculated the deviation function δf (or equivalently the g's), the transverse shear viscous coefficients can be extracted from the definition of the macroscopic momentum flux density tensor or the momentum flow tensor π^{ij}, which reads

$$\pi_{ij} = \int \frac{d^3p}{(2\pi)^3} v_i v_j \omega_{\boldsymbol{p}} \delta f = \sum_{n=0}^{n=4} \int \frac{d^3p}{(2\pi)^3} \omega_{\boldsymbol{p}} g_n v_i v_j v_k v_l V_{kl}^n \tag{6.19}$$

where in the last step, δf has been substituted from Eq. (6.4). Alternatively, the general tensorial decomposition of π^{ij} in terms of the velocity gradients can be written as

$$\pi_{ij} = \sum_{n=0}^{n=4} \eta_n V_{ij}^n \tag{6.20}$$

where η_n's are the shear viscosity coefficients in presence of external magnetic field. Making use of $V_{ij}^0 = 0$ for transverse shear viscous coefficients and comparing Eq. (6.19) and Eq. (6.20), we get after some algebra

$$\eta_n = \frac{2}{15} \int \frac{d^3p}{(2\pi)^3} \omega_{\boldsymbol{p}} g_n v^4 \quad , \qquad n = 1, 2, 3, 4. \tag{6.21}$$

Finally, substituting Eqs. (6.15)-(6.18) into Eq. (6.21), we obtain the following final expressions for the shear

viscosity coefficients

$$\eta_1 = \frac{g_\pi}{15T}\int\frac{d^3p}{(2\pi)^3}\frac{\boldsymbol{p}^4}{\omega_{\boldsymbol{p}}^2}\frac{\tau}{1+(2\tau\omega_c)^2}f_0(\omega_{\boldsymbol{p}})\{1+f_0(\omega_{\boldsymbol{p}})\}, \tag{6.22}$$

$$\eta_2 = \frac{g_\pi}{15T}\int\frac{d^3p}{(2\pi)^3}\frac{\boldsymbol{p}^4}{\omega_{\boldsymbol{p}}^2}\frac{\tau}{1+(\tau\omega_c)^2}f_0(\omega_{\boldsymbol{p}})\{1+f_0(\omega_{\boldsymbol{p}})\}, \tag{6.23}$$

$$\eta_3 = \frac{g_\pi}{15T}\int\frac{d^3p}{(2\pi)^3}\frac{\boldsymbol{p}^4}{\omega_{\boldsymbol{p}}^2}\frac{\tau^2\omega_c}{\frac{1}{2}+2(\tau\omega_c)^2}f_0(\omega_{\boldsymbol{p}})\{1+f_0(\omega_{\boldsymbol{p}})\}, \tag{6.24}$$

$$\eta_4 = \frac{g_\pi}{15T}\int\frac{d^3p}{(2\pi)^3}\frac{\boldsymbol{p}^4}{\omega_{\boldsymbol{p}}^2}\frac{\tau^2\omega_c}{1+(\tau\omega_c)^2}f_0(\omega_{\boldsymbol{p}})\{1+f_0(\omega_{\boldsymbol{p}})\}, \tag{6.25}$$

where, η_1 and η_2 are the shear viscosity coefficients in presence of magnetic field and η_3 and η_4 are Hall type shear viscosities as they vanish for vanishing magnetic field whereas $\eta_1 = \eta_2 = \eta$ for vanishing magnetic field.

6.2 Relaxation time in thermo-magnetic medium

Let us now calculate the relaxation time τ appearing in the electrical conductivity and shear viscosity expression. For the $2 \to 2$ scattering process $\pi(p) + \pi(k) \to \pi(p') + \pi(k')$, the inverse of the relaxation time τ is given by

$$\frac{1}{\tau(p)} = \frac{g}{4\omega_p}\iiint\frac{d^3k}{(2\pi)^3 2E_k}\frac{d^3p'}{(2\pi)^3 2E_{p'}}\frac{d^3k'}{(2\pi)^3 2E_{k'}}(2\pi)^4\delta^4\left(p+k-p'-k'\right)|\mathscr{M}|^2\frac{f_0^{\boldsymbol{p}}(1+f_0^{\boldsymbol{k'}})(1+f_0^{\boldsymbol{p'}})}{(1+f_0^{\boldsymbol{k}})} \tag{6.26}$$

where, $\mathscr{M}$ is the scattering amplitude, $f_0^{\boldsymbol{p}} = f_0(\omega_{\boldsymbol{p}})$, $f_0^{\boldsymbol{k'}} = f_0(\omega_{\boldsymbol{k'}})$ etc., and $g = 3$ is the degeneracy of the pions $(\pi^\pm, \pi^0)$. Integrating over the momenta d^3k' and d^3p', we get

$$\frac{1}{\tau(p)} = \frac{g}{2}\int\frac{d^3k}{(2\pi)^3}\left(\sigma\ v_{\rm rel}\right)f_0(\omega_k)\left\{1+f_0(\omega_k)\right\} \tag{6.27}$$

where, σ is the total $\pi\pi \to \pi\pi$ scattering cross section, and $v_{\rm rel}$ is the relative velocity between the initial state particles. We will now calculate the $\pi\pi \to \pi\pi$ cross section in a thermo-magnetic medium mediated by the vector meson ρ. The interaction Lagrangian (density) used is [141]

$$\mathscr{L}_{\rm int} = -g_{\rho\pi\pi}\partial_\mu\boldsymbol{\rho}_\nu\cdot(\partial^\mu\boldsymbol{\pi}\times\partial^\nu\boldsymbol{\pi}) \tag{6.28}$$

where, $\boldsymbol{\rho}_\nu$ and $\boldsymbol{\pi}$ are the iso-vector fields corresponding to ρ and π mesons respectively, and the coupling constant $g_{\rho\pi\pi} = 20.72\ \text{GeV}^{-2}$ is estimated from the experimental vacuum decay width of $\rho \to \pi\pi$ which is about $\Gamma_{\rho\to\pi\pi} \simeq 150$ MeV. It is useful to consider the isospin basis, so that the isospin averaged total cross section can be written as

$$\sigma = \frac{1}{64\pi^2 s}\int d\Omega\ \left(\frac{5}{9}|\mathscr{M}_2|^2 + \frac{1}{3}|\mathscr{M}_1|^2 + \frac{1}{9}|\mathscr{M}_0|^2\right) \tag{6.29}$$

where, $\mathscr{M}_I$ is the invariant amplitude in isospin channel(s) corresponding to the composite pionic isospin state(s) $|I, I_z\rangle$ having total isospin I (we note that, amplitudes are independent of the third component I_z of the isospin vector I). Using Eq. (6.28), the explicit expressions of $\mathscr{M}_I$'s come out to be [163]

$$\mathscr{M}_0 = g_{\rho\pi\pi}^2 \left[2\left(\frac{s-u}{t-m_\rho^2}\right) + 2\left(\frac{s-t}{u-m_\rho^2}\right)\right], \tag{6.30}$$

$$\mathscr{M}_1 = g_{\rho\pi\pi}^2 \left[2\left(\frac{t-u}{s-m_\rho^2-\frac{1}{3}g_{\mu\nu}\Pi^{\mu\nu}(\sqrt{s},\mathbf{0};T,B)}\right) + \left(\frac{s-u}{t-m_\rho^2}\right) - \left(\frac{s-t}{u-m_\rho^2}\right)\right], \tag{6.31}$$

$$\mathscr{M}_2 = g_{\rho\pi\pi}^2 \left[-\left(\frac{s-u}{t-m_\rho^2}\right) - \left(\frac{s-t}{u-m_\rho^2}\right)\right], \tag{6.32}$$

$$\tag{6.33}$$

where, s, t, u are the Mandelstam variables, m_ρ is the mass of the ρ meson, and $\Pi^{\mu\nu}(q^0, \boldsymbol{q}; T, B)$ is the thermo-magnetic self energy function of ρ-meson with momentum q.

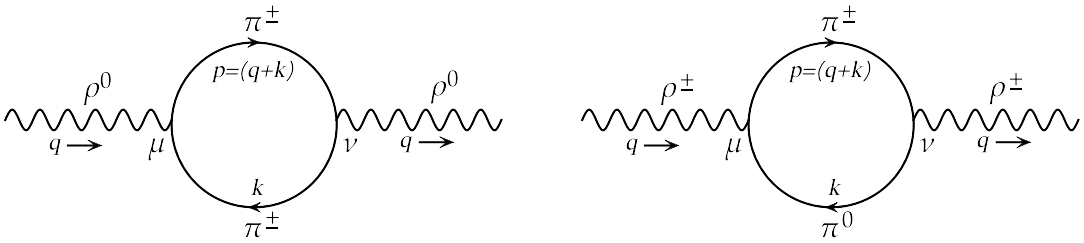

Figure 6.1: Feynman diagrams for the one-loop self energy of neutral and charged ρ meson.

We will now evaluate the one-loop self-energies of the ρ meson in a thermo-magnetic medium. Fig. 6.1 shows the Feynman diagrams for the one-loop self-energies of neutral and charged rho-mesons originating from the Lagrangian in Eq. (6.28). Unlike the zero magnetic field case, the self-energies of ρ^0 and $\rho^\pm$ become unequal in the presence of an external magnetic field. For calculating the thermo-magnetic self-energy of ρ-meson, we will use the real time formulation of thermal field theory in a magnetic background, in which the self-energy becomes 2×2 matrix [164, 165]. Applying the finite temperature Feynman rules to Fig. 6.1, the 11-components of the one-loop real time ρ^0 and $\rho^\pm$ meson self-energy matrices come out to be [166]

$$\Pi_{11,0}^{\mu\nu}(q;T,eB) = i\int \frac{d^4k}{(2\pi)^4} N^{\mu\nu}(q,k) D_{11}^{\rm mag}(k) D_{11}^{\rm mag}(p=q+k), \tag{6.34}$$

$$\Pi_{11,\pm}^{\mu\nu}(q;T,eB) = i\int \frac{d^4k}{(2\pi)^4} N^{\mu\nu}(q,k) D_{11}(k) D_{11}^{\rm mag}(p=q+k) \tag{6.35}$$

where $N^{\mu\nu}(q,k) = g_{\rho\pi\pi}^2 \left[q^4 k^\mu k^\nu + (q\cdot k)^2 q^\mu q^\nu - q^2(q\cdot k)(q^\mu k^\nu + k^\mu q^\nu)\right]$, $D_{11}(k)$ and $D_{11}^{\rm mag}(k)$ are the 11-component of the real time neutral and charged pion propagators respectively in a magnetic background (the π^0 propagator is not affected by the magnetic field). The explicit expressions of the π^0 and $\pi^\pm$

propagators read [166, 167]

$$D_{11}(k) = \left[\frac{-1}{k^2-m_\pi^2+i\epsilon}+2\pi i\eta(k^0)\delta(k^2-m_\pi^2)\right], \tag{6.36}$$

$$D_{11}^{\rm mag}(k) = \sum_{n=0}^{\infty}2(-1)^n e^{-\alpha_k}L_n(2\alpha_k)\left[\frac{-1}{k_\parallel^2-m_n^2+i\epsilon}+2\pi i\eta(k^0)\delta(k_\parallel^2-m_n^2)\right] \tag{6.37}$$

where, we have considered external magnetic field $\boldsymbol{B}=B\hat{\boldsymbol{z}}$ along the positive-$\hat{\boldsymbol{z}}$ direction, $\eta(x)=\Theta(x)f_0(x)+\Theta(-x)f_0(-x)$, n is the Landau level index, $\alpha_k=-k_\perp^2/eB>0$, e is the electric charge of a proton, $L_l(z)$ is Laguerre polynomial of order l, $m_n=\sqrt{m_\pi^2+(2n+1)eB}$, $p_{\parallel,\perp}^\alpha=g_{\parallel,\perp}^{\alpha\beta}p_\beta$ with $g_\parallel^{\mu\nu}=\text{diag}(1,0,0,-1)$ and $g_\perp^{\mu\nu}=\text{diag}(0,-1,-1,0)$.

Having obtained the 11-components of the self-energies, the analytic thermo-magnetic self-energy function $\Pi^{\mu\nu}(q;T,B)$ appearing in the expression of scattering amplitude in Eq. (6.31) can be obtained via relations [165, 164] $\text{Im}\Pi^{\mu\nu}(q)=\tanh\left(\frac{|q^0|}{2T}\right)\text{Im}\Pi_{11}^{\mu\nu}(q)$ and $\text{Re}\Pi^{\mu\nu}(q)=\text{Re}\Pi_{11}^{\mu\nu}(q)$. The imaginary parts of the self-energies can be simplified to obtain

$$\begin{aligned}\text{Im}\Pi_0^{\mu\nu}(q^0,\boldsymbol{q}=\boldsymbol{0}) = \frac{-1}{4q^0}\sum_{l=0}^{\infty}\sum_{n=0}^{\infty}\frac{1}{k_z'}\Big[&U_{1,nl}^{\mu\nu}(q^0,k_z')\Theta(q^0-m_n-m_l)+U_{2,nl}^{\mu\nu}(q^0,k_z')\Theta(-q^0-m_n-m_l)\\&+L_{1,nl}^{\mu\nu}(q^0,k_z')\Theta\left\{-q^0-\min(m_n-m_l,0)\right\}\Theta\left\{\max(m_n-m_l,0)+q^0\right\}\\&+L_{2,nl}^{\mu\nu}(q^0,k_z')\Theta\left\{q^0-\min(m_n-m_l,0)\right\}\Theta\left\{\max(m_n-m_l,0)-q^0\right\}\Big],\end{aligned} \tag{6.38}$$

$$\begin{aligned}\text{Im}\Pi_\pm^{\mu\nu}(q^0,\boldsymbol{q}=\boldsymbol{0}) = \frac{-\text{sign}(q^0)}{16\pi}\sum_{l=0}^{\infty}\sum_{s\in\{\pm\}}\Bigg[&\int_{\omega_0}^{\omega_-}\frac{d\omega_{\boldsymbol{k}}}{|\boldsymbol{k}|\cos\theta_0^+}U_{1,l}^{\mu\nu}\big(q^0,|\boldsymbol{k}|,s\cos\theta_0^+\big)\Theta(q^0-m_\pi-m_l)\\&+\int_{-\omega_0}^{-\omega_+}\frac{d\omega_{\boldsymbol{k}}}{|\boldsymbol{k}|\cos\theta_0^-}U_{2,l}^{\mu\nu}\big(q^0,|\boldsymbol{k}|,s\cos\theta_0^-\big)\Theta(-q^0-m_\pi-m_l)\\&+\int_{-\omega_-}^{-\omega_0}\frac{d\omega_{\boldsymbol{k}}}{|\boldsymbol{k}|\cos\theta_0^-}L_{1,l}^{\mu\nu}\big(q^0,|\boldsymbol{k}|,s\cos\theta_0^-\big)\Theta(-q^0-m_\pi+m_l)\Theta(q^0)\\&+\int_{\omega_+}^{\omega_0}\frac{d\omega_{\boldsymbol{k}}}{|\boldsymbol{k}|\cos\theta_0^+}L_{2,l}^{\mu\nu}\big(q^0,|\boldsymbol{k}|,s\cos\theta_0^+\big)\Theta(q^0-m_\pi+m_l)\Theta(-q^0)\Bigg]\end{aligned} \tag{6.39}$$

where $k_z'=\frac{1}{2q^0}\lambda^{1/2}(q_0^2,m_l^2,m_n^2)$, $\lambda(x,y,z)=x^2+y^2+z^2-2xy-2yz-2zx$ is the Källén function, $\omega_0=\frac{1}{2q^0}(q_0^2+m_\pi^2-m_l^2)$, $\omega_\pm=q^0\pm m_l$, and $\cos\theta_0^\pm=\frac{1}{|\boldsymbol{k}|}\sqrt{(q^0\mp\omega_k)^2-m_l^2}$. The explicit expressions of the tensors $U_{1,nl}^{\mu\nu}$, $U_{2,nl}^{\mu\nu}$, $L_{1,nl}^{\mu\nu}$, and $L_{2,nl}^{\mu\nu}$ appearing in Eq. (6.38) for the neutral rho-meson and $U_{1,l}^{\mu\nu}$, $U_{2,l}^{\mu\nu}$, $L_{1,l}^{\mu\nu}$, and $L_{2,l}^{\mu\nu}$ appearing in Eq. (6.39) for the charged rho-meson are provided in Appendix C. The imaginary parts of the ρ^0 as well as $\rho^\pm$ self energies have contributions from four terms (symbolically the U_1, U_2, L_1 and L_2) containing a number of step functions. These step functions represent the branch cuts of the self-energy function in the complex q^0 plane. They are termed as Unitary-I, Unitary-II, Landau-I and Landau-II cuts respectively as they appear in Eqs. (6.38) and (6.39). These cuts physically correspond to the kinematically

allowed scattering and decay processes in the thermomagnetic medium. The details of the calculation and an analysis of the analytic structure of the self-energy function can be found in Ref. [166]. Having obtained the thermo-magnetic self-energy functions $\Pi^{\mu\nu}_{0,\pm}$ of ρ^0 and $\rho^\pm$, we substitute them into the expression of scattering amplitude in Eq. (6.31) to obtain the isospin averaged $\pi\pi \to \pi\pi$ cross-section from Eq. (6.29) for a ρ^0 or $\rho^\pm$ exchange.

6.3 Numerical Results & Discussions

We begin this section by evaluating the numerical results for a generic isospin averaged $\pi\pi$ cross-section mediated by neutral and charged ρ mesons. The neutral and charged ρ mesons are affected differently in the presence of magnetic field as evident from the analytical calculation in the previous section.

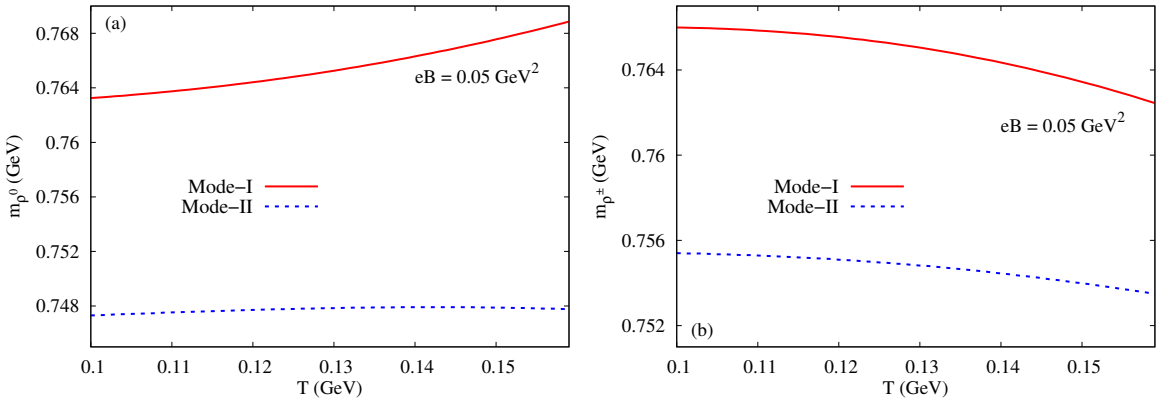

Figure 6.2: The effective masses of (a) ρ^0 and (b) $\rho^\pm$ vs T for $eB = 0.05$ GeV^2.

In Figs. 6.2 (a) and (b) we have shown the variation of effective masses of neutral and charged ρ meson as a function of temperature for $eB = 0.05$ GeV^2. The masses have been calculated from the poles of the exact ρ-meson propagator in a thermo-magnetic medium [166]. It is well known that in thermo-magnetic medium there are three distinct propagating modes of vector meson. However at vanishing transverse momentum of the vector meson, two modes are identical and hence we are left with two distinct modes denoted by Mode-I and Mode-II respectively [166]. From both the figures it is clear that the change in effective masses of both neutral and charged meson with temperature is marginal. It should be noted that, the variation of mass with temperature/magnetic field calculated using the Lagrangian (Eq. (6.28)) in which ρ and π mesons are basic degrees of freedom is expected to differ from that of other models such as Nambu–Jona-Lasinio (NJL) like models which are based on quark degrees of freedom and the mesons are generated by bosonization [168, 169, 170, 171].

We have plotted the $\pi\pi \to \pi\pi$ cross-section as a function of centre of mass energy for three different values of magnetic field- 0.005 GeV^2, 0.01 GeV^2 and 0.05 GeV^2 shown respectively in Fig.6.3(a), Fig.6.3(b) and Fig.6.3(c). In each of these plots temperature is taken to be 130 MeV. The numerical results of the cross-section has been computed in various media such as vacuum (V), thermal medium (T), magnetic

medium (M), and thermo-magnetic medium (TM).

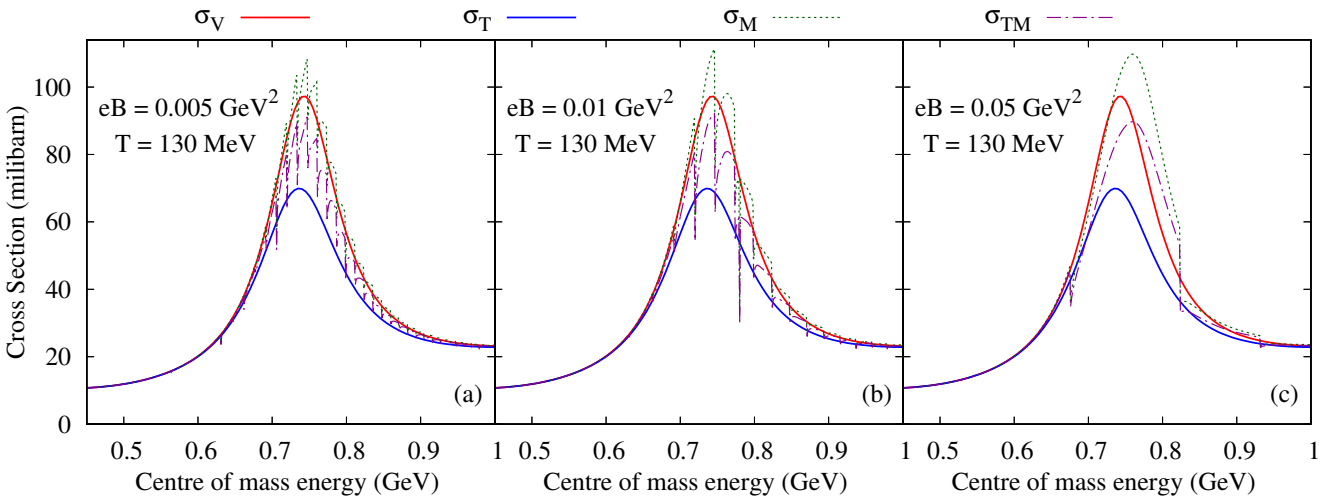

Figure 6.3: The variation of the isospin-averaged total $\pi\pi \to \pi\pi$ cross section at $T = 130$ MeV as a function of the center-of-mass energy for different media at (a) $eB = 0.005$ GeV^2, (b) $eB = 0.01$ GeV^2 and (c) $eB = 0.05$ GeV^2. The symbols $\sigma_{\rm V}$, $\sigma_{\rm M}$, $\sigma_{\rm T}$ and $\sigma_{\rm TM}$ denotes the $\pi\pi$ cross-section in vacuum, magnetic medium, thermal medium and thermo-magnetic medium respectively.

In Figs. 6.3(a) and (b) we observe the following trend for $\pi\pi$ cross-section: $\sigma_{\rm M} > \sigma_{\rm V} > \sigma_{\rm TM} > \sigma_{\rm T}$. We now attempt to explain this trend in the cross-section variation over different media. As the temperature is increased, the resonance spectral function experience in-medium broadening, owing to an increase in the imaginary part of the self-energy. This increase in the imaginary part of the self-energy in the thermal medium causes a decrease in the magnitude of thermal cross-section $\sigma_{\rm T}$ compared to the vacuum cross-section $\sigma_{\rm V}$. Physically, $\sigma_{\rm V} > \sigma_{\rm T}$ can be explained using the fact that in a thermal medium, ρ meson suffer additional decay and scattering thus lowering the $\pi\pi$ cross-section in thermal medium. In all the figures we observe the presence of spikes for finite values of the background magnetic field. The spikes are purely due to the presence of magnetic field. Particularly, it is due to the combined effects of threshold singularity appearing in the imaginary part of ρ^0 self energy for each Landau level and the Laguerre polynomials (which produces oscillations) appearing in the imaginary part of $\rho^{\pm}$ self energy. Physically, it corresponds to highly unstable ρ^0 meson at threshold values of q_0 decaying to π^+ and π^- in a purely magnetic medium. This explains the cross-section in magnetic medium being higher in magnitude compared to its vacuum counterpart ($\sigma_{\rm M} > \sigma_{\rm V}$). It is observed from the figure that the magnetic field causes nearly 10% increase in magnitude of cross-section compared to the vacuum cross-section and the thermal bath causes approximately 25-30% decrease in thermal medium dependent cross-section compared to the vacuum cross-section. This combined effect of temperature and magnetic-field causes the thermo-magnetic cross-section to be lower in magnitude than its vacuum counterpart as shown in Figs. 6.3(a) and (b). However, in Fig. 6.3(c) we observe the following trend - $\sigma_{\rm M} > \sigma_{\rm V} > \sigma_{\rm TM} > \sigma_{\rm T}$ for almost all values of centre of mass energy except for the region $0.75 \lesssim \sqrt{s} \lesssim 0.82$ GeV where $\sigma_{\rm TM} > \sigma_{\rm V}$. This suggests that the effect of magnetic field dominates over thermal contribution near resonance energies at higher eB values.

Next, we have studied the variation of average relaxation time $\langle\tau\rangle$ of pions as a function of temperature

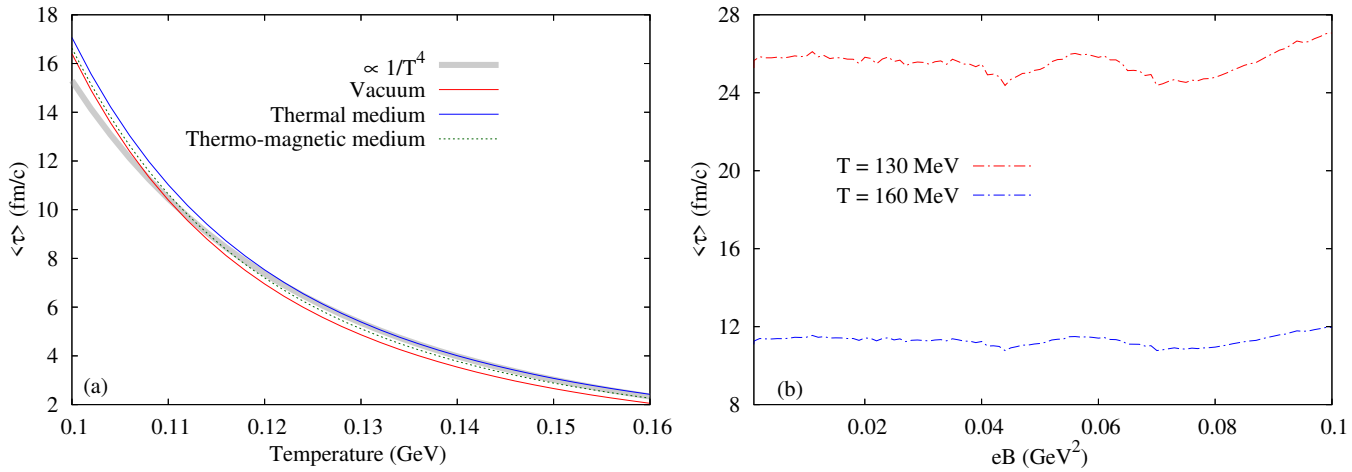

Figure 6.4: Variation of average relaxation time of pions as a function of (a) temperature at $eB = 0.01$ GeV^2, and (b) magnetic field at different temperatures.

at a magnetic field value of $eB = 0.01$ GeV^2 in Fig. 6.4 (a) and as a function of magnetic field at two different temperatures ($T = 130$ MeV and $T = 160$ MeV) in Fig. 6.4(b) respectively. In Fig. 6.3, it is seen that both the thermal and thermo-magnetic cross-section is suppressed with respect to the vacuum cross-section hence, the average relaxation time which is inversely related to the cross-section is enhanced in magnitude compared to its vacuum counterpart. As the relaxation time is a key dynamical input to the transport coefficients we will try to extract the leading behaviour of $\langle\tau\rangle$ as a function of temperature. For this we have fitted the variation of average relaxation time with $\frac{a_0}{T^4}$ (here a_0 is a constant) for qualitative understanding of the results of electrical conductivity and shear viscosity. Thus the leading order behaviour of the average relaxation will be approximated to $\langle\tau\rangle \sim \frac{1}{T^4}$. In Fig. 6.4(b), we observe a mild oscillatory variation of average relaxation time with respect to the magnetic field. As discussed earlier, this mild oscillatory behaviour is due to the combined effects of the threshold singularity appearing in the imaginary part of ρ^0 self-energy and Laguerre polynomial appearing in the $\rho^{\pm}$ self-energy.

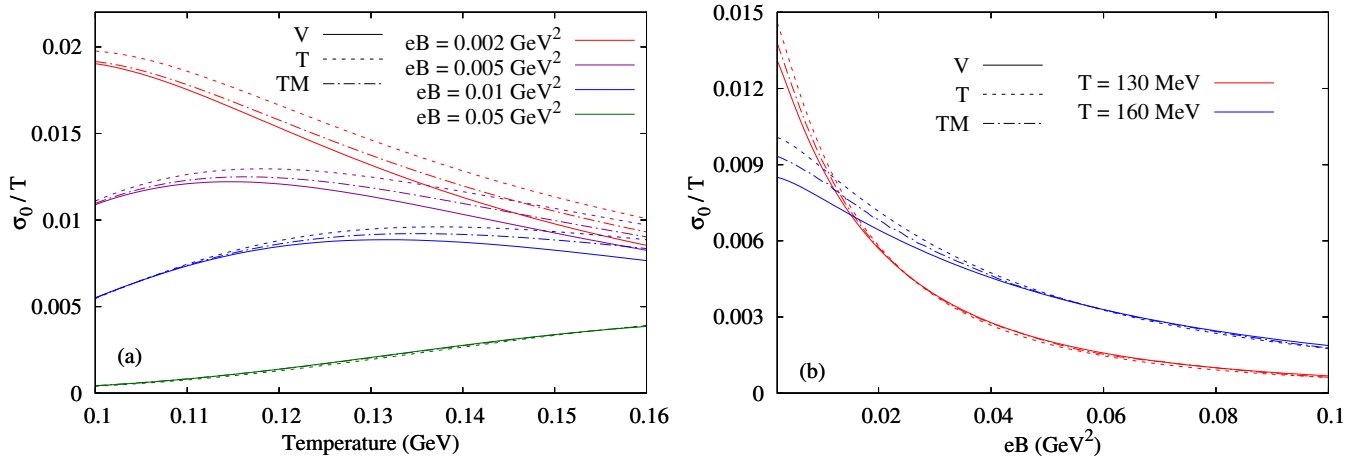

Figure 6.5: Variation of σ_0/T as a function of (a) temperature for different values of the magnetic field strength, and (b) magnetic field for different values of the temperature. Solid, dashed and dash-dotted lines of different colours respectively represent the consideration of vacuum, thermal and thermo-magnetic cross-sections while calculating the transport coefficients.

The numerical evaluation of electrical conductivity has been done using the electrical and hall conductivity expressions derived in Sec. 5.1. In Fig. 6.5(a) we have shown the variation of $\frac{\sigma_0}{T}$ with temperature for different values of magnetic field strength, and in Fig. 6.5(b) we have shown the variation of $\frac{\sigma_0}{T}$ as a function of magnetic field for different values of temperature. It must be noted that the transport coefficients calculated using thermal medium dependent cross-section experiences magnetic field influence only through cyclotron frequency ω_c, whereas in a thermo-magnetic medium magnetic field influence comes from ω_c and eB dependent $\langle\tau\rangle$ calculated using medium dependent cross-section. The variation of $\frac{\sigma_0}{T}$ with temperature can be explained with $\frac{\sigma_0}{T} \sim \frac{\tau T}{1+(\omega_c\tau)^2}$. We will make use of $\langle\tau\rangle \sim \frac{1}{T^4}$ to explain the temperature variation of electrical conductivity. We now explain the variation of electrical and Hall conductivities with temperature and magnetic field. For lower eB values $\omega_c\tau \ll 1$, thus $\frac{\sigma_0}{T} \sim \tau T \sim \frac{1}{T^3}$ whereas for higher eB values $\omega_c\tau \gg 1$, hence $\frac{\sigma_0}{T} \sim \frac{T}{\tau} \sim T^5$. This $\frac{1}{T^3}$ and T^5 variation respectively at lower and higher eB values can be seen in Fig. 6.5(a). The magnetic field dependence of $\frac{\sigma_0}{T}$ can be explained with $\frac{\sigma_0}{T} \sim \frac{\tau T}{1+(\omega_c\tau)^2}$. The two magnetic field dependent terms are ω_c and τ. As eB value increases, ω_c increases which results in the decrease of $\frac{\sigma_0}{T}$ for higher eB values as seen in Fig. 6.5(b). For lower eB values $\frac{\sigma_0}{T} \sim \tau$, thus we observe the trend $(\frac{\sigma_0}{T})_{\rm T} > (\frac{\sigma_0}{T})_{\rm TM} > (\frac{\sigma_0}{T})_{\rm V}$ which is in agreement to the trend in average relaxation time $\langle\tau\rangle_{\rm T} > \langle\tau\rangle_{\rm TM} > \langle\tau\rangle_{\rm V}$. However, this trend in $\frac{\sigma_0}{T}$ variation with magnetic field is not respected for higher eB values as $\frac{\sigma_0}{T} \sim \frac{1}{\tau}$ for higher eB values.

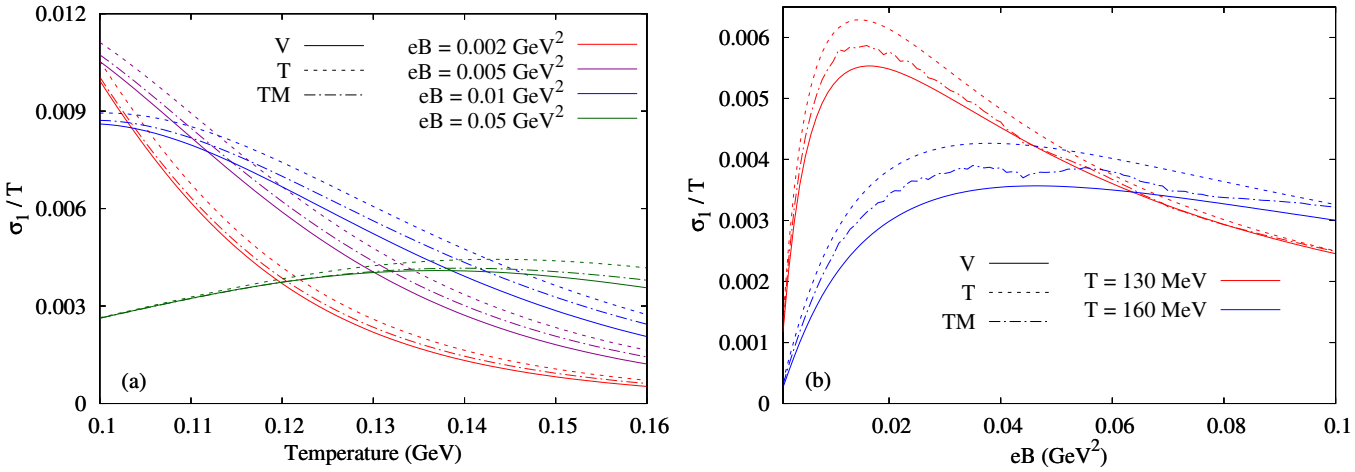

Figure 6.6: Variation of σ_1/T as a function of (a) temperature for different values of the magnetic field strength, and (b) magnetic field for different values of the temperature. Solid, dashed and dash-dotted lines of different colours respectively represent the consideration of vacuum, thermal and thermo-magnetic cross-sections while calculating the transport coefficients.

In Fig. 6.6(a) we have shown the plot for the variation of temperature scaled Hall conductivity $\frac{\sigma_1}{T}$ as a function of temperature for different values of magnetic field strength and in Fig. 6.6(b), we have shown the variation of $\frac{\sigma_1}{T}$ as a function of magnetic field for different values of temperature. The temperature variation of $\frac{\sigma_1}{T}$ can be understood with $\frac{\sigma_1}{T} \sim \frac{\tau^2\omega_c T}{1+(\omega_c\tau)^2}$. For lower eB values $\omega_c\tau \ll 1$, which results in $\frac{\sigma_1}{T} \sim \tau^2\omega_c T \sim \frac{\omega_c}{T^7}$ whereas for higher eB values $\omega_c\tau \gg 1$, resulting in $\frac{\sigma_1}{T} \sim \frac{T}{\omega_c}$. This variation can be observed in Fig. 6.6(a). The variation of $\frac{\sigma_1}{T}$ with magnetic field as seen in Fig. 6.6(b) can be understood using $\frac{\sigma_1}{T} \sim \frac{\tau^2\omega_c}{1+(\omega_c\tau)^2}$. The cyclotron frequency, ω_c renders a Breit-Wigner like function and τ^2 causes mild

oscillations in $\frac{\sigma_1}{T}$ for a thermo-magnetic medium due to the eB dependent $\pi\pi$ scattering cross-section. As the medium effect information is contained in the relaxation time τ and as $\frac{\sigma_1}{T} \sim \tau^2$, we observe in Figs. 6.6(a) and (b) that for any value of temperature and magnetic field, $\frac{\sigma_1}{T}$ evaluated for the medium (thermal and thermo-magnetic both) is higher than its vacuum counterpart.

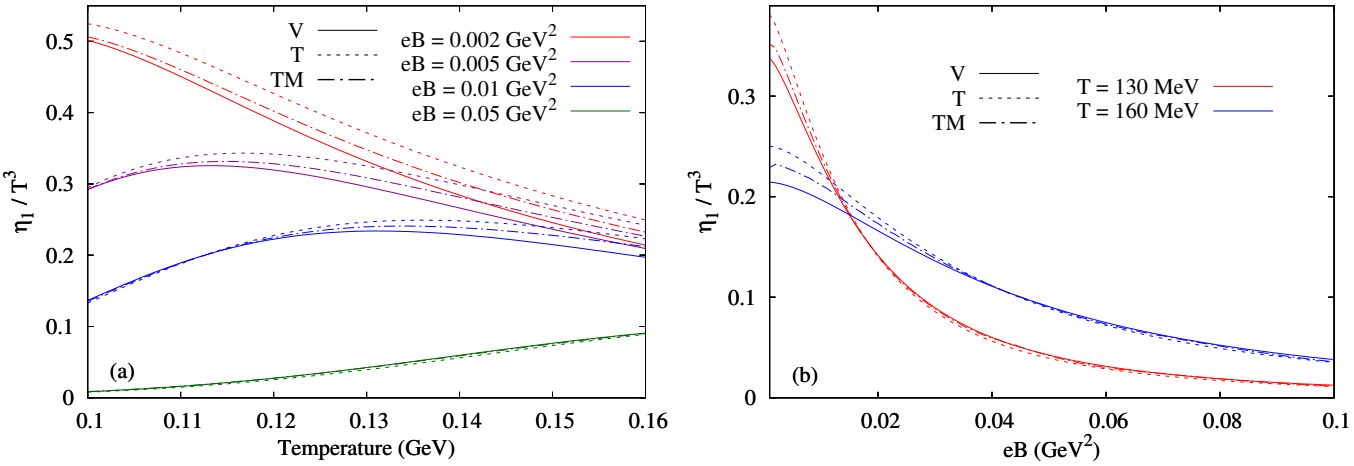

Figure 6.7: Variation of η_1/T as a function of (a) temperature for different values of the magnetic field strength, and (b) magnetic field for different values of the temperature. Solid, dashed and dash-dotted lines of different colours respectively represent the consideration of vacuum, thermal and thermo-magnetic cross-sections while calculating the transport coefficients.

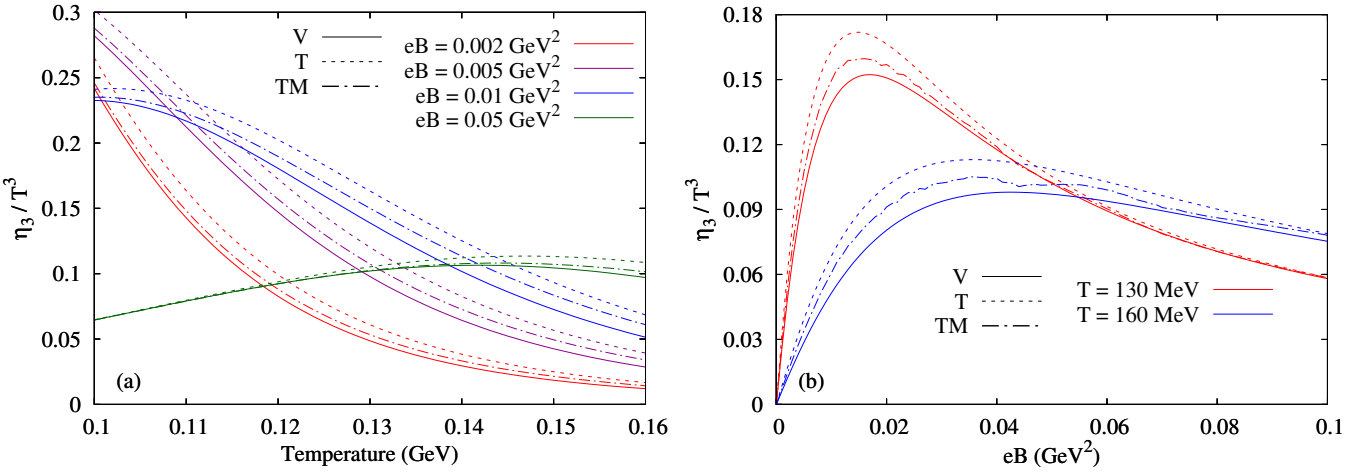

Figure 6.8: Variation of η_3/T as a function of (a) temperature for different values of the magnetic field strength, and (b) magnetic field for different values of the temperature. Solid, dashed and dash-dotted lines of different colours respectively represent the consideration of vacuum, thermal and thermo-magnetic cross-sections while calculating the transport coefficients.

The variation of temperature scaled normal shear viscosity $\frac{\eta_1}{T^3}$ with temperature for different values of magnetic field is shown in Fig. 6.7(a) and the variation of $\frac{\eta_1}{T^3}$ with magnetic field for different values of temperature is shown in Fig. 6.7(b). Using $\frac{\eta_1}{T^3} \sim \frac{\tau T}{1+(2\omega_c\tau)^2}$, we can explain the temperature dependence of $\frac{\eta_1}{T^3}$. For $\omega_c\tau \ll 1$ corresponding to lower eB values, $\frac{\eta_1}{T^3} \sim \tau T \sim \frac{1}{T^3}$ whereas for $\omega_c\tau \gg 1$ corresponding to higher eB values, $\frac{\eta_1}{T^3} \sim \frac{T}{\tau} \sim T^5$. At intermediate magnetic field values the variation of $\frac{\eta_1}{T^3}$ is non-monotonic which is due to the interplay of both temperature and eB. The variation of $\frac{\eta_1}{T^3}$ with magnetic field can be understood using $\frac{\eta_1}{T^3} \sim \frac{\tau}{1+(2\omega_c\tau)^2}$. As $\langle\tau\rangle$ is approximately constant (mild oscillations) with changing eB

as seen in Fig. 6.4(b), the $\frac{\eta_1}{T^3}$ variation with magnetic field can be explained using the values of ω_c. Thus, with the increase in ω_c corresponding to higher eB values, $\frac{\eta_1}{T^3}$ decreases monotonically. As observed earlier $\langle\tau\rangle_{\rm T} > \langle\tau\rangle_{\rm TM} > \langle\tau\rangle_{\rm V}$ and for lower eB values $\frac{\eta_1}{T^3} \sim \tau$, we observe the trend $(\frac{\eta_1}{T^3})_{\rm T} > (\frac{\eta_1}{T^3})_{\rm TM} > (\frac{\eta_1}{T^3})_{\rm V}$ for lower eB values in Fig. 6.7(a) and (b). The variation of $\frac{\eta_2}{T^3}$ with eB and temperature can be explained similar to that of $\frac{\eta_1}{T^3}$ as they differ only by a factor in the denominator.

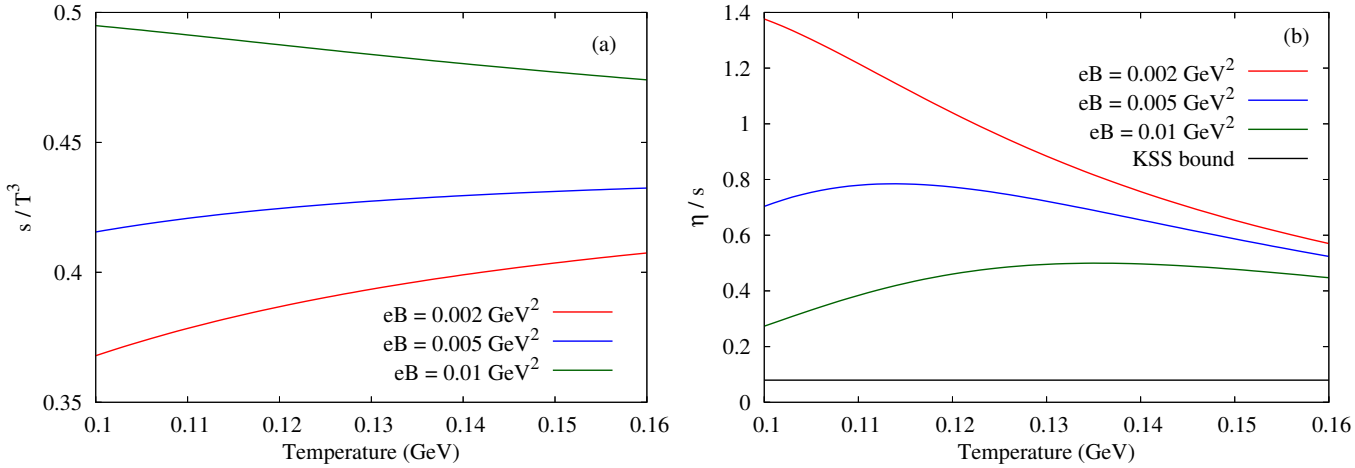

Figure 6.9: Variation of (a) entropy density (s), and (b) Specific shear viscosity (η/s) as a function of temperature for different values of the magnetic field strength.

In Fig. 6.8(a) we have shown the plot for the variation of temperature scaled Hall type shear viscosity η_3/T^3 as a function of temperature for different values of magnetic field whereas in Fig. 6.8(b) we have shown the variation of η_3/T^3 as a function of magnetic field for different values of temperature. η_3 is a purely Hall type quantity. It vanishes at zero magnetic field as can be seen from Fig. 6.8(b). The variation of $\frac{\eta_3}{T^3}$ with temperature can be understood with $\frac{\eta_3}{T^3} \sim \frac{\tau^2\omega_c T}{1+(2\omega_c\tau)^2}$. At low eB values $\omega_c\tau \ll 1$, thus $\frac{\eta_3}{T^3} \sim \tau^2\omega_c T \sim \frac{\omega_c}{T^7}$ whereas for higher eB values $\omega_c\tau \gg 1$, thus $\frac{\eta_3}{T^3} \sim \frac{T\tau^2}{\tau^2\omega_c T} \sim \frac{T}{\omega_c}$. This causes $\frac{\eta_3}{T^3}$ to monotonically decrease with increasing temperature at lower eB values and to monotonically increase with increasing temperature at higher eB values. The variation of $\frac{\eta_3}{T^3}$ with eB can be explained using $\frac{\eta_3}{T^3} \sim \frac{\tau^2\omega_c}{1+(2\omega_c\tau)^2}$. The quantity τ^2 appearing in the numerator has an effect of causing mild oscillations in $\frac{\eta_3}{T^3}$ calculated for the thermomagnetic medium. A Breit-Wigner like structure seen in Fig. 6.8(b) is due to the term $\frac{\omega_c}{1+(2\omega_c\tau)^2}$ occurring in $\frac{\eta_3}{T^3}$. Both Breit-Wigner form and mild oscillations in thermo-magnetic medium can be observed in Fig. 6.8(b). It can been observed from Figs. 6.8(a) and (b) that $\frac{\eta_3}{T^3}$ calculated in thermal and thermo-magnetic medium has higher magnitude for all values of eB compared to that of $\frac{\eta_3}{T^3}$ evaluated in the vacuum with finite B. This is in agreement with the fact that η_3 is a Hall type quantity and increasing magnetic field necessarily increases its value. The variation of $\frac{\eta_4}{T^3}$ as a function of temperature and magnetic field can be explained similar to that of $\frac{\eta_3}{T^3}$ since their expressions differ only by a factor in the denominator as can be noticed by comparing Eqs. (6.24) and (6.25).

In Fig. 6.9(a), we have shown the variation of scaled entropy density with temperature. The entropy density s has been calculated using the thermodynamic potential as shown in Appendix D. It is seen from the figure that for lower values of magnetic field s/T^3 increases with increasing temperature whereas for

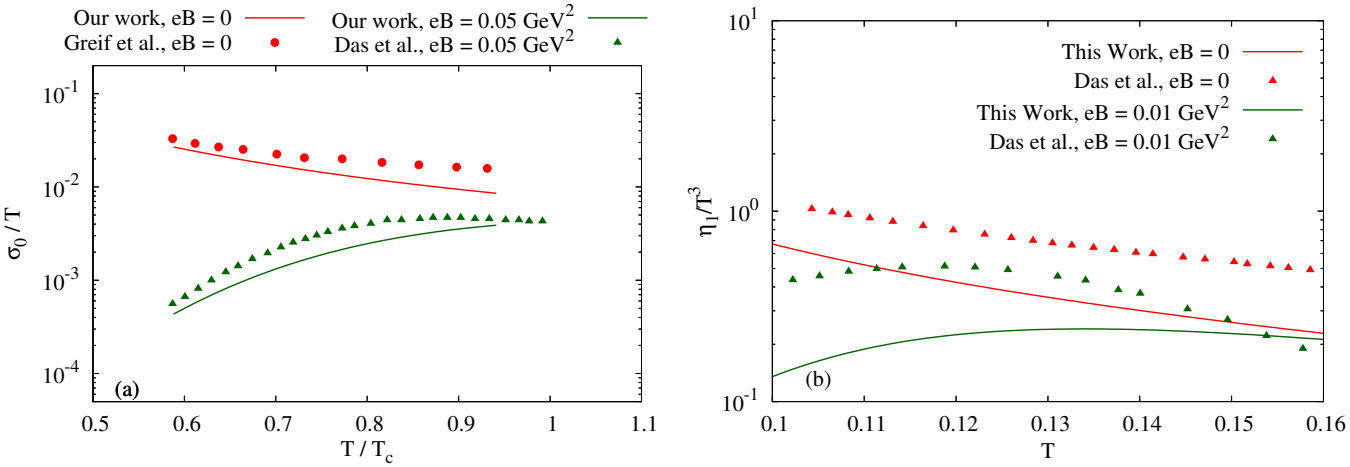

Figure 6.10: Comparison of (a) σ_0/T obtained in this work at zero magnetic field with Refs. [9] and [7] and at non-zero magnetic field with Refs. [10] and [12], and (b) η_1/T^3 obtained in this work with at zero and non-zero magnetic field with Ref. [13]

higher values of magnetic field strength s/T^3 decreases with increasing temperature. This shows that the increasing magnetic field reduces the randomness in pionic system under consideration. In Fig. 6.9(b), we have shown the variation of the specific shear viscosity (η/s) as a function of temperature for different values of magnetic field in a thermo-magnetic medium. As the magnitude of entropy density increases with the increase in magnetic field for a given temperature, it causes an increase in the magnitude of η/s compared to the magnitude of η_1/T^3. The obtained values of η/s are well within the KSS bound.

In Fig. 6.10(a), we have made a comparison of electrical conductivity obtained in our work with the other available results in literature. For zero magnetic field our results show a good match with the works of Greif et al. in Ref. [7]. Electrical conductivity results for $eB = 0.05GeV^2$ agrees well with the electrical conductivity calculated by Das et al. at the same eB value for a hadron resonance gas in Ref. [12]. Similarly in Fig. 6.10(b), we have shown a comparison of shear viscosity for both zero and non-zero magnetic field with that obtained by Das et al. in Ref. [13]. The difference in magnitude of shear viscosity can be attributed to the increased number density in a hadron resonance gas (used by Das et al.) which causes an increase in the magnitude of shear viscosity in Ref. [13].

Chapter 7

Summary and Outlook

The main aim of this thesis is to study the transport properties of the strongly interacting matter produced in the later stages of heavy ion collisions, from a kinetic theory approach. This study is motivated by the results of heavy ion collision experiments at RHIC which has shown clear indication that the matter produced in these experiments behave like strongly interacting fluid having small but finite value of shear viscosity to entropy density ratio. This has led to the study of different transport coefficients with an aim to obtain a realistic temperature dependence of these transport quantities in hot hadronic medium. Also, the generation of huge background magnetic field in heavy ion collision experiments at RHIC and LHC serves as a motivation to calculate magnetic field dependent transport coefficients. Thus, a detailed study of the effect of medium (both thermal and magnetic) dependent scattering cross section on the transport coefficients like thermal conductivity, shear viscosity, bulk viscosity and electrical conductivity has been made. As electrical conductivity is responsible for sustaining the magnetic field for a longer time in the medium, in this thesis we have focused on the calculation of electrical conductivity of a hadronic medium. We have made use of relaxation time approximation to calculate these transport coefficients of first-order hydrodynamics.

The earlier studies of transport coefficients of hot and hadronic medium using kinetic theory approach have considered either a constant cross-section or have treated cross-section as a free parameter to evaluate these transport coefficients. The scattering cross-section which is a key dynamical input to the calculation of these transport coefficient gets modified in the presence of hot and/or dense medium and also in the background magnetic field. This incorporation of the thermo-magnetic medium effects is the novelty of this thesis, as it provides a more realistic estimate of the transport coeffcieints. We will now summarize the essential results and discussions from each chapter below.

As the transport coefficients have been evaluated using the kinetic theory approach, in Chapter 2 we discuss in detail the basics of kinetic theory. In this chapter, various macroscopic quantities are discussed in detail in terms of the one-particle distribution function, and various conservation laws are also studied. The relativistic BTE has been derived both in the presence and absence of a background magnetic field.

In Chapter 3 the derivation of transport coefficients from BTE is discussed in detail. As the thermal medium effects on the bulk properties are being investigated, the RTF of the TFT is briefly studied, and

the thermal propagator of different fields is derived. For the sake of completeness and to illustrate the methodology of incorporating medium effects in transport coefficients, the shear viscosity of a pion gas in a thermal medium is evaluated. The results obtained in this chapter have provided strong motivation for a detailed study of transport coefficients in a medium using the medium-dependent cross section.

Having observed significant influence of the medium effects on the shear viscosity in Chapter 3, we now shift our focus to a multi-component hadronic mixture. Thus, in Chapter 4 a hot and dense hadronic gas mixture consisting of pions, kaons, and nucleons, which are the most important components of the system produced during the later stages of heavy ion collisions, has been considered. A systematic study of the relaxation times, viscous coefficients, and thermal conductivity for a system consisting only of pions, a system of pions and kaons, and finally for a pion-kaon-nucleon system has been presented using the BTE, which has been linearized using the Enskog expansion. The key ingredient is the use of in-medium cross-sections obtained using one-loop corrected thermal propagators in the matrix elements for $\pi\pi$, πK and πN scattering. The suppression of the in-medium cross-sections at finite temperature and density is reflected in the enhancement of relaxation times. This, in turn, results in observable modification of the temperature dependence of η, ζ and λ/T^2. However, the temperature dependence of η/s and ζ/s, where the entropy density s also contains the effect of interactions, is much less affected by the medium. On comparison, the value of η/s in the medium for vanishing chemical potentials is found to be in agreement with existing estimates in the literature.

After the study of thermal medium effects on the transport properties of hadronic system, we have swithced on the magnetic field in Chapter 5. As mentioned earlier, it is the electrical conductivity of the medium which sustains the otherwise transient magnetic field for a longer time. Thus, in this chapter the electrical conductivity tensor has been evaluated using the Boltzmann transport equation in a magnetic field, and hence, the electrical conductivity, Hall conductivity, and σ_2 for a system consisting of a pion gas have been assessed. The information pertaining to the dynamics of pion gas enters through the relaxation time into the expression of the three conductivities. The $\pi\pi$ cross section has been calculated in a thermal medium using the real time formalism of finite temperature field theory. The variation of these three conductivities with temperature for different values of the magnetic field has been shown. It is observed that electrical conductivity and Hall conductivity are very sensitive to the magnetic field strength and the in-medium cross sections. Moreover, as the LQ has not been considered in the dispersion relation of charged pions, the results are more accurate at low magnetic field values ($qH \lesssim m^2$), which is the realistic scenario for the later stages of HICs. Both the electrical and Hall conductivities have been found to increase with temperature for a given value of the magnetic field when the in-medium cross-section is used. For a given temperature there is no appreciable change (except at lower magnetic field values) in the electrical conductivity with the magnetic field when medium dependent cross section is used. A more detailed observation shows a monotonically increasing trend of electrical conductivity with the increase in temperature at higher values of the magnetic field. However, for a given temperature the conductivity is found to decrease monotonically as a function of the magnetic field. In the case of Hall conductivity, it is found that at lower values of the magnetic field, it

decreases with the increase in temperature more rapidly than the electrical conductivity, whereas at higher values of the magnetic field, a linear increase of the Hall conductivity with the temperature is observed. For a given temperature as long as it is low, a Breit-Wigner type structure in the Hall conductivity as a function of the magnetic field is seen. This structure disappears and tends to saturate at higher temperature. This behaviour can be attributed to the substantial spectral broadening of the exchanged particle at high temperature. The electrical conductivity obtained in this work has been shown to have both qualitative and quantitative agreement with earlier estimates available in the literature. Moreover, the calculated electrical conductivity is shown to be sufficient for causing a significant delay in the decay of external magnetic field in HIC. This leads to the conclusion that, weak magnetic field can be present in the later stage of HIC (in hadronic phase) and could be phenomenologically relevant.

In Chapter 6, we have considered the magnetic field influence on the transport coefficients through cyclotron frequency and magnetic field dependent cross-section. Here, we have studied the medium effects on two important transport coefficients- electrical conductivity and shear viscosity of a pion gas. These coefficients have been estimated using kinetic theory and relaxation time approximation. The dynamics of the pion gas in a thermo-magnetic medium have been taken into consideration by evaluating the $\pi\pi \to \pi\pi$ scattering cross-section using thermal field theory techniques in presence of background magnetic field. A medium dependent relaxation time obtained from the medium dependent cross-section has been used to calculate the electrical conductivity and shear viscosity of the pion gas. The electrical conductivity and shear viscosity are influenced by the magnetic field through the cyclotron frequency and the magnetic field-dependent relaxation time. It is observed that the relaxation time shows a mild oscillatory behaviour with the magnetic field, which is reflected in the electrical conductivity and shear viscosity evaluated in a thermo-magnetic medium. However, it must be noted that the magnetic field influence coming from the cyclotron frequency is higher in magnitude than the magnetic field influence from the relaxation time. Electrical conductivity and shear viscosity show an increase in magnitude with respect to temperature for a thermo-magnetic medium compared to its vacuum counterpart. Electrical conductivity σ_0/T and shear viscosity η_1/T^3 for a particular value of temperature show increased magnitude for lower magnetic field values and the magnitude gradually decreases for higher magnetic field values when thermo-magnetic effects are considered. However, the Hall type electrical conductivity σ_1/T and Hall type shear viscosity η_3/T^3 for a particular value of temperature are found to increase for all values of the magnetic field. The electrical conductivity and shear viscosity obtained in this work show a good agreement with the works available in the literature. Additionally, it has been observed that the estimated value of electrical conductivity in the range of 0.5-2 MeV causes a maximum magnetic field of strength 10^{-6}-10^{-5} GeV^2 to survive for a time $t \sim 10$ fm, which is sufficient to affect the dynamics and hence the evolution of hadronic matter produced in the later stage of HICs. It is to be noted that the interesting phenomenon of $\rho^+ - \pi^+$ mixing [168] as observed in NJL type models, has not been included. However such mixing cannot be achieved in the simplistic model that has been used in our work. Also the neutral pion remains unaffected by the magnetic field in this case. Moreover, for $eB = 0.05$ GeV^2 the Landau magnetic length is of the order of the radius of ρ and hence an

appropriate form factor is necessary to suppress the manifestation of quark structure of the mesons while calculating the cross-section. A few representative form factors, including that of [168], have been used to check this, but no appreciable change in the results has been observed.

In order to solve the BTE with collision term, we have made use of relaxation time approximation. In this approximation, only the distribution function of one of the incoming particles in a binary interaction is taken to be slightly away from equilibrium. Thus, this method simplifies the complex nature of particle collisions. In order to incorporate complex nature of particle interaction one can make use of Chapman Enskog approximation. In this method one systematically expands the distribution function in terms of a small parameter (the Knudsen number), leading to a series of approximations that can be improved iteratively.

It must be noted that we have only considered the magnetic field effects on the propagators and not on the external legs. For charged particles the magnetic field will modify the external legs which will affect the scattering cross-section. Though the influence of the magnetic field coming from the magnetic field dependent relaxation time is comparatively lower in magnitude than the magnetic field effect due to cyclotron frequency, a notable improvement to this work would be to include the magnetic field in the external legs to calculate the scattering cross-section.

Appendices

Appendix A

Thermodynamic quantities

The thermodynamic quantities like energy density, number density, pressure and enthalpy of the three component system consisting of pions, kaons and nucleons can be expressed in terms of the sum of series of Bessels function as $S_n^\alpha(z_\pi)$, $R_n^\alpha(z_K)$ and $T_n^\alpha(z_N)$, where $z_\pi = m_\pi/T$, $z_K = m_K/T$ and $z_N = m_N/T$. These quantities are given as:

$$n_\pi = g_\pi \int \frac{d^3p_\pi}{(2\pi)^3} f_\pi^{(0)}(p_\pi) = \left(\frac{g_\pi}{2\pi^2}\right) z_\pi^2 T^3 S_2^1(z_\pi) \ , \tag{A.1}$$

$$P_\pi = g_\pi \int \frac{d^3p_\pi}{(2\pi)^3} \frac{\vec{p_\pi}^{\,2}}{3E_{p_\pi}} f_\pi^{(0)}(p_\pi) = \left(\frac{g_\pi}{2\pi^2}\right) z_\pi^2 T^4 S_2^2(z_\pi) \ , \tag{A.2}$$

$$n_\pi e_\pi = g_\pi \int \frac{d^3p_\pi}{(2\pi)^3} E_{p_\pi} f_\pi^{(0)}(p_\pi) = \left(\frac{g_\pi}{2\pi^2}\right) z_\pi^2 T^4 \left[z_\pi S_3^1(z_\pi) - S_2^2(z_\pi)\right] , \tag{A.3}$$

$$n_\pi h_\pi = n_\pi z_\pi \frac{S_3^1(z_\pi)}{S_2^1(z_\pi)} \tag{A.4}$$

where $E_{p_\pi} = \sqrt{\vec{p}_\pi^2 + m_\pi^2}$ and $f_\pi^{(0)}(p_\pi) = [e^{\beta(E_{p_\pi} - \mu_\pi)} - 1]^{-1}$. Making use of the formula

$$[a-1]^{-1} = \sum_{n=1}^{\infty} (a^{-1})^n \quad \text{for} \quad |a| < 1 \ , \tag{A.5}$$

the distribution function can be expanded, so that the three momentum integrals in the above equations could be analytically performed and expressed in terms of the following infinite series

$$S_n^\alpha(z_\pi) = \sum_{k=1}^{\infty} \ e^{k\mu_\pi/T} \ k^{-\alpha} \ K_n(kz_\pi) \tag{A.6}$$

where $K_n(x)$ is the modified Bessel function of order n whose integral representation is

$$K_n(x) = \frac{2^n n!}{(2n)! \ x^n} \int_x^\infty d\tau (\tau^2 - x^2)^{n-\frac{1}{2}} e^{-\tau} \tag{A.7}$$

or

$$K_n(x) = \frac{2^n n!(2n-1)}{(2n)! x^n} \int_x^\infty \tau \ d\tau (\tau^2 - x^2)^{n-\frac{3}{2}} \ e^{-\tau}. \tag{A.8}$$

The expression for thermodynamic quantities mentioned above will be similar for kaons and nucleons except the term $S_n^\alpha(z_\pi)$ will be replaced by $R_n^\alpha(z_K)$ for kaons and $T_n^\alpha(z_N)$ for nucleons where

$$R_n^\alpha(z_K) = \sum_{k=1}^{\infty} e^{k\mu_K/T}\ k^{-\alpha}\ K_n(kz_K) \tag{A.9}$$

and

$$T_n^\alpha(z_N) = \sum_{k=1}^{\infty} (-1)^{k-1}\ e^{k\mu_N/T}\ k^{-\alpha}\ K_n(kz_N)\ . \tag{A.10}$$

Appendix B

Expressions for γ's

The transport equation for each species is given by

$$p^{\mu}\partial_{\mu}f_{k}^{(0)}(x,p) = -\frac{\delta f(x,p)}{\tau_{k}}E_{k} \tag{B.1}$$

where on the right hand side of the equation, we have made use of relaxation time approximation. The time and space derivatives (in the local rest frame) present in the left hand side of the above equation will be replaced by the derivatives of the thermodynamics parameters. The equation then reduces to

$$(p_k\cdot u)\left[\frac{p_k\cdot u}{T^2}DT + D\left(\frac{\mu_k}{T}\right) - \frac{p_k^{\mu}}{T}Du_{\mu}\right] + p^{\mu}\left[\frac{p_k\cdot u}{T^2}\nabla_{\mu}T + \nabla_{\mu}\left(\frac{\mu_k}{T}\right) - \frac{p_k^{\nu}}{T}\nabla_{\mu}u_{\nu}\right] = -\frac{\delta f(x,p)}{\tau_k}E_k\ . \tag{B.2}$$

The conservation equations

$$\partial_{\mu}N_k^{\mu} = 0, \quad Dn_k = -n_k\partial_{\mu}u^{\mu} \ \text{ and } \ \sum_k n_k De_k = -\sum_k P_k\partial_{\mu}u^{\mu} \tag{B.3}$$

with $N^{\mu} = nU^{\mu}$ and total $P = p_{\pi} + p_K + p_N$ can be expanded in terms of the derivative with respect to temperature and chemical potential over temperature as

$$\frac{\partial n_{\pi}}{\partial T}DT + \frac{\partial n_{\pi}}{\partial(\mu_{\pi}/T)}D\left(\frac{\mu_{\pi}}{T}\right) + \frac{\partial n_K}{\partial(\mu_K/T)}D\left(\frac{\mu_K}{T}\right) + \frac{\partial n_N}{\partial(\mu_N/T)}D\left(\frac{\mu_N}{T}\right) = -n_{\pi}\ \partial_{\mu}u^{\mu}\ , \tag{B.4}$$

$$\frac{\partial n_K}{\partial T}DT + \frac{\partial n_{\pi}}{\partial(\mu_{\pi}/T)}D\left(\frac{\mu_{\pi}}{T}\right) + \frac{\partial n_K}{\partial(\mu_K/T)}D\left(\frac{\mu_K}{T}\right) + \frac{\partial n_N}{\partial(\mu_N/T)}D\left(\frac{\mu_N}{T}\right) = -n_K\ \partial_{\mu}u^{\mu}\ , \tag{B.5}$$

$$\frac{\partial n_N}{\partial T}DT + \frac{\partial n_{\pi}}{\partial(\mu_{\pi}/T)}D\left(\frac{\mu_{\pi}}{T}\right) + \frac{\partial n_K}{\partial(\mu_K/T)}D\left(\frac{\mu_K}{T}\right) + \frac{\partial n_N}{\partial(\mu_N/T)}D\left(\frac{\mu_N}{T}\right) = -n_N\ \partial_{\mu}u^{\mu}\ , \tag{B.6}$$

$$\left[n_{\pi}\frac{\partial e_{\pi}}{\partial T} + n_K\frac{\partial e_K}{\partial T} + n_N\frac{\partial e_N}{\partial T}\right] + n_{\pi}\frac{\partial e_{\pi}}{\partial(\mu_{\pi}/T)}D\left(\frac{\mu_{\pi}}{T}\right)$$
$$+n_K\frac{\partial e_K}{\partial(\mu_K/T)}D\left(\frac{\mu_K}{T}\right) + n_N\frac{\partial e_N}{\partial(\mu_N/T)}D\left(\frac{\mu_N}{T}\right) = -P\partial_{\mu}u^{\mu}. \tag{B.7}$$

Making use of the expressions obtained in Appendix A in the above equations and then solving for DT, $D\left(\frac{\mu_\pi}{T}\right)$, $D\left(\frac{\mu_K}{T}\right)$ and $D\left(\frac{\mu_N}{T}\right)$ we get

$$DT = T\,(1-\gamma')\,\partial_\mu u^\mu\,, \tag{B.8}$$

$$TD\left(\frac{\mu_\pi}{T}\right) = [(\gamma''_\pi - 1) - T\gamma'''_\pi]\,\partial_\mu u^\mu\,, \tag{B.9}$$

$$TD\left(\frac{\mu_K}{T}\right) = [(\gamma''_K - 1) - T\gamma'''_K]\,\partial_\mu u^\mu\,, \tag{B.10}$$

$$TD\left(\frac{\mu_N}{T}\right) = [(\gamma''_N - 1) - T\gamma'''_N]\,\partial_\mu u^\mu \tag{B.11}$$

where

$$\begin{aligned}\gamma' = \frac{1}{X}\Bigg[& g_\pi\left\{z_\pi^3\left(4R_2^0S_2^0T_2^0S_3^1 + R_2^0T_2^0S_3^0S_2^1\right) + z_\pi^4\left(R_2^0T_2^0(S_2^0)^2 - R_2^0T_2^0(S_3^0)^2\right)\right\}\\ & + g_K\left\{z_K^3\left(4R_2^0S_2^0T_2^0R_3^1 + S_2^0T_2^0R_3^0R_2^1\right) + z_K^4\left(S_2^0T_2^0(R_2^0)^2 - S_2^0T_2^0(R_3^0)^2\right)\right\}\\ & + g_N\left\{z_N^3\left(4R_2^0S_2^0T_2^0T_3^1 + R_2^0S_2^0T_3^0T_2^1\right) + z_N^4\left(R_2^0S_2^0(T_2^0)^2 - R_2^0S_2^0(T_3^0)^2\right)\right\}\Bigg],\end{aligned} \tag{B.12}$$

$$\begin{aligned}\gamma''_\pi = \frac{1}{X}\Bigg[& g_\pi\left\{-5z_\pi^2R_2^0T_2^0(S_2^1)^2 + z_\pi^3\left(3R_2^0S_2^0T_2^0S_3^1 + 3R_2^0T_2^0S_3^0S_2^1\right) + z_\pi^4\left(R_2^0T_2^0(S_2^0)^2 - R_2^0T_2^0(S_3^0)^2\right)\right\}\\ & + g_K\left\{-z_K^2S_2^0T_2^0(R_2^1)^2 + z_K^3\left(3R_2^0S_2^0T_2^0R_3^1 + 2R_3^0S_2^0T_2^0R_2^1\right) + z_K^4\left(S_2^0T_2^0(R_2^0)^2 - S_2^0T_2^0(R_3^0)^2\right)\right\}\\ & + g_N\left\{-z_N^2R_2^0S_2^0(T_2^1)^2 + z_N^3\left(3R_2^0S_2^0T_2^0T_3^1 + 2R_2^0S_2^0T_3^0T_2^1\right) + z_N^4\left(R_2^0S_2^0(T_2^0)^2 - R_2^0S_2^0(T_3^0)^2\right)\right\}\Bigg],\end{aligned} \tag{B.13}$$

$$\begin{aligned}\gamma'''_\pi = \frac{1}{X}\Bigg[& g_\pi\left\{z_\pi^4R_2^0T_2^0S_2^0S_2^1\right\} + g_K\left\{z_K^3\left(4R_2^0T_2^0S_2^1R_3^1 + T_2^0R_3^0R_2^1S_2^1\right) + z_K^4\left(T_2^0S_2^1(R_2^0)^2 - T_2^0S_2^1(R_3^0)^2\right)\right.\\ & \left. - z_\pi z_K^2T_2^0S_3^0(R_2^1)^2 + z_\pi z_K^3\left(R_3^0S_3^0T_2^0R_2^1 - R_2^0S_3^0T_2^0R_3^1\right)\right\} + g_N\left\{z_N^3\left(4R_2^0T_2^0S_2^1T_3^1 + R_2^0T_3^0S_2^1T_2^1\right)\right.\\ & \left. + z_N^4\left(R_2^0S_2^1(T_2^0)^2 - R_2^0S_2^1(T_3^0)^2\right) - z_\pi z_N^2R_2^0S_3^0(T_2^1)^2 + z_\pi z_N^3\left(R_2^0S_3^0T_3^0T_2^1 - R_2^0S_3^0T_2^0T_3^1\right)\right\}\Bigg],\end{aligned} \tag{B.14}$$

$$\begin{aligned}\gamma''_K = \frac{1}{X}\Bigg[& g_\pi\left\{-z_\pi^2R_2^0T_2^0(S_2^1)^2 + z_\pi^3\left(3R_2^0S_2^0T_2^0S_3^1 + 2R_2^0T_2^0S_3^0S_2^1\right) + z_\pi^4\left(R_2^0T_2^0(S_2^0)^2 - R_2^0T_2^0(S_3^0)^2\right)\right\}\\ & + g_K\left\{-5z_K^2S_2^0T_2^0(R_2^1)^2 + z_K^3\left(3R_2^0S_2^0T_2^0R_3^1 + 3R_3^0S_2^0T_2^0R_2^1\right) + z_K^4\left(S_2^0T_2^0(R_2^0)^2 - S_2^0T_2^0(R_3^0)^2\right)\right\}\\ & + g_N\left\{-z_N^2R_2^0S_2^0(T_2^1)^2 + z_N^3\left(3R_2^0S_2^0T_2^0T_3^1 + 2R_2^0S_2^0T_3^0T_2^1\right) + z_N^4\left(R_2^0S_2^0(T_2^0)^2 - R_2^0S_2^0(T_3^0)^2\right)\right\}\Bigg],\end{aligned} \tag{B.15}$$

$$\gamma'''_K = \frac{1}{X}\Bigg[g_\pi\left\{z_\pi^3\left(4T_2^0S_2^0R_2^1S_3^1+T_2^0S_3^0R_2^1S_2^1\right)+z_\pi^4\left(T_2^0R_2^1(S_2^0)^2-T_2^0R_2^1(S_3^0)^2\right)-z_Kz_\pi^2T_2^0R_3^0(S_2^1)^2 \\ +z_Kz_\pi^3\left(T_2^0R_3^0S_3^0S_2^1-T_2^0R_3^0S_2^0S_3^1\right)\right\}+g_K\left\{z_k^4S_2^0T_2^0R_2^0R_2^1\right\}+g_N\left\{z_N^3\left(4T_2^0S_2^0R_2^1T_3^1+S_2^0T_3^0R_2^1T_2^1\right) \\ +z_N^4\left(S_2^0R_2^1(T_2^0)^2-S_2^0R_2^1(T_3^0)^2\right)-z_Kz_N^2S_2^0R_3^0(T_2^1)^2+z_Kz_N^3\left(S_2^0R_3^0T_3^0T_2^1-S_2^0R_3^0T_2^0T_3^1\right)\right\}\Bigg], \quad \text{(B.16)}$$

$$\gamma''_N = \frac{1}{X}\Bigg[g_\pi\left\{-z_\pi^2R_2^0T_2^0(S_2^1)^2+z_\pi^3\left(3R_2^0S_2^0T_2^0S_3^1+2R_2^0T_2^0S_3^0S_2^1\right)+z_\pi^4\left(R_2^0T_2^0(S_2^0)^2-R_2^0T_2^0(S_3^0)^2\right)\right\} \\ +g_K\left\{-z_K^2S_2^0T_2^0(R_2^1)^2+z_K^3\left(3R_2^0S_2^0T_2^0R_3^1+2R_3^0S_2^0T_2^0R_2^1\right)+z_K^4\left(S_2^0T_2^0(R_2^0)^2-S_2^0T_2^0(R_3^0)^2\right)\right\} \\ +g_N\left\{-5z_N^2R_2^0S_2^0(T_2^1)^2+z_N^3\left(3R_2^0S_2^0T_2^0T_3^1+3R_2^0S_2^0T_3^0T_2^1\right)+z_N^4\left(R_2^0S_2^0(T_2^0)^2-R_2^0S_2^0(T_3^0)^2\right)\right\}\Bigg], \quad \text{(B.17)}$$

$$\gamma'''_N = \frac{1}{X}\Bigg[g_\pi\left\{z_\pi^3\left(4S_2^0R_2^0T_2^1S_3^1+R_2^0S_3^0T_2^1S_2^1\right)+z_\pi^4\left(R_2^0T_2^1(S_2^0)^2-R_2^0T_2^1(S_3^0)^2\right)-z_Nz_\pi^2R_2^0T_3^0(S_2^1)^2 \\ +z_Nz_\pi^3\left(R_2^0S_3^0T_3^0S_2^1-R_2^0S_2^0T_3^0S_3^1\right)\right\}+g_N\left\{z_N^4S_2^0T_2^0R_2^0T_2^1\right\}+g_K\left\{z_K^3\left(4R_2^0S_2^0T_2^1R_3^1+R_3^0S_2^0R_2^1T_2^1\right) \\ +z_K^4\left((R_2^0)^2S_2^0T_2^1-(R_3^0)^2S_2^0T_2^1\right)-z_Nz_K^2S_2^0T_3^0(R_2^1)^2+z_Nz_K^3\left(S_2^0R_3^0T_3^0R_2^1-R_2^0S_2^0T_3^0R_3^1\right)\right\}\Bigg], \quad \text{(B.18)}$$

and the term X appearing in the above expressions of γ's is given by

$$X = g_\pi\left[-z_\pi^2R_2^0T_2^0(S_2^1)^2+z_\pi^3\left(3R_2^0S_2^0T_2^0S_3^1+2R_2^0T_2^0S_3^0S_2^1\right)+z_\pi^4\left(R_2^0T_2^0(S_2^0)^2-R_2^0T_2^0(S_3^0)^2\right)\right] \\ +g_K\left[-z_K^2S_2^0T_2^0(R_2^1)^2+z_K^3\left(3R_2^0S_2^0T_2^0R_3^1+2R_3^0S_2^0T_2^0R_2^1\right)+z_K^4\left(S_2^0T_2^0(R_2^0)^2-S_2^0T_2^0(R_3^0)^2\right)\right] \\ +g_N\left[-z_N^2R_2^0S_2^0(T_2^1)^2+z_N^3\left(3R_2^0S_2^0T_2^0T_3^1+2R_2^0S_2^0T_3^0T_2^1\right)+z_N^4\left(R_2^0S_2^0(T_2^0)^2-R_2^0S_2^0(T_3^0)^2\right)\right]. \quad \text{(B.19)}$$

Appendix C

Tensors Appearing in the Imaginary Parts of Self-Energies

In this appendix, we provide the explicit expressions of the tensors $U^{\mu\nu}_{1,nl}$, $U^{\mu\nu}_{2,nl}$, $L^{\mu\nu}_{1,nl}$, and $L^{\mu\nu}_{2,nl}$ appearing in Eq. (6.38) and $U^{\mu\nu}_{1,l}$, $U^{\mu\nu}_{2,l}$, $L^{\mu\nu}_{1,l}$, and $L^{\mu\nu}_{2,l}$ appearing in Eq. (6.39). These are given by

$$
\begin{aligned}
U^{\mu\nu}_{1,nl}(q^0,k_z) &= \Big\{1+f_0(\omega^n_k)+f_0(\omega^l_k)\Big\}\,N^{\mu\nu}_{nl}(k_0=\omega^n_k), && \text{(C.1)}\\
U^{\mu\nu}_{2,nl}(q^0,k_z) &= \Big\{-1-f_0(\omega^n_k)-f_0(\omega^l_k)\Big\}\,N^{\mu\nu}_{nl}(k_0=-\omega^n_k), && \text{(C.2)}\\
L^{\mu\nu}_{1,nl}(q^0,k_z) &= \Big\{f_0(\omega^n_k)-f_0(\omega^l_k)\Big\}\,N^{\mu\nu}_{nl}(k_0=-\omega^n_k), && \text{(C.3)}\\
L^{\mu\nu}_{2,nl}(q^0,k_z) &= \Big\{-f_0(\omega^n_k)+f_0(\omega^l_k)\Big\}\,N^{\mu\nu}_{nl}(k_0=\omega^n_k), && \text{(C.4)}\\
U^{\mu\nu}_{1,l}\big(q^0,|\boldsymbol{k}|,\cos\theta\big) &= 2(-1)^l e^{-\alpha_k}L_l(2\alpha_k)\Big\{1+f_0(\omega^l_k)+f_0(\omega_{\boldsymbol{k}})\Big\}\,N^{\mu\nu}(q,k^0=\omega_{\boldsymbol{k}},\boldsymbol{k}), && \text{(C.5)}\\
U^{\mu\nu}_{2,l}\big(q^0,|\boldsymbol{k}|,\cos\theta\big) &= 2(-1)^l e^{-\alpha_k}L_l(2\alpha_k)\Big\{-1-f_0(\omega^l_k)-f_0(\omega_{\boldsymbol{k}})\Big\}\,N^{\mu\nu}(q,k^0=-\omega_{\boldsymbol{k}},\boldsymbol{k}), && \text{(C.6)}\\
L^{\mu\nu}_{1,l}\big(q^0,|\boldsymbol{k}|,\cos\theta\big) &= 2(-1)^l e^{-\alpha_k}L_l(2\alpha_k)\Big\{f_0(\omega^l_k)-f_0(\omega_{\boldsymbol{k}})\Big\}\,N^{\mu\nu}(q,k^0=-\omega_{\boldsymbol{k}},\boldsymbol{k}), && \text{(C.7)}\\
L2^{\mu\nu}_{1,l}\big(q^0,|\boldsymbol{k}|,\cos\theta\big) &= 2(-1)^l e^{-\alpha_k}L_l(2\alpha_k)\Big\{-f_0(\omega^l_k)+f_0(\omega_{\boldsymbol{k}})\Big\}\,N^{\mu\nu}(q,k^0=\omega_{\boldsymbol{k}},\boldsymbol{k}), && \text{(C.8)}
\end{aligned}
$$

where,

$$
\begin{aligned}
\mathcal{N}^{\mu\nu}_{nl}(q^0,k^0,k_z) &= g^2_{\rho\pi\pi}(-1)^{n+l}\left(\frac{eB}{2\pi}\right)\Big[\Big\{q^4_\parallel k^\mu_\parallel k^\nu_\parallel+(q_\parallel.k_\parallel)^2q^\mu_\parallel q^\nu_\parallel-q^2_\parallel(q_\parallel.k_\parallel)(q^\mu_\parallel k^\nu_\parallel+q^\nu_\parallel k^\mu_\parallel)\Big\}\delta^n_l\\
&\quad-\frac{eB}{4}q^4_\parallel g^{\mu\nu}_\perp\Big\{(2n+1)\delta^n_l-n\delta^{n-1}_l-(n+1)\delta^{n+1}_l\Big\}\Big], && \text{(C.9)}
\end{aligned}
$$

$\omega^n_k=\sqrt{k^2_z+m^2_n}$ and $N^{\mu\nu}$ is defined below Eq. (6.35).

Appendix D

Calculation of Entropy Density

In order to derive the expression for entropy density for a system of pion gas, we make use of the thermodynamic potential following [172, 173, 174, 175, 176, 177, 178]. The normalized thermodynamic potential Ω in the absence of magnetic field is given as

$$\Omega^{\rm norm}(T) = gT \int \frac{d^3k}{(2\pi)^3} \ln(1 - e^{-\omega_{\boldsymbol{k}}/T}) \tag{D.1}$$

where $\omega_{\boldsymbol{k}} = \sqrt{\boldsymbol{k}^2 + m_\pi^2}$ and $g = 3$ is the pion degeneracy. Here the normalization is done in the usual manner by subtracting the divergent vacuum contribution. The other relevant thermodynamic quantities can be calculated using the normalized thermodynamic potential as

$$P = -\Omega^{\rm norm}(T), \tag{D.2}$$

$$\epsilon = -T^2 \frac{\partial}{\partial T}\left(\frac{\Omega^{\rm norm}}{T}\right) \tag{D.3}$$

where P is the pressure and ϵ is the energy density. The entropy density is then obtained from $s = \left(\frac{\epsilon + P}{T}\right)$.

The presence of background magnetic field can be incorporated by modifying the momentum integral for charged pions in the following manner [173]

$$\int \frac{d^3k}{(2\pi)^3} f(\omega_k) \longrightarrow \sum_{l=0}^{\infty} \frac{|eB|}{2\pi} \int_{-\infty}^{\infty} \frac{dk_z}{2\pi} f(\omega_k^l). \tag{D.4}$$

Here $\omega_k^l(k_z) = \sqrt{k_z^2 + (2l+1)eB + m_\pi^2}$ is the Landau quantized energy eigen value of the charged pions. Thus the normalized thermodynamic potential for a pion gas in presence of external magnetic field is then given by

$$\Omega_B^{\rm norm}(T, eB) = T \int \frac{d^3k}{(2\pi)^3} \ln(1 - e^{-\omega_{\boldsymbol{k}}/T}) + 2T \sum_{l=0}^{\infty} \frac{|eB|}{2\pi} \int_{-\infty}^{\infty} \frac{dk_z}{2\pi} \ln(1 - e^{-\omega_k^l/T}) \tag{D.5}$$

where, the first term on the rhs is the contribution from the neutral pions which are not affected by the

magnetic field. The entropy density in presence of magnetic field is given by [172, 173]

$$s_B = \frac{\epsilon_B + P_\parallel}{T} \tag{D.6}$$

where, $P_\parallel = -\Omega_B^{\rm norm}$ is the longitudinal pressure and

$$\epsilon_B = \frac{1}{3}\epsilon + 2\sum_{l=0}^{\infty}\frac{|eB|}{2\pi}\int_{-\infty}^{\infty}\frac{dk_z}{2\pi}\frac{\omega_k^l}{e^{\omega_k^l/T}-1}. \tag{D.7}$$

Bibliography

[1] M. Luzum and P. Romatschke, *Conformal relativistic viscous hydrodynamics: Applications to rhic results at* $\sqrt{s_{NN}} = 200$ *gev*, *Phys. Rev. C* **78** (2008) 034915.

[2] D. E. Kharzeev, *The Chiral Magnetic Effect and Anomaly-Induced Transport*, *Prog. Part. Nucl. Phys.* **75** (2014) 133 [1312.3348].

[3] M. Prakash, M. Prakash, R. Venugopalan and G. Welke, *Nonequilibrium properties of hadronic mixtures*, *Phys. Rept.* **227** (1993) 321.

[4] N. Demir and S. A. Bass, *Shear-viscosity to entropy-density ratio of a relativistic hadron gas*, *Phys. Rev. Lett.* **102** (2009) 172302.

[5] P. Romatschke and S. Pratt, *Extracting the shear viscosity of a high temperature hadron gas*, 1409.0010.

[6] J.-B. Rose, J. M. Torres-Rincon, A. Schäfer, D. R. Oliinychenko and H. Petersen, *Shear viscosity of a hadron gas and influence of resonance lifetimes on relaxation time*, *Phys. Rev. C* **97** (2018) 055204.

[7] M. Greif, C. Greiner and G. S. Denicol, *Electric conductivity of a hot hadron gas from a kinetic approach*, *Phys. Rev. D* **93** (2016) 096012 [1602.05085].

[8] D. Fernandez-Fraile and A. Gomez Nicola, *The Electrical conductivity of a pion gas*, *Phys. Rev. D* **73** (2006) 045025 [hep-ph/0512283].

[9] A. Amato, G. Aarts, C. Allton, P. Giudice, S. Hands and J.-I. Skullerud, *Electrical conductivity of the quark-gluon plasma across the deconfinement transition*, *Phys. Rev. Lett.* **111** (2013) 172001 [1307.6763].

[10] B. Feng, *Electric conductivity and Hall conductivity of the QGP in a magnetic field*, *Phys. Rev.* **D96** (2017) 036009.

[11] A. Das, H. Mishra and R. K. Mohapatra, *Electrical conductivity and Hall conductivity of a hot and dense hadron gas in a magnetic field: A relaxation time approach*, *Phys. Rev. D* **99** (2019) 094031 [1903.03938].

[12] A. Das, H. Mishra and R. K. Mohapatra, *Electrical conductivity and Hall conductivity of a hot and dense quark gluon plasma in a magnetic field: A quasiparticle approach*, *Phys. Rev. D* **101** (2020) 034027 [1907.05298].

[13] A. Das, H. Mishra and R. K. Mohapatra, *Transport coefficients of hot and dense hadron gas in a magnetic field: a relaxation time approach*, *Phys. Rev. D* **100** (2019) 114004 [1909.06202].

[14] K. G. Wilson, *Confinement of Quarks*, *Phys. Rev. D* **10** (1974) 2445.

[15] C. Ratti, *Lattice QCD and heavy ion collisions: a review of recent progress*, *Rept. Prog. Phys.* **81** (2018) 084301 [1804.07810].

[16] R. Hagedorn, *How We Got to QCD Matter from the Hadron Side: 1984*, *Lect. Notes Phys.* **221** (1985) 53.

[17] R. Venugopalan and M. Prakash, *Thermal properties of interacting hadrons*, *Nucl. Phys. A* **546** (1992) 718.

[18] F. Karsch, K. Redlich and A. Tawfik, *Hadron resonance mass spectrum and lattice QCD thermodynamics*, *Eur. Phys. J. C* **29** (2003) 549 [hep-ph/0303108].

[19] F. Karsch, K. Redlich and A. Tawfik, *Thermodynamics at nonzero baryon number density: A Comparison of lattice and hadron resonance gas model calculations*, *Phys. Lett. B* **571** (2003) 67 [hep-ph/0306208].

[20] P. Huovinen and P. Petreczky, *QCD Equation of State and Hadron Resonance Gas*, *Nucl. Phys. A* **837** (2010) 26 [0912.2541].

[21] Y. Nambu and G. Jona-Lasinio, *Dynamical model of elementary particles based on an analogy with superconductivity. ii*, *Phys. Rev.* **124** (1961) 246.

[22] Y. Nambu and G. Jona-Lasinio, *Dynamical model of elementary particles based on an analogy with superconductivity. i*, *Phys. Rev.* **122** (1961) 345.

[23] S. P. Klevansky, *The nambu—jona-lasinio model of quantum chromodynamics*, *Rev. Mod. Phys.* **64** (1992) 649.

[24] B.-J. Schaefer, J. M. Pawlowski and J. Wambach, *Phase structure of the polyakov-quark-meson model*, *Phys. Rev. D* **76** (2007) 074023.

[25] V. Skokov, B. Stokić, B. Friman and K. Redlich, *Meson fluctuations and thermodynamics of the polyakov-loop-extended quark-meson model*, *Phys. Rev. C* **82** (2010) 015206.

[26] T. K. Herbst, J. M. Pawlowski and B.-J. Schaefer, *The phase structure of the polyakov–quark–meson model beyond mean field*, *Physics Letters B* **696** (2011) 58.

[27] J. Adams, M. Aggarwal, Z. Ahammed, J. Amonett, B. Anderson, D. Arkhipkin et al., *Experimental and theoretical challenges in the search for the quark–gluon plasma: The star collaboration's critical assessment of the evidence from rhic collisions*, *Nuclear Physics A* **757** (2005) 102.

[28] K. Adcox, S. Adler, S. Afanasiev, C. Aidala, N. Ajitanand, Y. Akiba et al., *Formation of dense partonic matter in relativistic nucleus–nucleus collisions at rhic: Experimental evaluation by the phenix collaboration*, *Nuclear Physics A* **757** (2005) 184.

[29] I. Arsene, I. Bearden, D. Beavis, C. Besliu, B. Budick, H. Bøggild et al., *Quark–gluon plasma and color glass condensate at rhic? the perspective from the brahms experiment*, *Nuclear Physics A* **757** (2005) 1.

[30] B. Back, M. Baker, M. Ballintijn, D. Barton, B. Becker, R. Betts et al., *The phobos perspective on discoveries at rhic*, *Nuclear Physics A* **757** (2005) 28.

[31] ALICE collaboration, *Charged-particle multiplicity density at midrapidity in central pb-pb collisions at* $\sqrt{s_{NN}} = 2.76$ TeV, *Phys. Rev. Lett.* **105** (2010) 252301.

[32] ALICE collaboration, *Elliptic flow of charged particles in pb-pb collisions at* $\sqrt{s_{NN}} = 2.76$ TeV, *Phys. Rev. Lett.* **105** (2010) 252302.

[33] ALICE collaboration, *Centrality dependence of the charged-particle multiplicity density at midrapidity in pb-pb collisions at* $\sqrt{s_{\rm NN}} = 2.76$ TeV, *Phys. Rev. Lett.* **106** (2011) 032301.

[34] ALICE collaboration, *Higher harmonic anisotropic flow measurements of charged particles in pb-pb collisions at* $\sqrt{s_{NN}} = 2.76$ TeV, *Phys. Rev. Lett.* **107** (2011) 032301.

[35] HotQCD collaboration, *Equation of state in (2+1)-flavor QCD*, *Phys. Rev. D* **90** (2014) 094503 [1407.6387].

[36] C. Y. Wong, *Introduction to high-energy heavy ion collisions*. 1995.

[37] J. e Alam, S. Sarkar, P. Roy, T. Hatsuda and B. Sinha, *Thermal photons and lepton pairs from quark gluon plasma and hot hadronic matter*, *Annals of Physics* **286** (2000) 159.

[38] S. Sarkar, H. Satz and B. Sinha, eds., *The physics of the quark-gluon plasma*, vol. 785. 2010, 10.1007/978-3-642-02286-9.

[39] F. Geurts and R.-A. Tripolt, *Electromagnetic probes: Theory and experiment*, *Prog. Part. Nucl. Phys.* **128** (2023) 104004 [2210.01622].

[40] A. M. Poskanzer and S. A. Voloshin, *Methods for analyzing anisotropic flow in relativistic nuclear collisions*, *Phys. Rev. C* **58** (1998) 1671.

[41] J.-Y. Ollitrault, *Anisotropy as a signature of transverse collective flow*, *Phys. Rev. D* **46** (1992) 229.

[42] S. A. Voloshin, A. M. Poskanzer and R. Snellings, *Collective phenomena in non-central nuclear collisions*, *Landolt-Bornstein* **23** (2010) 293 [0809.2949].

[43] P. F. Kolb and U. W. Heinz, *Hydrodynamic description of ultrarelativistic heavy ion collisions*, nucl-th/0305084.

[44] S. Voloshin and Y. Zhang, *Flow study in relativistic nuclear collisions by Fourier expansion of Azimuthal particle distributions*, *Z. Phys. C* **70** (1996) 665 [hep-ph/9407282].

[45] N. Herrmann, J. P. Wessels and T. Wienold, *Collective flow in heavy ion collisions*, *Ann. Rev. Nucl. Part. Sci.* **49** (1999) 581.

[46] H. Stoecker, *Collective flow signals the quark gluon plasma*, *Nucl. Phys. A* **750** (2005) 121 [nucl-th/0406018].

[47] H. Sorge, *Elliptical flow: A Signature for early pressure in ultrarelativistic nucleus-nucleus collisions*, *Phys. Rev. Lett.* **78** (1997) 2309 [nucl-th/9610026].

[48] B. Alver and G. Roland, *Collision geometry fluctuations and triangular flow in heavy-ion collisions*, *Phys. Rev. C* **81** (2010) 054905 [1003.0194].

[49] STAR collaboration, *Experimental and theoretical challenges in the search for the quark gluon plasma: The STAR Collaboration's critical assessment of the evidence from RHIC collisions*, *Nucl. Phys. A* **757** (2005) 102 [nucl-ex/0501009].

[50] ALICE collaboration, *Elliptic flow of charged particles in Pb-Pb collisions at 2.76 TeV*, *Phys. Rev. Lett.* **105** (2010) 252302 [1011.3914].

[51] Z.-W. Lin, C. M. Ko, B.-A. Li, B. Zhang and S. Pal, *Multiphase transport model for relativistic heavy ion collisions*, *Phys. Rev. C* **72** (2005) 064901.

[52] M. Bleicher, E. Zabrodin, C. Spieles, S. A. Bass, C. Ernst, S. Soff et al., *Relativistic hadron-hadron collisions in the ultra-relativistic quantum molecular dynamics model*, *Journal of Physics G: Nuclear and Particle Physics* **25** (1999) 1859.

[53] W. Cassing and E. L. Bratkovskaya, *Parton transport and hadronization from the dynamical quasiparticle point of view*, *Phys. Rev. C* **78** (2008) 034919 [0808.0022].

[54] H. Petersen, D. Oliinychenko, M. Mayer, J. Staudenmaier and S. Ryu, *Smash – a new hadronic transport approach*, *Nuclear Physics A* **982** (2019) 399.

[55] P. Danielewicz and M. Gyulassy, *Dissipative Phenomena in Quark Gluon Plasmas*, *Phys. Rev. D* **31** (1985) 53.

[56] H. Song and U. W. Heinz, *Extracting the QGP viscosity from RHIC data - A Status report from viscous hydrodynamics*, *J. Phys. G* **36** (2009) 064033 [0812.4274].

[57] A. Chaudhuri, *Nearly perfect fluid in Au+Au collisions at RHIC*, *Phys. Lett. B* **681** (2009) 418 [0909.0391].

[58] P. Bożek, *Components of the elliptic flow in pb–pb collisions at s=2.76 tev*, *Physics Letters B* **699** (2011) 283.

[59] D. E. Kharzeev, L. D. McLerran and H. J. Warringa, *The Effects of topological charge change in heavy ion collisions: 'Event by event P and CP violation'*, *Nucl. Phys. A* **803** (2008) 227 [0711.0950].

[60] V. Skokov, A. Illarionov and V. Toneev, *Estimate of the magnetic field strength in heavy-ion collisions*, *Int. J. Mod. Phys. A* **24** (2009) 5925 [0907.1396].

[61] K. Tuchin, *Particle production in strong electromagnetic fields in relativistic heavy-ion collisions*, *Adv. High Energy Phys.* **2013** (2013) 490495 [1301.0099].

[62] K. Fukushima, D. E. Kharzeev and H. J. Warringa, *The Chiral Magnetic Effect*, *Phys. Rev. D* **78** (2008) 074033 [0808.3382].

[63] D. E. Kharzeev and H. J. Warringa, *Chiral Magnetic conductivity*, *Phys. Rev. D* **80** (2009) 034028 [0907.5007].

[64] G. Bali, F. Bruckmann, G. Endrodi, Z. Fodor, S. Katz, S. Krieg et al., *The QCD phase diagram for external magnetic fields*, *JHEP* **02** (2012) 044 [1111.4956].

[65] I. A. Shovkovy, *Magnetic Catalysis: A Review*, vol. 871, pp. 13–49. 2013. 1207.5081. 10.1007/978-3-642-37305-3_2.

[66] V. Gusynin, V. Miransky and I. Shovkovy, *Catalysis of dynamical flavor symmetry breaking by a magnetic field in (2+1)-dimensions*, *Phys. Rev. Lett.* **73** (1994) 3499 [hep-ph/9405262].

[67] V. Gusynin, V. Miransky and I. Shovkovy, *Dynamical flavor symmetry breaking by a magnetic field in (2+1)-dimensions*, *Phys. Rev. D* **52** (1995) 4718 [hep-th/9407168].

[68] V. Gusynin, V. Miransky and I. Shovkovy, *Dimensional reduction and catalysis of dynamical symmetry breaking by a magnetic field*, *Nucl. Phys. B* **462** (1996) 249 [hep-ph/9509320].

[69] V. Gusynin, V. Miransky and I. Shovkovy, *Theory of the magnetic catalysis of chiral symmetry breaking in QED*, *Nucl. Phys. B* **563** (1999) 361 [hep-ph/9908320].

[70] F. Preis, A. Rebhan and A. Schmitt, *Inverse magnetic catalysis in dense holographic matter*, *JHEP* **03** (2011) 033 [1012.4785].

[71] F. Preis, A. Rebhan and A. Schmitt, *Inverse magnetic catalysis in field theory and gauge-gravity duality*, vol. 871, pp. 51–86. 2013. 1208.0536. 10.1007/978-3-642-37305-3_3.

[72] P. Elmfors, K. Enqvist and K. Kainulainen, *Strongly first order electroweak phase transition induced by primordial hypermagnetic fields*, *Phys. Lett. B* **440** (1998) 269 [hep-ph/9806403].

[73] V. Skalozub and M. Bordag, *Ring diagrams and electroweak phase transition in a magnetic field*, *Int. J. Mod. Phys. A* **15** (2000) 349 [hep-ph/9904333].

[74] N. Sadooghi and K. Anaraki, *Improved ring potential of QED at finite temperature and in the presence of weak and strong magnetic field*, *Phys. Rev. D* **78** (2008) 125019 [0805.0078].

[75] J. Navarro, A. Sanchez, M. E. Tejeda-Yeomans, A. Ayala and G. Piccinelli, *Symmetry restoration at finite temperature with weak magnetic fields*, *Phys. Rev. D* **82** (2010) 123007 [1007.4208].

[76] S. Fayazbakhsh and N. Sadooghi, *Color neutral 2SC phase of cold and dense quark matter in the presence of constant magnetic fields*, *Phys. Rev. D* **82** (2010) 045010 [1005.5022].

[77] S. Fayazbakhsh and N. Sadooghi, *Phase diagram of hot magnetized two-flavor color superconducting quark matter*, *Phys. Rev. D* **83** (2011) 025026 [1009.6125].

[78] V. Skokov, *Phase diagram in an external magnetic field beyond a mean-field approximation*, *Phys. Rev. D* **85** (2012) 034026 [1112.5137].

[79] K. Fukushima and J. M. Pawlowski, *Magnetic catalysis in hot and dense quark matter and quantum fluctuations*, *Phys. Rev. D* **86** (2012) 076013 [1203.4330].

[80] M. Chernodub, *Spontaneous electromagnetic superconductivity of vacuum in strong magnetic field: evidence from the Nambu–Jona-Lasinio model*, *Phys. Rev. Lett.* **106** (2011) 142003 [1101.0117].

[81] M. Chernodub, J. Van Doorsselaere and H. Verschelde, *Electromagnetically superconducting phase of vacuum in strong magnetic field: structure of superconductor and superfluid vortex lattices in the ground state*, *Phys. Rev. D* **85** (2012) 045002 [1111.4401].

[82] K. Tuchin, *Time and space dependence of the electromagnetic field in relativistic heavy-ion collisions*, *Phys. Rev. C* **88** (2013) 024911 [1305.5806].

[83] U. Gursoy, D. Kharzeev and K. Rajagopal, *Magnetohydrodynamics, charged currents and directed flow in heavy ion collisions*, *Phys. Rev. C* **89** (2014) 054905 [1401.3805].

[84] K. Tuchin, *Initial value problem for magnetic fields in heavy ion collisions*, *Phys. Rev. C* **93** (2016) 014905 [1508.06925].

[85] A. Das, S. S. Dave, P. Saumia and A. M. Srivastava, *Effects of magnetic field on plasma evolution in relativistic heavy-ion collisions*, *Phys. Rev. C* **96** (2017) 034902 [1703.08162].

[86] R. C. Duncan and C. Thompson, *Formation of very strongly magnetized neutron stars - implications for gamma-ray bursts*, *Astrophys. J.* **392** (1992) L9.

[87] C. Thompson and R. C. Duncan, *Neutron star dynamos and the origins of pulsar magnetism*, *Astrophys. J.* **408** (1993) 194.

[88] T. Vachaspati, *Magnetic fields from cosmological phase transitions*, *Phys. Lett. B* **265** (1991) 258.

[89] L. Campanelli, *Origin of Cosmic Magnetic Fields*, *Phys. Rev. Lett.* **111** (2013) 061301 [1304.6534].

[90] S. R. De Groot, *Relativistic Kinetic Theory. Principles and Applications*. 1980.

[91] S. Weinberg, *Entropy generation and the survival of protogalaxies in an expanding universe*, *Astrophys. J.* **168** (1971) 175.

[92] P. Polak, W. van Leeuwen and S. de Groot, *On relativistic kinetic gas theory: X. transport coefficients in the intermediate relativistic regime. values for special models*, *Physica* **66** (1973) 455 .

[93] S. R. De Groot, *Relativistic Kinetic Theory. Principles and Applications*. 1980.

[94] A. Wiranata and M. Prakash, *Shear Viscosities from the Chapman-Enskog and the Relaxation Time Approaches*, *Phys. Rev.* **C85** (2012) 054908 [1203.0281].

[95] S. Plumari, A. Puglisi, F. Scardina and V. Greco, *Shear Viscosity of a strongly interacting system: Green-Kubo vs. Chapman-Enskog and Relaxation Time Approximation*, *Phys. Rev.* **C86** (2012) 054902 [1208.0481].

[96] B. D. Serot and J. D. Walecka, *The Relativistic Nuclear Many Body Problem*, *Adv. Nucl. Phys.* **16** (1986) 1.

[97] S. Mitra, S. Ghosh and S. Sarkar, *Effect of a spectral modification of the ρ meson on the shear viscosity of a pion gas*, *Phys. Rev. C* **85** (2012) 064917.

[98] A. Dobado, F. J. Llanes-Estrada and J. M. Torres-Rincon, *Minimum of η/s and the phase transition of the linear sigma model in the large-n limit*, *Phys. Rev. D* **80** (2009) 114015.

[99] V. Ozvenchuk, O. Linnyk, M. I. Gorenstein, E. L. Bratkovskaya and W. Cassing, *Shear and bulk viscosities of strongly interacting "infinite" parton-hadron matter within the parton-hadron-string dynamics transport approach*, *Phys. Rev. C* **87** (2013) 064903.

[100] L. P. Csernai, J. I. Kapusta and L. D. McLerran, *Strongly interacting low-viscosity matter created in relativistic nuclear collisions*, *Phys. Rev. Lett.* **97** (2006) 152303.

[101] C. Sasaki and K. Redlich, *Transport coefficients near chiral phase transition*, *Nucl. Phys.* **A832** (2010) 62 [0811.4708].

[102] P. K. Kovtun, D. T. Son and A. O. Starinets, *Viscosity in strongly interacting quantum field theories from black hole physics*, *Phys. Rev. Lett.* **94** (2005) 111601.

[103] D. Kharzeev and K. Tuchin, *Bulk viscosity of QCD matter near the critical temperature*, *JHEP* **09** (2008) 093 [0705.4280].

[104] J.-W. Chen and J. Wang, *Bulk viscosity of a gas of massless pions*, *Phys. Rev. C* **79** (2009) 044913.

[105] D. Fernández-Fraile and A. G. Nicola, *Bulk viscosity and the conformal anomaly in the pion gas*, *Phys. Rev. Lett.* **102** (2009) 121601.

[106] T. Ullrich, B. Wyslouch and J. W. Harris, *Proceedings, 23rd International Conference on Ultrarelativistic Nucleus-Nucleus Collisions : Quark Matter 2012 (QM 2012)*, *Nucl. Phys.* **A904-905** (2013) pp. 1c.

[107] S. Gavin, *TRANSPORT COEFFICIENTS IN ULTRARELATIVISTIC HEAVY ION COLLISIONS*, *Nucl. Phys.* **A435** (1985) 826.

[108] D. Davesne, *Transport coefficients of a hot pion gas*, *Phys. Rev. C* **53** (1996) 3069.

[109] A. Dobado and S. N. Santalla, *Pion gas viscosity at low temperature and density*, *Phys. Rev. D* **65** (2002) 096011.

[110] A. Dobado and F. J. Llanes-Estrada, *Viscosity of meson matter*, *Phys. Rev. D* **69** (2004) 116004.

[111] J.-W. Chen, Y.-H. Li, Y.-F. Liu and E. Nakano, *Qcd viscosity to entropy density ratio in the hadronic phase*, *Phys. Rev. D* **76** (2007) 114011.

[112] K. Itakura, O. Morimatsu and H. Otomo, *Shear viscosity of a hadronic gas mixture*, *Phys. Rev. D* **77** (2008) 014014.

[113] D. Fernandez-Fraile and A. Gomez Nicola, *Transport coefficients and resonances for a meson gas in Chiral Perturbation Theory*, *Eur. Phys. J.* **C62** (2009) 37 [0902.4829].

[114] J. Noronha-Hostler, J. Noronha and C. Greiner, *Transport coefficients of hadronic matter near T_c*, *Phys. Rev. Lett.* **103** (2009) 172302.

[115] C. Sasaki and K. Redlich, *Bulk viscosity in quasiparticle models*, *Phys. Rev. C* **79** (2009) 055207.

[116] A. Dobado and J. M. Torres-Rincon, *Bulk viscosity and the phase transition of the linear sigma model*, *Phys. Rev. D* **86** (2012) 074021.

[117] A. Dobado, F. J. Llanes-Estrada and J. M. Torres Rincon, *Heat conductivity of a pion gas*, in *Quarks and nuclear physics. Proceedings, 4th International Conference, QNP 2006, Madrid, Spain, June 5-10, 2006*, 2007, hep-ph/0702130.

[118] D. Fernandez-Fraile and A. Gomez Nicola, *Transport properties of a meson gas*, *Int. J. Mod. Phys.* **E16** (2007) 3010 [0706.3561].

[119] M. Greif, F. Reining, I. Bouras, G. S. Denicol, Z. Xu and C. Greiner, *Heat conductivity in relativistic systems investigated using a partonic cascade*, *Phys. Rev. E* **87** (2013) 033019.

[120] G. S. Denicol, H. Niemi, I. Bouras, E. Molnar, Z. Xu, D. H. Rischke et al., *Solving the heat-flow problem with transient relativistic fluid dynamics*, *Phys. Rev.* **D89** (2014) 074005 [1207.6811].

[121] P. Danielewicz and M. Gyulassy, *Dissipative phenomena in quark-gluon plasmas*, *Phys. Rev. D* **31** (1985) 53.

[122] A. Hosoya and K. Kajantie, *Transport Coefficients of QCD Matter*, *Nucl. Phys.* **B250** (1985) 666.

[123] P. B. Arnold, G. D. Moore and L. G. Yaffe, *Transport coefficients in high temperature gauge theories. 1. Leading log results*, *JHEP* **11** (2000) 001 [hep-ph/0010177].

[124] P. B. Arnold, G. D. Moore and L. G. Yaffe, *Transport coefficients in high temperature gauge theories. 2. Beyond leading log*, *JHEP* **05** (2003) 051 [hep-ph/0302165].

[125] M. Rahaman, S. Ghosh, S. Ghosh, S. Sarkar and J.-e. Alam, *Contribution of a kaon component in the viscosity and conductivity of a hadronic medium*, *Phys. Rev. C* **97** (2018) 035201.

[126] S. Ghosh, G. Krein and S. Sarkar, *Shear viscosity of a pion gas resulting from $\rho\pi\pi$ and $\sigma\pi\pi$ interactions*, *Phys. Rev.* **C89** (2014) 045201 [1401.5392].

[127] S. Ghosh, *Nucleon thermal width owing to pion-baryon loops and its contributions to shear viscosity*, *Phys. Rev.* **C90** (2014) 025202 [1503.06927].

[128] S. Ghosh, *Shear viscosity of pionic and nucleonic components from their different possible mesonic and baryonic thermal fluctuations*, *Braz. J. Phys.* **45** (2015) 687 [1507.01705].

[129] L. Pitaevskii and E. Lifshitz, *Physical Kinetics*, no. v. 10. Elsevier Science, 2012.

[130] F. Reif, *Fundamentals of statistical and thermal physics / [by] F. Reif*. McGraw-Hill Kogakusha Tokyo, international student ed. ed., 1965.

[131] R. Kubo, *Statistical mechanical theory of irreversible processes. 1. General theory and simple applications in magnetic and conduction problems*, *J. Phys. Soc. Jap.* **12** (1957) 570.

[132] S. Sarkar, *Viscous Coefficients of a Hot Pion Gas*, *Adv. High Energy Phys.* **2013** (2013) 627137 [1308.1771].

[133] S. Jeon, *Hydrodynamic transport coefficients in relativistic scalar field theory*, *Phys. Rev.* **D52** (1995) 3591 [hep-ph/9409250].

[134] S. Jeon and L. G. Yaffe, *From quantum field theory to hydrodynamics: Transport coefficients and effective kinetic theory*, *Phys. Rev.* **D53** (1996) 5799 [hep-ph/9512263].

[135] E. Lu and G. D. Moore, *Bulk viscosity of a pion gas*, *Phys. Rev. C* **83** (2011) 044901.

[136] S. Mitra and S. Sarkar, *Medium effects on the viscosities of a pion gas*, *Phys. Rev. D* **87** (2013) 094026.

[137] S. Mitra and S. Sarkar, *Medium effects on the thermal conductivity of a hot pion gas*, *Phys. Rev. D* **89** (2014) 054013.

[138] U. Gangopadhyaya, S. Ghosh, S. Sarkar and S. Mitra, *In-medium viscous coefficients of a hot hadronic gas mixture*, *Phys. Rev. C* **94** (2016) 044914.

[139] R. Lang, N. Kaiser and W. Weise, *Shear Viscosity of a Hot Pion Gas*, *Eur. Phys. J.* **A48** (2012) 109 [1205.6648].

[140] A. Wiranata, V. Koch, M. Prakash and X. N. Wang, *Shear viscosity of hadrons with K-matrix cross sections*, *Phys. Rev.* **C88** (2013) 044917 [1307.4681].

[141] O. Krehl, C. Hanhart, S. Krewald and J. Speth, *What is the structure of the roper resonance?*, *Phys. Rev. C* **62** (2000) 025207.

[142] C. M. Ko and D. Seibert, *What can we learn from a second phi meson peak in ultrarelativistic nuclear collisions?*, *Phys. Rev. C* **49** (1994) 2198.

[143] S. Ghosh, S. Sarkar and S. Mitra, Δ *self-energy at finite temperature and density and the* πn *cross section*, *Phys. Rev. D* **95** (2017) 056010.

[144] H. Bebie, P. Gerber, J. L. Goity and H. Leutwyler, *The Role of the entropy in an expanding hadronic gas*, *Nucl. Phys.* **B378** (1992) 95.

[145] P. Buividovich, M. Chernodub, D. Kharzeev, T. Kalaydzhyan, E. Luschevskaya and M. Polikarpov, *Magnetic-Field-Induced insulator-conductor transition in SU(2) quenched lattice gauge theory*, *Phys. Rev. Lett.* **105** (2010) 132001 [1003.2180].

[146] S. Pu, S.-Y. Wu and D.-L. Yang, *Chiral Hall Effect and Chiral Electric Waves*, *Phys. Rev. D* **91** (2015) 025011 [1407.3168].

[147] D. Satow, *Nonlinear electromagnetic response in quark-gluon plasma*, *Phys. Rev. D* **90** (2014) 034018 [1406.7032].

[148] E. Gorbar, I. Shovkovy, S. Vilchinskii, I. Rudenok, A. Boyarsky and O. Ruchayskiy, *Anomalous Maxwell equations for inhomogeneous chiral plasma*, *Phys. Rev. D* **93** (2016) 105028 [1603.03442].

[149] A. Harutyunyan and A. Sedrakian, *Electrical conductivity of a warm neutron star crust in magnetic fields*, *Phys. Rev. C* **94** (2016) 025805 [1605.07612].

[150] B. Kerbikov and M. Andreichikov, *Electrical Conductivity of Dense Quark Matter with Fluctuations and Magnetic Field Included*, *Phys. Rev. D* **91** (2015) 074010 [1410.3413].

[151] M. G. Alford, H. Nishimura and A. Sedrakian, *Transport coefficients of two-flavor superconducting quark matter*, *Phys. Rev. C* **90** (2014) 055205 [1408.4999].

[152] S.-i. Nam, *Electrical conductivity of quark matter at finite T under external magnetic field*, *Phys. Rev. D* **86** (2012) 033014 [1207.3172].

[153] X.-G. Huang, A. Sedrakian and D. H. Rischke, *Kubo formulae for relativistic fluids in strong magnetic fields*, *Annals Phys.* **326** (2011) 3075 [1108.0602].

[154] S. I. Finazzo, R. Critelli, R. Rougemont and J. Noronha, *Momentum transport in strongly coupled anisotropic plasmas in the presence of strong magnetic fields*, *Phys. Rev. D* **94** (2016) 054020 [1605.06061].

[155] K. Fukushima, K. Hattori, H.-U. Yee and Y. Yin, *Heavy Quark Diffusion in Strong Magnetic Fields at Weak Coupling and Implications for Elliptic Flow*, *Phys. Rev. D* **93** (2016) 074028 [1512.03689].

[156] S. Li, K. A. Mamo and H.-U. Yee, *Jet quenching parameter of the quark-gluon plasma in a strong magnetic field: Perturbative QCD and AdS/CFT correspondence*, *Phys. Rev. D* **94** (2016) 085016 [1605.00188].

[157] K. Hattori and D. Satow, *Electrical Conductivity of Quark-Gluon Plasma in Strong Magnetic Fields*, *Phys. Rev.* **D94** (2016) 114032 [1610.06818].

[158] K. Fukushima and Y. Hidaka, *Electric conductivity of hot and dense quark matter in a magnetic field with Landau level resummation via kinetic equations*, *Phys. Rev. Lett.* **120** (2018) 162301 [1711.01472].

[159] A. Dash, S. Samanta, J. Dey, U. Gangopadhyaya, S. Ghosh and V. Roy, *Anisotropic transport properties of Hadron Resonance Gas in magnetic field*, 2002.08781.

[160] K. Tuchin, *Synchrotron radiation by fast fermions in heavy-ion collisions*, *Phys. Rev. C* **82** (2010) 034904 [1006.3051].

[161] H.-T. Ding, A. Francis, O. Kaczmarek, F. Karsch, E. Laermann and W. Soeldner, *Thermal dilepton rate and electrical conductivity: An analysis of vector current correlation functions in quenched lattice QCD*, *Phys. Rev. D* **83** (2011) 034504 [1012.4963].

[162] G. Aarts, C. Allton, J. Foley, S. Hands and S. Kim, *Spectral functions at small energies and the electrical conductivity in hot, quenched lattice QCD*, *Phys. Rev. Lett.* **99** (2007) 022002 [hep-lat/0703008].

[163] S. Mitra, S. Ghosh and S. Sarkar, *Effect of spectral modification of ρ on shear viscosity of a pion gas*, *Phys. Rev. C* **85** (2012) 064917 [1204.2388].

[164] M. L. Bellac, *Thermal Field Theory*, Cambridge Monographs on Mathematical Physics. Cambridge University Press, 3, 2011, 10.1017/CBO9780511721700.

[165] S. Mallik and S. Sarkar, *Hadrons at Finite Temperature*. Cambridge University Press, Cambridge, 2016, 10.1017/9781316535585.

[166] S. Ghosh, A. Mukherjee, M. Mandal, S. Sarkar and P. Roy, *Thermal effects on ρ meson properties in an external magnetic field*, *Phys. Rev. D* **96** (2017) 116020 [1704.05319].

[167] A. Ayala, P. Mercado and C. Villavicencio, *Magnetic catalysis of a finite size pion condensate*, *Phys. Rev. C* **95** (2017) 014904 [1609.02595].

[168] J. P. Carlomagno, D. Gomez Dumm, M. F. I. Villafañe, S. Noguera and N. N. Scoccola, *Charged pseudoscalar and vector meson masses in strong magnetic fields in an extended NJL model*, *Phys. Rev. D* **106** (2022) 094035 [2209.10679].

[169] M. A. Andreichikov, B. O. Kerbikov, E. V. Luschevskaya, Y. A. Simonov and O. E. Solovjeva, *The Evolution of Meson Masses in a Strong Magnetic Field*, *JHEP* **05** (2017) 007 [1610.06887].

[170] S. Ghosh, A. Mukherjee, N. Chaudhuri, P. Roy and S. Sarkar, *Thermo-magnetic spectral properties of neutral mesons in vector and axial-vector channels using NJL model*, *Phys. Rev. D* **101** (2020) 056023 [2003.02024].

[171] E. V. Luschevskaya, O. E. Solovjeva and O. V. Teryaev, *Determination of the properties of vector mesons in external magnetic field by Quenched $SU(3)$ Lattice QCD*, *JHEP* **09** (2017) 142 [1608.03472].

[172] M. Strickland, V. Dexheimer and D. P. Menezes, *Bulk Properties of a Fermi Gas in a Magnetic Field*, *Phys. Rev. D* **86** (2012) 125032 [1209.3276].

[173] J. O. Andersen, W. R. Naylor and A. Tranberg, *Phase diagram of QCD in a magnetic field: A review*, *Rev. Mod. Phys.* **88** (2016) 025001 [1411.7176].

[174] G. Endrődi, *QCD equation of state at nonzero magnetic fields in the Hadron Resonance Gas model*, *JHEP* **04** (2013) 023 [1301.1307].

[175] N. Chaudhuri, S. Ghosh, S. Sarkar and P. Roy, *Effects of quark anomalous magnetic moment on the thermodynamical properties and mesonic excitations of magnetized hot and dense matter in PNJL model*, *Eur. Phys. J. A* **56** (2020) 213 [2003.05692].

[176] N. Chaudhuri, S. Ghosh, P. Roy and S. Sarkar, *Anisotropic pressure of magnetized quark matter with anomalous magnetic moment*, *Phys. Rev. D* **106** (2022) 056020 [2209.02248].

[177] D. Atta, N. Chaudhuri and S. Ghosh, *Finite size effect on the thermodynamics of a hot and magnetized hadron resonance gas*, *Mod. Phys. Lett. A* **37** (2022) 2250211 [2212.05834].

[178] S. S. Avancini, R. L. S. Farias, M. B. Pinto, T. E. Restrepo and W. R. Tavares, *Regularizing thermo and magnetic contributions within nonrenormalizable theories*, *Phys. Rev. D* **103** (2021) 056009 [2008.10720].